ABSTRACT

Title of Dissertation:	LEVERAGING BIOMATERIALS TO DIRECT IMMUNE FUNCTION IN CANCER AND AUTOIMMUNITY
	Shannon J. Tsai, Doctor of Philosophy, 2022
Dissertation directed by:	Christopher M. Jewell Professor Fischell Department of Bioengineering

Immune dysregulation and difficulties in directing immune function in cancer and autoimmune disease pose complex challenges for existing vaccines and immunotherapies. In cancer, tumor cells exploit processes to evade the immune system. Conversely, autoimmune diseases such as multiple sclerosis (MS) occur when immune cells incorrectly attack healthy host tissue and cells. To address the dichotomy of dysregulated immune responses that can arise, next generation vaccines and immunotherapies demand better control over the specificity and types of immune of responses generated within lymph nodes (LNs).

This dissertation investigated two approaches to improve immune signal delivery for precision control over immune responses. In the first approach, self-assembling vaccine nanoparticles were engineered with tunable charge and cargo loading to efficiently deliver immune signals in specific combinations and doses without compromising function. These studies offer new insight into biomaterial design for therapeutic cancer vaccines and demonstrate that

the physiochemical properties of biomaterials - particularly the interplay between charge, uptake, and affinity - play an important role in the immune signals that can promote T cell expansion against tumor antigens.

In the second approach, a biomaterial-based platform is used to control immune signal delivery to LNs during autoimmunity. Direct injections of therapeutic vaccine carriers into the LNs of mice offer new insight into how the localized combination of myelin peptide (MOG) and rapamycin (Rapa) - an immunomodulatory signal, promote potent and selective immune tolerance. This body of work demonstrates that immune function is highly localized to the signals delivered to the LNs, requiring an idealized combination of both self-antigen and immunomodulatory signal to promote the proliferation, retention, and polarization of antigen specific T cells towards regulatory T cells that can selectively limit inflammatory T cell phenotypes and combat autoimmunity.

Together, these two approaches offer new insight into how biomaterials can be rationally harnessed to direct immune function across cancer and autoimmune disease.

LEVERAGING BIOMATERIALS TO DIRECT IMMUNE FUNCTION IN CANCER AND AUTOIMMUNITY

by

Shannon J. Tsai

Dissertation submitted to the Faculty of the Graduate School of the
University of Maryland, College Park, in partial fulfillment
of the requirements for the degree of
Doctor of Philosophy
2022

Advisory Committee:
Professor Christopher M. Jewell, Chair
Assistant Professor Gregg A. Duncan
Associate Professor Steven M. Jay
Assistant Professor Katharina Maisel
Professor David M. Mosser, Dean's Representative

Acknowledgements

To Chris, thank you for supporting me and being my biggest advocate. I will be forever grateful for how much you've driven my career and personal development so I could achieve my goals. To my committee – thank you for your time, guidance, and support – for asking the tough questions and offering insight to support my work. To past and current member of the Jewell lab, thank you for all of the advice and assistance you have provided throughout the years, for sharing in the experimental struggles and making the work in this dissertation possible, and putting up with Taylor Swift. To my family and friends, thank you for the emotional support and patience throughout the years, for lifting me up through my lows and celebrating my highs, and instilling the confidence that I needed when I fell short. To Marshall, there aren't enough words. Thank you for your unwavering support and belief in me. I love you.

Table of Contents

List of Tables

List of Figures

List of Abbreviations

1,2-distearoyl-sn-glycero-3-phosphoethanolamine-N-PEG	DSPE-PEG
4′,6-diamidino-2-phenylindole	DAPI
5(6)Carboxy-fluorescein diacetate N-succinimidyl ester	CFSE
Aluminum oxyhydroxide nanorods	ALNR
Analysis of variance	ANOVA
Antigen	Ag
Antigen presenting cell	APC
Antigen presenting cell mimetic scaffold	APC-ms
Artificial antigen presenting cell	aAPC
Bone marrow derived dendritic cell	BMDC
Central Nervous System	CNS
Complete Freund's Adjuvant	CFA
Dendritic cell	DC
Deoxyribonucleic acid	DNA
Enzyme-linked immunosorbent Assay	ELISA
Experimental autoimmune encephalomyelitis	EAE
Extracellular matrix	ECM
Gold nanoparticle	AuNP
Hyaluronic acid	HA
Interferon	IFN
Interleukin	IL

Intra-lymph node	iLN
Intraperitoneal	i.p.
Intravenous	i.v.
Lipopolysaccharide	LPS
Lymph node	LN
Major histocompatibility complex	MHC
Median Fluorescence Intensity	MFI
Micro bicinchoninic acid protein assay	mBCA
Microparticle	MP
Molecular target of rapamycin	mTOR
Molecular weight	MW
Multiple sclerosis	MS
Nanoparticles	NP
Natural killer cell	NK cell
Ovalbumin	OVA
Pathogen associated molecular patterns	PAMP
Pattern recognition receptors	PRRs
Peptide amphiphile micelles	PAM
Peptide-Major histocompatibility complex	pMHC
Phosphate buffered saline	PBS
Poly(beta amino ester)	PBAE
Poly(ethylene glycol)	PEG

Poly(lactic-glycolic acid)	PLGA
Poly(lactic-glycolic)	PLG
Polyvinyl alcohol	PVA
Rapamycin	Rapa
Regulatory T cell	Treg
Ribonucleic acid	RNA
Spherical nucleic acids	SNA
Standard error of the mean	SEM
Subcutaneous	s.c.
T cell receptor	TCR
Toll-like receptor	TLR
Toll-like receptor agonist	TLRa

Chapter 1: Introduction

The work in this dissertation draws on a mix of engineering and immunology to study how biomaterials can be leveraged to improve immunotherapies for both cancer and autoimmune disease. **Chapter 1** provides an orientation to understand the subsequent chapters.

1.1 Background

1.1.1 Considerations for the development and design of vaccines and immunotherapies

Vaccines and immunotherapies have produced some of the greatest impacts on public health, effectively eradicating diseases such as polio and small pox and improving outcomes and quality of life for millions of patients across cancer and autoimmune disease.[1] Vaccines arm the immune system against future encounters with pathogens through delivery of unique specific markers – antigens – that are recognized as foreign. This priming of the immune system enables immune cells to mount robust, highly selective immune responses against their target. Similarly, immunotherapies offer precise control by initiating, enhancing or suppressing immune cells in settings where disease is already present. These treatments target specific immune pathways to generate immune responses with distinct characteristics. However, many diseases continue to pose complex challenges for existing vaccine and immunotherapy strategies. For example, immune dysregulation can lead to cancer or autoimmune disorders. Cancer cells develop strategies to evade the immune system. While therapeutic cancer vaccines that arm immune cells against antigens over-expressed on cancer cells have the potential to transform cancer therapy, they have been hindered by inefficient expansion of T cells against tumor antigens, an inability to maintain anti-tumor response in the immune-suppressive tumor microenvironment, and poor generation of

tumor-specific T cell memory to prevent relapse. Conversely, autoimmune diseases such as multiple sclerosis (MS) occur when immune cells incorrectly attack healthy host tissue and cells. Current therapies for MS partially ameliorate symptoms of disease but fail to differentiate between healthy and self-reactive disease associated immune cells. As a more targeted approach, experimental strategies are employing vaccine-like approaches to selectively reprogram the immune system to induce regulatory T cells (Tregs) that can suppress inflammatory cells and ameliorate disease with high selectivity. However, improved knowledge in triggering antigen-specific Treg activation, differentiation, and expansion is needed. To address the dichotomy of dysregulated immune responses that can arise, developing next generation vaccines and immunotherapies requires better control over the specificity and types of immune of responses generated within lymph nodes.

1.1.2 Lymph nodes are a key tissue that organizes immune cells, signals, and responses

Lymph nodes (LNs) are key tissue that orchestrates immunity.[1,2] In these tissues, antigen presenting cells such as dendritic cells (DCs) process and present antigen to activate naive T cells and B cells against these molecules. Immune cells can be directed towards inflammatory or tolerogenic phenotypes, depending on the soluble factors, structural components, and surface markers encountered in LNs. During a proimmune response, APCs can recognize "danger signals," molecular motifs commonly found on pathogens, but absent in healthy host cells, resulting in upregulation of co-stimulatory signals. Presentation of a specific antigen in the presence of costimulatory molecules by APCs leads to activation of T cells specific to the presented antigen through the T cell receptor (TCR). B cells share many of the same features of T cell activation, and become activated following recognition of a cognate antigen. B cells also play important roles

in the generation of antigen-specific antibody responses.[3] However, the focus of this dissertation has primarily been on T cells. Upon activation, T cells leave LNs or spleen and return to sites of infection or disease to selectively combat the pathogen the cell is now armed against. In contrast, T cells that encounter self-antigen in the absence of costimulatory signals receive incomplete priming signals, which can lead to either deletion or anergy (i.e. nonreactivity) of effector T cells or the induction of T_{REGS} that can suppress inflammatory cells. Co-delivery of antigen with immunomodulatory cytokines (e.g. IL-10, TGF-β) or immunosuppressants (e.g. rapamycin) may further attenuate T cell responses.[4–7] Thus, antigen presentation, costimulatory molecules, and cytokines are all cues that initiate and maintain immune responses towards pro-inflammatory or tolerogenic pathways.[8,9]

1.1.3 New immunotherapies would benefit from rational design criteria

Many challenges remain in developing functionally robust T cells for controlling cancer and autoimmune diseases *in vivo*. This is due in part to the complexity of immune signaling, and the lack of clear design rules to drive particular immune responses. Nevertheless, fundamental understanding of some of the key mechanisms governing adaptive immune responses offer insight into approaches to control and regulate immune response. One paradigm in immunology is that the strength of immune responses is shaped by antigen dose, localization, and costimulatory signals. From this perspective, control over the total dose, signal density, relative signal concentration, signal localization and delivery kinetics has the potential to polarize and enhance immune responses.

First, careful vaccine and immunotherapy dosing strategies can modulate the strength of TCR signaling. The capacity of APCs to induce TCR signaling can be modulated by antigen load, the quality of peptide presented, and the combinations of co-stimulatory molecules. This is of particular significance because several labs have shown that TCR signal strength controls the differentiation of T cells.[10–13] For instance, low doses of peptide presentation by APCs trigger weak TCR signaling resulting in increased Treg phenotypes while stimulation with APCs presenting a high dose of peptide can lead to the induction of inflammatory T_H1 cells that play important roles in cell mediated immunity and inflammation.[14,15]

Additionally, the density of delivered signals offer an opportunity to impact TCR cross-linking and the stability of APC-T cell interactions. Because the TCR is comprised of monovalent and multivalent complexes with low binding affinity, TCR activation occurs by formation of nanoclusters that bind peptide-MHC to promote TCR cross-linking.[16,17] This allows for sensing of both high and low concentrations of peptide-MHC, while maintaining high specificity.[7] Importantly, the cross-linking of TCRs can help stabilize APC-TCR interactions.[11] Thus, TCR signaling can also be controlled by improved cross-linking of the receptor. Together, these mechanisms offer an immunological basis for the dependency of immune responses based on dose, density, and the combination of immune signals.

Third, immune signals act synergistically to modulate immune responses. Immune modulation is dependent on the intricate balance between antigen presentation, costimulatory molecules, and cytokines. Ultimately, the immune response generated is dependent on the sum of immune signals present. For example, while antigen alone can stimulate immune responses, the addition of strong immunostimulators can drastically reducing the dose of antigen needed to

achieve similar levels of activation.[18–20] Thus, in the context of multiple immune signals, the relative concentrations of signals can play an important role in driving specific immune responses.

Finally, as highlighted above, immune signal localization to LNs is critical to the generation of immune responses. Given that immune responses rely on a combination of signals, another key aspect to the delivery of effective immunotherapies for modulating specific responses is co-delivery of multiple cargos and controlled release to spatially control the localization of signals. Adaptive immune responses by T and B cells can only be induced in lymphoid tissues. Additionally, immune signals must be present at the appropriate amounts. Signals that do not reach LNs in minimum doses or for sufficiently long time periods are immunologically ignored.[21–23] Antigen that either usually exists in the LN or persists in excessive amounts for long periods of time can lead to deletion of T cells.[24,25] These findings suggest that the location in which immune signals are retained can heavily influence immunological reactivity.

1.1.4 Biomaterials offer a breadth of opportunities to generate and improve therapeutic immune responses

The term "biomaterials" spans a broad range of both organic and inorganic compounds used in biological applications. Many of these classes are useful because they are easily modified for chemical and physiochemical properties. Organic biomaterials may be comprised on natural and synthetic polymers, including peptides and nucleic acids, or even cells. Inorganic materials (e.g. gold, silicon, carbon), while often non-biodegradable, have also been explored as important classes of biomaterials.[26] These materials can be engineered into many forms, including liposomes,

polymer nanoparticles and microparticles (MPs), self-assembled particles, polymer scaffolds, and microneedles (**Fig. 1.1**).

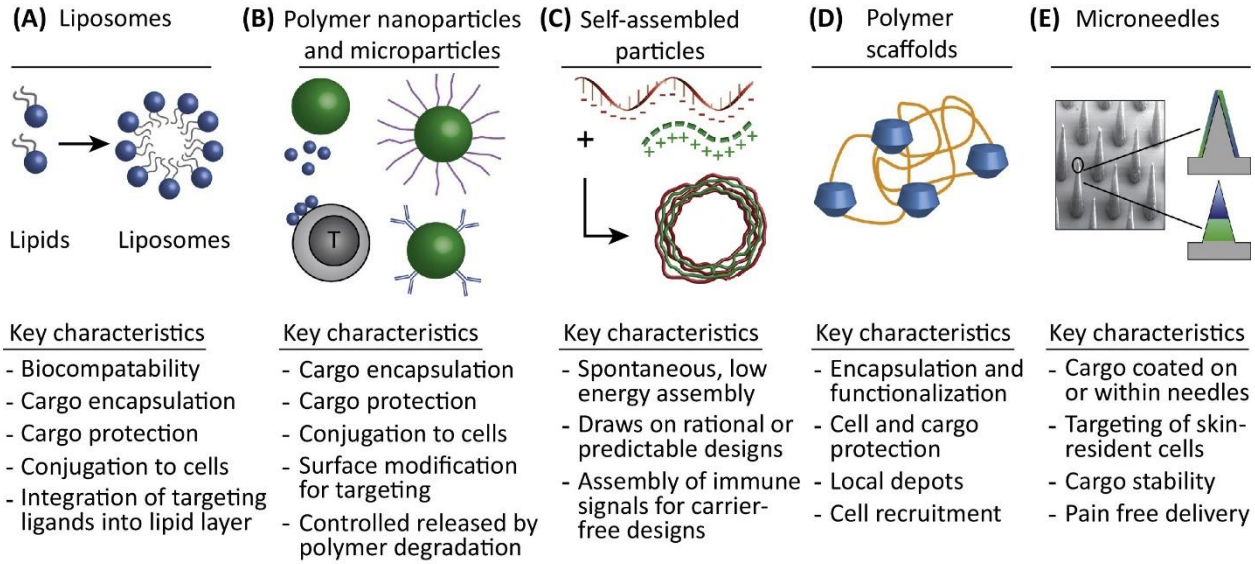

Figure 1.1 Examples of biomaterials in immune engineering
Biomaterials in immune signal delivery take on a variety of forms, each of which offer distinct advantages. These forms include: (**A**) liposomes (**B**) polymer particles (**C**) self-assembled particles, (**D**) polymer scaffolds and (**E**) microneedles. Adapted from *Trends in Immunology*, **2018**. [27]

Biomaterials present a new realm for the generation, enhancement, inhibition, or other selective direction of immune responses. These materials offer several generally important design benefits, including cargo protection, controlled release, and dose sparing to minimize local and systemic toxicity. Further, biomaterials can be functionalized to improve targeting to immune cells or organs. While the characteristics just summarized are generally useful for drug delivery, biomaterials also exhibit features of particular interest for vaccines and immunotherapies. The immune system responds to specific cues across multiple dimensions, including the physiological location, the combination and relative concentration of signals present, the molecular conformation of the signals, and the types of immune cells and migration patterns involved; all of these factors influence the activation, maintenance, and resolution of immune response. Biomaterials can be engineered to interact with the immune system in specific ways, allowing for

presentation of physical and chemical signals with the spatiotemporal accuracy to better direct immune responses. Nanoparticles and microparticles in particular are increasingly being employed to deliver disease-relevant antigens and molecules that can target and enhance occurring immune pathways to generate therapeutic immune responses across infection, cancer, and autoimmune disease. As one recent example, liposomal carriers – particles composed of amphipathic lipid molecules surrounding an inner aqueous core – encapsulate Pfizer and Moderna's mRNA vaccine against SARS-CoV-2, playing a critical role in the response against COVID-19.[28]

1.2 Significance

My doctoral work has focused on understanding how biomaterials can be leveraged to provide the appropriate control needed to tune immune responses. Given that immune responses are the result of a complex integration of signals, it is critical to understand how specific features of materials alter immune responses. Understanding the link between materials features and the resulting immune functions will increasingly support guidelines for rational design of biomaterials for vaccines and immunotherapies.[29] The studies in this dissertation utilize biomaterials to elucidate rational design considerations in promoting robust immune function against cancer and autoimmune disease. During cancer, the goal is to enhance the immunogenicity of administered therapies to stimulate robust immune responses and circumvent immune tolerance to target over-expressed self-antigens in tumors. Conversely, in autoimmune disease, immune cells incorrectly attack self-tissue, requiring treatments that can selectively promote immune tolerance. While these two areas of disease present opposing goals, they share a need for improved delivery and control over the type of immune responses generated. This is accomplished in two ways.

First, I engineer vaccine nanoparticles with tunable charge and cargo loading that can efficiently deliver pro-immune signals in the right combination and doses without compromising function. These studies offer new insight into biomaterial design for therapeutic cancer vaccines and demonstrate that the physiochemical properties of biomaterials, particularly the interplay between charge, uptake, and affinity, play an important role in determining the nature and efficacy of the immune response generated.

In my second approach, a biomaterial-based platform is employed to control immune signal delivery and gain new insight into how the localized combination of MOG and Rapa promote immune tolerance. Therapies injected via typical delivery routes such as subcutaneously (*s.c.*) or intramuscularly (*i.m.*), are often rapidly cleared from draining lymph nodes, limiting exposure times for antigen uptake by DCs. Meanwhile, poor targeting efficiency prevents direct control over the combinations and dosage of signals that reach LNs. This is a major limitations for many existing treatments in MS, which expose patient to systemic, repeated dosing of immunosuppresants, presenting safety concerns related to the lack of specificity and global immunosuppression. To address this challenge, this direction uses a non-surgical technique for directly injecting vaccine carriers into the LNs of mice. Intra-lymph node (*i.LN*) injection provides a unique platform to directly study how changes in immune signal combinations, dose, and concentration, impact development or enhancement of immune response. In this platform, microparticles (MPs) are synthesized using double emulsion to prepare MPs that are too large to drain from the LN. Instead, the MPs slowly degrade to locally release peptide antigens and molecular immunomodulatory signals in the LN microenvironment allowing for studies to explore the role of dose and combinations of immune signals within LNs in inducing immune tolerance.

Excitingly, iLN treatment with traditional soluble antigens has recently been tested in clinical trials using ultrasound guidance and has shown promise for allergy therapy[30,31] and cancer,[32,33] highlighting a path towards translation.

1.3 Thesis Goals and Organization

My dissertation combines immunology and materials science to explore the role of biomaterials in promoting robust immune responses by enabling immune signal delivery with control over the dose, combination, and location. I use two different biomaterial-based platforms to achieve this goal. This is accomplished first through direct engineering of biomaterials-based vaccines and immunotherapies to control immune signal uptake and processing in cancer vaccination. Under this approach, I exploit self-assembly of charged polymers, peptides and oligonucleotides to synthesize immune signal complexes with tunable loading, charge, and interaction strength. In my second approach, a direct LN injection technique was used to spatially control immune signal delivery and localization, garnering new insight into the roles of myelin peptide and rapamycin, an immunomodulator in generating tolerance. The work in this dissertation required expertise in immunology, biomaterials, drug delivery, formulation development and characterization, and animal models.

To understand the roles and limitations that biomaterials may play in delivering immune signals, my doctoral work focused on three central goals:

1. Identify key features of biomaterials based vaccines and immunotherapies that can enable efficient deliver immune signals in the right combination and doses without compromising function

2. Leverage biomaterials for spatial and dose control to isolate role of individual immune signals in generating systemic tolerance.
3. Develop new insights into therapeutic formulations to promote advancement of therapies towards translation

The completed work supports the overall goal of generating insight that will promote more robust biomaterial-based immunotherapies. This dissertation first outlines how biomaterials can be leveraged to modulate immune responses in **Chapter 2**. This review begins with an overview of how antigen-specific immune responses are generated, followed by a discussion on the state of the immune engineering field with specific examples that highlight engineering strategies that can be leveraged to control delivery of immune signals and tune immune function. **Chapters 3** and **4** investigate delivery of immune signals using polyplexes –nanoparticles built entirely from immune signals using self-assembly – to drive proimmune function. **Chapter 3** lays the groundwork focusing on delivery of a single immune signal to activate immune responses. Building on this work, **Chapter 4** then explores co-delivery of multiple immune signals in the absence of a delivery vehicle. In a second approach to leveraging biomaterials to improve immune responses, **Chapter 5** explores iLN as a tool to control delivery of immune signals and gain new insight into how immune signals localized within LNs promote immune tolerance in a mouse model of MS. **Chapter 6** details ongoing and future research directions to explore in support of the presented work, including opportunities to improve the durability of generated immune responses and studies in male mice to improve rigor of studies. My contributions to the field are summarized in **Chapter 7**. This dissertation concludes with an **Appendix** listing the publications that I have authored as a part of this dissertation and list of **References** used in this work.

Chapter 2: Leveraging the modularity of biomaterial carriers to tune immune responses †

2.1 Introduction

Biomaterial carriers offer modular features to control the delivery and presentation of vaccines and immunotherapies. This tunability is a distinct capability of biomaterials. Understanding how tunable material features impact immune responses is important to improve vaccine and immunotherapy design, as well as clinical translation. Here we discuss the modularity of biomaterial properties as a means of controlling encounters with immune signals across scales – tissue, cell, molecular, and time – and ultimately the stimulation or regulation of immunity. We highlight these advances using illustrations from recent literature across infectious disease, cancer, and autoimmunity. As the immune engineering field matures, informed design criteria could support more rational biomaterial carriers for vaccination and immunotherapy.

2.2 Biomaterials offer modularity that can be exploited for vehicles to improve vaccines and immunotherapies

As introduced in **Chapter 1,** vaccines and immunotherapies are unique in their ability to exert specific and long-lasting effects to combat infection and disease. Advances in our understanding of the underlying cellular processes that govern these responses have paved the way for new vaccines and immunotherapies, but putting this new insight into practice is a work in progress.[34–37] One ongoing hurdle facing new strategies is the evolving nature of pathogens and cancerous cells that constantly mutate to evade immune recognition. Likewise, coaxing the immune system to recognize a particular fragment of a particular pathogen to mount a response –

†Adapted from: **Tsai SJ**, Black SB, Jewell CM. "Leveraging the modularity of biomaterial carriers to tune immune responses."*Advanced Functional Materials.* **2020**.

and determining which fragments to focus on – represent other key challenges. Additionally, emerging pathogens such as Zika and SARS-CoV-2 – the cause of novel COVID-19 – highlight the challenges of quickly identifying targetable antigens – molecular fragments of pathogens – without raising safety concerns.[38–40] Because the immune system is a complex amplification system, changes in immune activity can lead to broad effects, which underscores the constant need for safety considerations as new technologies are developed for the clinic. These challenges are true not only in vaccines for infectious disease, but also cancer immunotherapies aimed at enabling selective immune responses to destroy tumors. Likewise, similar hurdles are faced in designing better immunotherapeutics to tackle aberrant immune recognition that may occur in autoimmune disease (i.e. multiple sclerosis, type 1 diabetes), transplantation, and allergies. Current treatments for these areas seek to control excess inflammation and dysfunctional immune attack, but often lead to side effects. For example, immunotherapies for autoimmune diseases – in which immune cells mistakenly identify self-molecules as foreign – often leave patients immunocompromised and are non-curative, requiring frequent and life-long treatment.[41] As such, new strategies that offer safer and more controlled modulation of the immune system are critical for new options across infectious disease vaccines and cancer immunotherapy, as well as for therapeutics that maintain immunological tolerance in autoimmune or inflammatory settings.

Many strategies are exploring biomaterials as carriers for immune signals for the generation, enhancement, inhibition, or other selective direction of immune responses.[42–45] A defining feature motivating this interest is the modularity that biomaterials offer. The immune system integrates and responds to multi-dimensional cues including physiological location, the combination and relative concentration of signals present, the types of immune cells involved, the

molecular conformation of the signals, as well as the kinetics at which these processes progress. These factors influence the generation, maintenance, and resolution of immune responses (**Figure 2.1**). Thus, the unique tunability of engineered materials enable the design of vaccines and immunotherapies that can specifically interact with the immune system to achieve these requirements.

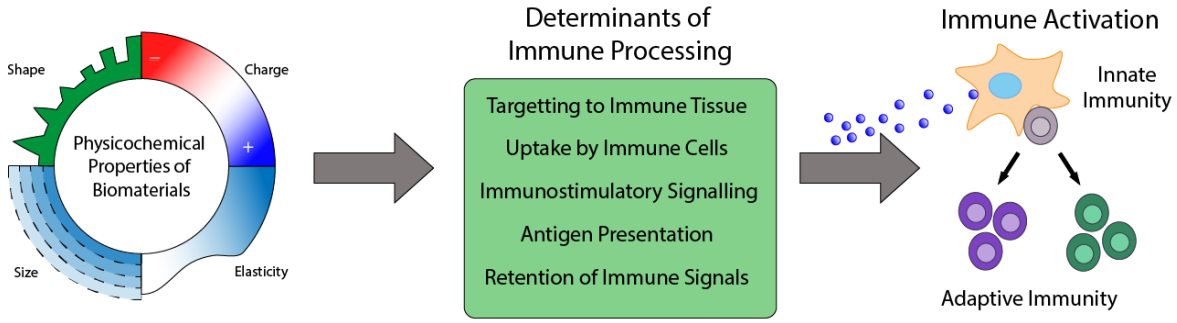

Figure 2.1 The physicochemical properties of biomaterials can be harnessed to improve vaccines and immunotherapies
Biomaterials exhibit tunable properties which can facilitate their trafficking throughout the host, as well as their interactions with immune cells. The physicochemical properties of biomaterials offer control over several key determinants of immune processing to facilitate activation of specific immune responses.

The immune engineering field has rapidly blossomed by drawing on the drug delivery space to explore carriers spanning organic and inorganic compounds; all of these offer facile opportunities to modify physiochemical properties. For the purposes of this chapter, we restrict our discussion to scaffolds and particles designed as biomaterial carriers for vaccination and immunotherapy. Within these areas, we explore organic biomaterial carriers comprised of natural and synthetic polymers, including peptides and nucleic acids, or even cells. Polymers such as chitosan, poly(lactic-glycolic acid) (PLGA), agarose, and hyaluronic acid (HA) are well-studied in this class and have been widely explored due to their biocompatibility and biodegradability. Additionally, many organic materials allow for customizable architectures or properties that mimic

natural aspects of natural tissue, or for tunable degradation rates. Our scope also includes inorganic material carriers (e.g. gold, silicon, carbon, aluminum), which while often non-biodegradable, have also been explored as important classes of biomaterials.[26] Inorganic material carriers – such as quantum dots and metal nanoparticles (NPs) – are also often easily-functionalized to alter physicochemical properties, providing stable templates and precision synthesis. Many also offer unique optical or electrical properties. While there are other large bodies of work involving biomaterials interacting with the immune system, such as tissue engineering and host response to implants, these are beyond the specific scope of this report, which focuses on biomaterial carriers with a primary focus of manipulating and delivering immune function.

Excitingly, the potential of biomaterials to improve immune outcomes is also already being explored in a number of clinical trials. For example, the potential for multivalent virus-like particles as improved vectors against HPV (NCT00943722[46]) and influenza (NCT04120194[47]) are being explored in Phase III clinical trials by Merck and Novavax, respectively. Combination vaccines delivered in liposomes are being assessed to prevent HIV infection (NCT03961438[48]), a disease that lacks an effective vaccine. A poly(lactic-glycolic) (PLG) scaffold vaccine against melanoma is being investigated in a phase I clinical trial (NCT01753089[49]), with parts of this technology now licensed by Novartis, suggesting interest in the pharmaceutical industry for the adoption of these approaches. Antigen loaded microparticles are being explored to shift the balance of immune cell types to combat celiac disease (NCT03738475[50]). Gold nanoparticles with surface coupled antigen are being explored in the treatment of Type I diabetes (NCT02837094[51]), which currently lacks a cure. While not exhaustive, these examples highlight the therapeutic potential that biomaterials enable in the vaccine and immunotherapy space.

Over the past decade, biomaterial systems for vaccines and immunotherapies have been intensely studied [19,52–54]. As alluded to above, distilling the driving tenants of this body of work, a unique feature is the ability to create tunable materials platforms that control how the immune system interacts with vaccine and immunotherapy components. For example, surface functionalization through absorbed proteins, intrinsic topographical materials features, and carrier geometries that mimic bacteria or promote certain cell-biomaterial interactions, are all routes explored along these lines. Likewise, carrier/scaffold size, shape, charge, hydrophobicity, and mechanical properties are now documented as playing important roles in determining immune cell function and differentiation.[27,53,55–57] While it is clear that the physicochemical properties of materials can impact immune responses, there remains a lack of comparative measures for the gestalt of emerging immune engineering platforms. Thus, another important need in the field is systematic studies and standardized approaches to benchmark trade-offs in design approaches and connect materials properties to modulating immune responses.[29,58]

In this progress report, we use studies from the most recent five years to highlight central ways in which the modularity of biomaterials can be leveraged to direct immune outcomes. In particular, we connect tuning of material properties – such as size, charge, shape, elasticity, topography, and stability – to manipulating immune processes at several scales, including tissue, cell, molecular, and time. For example, altering design parameters can be used to control biodistribution and improve targeting to LNs or other important immune tissues (**Figure 2.1A**). Once contacting antigen presenting cells (APCs), many of these same properties can be exploited to promote or limit uptake and activation of immune cells (**Figure 2.1B**). Ultimately, the ability to control the distribution in immune tissues and cells, along with control over the context in which

specific immune signals are received, plays a major role in programming APCs and subsequently the types of T and B cells responses that occur (**Figure 2.1C**). Additionally, carefully engineered designs can further improve the quality of generated immune responses by tuning the kinetics with which immune signals are encountered or displayed (**Figure 2.1D**). In the next section – **Section 2.3 –** we provide concise immunological background to introduce some of the key steps in immune response that biomaterial carriers are commonly designed to interact with. Moving to recent literature, we begin with **Section 2.4**, which focuses on improving targeting at the immune tissue scale by tuning size, charge, shape, and stiffness. **Section 2.5** probes a shorter length scale – trafficking within immune cells – by highlighting how altering material designs can impact uptake and localization of immune signals to specific intracellular compartments. Having considered targeting at the tissue and cell level, in **Section 2.6,** we narrow in on manipulating material design for delivery of specific immune signals classes, beginning with the delivery of adjuvants to prime early, non-specific functions of innate immune cells. Maintaining the theme of molecular encounter, in **Section 2.7** we focus on using biomaterials to control the context with which antigen is delivered to impact the slower, but highly specific functions of adaptive immune response. We conclude in **Section 2.8** by discussing how biomaterial properties are being engineered to control the kinetics and persistence of immune signals. Examples of the recent pre-clinical approaches that modulate these areas of immune signal delivery, which we discuss in this chapter, are summarized in **Table 1**.

Table 2.1 Key Examples of Control Over Immune Processing by Tuning Material Properties

Immunological Process to be Controlled	Biomaterial Parameter	Technique/Approach	Biological Outcome	Ref

Targeting to lymphoid organs	Size	Altering organic:water volumetric ratio during flash nanoprecipatiation	20nm NPs rapidly drain to LNs, but 100nm NPs show minimal accumulation	[59]
	Shape	Different NP seeding protocols from aqueous solution	Sphere and star-like particles accumulate in spleen	[60]
	Charge	Addition of cationic or anionic amino acids to the end of displayed antigen peptide sequence	Zwitterionic micelles promotes a combination of LN accumulation and cellular interactions	[61]
	Surface functionalization	PEGylation	Increased active transport of antigen to LNs, decreased ECM interactions with increasing MW of PEG	[62,63]
		Conjugating antigen to targetting moieties	Cell-mediated trafficking of antigen to LNs, enhanced LN accumulation	[64–66]
	Elasticity	Electrostatic layer-by-layer assembly, followed by removal of template core to form hollow capsules	Hollow particles can pass through pores up to 4x smaller in size to faciliate LN trafficking	[67]
Targeting APCs	Elasticity	Pickering emulsions	Highly deformable NPs due to raspeberry-like structure of pickering emulsions improves particle interactions with DCs	[68]
		Varying polymer content (i.e. PLGA:PEG ratio)	Stiffer nanodiscs improve uptake by macrophages by increasing material-cell interaction times	[69]
	Charge	Anionic modification of self-assembling polymer	Intermediate levels of negative charge	[70]

		chains with different chain lengths of carboxyl group substitution	displays highest level of uptake; highly negatively charged particles are taken less eficiently by cells.	
		Formation of amine containing hydrogels using Particle Replication In Non-wetting Templates (PRINT), followed by protonation/deprotonation of amine groups	In lung, cationic NPs are preferentially taken up by DCs, while anionic NPs are preferentially taken up by macrophages	[71]
	Surface functionalization	Conjugating bacterial sugars or mimics to polymer NP surface	Increased intracellular accumulation targetting endoplasmic reticulum	[72]
	Hydrophobicity	Preparation of dendritic mesoporous organosilica and pure silica NPs	Hydrophobic particles facilitate lysosomal escape for delivery into the cytosol	[73]
	Charge	Altering number of basic amino acid arms on dendrimer	Positively charge NPs can rupture lysosomes to enter cytosol and improve inflammazome activation	[74]
		Functionalization with quarternary ammonium groups to polymer backbone	Positively charged hydrophobic microgels improve membrane disrupting potential to promote cytosolic delivery	[75]
	Controlled Release	Materials selection: polymers with different degradation profiles	Faster release under acidic conditions enhances antigen presentation	[76]
Delivery of Immunostimulatory Cues	Shape	Computationally designed nucleic acid sequences that self-assemble into 2D and 3D structures	Inflammatory cytokine secretion can be tuned based on dimensions (i.e. 2D vs. 3D), and the	[77,78]

			number of sides on polygonal structures	
		Conjugating poorly immunogenic RNA adjuvant to gold NP	Nanorods improve adjuvanticity	[79]
	Controlled Release	Materials selection: polymers degradable by hydrolysis or degraded under acidic conditions	Products of polymer degradation can modulate immune activity	[80–82]
		Alter binding affinity of polymer to TLRa by using softer chained polymers or varying polymer:TLRA ratio	Reduction in adjuvanticity of TLRa with increased interaction strength of polymer carrier	[83,84]
	Surface functionalization (ligand density)	Covalent linking of TLRa at different densities to polymer backbone allowing for chemically defined controlled loading	Higher density induces particle formation and improved activation of DCs and macrophages	[85]
	Topography	Hydrothermal assembly of titanium oxide nanostructural bundles to form nanospikes	Mechanical stress induced by nanospikes activates inflammasome pathway	[86]
Antigen Presentation	Size	Covalent linkage of TLRa to polymers with different chain architectures with distinct hydrodynamic characteristics	Induction of $CD8^+$ T cell responses increases with increasing polymer hydrodynamic radius	[87]
		NPs of different sizes coated with pMHC and anti-CD28 to form aAPCs	Smaller aAPCs require saturated doses of pMHC or artificial magnetic clustering to activate T cells at similar levels compared to larger particles.	[17]
	Controlled Release	Conjugation of antigen to adjuvant using a pH sensitive reversible linker	Release of unmodified antigen improves expansion of T cells	[88]

	Antigen localization	Surface conjugation of antigen and encapsulation of antigen onto polymers	Encapsulated antigens preferentially promote antigen presentation on MHC-I to enhance $CD4^+$ resposnes. Surface conjugated antigens promote antigen presentation on MHC-II, enhancing $CD8^+$ responses	[89–91]
	Surface functionalization	Biotinylated liposomes coated onto mesoprous silica microrods, followed by attachment of anti-CD8 and anti-CD3 antibodies	Fluidity of lipid bilayers allows for robust expnasion of T cells even with lower density of stimulatory cues	[16]
		Site specific binding of antigen to alum via multivalent phosphorylated serine groups that bind hydroxyl groups on alum.	Stable binding of antigen to alum offers conformational control over antigen presentation, allowing for tuning of B cell specificity towards specific antigen epitopes	[92]
	Ligand density	Iron oxide NPs conjugated with pMHC	pMHC must exceed a threshold density for T cell activation to occur	[93]
		Antigen adsorbed to quantum dots	Controlling antigen display to APCs alters T cell responses	[94]
Immune Signal Retention	Controlled Release	Altering linker chemistry (e.g. thioether vs. dssulfide linker) between antigen and polymer	Slower release of antigen prolongs antigen release and antigen presentation over time leading to improved immune response	[95]

	Altering MW and varying degree of cyclic acetal groups on acetylated-dextra MPs	Faster degrading MPs promote strong humoral and cellular responses at earlier timepoints. Slow-degrading MPs drive stronger responses at later timepoints	[96]
Size	Antigen conjugated to different sized NPs using carbodiimide-mediate coupling to control antigen dose	Larger particles prolong antigen presentation by APCs, resulting in improved antibody production	[97]
	Different gold NP seeding protocols	Retention of 50-100nm NPs on dendrites of FDCs in LNs	[98]
Surface Functionalization	Peptide conjugated to nucleic acid adjuvant and adsorbed to liposome via hydrophobic anchoring group (cholesterol)	Co-delivery of antigen and adjuvant allows for synchronized peptide presentation and expression of costimulatory markers, improving generation of memory T cells	[99]

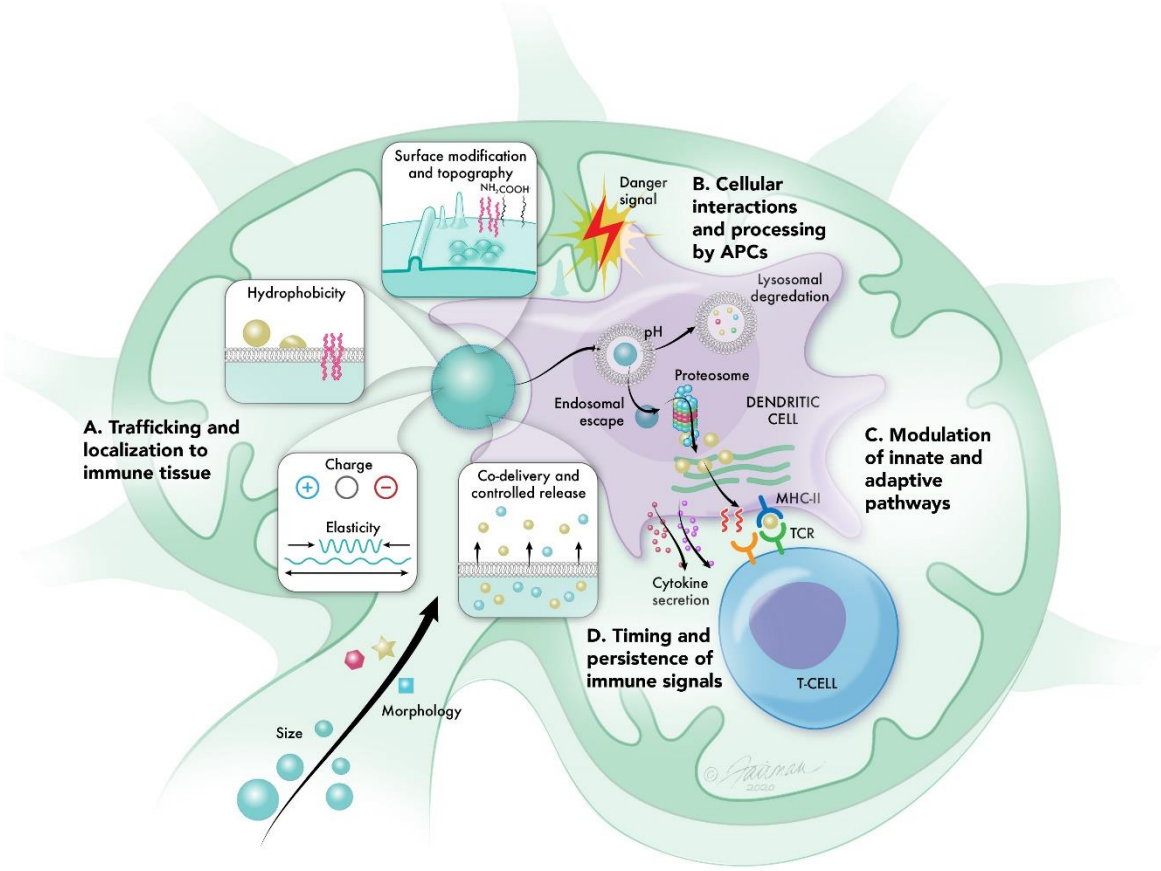

Figure 2.2 The physicochemical properties of biomaterials can be tuned to program immune responses

Properties such as size and morphology can **A)** promote trafficking of materials to immune tissues such as LNs (**Section 3**). These same properties in addition to surface modifications, hydrophobicity, charge, elasticity, and controlled release can **B)** impact the interactions of biomaterial carriers with APCs, altering their uptake and processing by immune cells (**Section 2.4**). Because APCs are key initiators of adaptive immune responses, molecular control over the delivery of immunostimulatory cues (**Section 2.5)** and antigen (**Section 2.6**) by biomaterial carriers can **C)** modulate innate and downstream adaptive immune pathways to generate potent specific immune responses. The modularity of biomaterials further allows for tuning over **D)** the lengthscales in which immune signals persist to control the quality and maintenance of responses (**Section 2.7**). Credit: printed with permission from © Fairman Studios, LLC

2.3 Immune responses arise from complex interactions between immune cell populations across distinct tissues and time scales

Immune responses are categorized into two major classes, innate and adaptive. Innate responses provide rapid defense against infection by non-specifically removing pathogens, infected cells, and damaged tissue. In contrast, adaptive immune responses develop more slowly, but are highly specific responses that are initiated within lymphoid organs such as the spleen and lymph nodes (LNs). In these tissues, resident B and T cells can differentiate into long-lived memory cells that provide rapid protection upon re-exposure to a pathogen. This section describes the key features of these two systems and how they interact.

2.3.1 The innate immune system is a rapid first line of defense, but lacks specificity

Innate immunity offers a quick-acting but less-specific defense mechanism comprised of both molecular and cellular components able to recognize general patterns common in frequently encountered pathogens. Biomaterial carriers can trigger innate immunity through surface engineering of molecules found on the cell walls of bacteria or through fabrication of particles with similar size scales and topographical features to pathogens. When encountered, cells express surface proteins and secrete cytokines – the protein signals of the immune system that play key roles in the activation and polarization of most immune cells. Additionally, a variety of innate immune cells survey the body for pathogens such as natural killer (NK) cells and APCs. APCs are specialized innate immune cells that are important in the detection and processing of pathogens and include macrophages and dendritic cells (DCs). Because they efficiently phagocytose or internalize fragments of pathogens – termed antigens, these cells can quickly generate non-specific

inflammatory responses against pathogens. Equally important, APCs bridge the innate and adaptive immune system, providing signaling cues to initiate more specific responses.

Recognition and activation of APCs is dependent on surface receptor interactions and soluble signals (i.e. cytokines) that can be used to sense pathogens. APCs can recognize molecular motifs commonly found on pathogens but absent in healthy host cells, termed pathogen associated molecular patterns (PAMPs). PAMP recognition results in upregulation of co-stimulatory signals that help initiate immune response. Pattern recognition receptors (PRRs) on APCs can sense PAMPS and help identify a diverse range of these "warning signals", making them a key target of interest in engineering immune responses. One major class of PRRs are Toll-like receptors (TLRs), a family of membrane bound receptors that recognize ligands on pathogens, leading to activation of inflammatory responses. Signaling may occur on the APC outer membrane surface through receptors evolved to detect extracellular pathogens. In contrast, many of the TLRs exist within specific intra-cellular domains such as endosomes to detect pathogens taken up by endocytosis or intracellular components exposed after pathogen degradation, such as viral RNA. Other PRRs, such as the inflammasome, can detect PAMPs within the cytosol. The inflammasome is a complex of proteins which ultimately triggers secretion of IL-1β, a key cytokine involved in initiating inflammatory processes. Of particular relevance, biomaterial carriers can promote internalization of immune signals to facilitate activation of these pathways.

Concurrent with PRR activation, internalization of antigens triggers processing and loading onto major histocompatibility complex (MHC) by APCs. Antigens are loaded onto either MHC-I or MHC-II, depending on the intracellular processing mechanisms that the antigen undergoes. Endocytosed materials are degraded in endosomal/lysosomal compartments and presented in

MHC-II. On the other hand, MHC-I predominantly presents antigens localized within the cytosol. Importantly, endocytosed materials can also enter the cytosol and be presented via MHC-I through various mechanisms reviewed by others[100–103] such as lysosomal escape, through a process called "cross-presentation." Biomaterial carriers offer features for improved delivery of immune cargo (i.e. co-delivery of signals, efficient internalization, tunable kinetics, cargo protection), which can better direct these outcomes. This is important because together, internalization of antigen and engagement of PRRs results in DC maturation and migration to spleen or LNs where these APCs can prime T cells. As such, APC activation and antigen presentation are not only important for the elimination of pathogens, but also provide signaling cues that can greatly influence the adaptive immune responses. The interactions of APCs with T and B cells within lymphoid organs are highly dependent on the appropriate signals being presented by APCs. Additionally, T cells recognize the antigen they are specific for – the "cognate" antigen, only when loaded within an MHC complex displayed by a DC or other APCs. As highlighted in several comprehensive reviews, these cells are thus frequent targets for vaccines and immunotherapies.[104–106] Current vaccination strategies employ adjuvants, molecules that mimic immune warning signals to trigger activation through co-stimulation and other mechanisms. Importantly, the immune pathways activated by pathogens and other foreign molecules can also sometimes be triggered by biomaterials. The particulate nature of many biomaterial carriers (e.g., NPs) also facilitates uptake by APCs. These features, along with the prominent role of APCs in initiating adaptive immunity, have made APC populations a major target for materials-based strategies.

2.3.2 Adaptive immune responses develop more slowly but are high specialized and highly specific

Generation of specific, long-lasting immunity involves the activation of adaptive lymphocytes that respond to a particular antigen in LNs and spleens. Thus, one way in which nanocarriers and microcarriers facilitate adaptive immune responses is through targeting immune signals to these sites. Adaptive immunity is a highly selective response that is initiated by interactions between APCs and lymphocytes, such as T and B cells. While T and B cells are responsible for carrying out processes to combat and remove pathogens, APCs are responsible for activating these cells. As discussed above, APCs take up, process, and display antigen peptide fragments to molecularly-specific receptors on lymphocytes by loading antigens into MHC. These complexes can then be presented in combination with costimulatory molecules to, for example, T cell receptors (TCRs) on the T cells, leading to activation of T cells specific to the presented antigen. The activated T cells then leave LNs or spleen and return to sites of infection or disease to selectively combat the pathogen the cell is now armed against. A small number of activated cells can become long-lasting memory cells that persist in the body to quickly mount protective immune responses if the pathogens these cells are armed against are re-encountered in the years or decades to come.

Antigen presentation, costimulatory molecules, and cytokines are all cues that initiate and maintain immune response against pathogens, tumors, or other targets. The intricate balance between these signals is also important in maintaining immunological tolerance that prevents host tissue from being attacked. For example, T cell activation results when these costimulatory signals occur in tandem with presentation of an antigen that the T cell engaging the APC is specific for. Conversely, the absence of costimulatory signals during antigen presentation can give rise to

different outcomes, such as the generation of regulatory T cells (T_{REGs}) that can help regulate immune response and combat autoimmunity, conditions in which immune cells mistaken recognize self-antigen as foreign. Synthetic microparticles (MPs) present another opportunity for biomaterials to engage with immune responses, through the engineering of APC mimics that can directly interacting with T cells to regulate their differentiation and function.

Depending on the signals that T cells receive, a number of different T cell subsets can arise. For example, recognition of peptide antigens in MHC are restricted to particular T cell types such that $CD8^+$ T cells recognize cognate antigen displayed in MHC I and $CD4^+$ T cells recognize antigen displayed in MHC II. $CD8^+$ T cells, become cytotoxic T lymphocytes (CTLs) upon activation. These cells directly target and destroy diseased host cells – such as those infected with intracellular pathogens (e.g., viruses) – to prevent spread of infection; these cells are also sometimes able to destroy cancerous cells. Activated $CD4^+$ T cells, on the other hand, become T helper (T_H) cells. T_H cells exhibit specific phenotypes, such as T_{H1} and T_{H2} function, that provide support to other immune cells through secretion of signaling molecules called cytokines.

B cells are also important components of adaptive immunity. These cells share some of the same features of T cell activation, including the ability to generate memory cells. B cells become activated following recognition of a cognate antigen. Importantly, B cell activation requires cross-linking of the B cell receptors displayed on the surface of these cells by the antigen. However, maturation and long-live antibody-production requires additional activation from T_H cells. Development of B cell memory and long-live antibody-production requires that B and T cells organize into specialized domains that form in lymph nodes called germinal centers (GCs); the resulting activated B cells produce more potent strongly-binding antibodies.[107,108] This brief

description demonstrates an important point, that generation of strong antibody responses requires activation of both B and T cell subsets. This is one more example of the inter-connected nature of the immune system, motivating the need to understand how biomaterial properties can be tuned to control the cues governing adaptive immunity. Along these lines, in the following section we focus on how materials can be engineered to improve targeting to immune tissue.

2.4 Biomaterial properties can be engineered to target or enrich immune signals in lymphoid tissues.

As discussed in **Section 2.3**, lymphoid organs such as the spleen and LNs are the sites where APCs present antigen and co-stimulatory signals to drive differentiation and proliferation of the T and B cells residing in these sites.[109] For this reason, LNs and spleen are the tissue target of many vaccines and other immune signal delivery applications.[19,53,110] Reaching these sites is important in quickly generating strong and selective immune responses, using doses that minimize toxicity or off-target effects. Efficient delivery of materials to LNs is also important to minimize toxicity of the carriers themselves, as the biocompatibility of candidate biomaterial carriers can be highly dependent on microenvironment, further underscoring the importance of directed targeting to lymphoid organs.[111] A number of approaches now exist that enable vaccines and immunotherapies – typically administered peripherally in muscle or under the skin – to accumulate at high levels in LNs.[112,113] We begin by discussing targeting and accumulation of biomaterial carriers to lymphoid organs by tuning biomaterials, focusing on design parameters that promote passive targeting, strategies to overcome barriers that impede entry, and active targeting approaches.

2.4.1 Design parameters can be tailored to promote passive targeting to spleen and LNs

While conventional non-biomaterial vaccines rely on free drainage to LNs or trafficking by APCs that encounter the vaccine, biomaterials offer additional properties to leverage in directing the trafficking and targeting of vaccines and immunotherapies after injection. For example, the ability to control size has been pivotal in improving LN drainage following injection. Howard et. al investigated the "size gate" for effective LN drainage by synthesizing PLGA-b-PEG NPs with average diameters of 20,40 and 100-nm. Following subcutaneous (s.c.) administration in mice, 20-nm NPs were found to drain rapidly across proximal and distal LNs and displayed improved retention compared to NPs with an average diameter of 40-nm. The drainage of 100-nm NPs was negligible.[59] These results support seminal studies that polypropylene sulfide NPs larger than 100 nm do not passively diffuse to LNs, relying instead on uptake and trafficking by APCs at the site of injection.[114] Another opportunity that biomaterials offer is the ability to control size to assist in the delivery of small molecules. As one example, mellitin is a small molecule adjuvant that preferentially enters the blood. Encapsulation of the mellitin, a small molecule adjuvant, into nanolipids 10-20 nm in size has been shown to promote LN accumulation of melittin, but not other organs.[115]

Manipulation of multiple parameters offers an additional layer of control. The size and shape of gold NPs (AuNP) has been leveraged to impact the biodistribution and trafficking to spleen.[60] In particular, this study revealed AuNPs of 50 nm diameter accumulated more in the spleen than AuNPs of 10 nm. When using AuNPs of similar size but with different shapes – spheres, star-like, and rod shaped – only spheres and star-like particles accumulated in the spleen. In contrast, rod-shaped particles displayed a poor ability to penetrate organs and were rapidly

cleared. In another example, the icosahedral-shaped cowpea mosaic virus has been found to display superior transport and retention to LNs compared to the filamentous-shaped potato virus (**Figure 2.3A**).[116]

In addition to size and shape, charge is another property that can be leveraged to promote LN targeting. For example, the charge on peptide amphiphile micelles (PAMs) can be readily modified through the addition of positively charge lysine or negatively charge glutamic acid residues, while maintaining similar shape and size, ranging 60-70nm (**Figure 2.3B**).[61] Entry of these PAMs and their subsequent interactions with APCs in the LNs has been shown to be maximized when the PAM surface was zwitterionic. Anionic surfaces allowed accumulation in LNs but failed to interact with APCs, eliminating immune activation. Cationic surfaces on the other hand, had significantly lower accumulation in the LN than both zwitterionic and anionic, but were able to interact with APCs in circulation and peripheral tissues; this binding however was relatively non-specific, as the cationic PAMs also bound non-phagocytic cells. Only zwitterionic PAMs provided the appropriate combination of LN accumulation and LN interactions. Collectively, these results demonstrate another biomaterial property lever – charge – to promote or diminish access and interaction with immune cells and tissues.

Thus, a range of biomaterials properties – size, shape, and charge– each have significant roles in enhancing trafficking to LNs and spleen. This is important as lymphoid organs control many aspects of immune function; this targeting also provides dose-sparing which can minimize systemic toxicity. Although the trends examined here may not apply across all platforms or biomaterials, they highlight different opportunities to improve targeting to lymphoid organs by altering biomaterial design parameters. It is important to note, however, that the examples

presented here reflect only carriers within size ranges below 100 nm, which, as discussed, favor efficient LN drainage. While size remains a critical component to effective LN drainage, a number of biomaterial-based approaches vary by orders of magnitude between 100-1000 nm, yet still display efficient LN targeting. Similarly, some positively charged NPs have been observed to accumulate within LNs. Critically, biomaterials modulate immune function through an interplay of multiple design parameters, which enables additional modalities to overcome barriers to LN trafficking; this topic is the focus of the next subsection.

2.4.2. Rational design enables biomaterials carriers to overcome barriers to entry into LNs

Although the examples in the previous section highlight how the tunability of biomaterial carriers allows for their accumulation in lymphoid organs, there are many physiological barriers that limit efficient delivery of vaccines and immunotherapies from peripheral injections sites to LNs. While entry into the lymphatics offers a direct route to LNs, biomaterial-based vaccines and immunotherapies that enter systemic circulation – passively from the injection site or through direct intravenous (i.v.) injection – require design strategies to promote prolonged circulation. As previously mentioned, most traditional vaccines are administered into muscle or under the skin. At the site of injection, administered agents must navigate a collection of extravascular fluid, solute, extracellular matrix (ECM), and cellular environment. The pore size and highly negatively charged moieties within the ECM present another obstacle for larger positively charged carriers. Thus, biomaterials must also be tuned to overcome these hurdles.

Work by the Collier lab has shown that for sublingual delivery of vaccines, in which the network of mucin presents similar obstacles to those found in ECM, nanofiber interactions with

mucin were found to decrease as a function of increasing MW of PEG.[62] Increasing MW of PEG elicited larger antibody responses, suggesting a role for improving immune responses by making biomaterial carriers more inert against extracellular environments. Utilizing a similar principle, De Koker et al. has approached this design need by PEGylating 200 nm PMA hydrogel particles (**Figure 2.3C**).[63] These studies revealed that the addition of PEG increased lymphatic draining and the active transport of antigen to the LN. This observation was attributed to the blocking of redox-sensitive groups on the PMA particles upon addition of PEG, which may have increased mobility through the ECM and the circulation half-life. The association of the particles to immune cells also increased with PEGylation. A similar outcome has been observed by conjugating peptide antigens to 5(DSPE-PEG) to enhance lymphatic drainage.[117] After conjugation these peptides traveled to nearby and distant LNs. These findings build on established drug delivery approaches based on PEGylation of liposomes or small molecular drugs to increase circulation.[118]

In an alternative approach to PEGylation, Hasani-Sadrabadi et al. described polymeric gel alginate particles with elastic moduli that mimic naive and activated helper T cells ($CD4^+$).[119] Naïve and activated T cells are able to pass though capillaries of much smaller size than their diameters, thus, the investigators created a microfluidic chip model using capillary channels with diameters of 5 μm to study the traversal of 12 μm diameter particles. Only softer particles (e.g., modulus of 3. 3 kPa) were able to pass through the pores, then regain their shape (**Figure 2.3D**). Even when chemotaxis – movement of cells towards a chemical attractant – was simulated using magnetic fields, stiffer particles (e.g., modulus of 11.1 kPa) were unable to traverse the microfluidic channels. This result highlights the importance of deformability for larger particles to navigate smaller pore sizes. In addition to simulating $CD4^+$ T cell movement across barriers, the

particles could also be readily loaded for immune signaling molecules, interleukin-2 (IL-2) and interferon γ (IFN-γ), demonstrating the potential of softer particles to improve delivery of immune signals.

Supporting the importance of deformability to facilitate entry into LNs, the Moon lab has developed nanocapsules 220nm in size with a hollow core and shell composed of microbial polysaccharides to mimic the structural and immunological properties of bacterial cell walls.[67] The nanocapsules were developed using a layer-by-layer assembly technique onto a rigid silica NP core template, followed by removal of the silica template. Hollow nanocapsules administered s.c. were found to efficiently drained to inguinal LNs compared to NPs which maintained the rigid silica core. These differences were attributed to the hollow design which allowed for high deformability while NPs with the rigid cores maintained their structure. Additional studies revealed that hollow particles easily passed through 100nm pores and 30% of the hollow particles were still recovered when hollow particles were flowed through a 50nm pore membrane. On the other hand, NPs that maintained the rigid silica core failed to pass through even a 200nm sized pore membrane, supporting design of elastic materials to enable improved delivery of NPs larger than 100nm.

While the above examples highlight ways in which biomaterials have been designed to improve passive drainage to LNs, active targeting approaches are also being developed for efficient delivery to these immune tissues. One common target is albumin, a protein that regularly filters through LN. In these approaches, the natural shuttling ability of albumin to LNs is exploited by conjugating peptide antigens or vaccine adjuvants to albumin-binding structures to enhance

LN trafficking.[64,120] Alternatively, biomaterials can target mannose receptors on DCs to promote

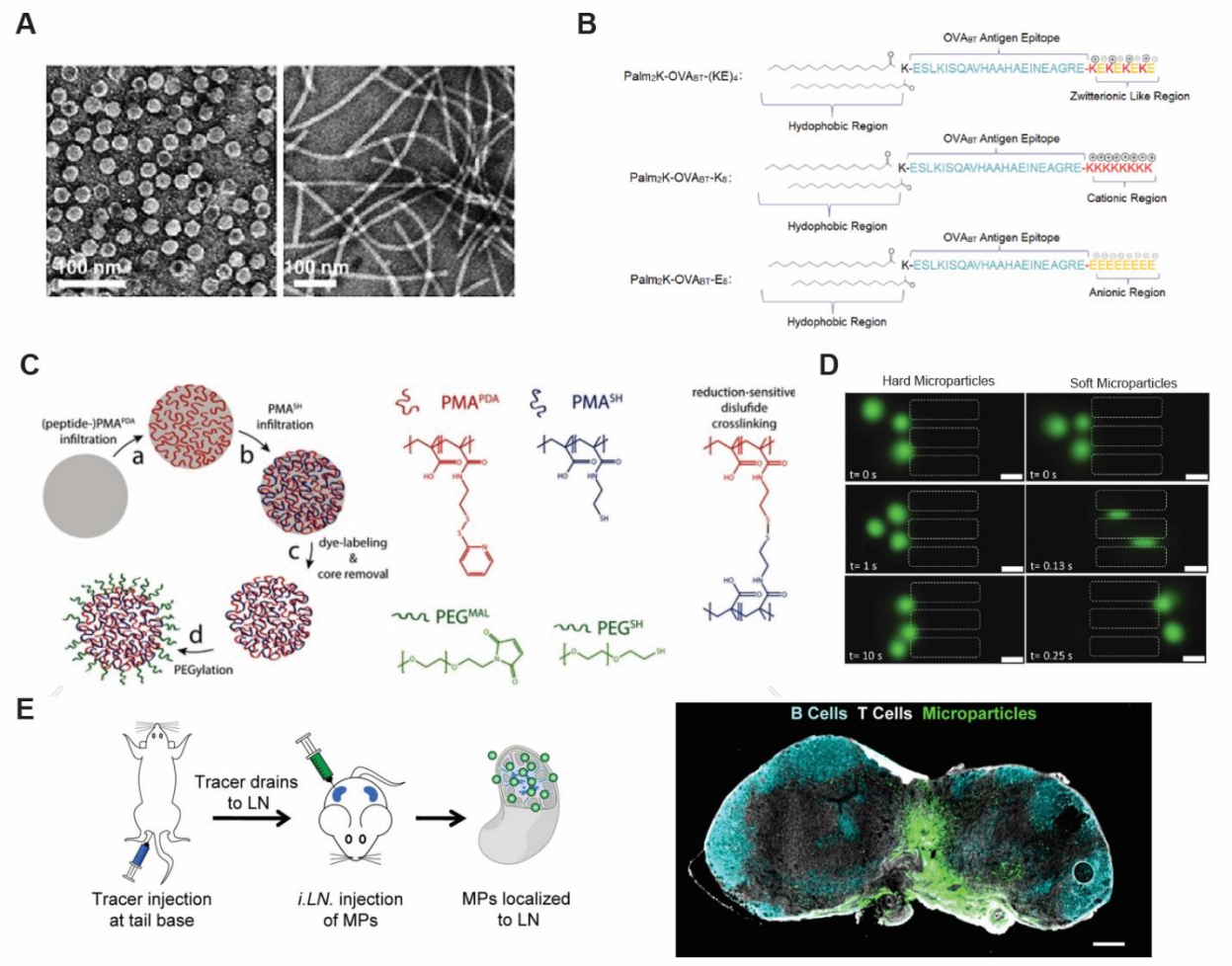

Figure 2.3 Engineering biomaterial properties to target LNs

A) Morphology of viral nanoparticles improves transport and retention within LNs. Reproduced with permission.[116] Copyright 2017 , Elsevier. B) Engineering of PAM charge influences lymph node accumulation and cell association, with cationic PAMS exhibiting less accumulation in LN than zwitterionic or anionic PAMs. Macrophages incubated with anionic PAMs display reduced uptake compared with other tested formulations. Highly charged PAMS induce lower antibody responses, compared to zwitterionic particles. Reproduced with permission.[61] Copyright 2018, American Chemical Society. C) PEGylation of PMA particles improves particle stability, blocking unfavorable interactions of PMA side chains with the ECM that would otherwise hinder particle mobility and transport through the lymphatics. Reproduced with permission.[63] Copyright 2015, Wiley-VCH. D) Deformability supports the passage of soft MPs through confined microchannels, whereas hard MPs exhibit poor migration (scale bar= 30um). Reproduced with permission.[119] Copyright Wiley-VCH 2018. E) Direct LN injection to locally deposits vaccine depots into LNs. A tracer dye is injected subcutaneously at the tail base which then drains to inguinal LNs allowing for visualization of LNs through the skin. MP depots can then be injected into the skin. MPs are

retained within LN 28 days following injection of LN with fluorescent depots (scale bar= 200um). Reproduced according to the terms of the Creative Commons Attribution 4.0 International License.[1] Copyright 2016, Springer US.

LN accumulation through cell-mediated trafficking.[65] While the above strategies describe targeting of LNs through the lymphatics, systemic circulation offers an alternative transport route to LNs. In one study, NPs were conjugated to an antibody that efficiently targeted high endothelial venules – the vasculature structure through which lymphocytes enter LNs from circulation – to enhance LN accumulation.[66] This is important as systemic administration has been shown to be the superior route of administration for some vaccines.[121,122] We have developed an alternate idea based on direct delivery of biomaterials depots directly to LNs (**Figure 2.3E**). These particles are synthesized to be too large to freely drain from the sites and are thus mechanically restricted. Instead, the depots slowly degrade, releasing stimulatory or regulatory cues to reprogram the local LN microenvironment. For example, this strategy can be used to deliver antigens or immunostimulatory adjuvants,[1,123,124] as well as signals to promote immune tolerance and combat autoimmune disease.[125] This core concept is utilized to study tolerance in **Chapter 5**.

2.5 Biomaterial properties can impact single cell interactions, uptake and processing

While in **Section 2.4** we discussed how biomaterial properties are being manipulated to target delivery to immune tissues across the body, we now turn to a much shorter length scale, focusing on how the properties of biomaterials can influence their interactions with and within immune cells. We discuss how biomaterial carriers can be engineered to influence binding, internalization, and immune signal processing by APCs within these cells. In the context of immune engineering, the studies highlighted in this section suggest that strategies to enhance the

immunogenicity of biomaterial-enabled vaccines and immunotherapies can be achieved through more direct targeting to LNs.

2.5.1 Biomaterial stiffness and charge alters interactions with immune cells to promote uptake

In **Section 2.4** we discussed how physicochemical properties are important for tissue-level biodistribution, but some of these same parameters impact how biomaterials interact and are processed by immune cells. Internalization of materials requires direct and effective immune cell-material interactions. Recent studies have generated increasing evidence that physical properties – including size, shape, charge and stiffness – play significant roles in the internalization of particles by APCs, by favorably associating with cell membranes allowing for improved uptake. However, it remains difficult to define how each parameter affects particle fate and function, and some inconsistencies exist across the literature findings. For example, in studies using micron-sized polymer particles, the effect of stiffness on uptake has been found to be shape-dependent, such that only softer variants of rods display increased uptake, while spheres displayed no enhancement in uptake as stiffness was varied.[126] However, in these studies, the effects of shape and stiffness were eclipsed by the effect of size, whereby larger particles (6μm) resulted in poor uptake. These larger sized particles may exhibit limited uptake due to the higher membrane deformation energy required for cells to engulf these particles, highlighting the importance of particle-cell interactions in the uptake of biomaterials.

Recognizing that internalization of particles requires increased contact areas and multivalent interactions with APCs, the Ma lab designed PLGA NP-stabilized Pickering emulsions (PPAS) (**Figure 2.4A**).[68] In this design, NPs form a fluid raspberry-like structure to stabilize a

hydrophobic core, resulting in particles that can readily deform under mechanical stress. PPAS exhibited significantly improved uptake compared to traditional PLGA NPs stabilized with surfactant. Confocal microscopy revealed that deformability of particles during uptake improved the ability of DCs to wrap around NPs and allowed for increased contact area with the DC, and thus more multivalent interactions; together, these features facilitated phagocytosis. In contrast, PLGA NPs with smoother surfaces appeared to hinder the ability for cells to interact with NPs, resulting in sterically blocked DC interactions. Thus, in addition to improving LN accumulation, softer particles can also improve immune cell interactions.

Contrary to these findings, soft silica nanocapsules have been reported to have 3 times less uptake than their stiffer counterparts.[127] In this study, functionalization with folic acid to improve uptake by macrophages was shown to only affect stiffer particles. In a similar vein, Palomba et. al developed polymeric nanodiscs of defined shapes and size.[69] The stiffness of each particle was readily tunable over several orders of magnitude by varying the relative ratio of PLGA and PEG. Regardless of shape and size, softer nanoconstructs were taken up less efficiently compared to rigid constructs, although it was noted that soft elliptical particles were also readily internalized. Live cell microscopy indicated that soft nanodiscs experienced short-lived interactions, diminishing their likelihood of recognition and internalization by macrophages (**Figure 2.4B**). Further analysis identified the bending stiffness of nanodiscs as a discriminating factor for uptake: nanodiscs with bending stiffnesses much higher or lower than cells facilitated internalization, while a bending stiffness similar to cells opposed internalization. Although the data set is not yet complete, these studies highlight that stiffness is a key parameter for modulating interactions with the immune system to improve cellular uptake. Importantly, the role of stiffness in facilitating

uptake may be dependent on the type of APC. While softer particles were found to improve uptake in DCs, as highlight by the Ma lab, the above studies suggest that stiffer particles facilitate uptake by macrophages. These differences suggest that stiffness can also be leveraged to target specific APCs.

Charge is another parameter that can be tuned to improve uptake. In several studies, positively charged particles have been found promote interactions with cells through electrostatic interactions with the cell membrane, which is often negatively charged [128,129] This interaction can translate to improved uptake that affects processing of biomaterials and immune cargo by the APC. On the other hand, negatively charged materials or assemblies have been found to hinder uptake by APCs, impeding signal processing and the ultimate downstream T cell and antibody responses. These findings, however, are not universally true. In one study, negatively charged polysaccharide nanogels modified with varying levels of carboxyl groups showed preferential uptake by APCs in LNs over unmodified nanogels.[70] Importantly, however, the level of uptake was greatest in nanogels that displayed intermediate levels of charge; highly negatively charged particles were less efficiently taken up by cells. One possibility is that highly negatively charged particles offered improved trafficking to LNs (as discussed in **Section 2.4**) however were taken up less efficiently by APCs, once within LNs. Nanogels that displayed intermediate levels of negative charges, on the other hand, could still be taken up efficiently, while offering improved LN targeting. These findings illustrate a critical design dilemma that can arise in designing vehicles that can efficiently be internalized by APCs: material properties that promote lymph node accumulation can hinder internalization by APCs. As such, in the development of carriers that can efficiently deliver immune signals to cells and tissue, systematic studies of material design parameters are important

to balance opposing design needs. This task that is readily accomplished through the tunability of materials.

In addition to improving material-cell interactions to promote uptake, biomaterials can also be targeted to specific populations of APCs. For example, while the underlying mechanisms are unknown, ferritin NPs demonstrate intrinsic preferential capture by specific APC subsets both *in vivo* and *in vitro*.[130] Studies in pulmonary antigen delivery to the lungs suggest that particle charge can also differentially affect uptake by specific cell types.[71] In one report, cationic NPs were found to be preferentially taken up by DCs, the targeted APC in this study. Conversely, anionic NPs were preferentially taken up by alveolar macrophages, whose primary function is in maintenance and clearance of air spaces from foreign particulates. Thus, uptake by specific APCs can be manipulated by surface charge, presenting another important variable through which biomaterials can regulate immunogenicity.

Functionalization of biomaterial carriers to alter the surface chemistry of particles is another important strategy, offering two layers of control over cell interaction and uptake: i) an additional method to influence interactions with immune cells and ii) the mode of uptake. As one example, polyanhydride NPs were modified with a glycolic acid linker conjugated to di-mannose, a sugar found on bacteria, or with glycolic acid linker alone (**Figure 2.4C**).[72] Both linkers exhibited 8-fold higher uptake by DC *in vitro* compared to unfunctionalized polyanhydride, which was attributed in part to the positive charge of the NPs after modifications. Interestingly, d-mannose-functionalized NPs caused increased intracellular accumulation compared to NPs functionalized with glycolic acid linker alone. Both linker types also resulted in markedly different levels of cytokine secretion and activation marker expression, suggesting that uptake may occur through

different pathways depending on surface modification. Additionally, in contrast with non-functionalized particles, a fraction of the linker-functionalized NPs was found to co-localize to the endoplasmic reticulum, further supporting different mechanisms of uptake between NPs. These findings highlight that surface functionalization may play a role not just in mediating the initial material-cell association and the level of uptake, but also in the mechanisms by which biomaterials are internalized. This is important because the mechanism of uptake affects intracellular processing and control antigen presentation by APCs, as discussed in the follow section.

2.5.2 Hydrophobicity and charge can regulate intracellular processing pathways

In addition to efficient uptake, the ability to control compartmentalization of biomaterials within particular intracellular locations is critical for proper antigen processing, detection of danger signals, and initiation of specific immune responses. A key concern for the delivery of antigens and adjuvants is the array of cellular compartments that can be targeted. For example, immune recognition of PAMPs – described in **Section 2.3 -** can occur in either intracellular structures (e.g., endosomes) or within the cytosol. Nucleic acid based PAMPs such as viral RNA or bacterial DNA are recognized within endosomal membranes, while intracellular danger sensors such as the inflammasome reside in the cytosol. As such, activation of certain pathways requires that immune signals are able to escape endosomal membranes following uptake to deliver immune signals to the cytosol. Furthermore, activation of specific adaptive immune responses is dependent on antigen internalization by APCs and processing. Antigen that ultimately reaches the cytosol is presented on MHC-I, while antigen that remains in the endosome is presented on MHC-II, resulting in engagement of different subsets of T cells. Thus, the intracellular fate of immune signals (i.e., degradation, localization to specific cellular compartments, agglomeration) within

APCs shapes both the innate response and downstream adaptive immune responses. As such, materials must not only be designed for efficient internalization of immune signals, but also for delivery to the appropriate cellular compartments for a particular signal or application.[131,132]

Hydrophobicity and charge emerge as key parameters to control how biomaterials interact with membranes to deliver immune signals to the cytosol. This is largely due to membranes being comprised of negatively charged lipids. For example, in one study, hydrophobic mesoporous organosilica NPs have been shown to better facilitate lysosomal escape into the cytosol compared to hydrophilic silica particles.[73] In another example, aluminum oxyhydroxide nanorods (ALNRs) were functionalized with either $-NH_2$ or $-SO_3H$ to alter surface charge and assessed for cellular uptake.[133] Although all ALNRs were taken up by immune cells with similar efficiencies, $-NH_2$ functionalized ALNRs exhibited higher levels of lysosomal damage and activation than $-SO_3H$ functionalized ALNRs and unfunctionalized ALNRs.

In addition to facilitating membrane penetration by physical interactions of materials with the membrane, charge also plays a role due to its effect on the capacity of materials to buffer pH. Following initial uptake of materials by cells into endosomes, cells naturally lower the intravessicular pH as endosomes mature into lysosomes to support degradation into resources cells can use. The reductive environment and relative low pH of lysosomes create opportunities for materials that exhibited altered properties or triggered response when these changing environmental cues occur. For example, positively charged polymer particles containing pH-buffering units can induce an osmotic pressure buildup leading to lysosomal disruption for cytosol delivery. In one study, increasing the number of histidine residues on side arms of dendrimers offers more protonation sites under acidic endosomal conditions, altering the osmolarity in the

intracellular compartment, leading to increased lysosomal disruption.[74] Importantly, tuning the ability of particles to rupture lysosomes and enter the cytosol has been shown to modulate activation the inflammasome (**Figure 2.4D**). Following a similar mechanism, adsorption of cationic PEI to mesoporous silicon microrods also allows for lysosomal rupture following uptake.[134] These results exemplify that positively charged particles can facilitate lysosomal escape.

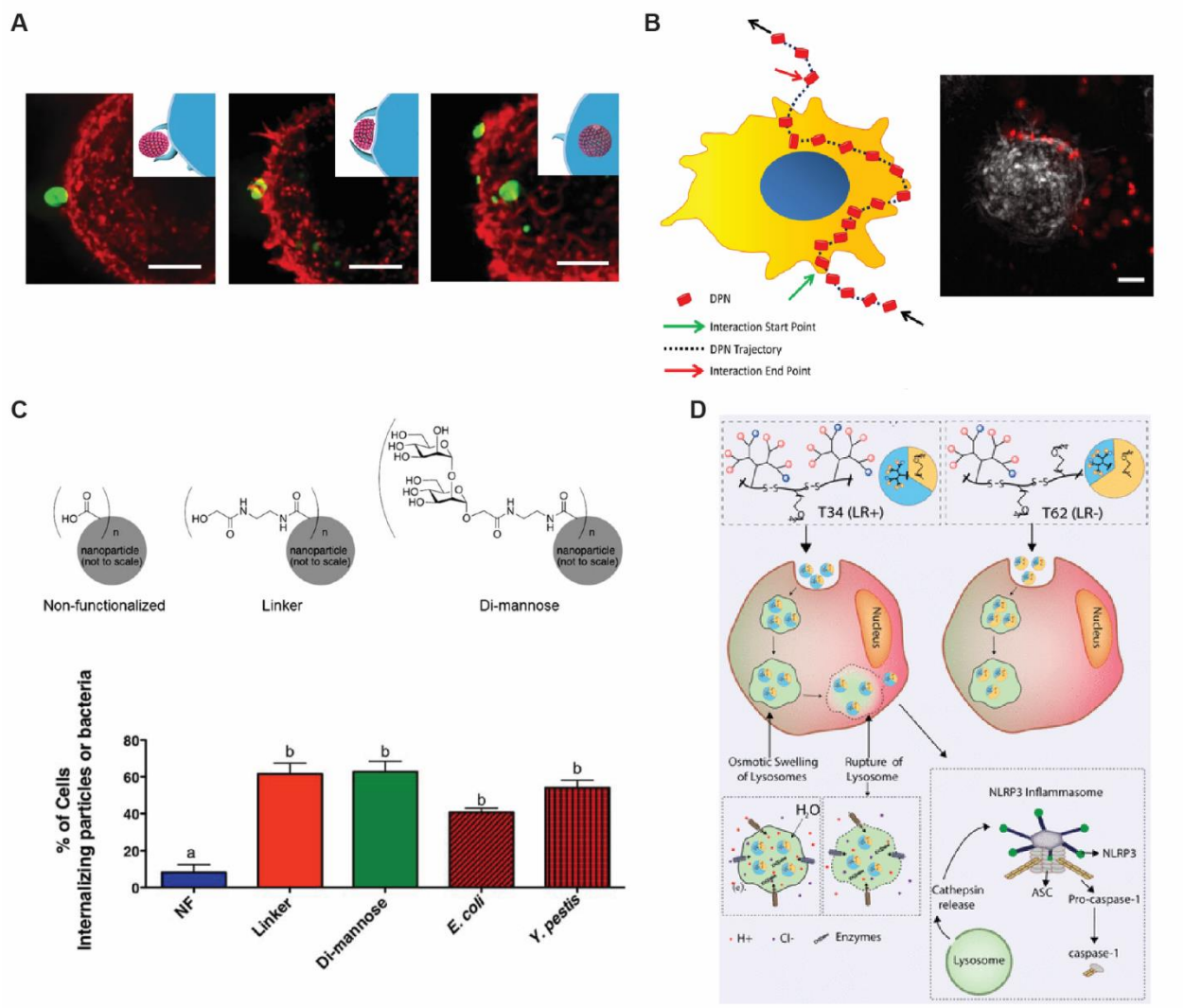

Figure 2.4 Biomaterials can be designed to improve uptake and processing by APCs
A) Pickering emulsions allow for improved deformability, which facilitates uptake of NPs by APCs. Reproduced with permission.[68] Copyright 2018, Nature Publishing Group. B) Time-lapse microscopy analysis of NPs to observe cell-particle interactions. Rigid constructs have prolonged

interactions with cells compared to soft constructs. Reproduced with permission.[69] C) Functionalization of polyanhydride NPs with di-mannose via a glycolic acid linker to mimic bacterial surfaces promotes internalization of NPs. Enhanced uptake is observed even with the glycolic acid alone. Copyright 2018, American Chemical Society. Reproduced with permission.[72] D) Modification of a single amino acid can alter intracellular processing. Reproduced with permission.[74] Copyright 2018, American Chemical Society.

The relative roles of charge and hydrophobicity has been investigated by the Su group.[75] In these studies, chitosan microgels were evaluated for their uptake efficiency and ability to activate bone marrow derived DCs (BMDCs) depending of the extent of functionalization of positively-charged quaternary ammonium groups to a chitosan backbone; this level was termed the "quartenization". Importantly, quartenization was a critical factor in dictating the microgel hydrophobicity and charge. While low quartenization microgels possess high hydrophobicity and lower surface charge, higher quartenization results in lower hydrophobicity and higher surface charge. Only moderate quartenization microgels display both high, positive surface charge and high hydrophobicity. Although lower quartenization exhibited increased uptake, microgels with moderate quartenization elicited the strongest immune responses, displaying improved stimulation of BMDCs *in vitro*; this was true even at lower antigen doses. These findings were attributed to the improved ability of highly charged hydrophobic microgels to disrupt membranes. Thus, the membrane disrupting potential of materials is impacted by the combination of hydrophobic and electrostatic interactions. These differences in uptake are particularly important in biomaterials designed to deliver antigen, because the mode of uptake affects which molecular machinery in immune cells encounter the antigen, which in turn determines how antigen is processed.

While the examples above present ways in which biomaterials can be tuned to promote immune signal localization to specific compartments within cells, it is equally important that immune signals are then released from biomaterial carriers in a manner that will enable processing

by their target pathways (e.g. MHC, TLRs, inflammasome). The ability for carriers to quickly degrade and release cargo within the endosome is important for targeting immune receptors localized within this compartment. Biomaterials can be engineered to quickly release antigen under acidic conditions within endosomes to facilitate antigen processing and presentation. For example, poly(orthoester)s that rapidly degraded at pH 5.0 were found to enhance antigen presentation over PLGA NPs, suggesting that faster release kinetics improved antigen processing.[76] Additionally, the accumulation of particles within immune cells can pose problems. Accumulation of particles can lead to endosomal dysfunction, leading to blockage of other key cellular functions. For example, increased localization of smaller NPs in endosomes was associated with slowed antigen degradation into peptides in endosomes, a critical step for intracellular processing of antigen onto MHC.[135] Thus, controlled release and polymer degradation characteristics offer an avenue to facilitate the pacing of immune signal processing by cells. Control over the timing of immune signal delivery and availability will be addressed in further detail in **Section 2.8**.

2.6 Material Properties Regulate the Delivery of Immunostimulatory Cues to Control Immune Activation

In the previous two sections we focused on general targeting at the immune cell and immune tissue scales. Here, we focus on how the molecular control provided by biomaterials can direct delivery of immune signals, beginning with immunostimulatory cues to immune cells. As reviewed in **Section 2.3**, innate responses serve as the first line of defense against pathogens and allow for rapid protection by activating APCs and stimulating the release of inflammatory cytokines. Thus – owing to some of the same design capabilities explained in **Sections 2.4 and 2.5** – biomaterial carriers can directly or indirectly (i.e. delivery of payload) drive generalized

inflammation and concentrate immune signals to activate innate and subsequently adaptive immune cells. This is of particular interest from a design perspective due to the innate immune system's role in initiating cellular and humoral immune responses needed in vaccines and immunotherapies. As such, APCs remain a frequent target in immune engineering.[103,106,136–138]

2.6.1 Biomaterials exhibit intrinsic immunogenic features that can trigger innate immune function

Many biomaterials are inherently immunogenic, in other words, the material itself can trigger or modulate immune function. While this activity can create problems – for example, in the context of autoimmune disease where carrier-induced inflammation could exacerbate the activity of the dysfunctional immune cells – the intrinsic immunogenicity of materials can also be harnessed to promote immune function for vaccines and immunotherapies against infectious disease and cancer. As one illustration, arginine rich polymers have been shown to activate the complement system, an innate immune pathway for the clearance of pathogens.[139] Different forms of the same material can also trigger different immune responses. Gold nanoparticles have been reported to preferentially activate different innate pathways depending on size.[140] Likewise, Chen et. al offer insight using thiolated poly(methacrylic acid) polymer capsules consisting of spheres and rods that demonstrate similar levels of uptake by macrophages.[141] In these studies, short rod-shaped capsules were found to promote a larger increase in inflammatory TNF and IL-8 cytokine secretion. Neither intracellular fate nor capsule size and volume appeared to play a role in the observed differences in cytokine secretion, suggesting that inflammatory cytokine secretion is dependent on shape.

The dependence on shape in altering intrinsic immune activity and innate immune cell interactions is not confined to polymer-based biomaterials. Nucleic acids offer a facile way to study size and morphology due to the relative ease of forming structures with well-defined configurations and have been studied by several labs.[77,142–144] As one example, the Afonin lab constructed a library of RNA and DNA based NPs of different sizes and shapes with the inclusion of fibrous and globular structures, in addition to planar structures with multiple facets (**Figure 2.5A**).[78] These NPs only stimulate immune responses when complexed to a polymer carrier; nucleic acid structures or carrier alone displayed no immunogenicity. This finding illustrates one way in which biomaterial structure can directly impact immunogenicity. DNA NPs were found to be overall less immunostimulatory than RNA based NPs. Again, shape and structure were found to influence immunogenicity with globular structures being more immunogenic than fibers, which were more immunogenic than planar structures.

Furthering these findings, the Guo lab has developed a library of RNA based NPs comprised of triangle, square, pentagon, and tetrahedron shapes of different sizes. For each shape, extended nucleic acid sequences were attached at each vertice to form an additional set of RNA structures with "arms"[77] Only NPs with extended sequences stimulated production of TNF and IL-6 by macrophages; and immunogenicity was also sequence dependent. When size was kept constant, inflammatory cytokine secretion levels correlated with the number of sides on polygons such that triangles exhibited the lowest secretion levels. This finding may have been influenced by the presence of additional extended sequences on higher ordered polygons. Additionally, the tetrahedron structure exhibited the highest level of cytokine secretion of all NPs, again, suggesting a role of dimensionality (i.e. planar vs. three-dimensional structure) in stimulating inflammatory

responses. Importantly these results offer the potential of tunable immunogenicity to produce either a minimal immune response allowing for NPs that can serve as immunologically-inert therapeutic vectors, or a strong adjuvant immune response, such as those useful in vaccines and cancer immunotherapies.

In addition to shape, controlled release offered by degradable polymers can also lead to activation of immune responses by biomaterials themselves. Given that the properties of polymers are altered during degradation, our lab has explored how degradation of biodegradable polymeric carriers impacts immunogenicity over time. NPs comprised of poly(beta-amino ester) (PBAEs), a class of rapidly degradable polymers, exhibit changes in charge, size, and molecular weight as the polymers degrade.[80] Notably, PBAEs were observed to be immunogenic only in particulate form, with free polymer failing to activate DCs. Activation of DCs by polymer alone was dependent on the extent of degradation. Further studies have revealed that regardless of the starting molecular weight of the polymer, the immunogenicity was identified to be greatest when the molecular weight of degrading PBAEs decreased to a range of 1.5-3kDa, below which immunogenicity was eventually lost.[81] These studies demonstrate that the intrinsic immunogenicity of polymers evolves with degradation, highlighting another important consideration in biomaterial design in the control of APCs and other immune cells. This is particularly important in controlled release to prolong immune signal retention, which will be addressed in **Section 2.8**.

Similarly, PLGA, one of the most investigated biomaterials for particulate based immunoengineering, has also been shown to exhibit degradation-dependent immunomodulation of APCs. Allen et. al investigated the immunomodulatory properties of PLGA across multiple molecular weights over time.[82] In this studies, empty PLGA MPs with differing MW (10kDa,

22kDa, and 90kDa) were prepared. Notably, variations in the molecular weight and composition used influenced the degradation of PLGA. Treatment of DCs with PLGA MPs alone resulted in a time-dependent decreased expression of stimulatory markers MHC-II, CD80, and CD86 in the maturation level of cells. Even when challenged with LPS to stimulate DC activation, MP-treated cells resulted in a marked decreased expression of stimulatory markers and decreased inflammatory IL-12 secretion compared to treatment with LPS alone. The observed immune inhibition was correlated to increased lactic acid, both intracellularly and extracellularly. Importantly, lactic acid is a product of PLGA degradation and has been shown to be immunosuppressive in the tumor environment.[13,145] As such, accumulation of lactic acid as phagocytosed PLGA MPs degraded creates another mechanism that impacts innate immunity. This idea was further supported by findings that immunosuppression was dependent on MW; slower degrading high MW polymers that produce lactic acid more slowly required longer incubation times to produce comparable dampening of DC activation. Together, these results demonstrate that PLGA degradation can lead to immunosuppression of DCs via the accumulation of lactic acid byproducts. These studies illustrate how degradation alters biomaterial modulation of the local immune environment, highlighting the need for further studies to better understand the evolving immunogenicity of materials.

2.6.2 Biomaterials modify adjuvant function to direct innate and adaptive immune responses

Moving from intrinsic properties of biomaterials as stimulatory cues that direct immunity, here we focus on biomaterials to deliver adjuvants and stimulatory signals that activate APCs or other innate cells. For example, Loftus et. al demonstrated that conjugating innate-activating antibody ligands to a graphene oxide template can be used to stimulate specialized innate immune

cells – NK cells – much more effectively than the soluble antibody cues.[146] Additionally, some immunostimulants can cause serious adverse immune-toxicity effects if disseminated via systemic circulation. This constraint creates an additional challenge when multiple adjuvants are involved, which sometimes generate synergistic or self-amplifying responses.[20] Encapsulation of adjuvants can reduce systemic exposure, limiting delivery of immunostimulatory cues to targeted cells and tissues as described in **Sections 2.4** and **2.5**. Further, encapsulation can also enhance uptake by APCs, offering the ability to deliver multiple adjuvants to the same innate-immune cells and control adjuvant display density. These materials can also be used to mimic common physiological properties of particulate pathogens – such as size, shape, or stiffness. Biomaterial carriers can be tuned to deliver cues in a manner that mimics the pathogens immune cells are specialized to detect and internalize, allowing for improved potency relative to soluble adjuvants or signals that innate immune cells may not as easily sense.

The ability to carefully tune polymer chemistry presents another mode of modularity for biomaterials. For example, PBAE chemistry can be readily tuned for hydrophobicity and charge density. In recent studies, a large library of PBAEs NP encapsulating the adjuvant polyIC were used to identify formulations that enhanced the magnitude and duration of antibody responses following vaccination.[147] These studies offer a path to improve our understanding of the role of polymer chemical and structural features in the effective delivery of adjuvants to enable the rational design of biomaterials based vaccines and immunotherapies. Importantly, Sofias et. al have demonstrated that the chemistry by which surface ligands are attached can also have a large effect on immune responses[148], reflecting a need for careful consideration over how adjuvants are conjugated to biomaterials.

The Seder lab has investigated how optimal delivery of TLRs can enhance delivery of immunostimulatory cues to APCs and improve vaccine immunogenicity.[85] TLR7/8a was conjugated to a polymer scaffold to generate a library of adjuvant-linked polymers (Poly-7/8a) with different densities of TLR7/8a displayed on the polymer (**Figure 2.5B**). In aqueous conditions, increasing density of TLR7/8a resulted in assembly of the Poly-7/8a into structures, such that low to intermediate densities produced random coils arrangements, while higher densities promoted formation of particles (**Figure 2.5C**). Higher density particles increased cytokine secretion and activation of DCs and macrophages relative to lower density particles, despite the overall dose of TLR7/8a being constant across formulations. Thus, particle formation, increasing densities of TLR-7/8a on the polymers, or both, were critical in determining the potency of immune responses. In similar studies, CpG – a TLR9 agonist, was conjugated to poly (L-glutamic acid) (PGA) via disulfide bonds that could readily be reduced under the acidic environment within lysosomes to release CpG.[149] The elasticity and cargo loading of these PGA-CpG conjugate NPs could be readily be tuned by varying crosslinking density. During *in vitro* experiments, activation levels of DCs could be readily varied by altering crosslinking density. Higher crosslinking density resulted in higher loading capacity, which led to increased DC activation. Together these studies highlight how biomaterials can alter adjuvant delivery to improve innate responses.

As alluded to above using the example of particular versus soluble signals, biomaterial can also improve innate immune cell activation and subsequent downstream responses by mimicking other features not present on soluble adjuvants. Wang et. al designed titanium oxide (TiO_2) MPs decorated with nanospikes.[86] These spiky NPs were shown to activate and amplify innate immune responses. Bone marrow macrophages were incubated with spiky or rough particles or nanorods.

Following priming with TLR4 agonist, lipopolysaccharide (LPS), spiky particles triggered inflammatory IL-1β secretion (**Figure 2.5D**). Additional studies revealed that mechanical stress exerted on the cell membrane during uptake of spiky TiO_2 MPs by macrophages stimulated potassium efflux, resulting in inflammasome activation and increased IL-1β. Importantly, these findings were LPS-dependent; treatment with TiO_2 MPs alone resulted in no significant changes. As such, while activation of innate immunity requires the presence of danger signals, morphology can play a role in potentiating the response.

From the above study, is it clear that co-administration of biomaterials with adjuvants can alter how APCs respond to these immunostimulatory signals. The Fahmy lab explored the effect that NPs may have in these skewing responses.[150] Silica NPs were coated with different poly(amino acid)s to form a library of NPs of different size, charge, and hydrophobicity. When DCs were treated with NPs in conjunction with TLR3/4 agonists, IL-1β secretion was dependent on size and hydrophobicity. Charge, on the other hand, did not have a significant effect on the generation of innate immune responses. However, cationic NPs were found to improve proliferation of T cells. These findings highlight that biomaterials can be used to enhance or alter the immune system's response to an adjuvant. Intrinsic properties of biomaterials can also alter cytokine secretion profiles, which regulate and direct immune responses. Thus, material properties that exhibit intrinsic immunogenic effects as described in **Section 2.6.1** can also enhance weakly immunogenic adjuvants. For instance, Tazaki et. al conjugated a safer (i.e., less toxic), but poorly

immunogenic RNA adjuvant to gold NPs. In these studies, it was observed that nanorods, but not spheres, enhanced the adjuvanticity improving suppression of influenza infection in mice

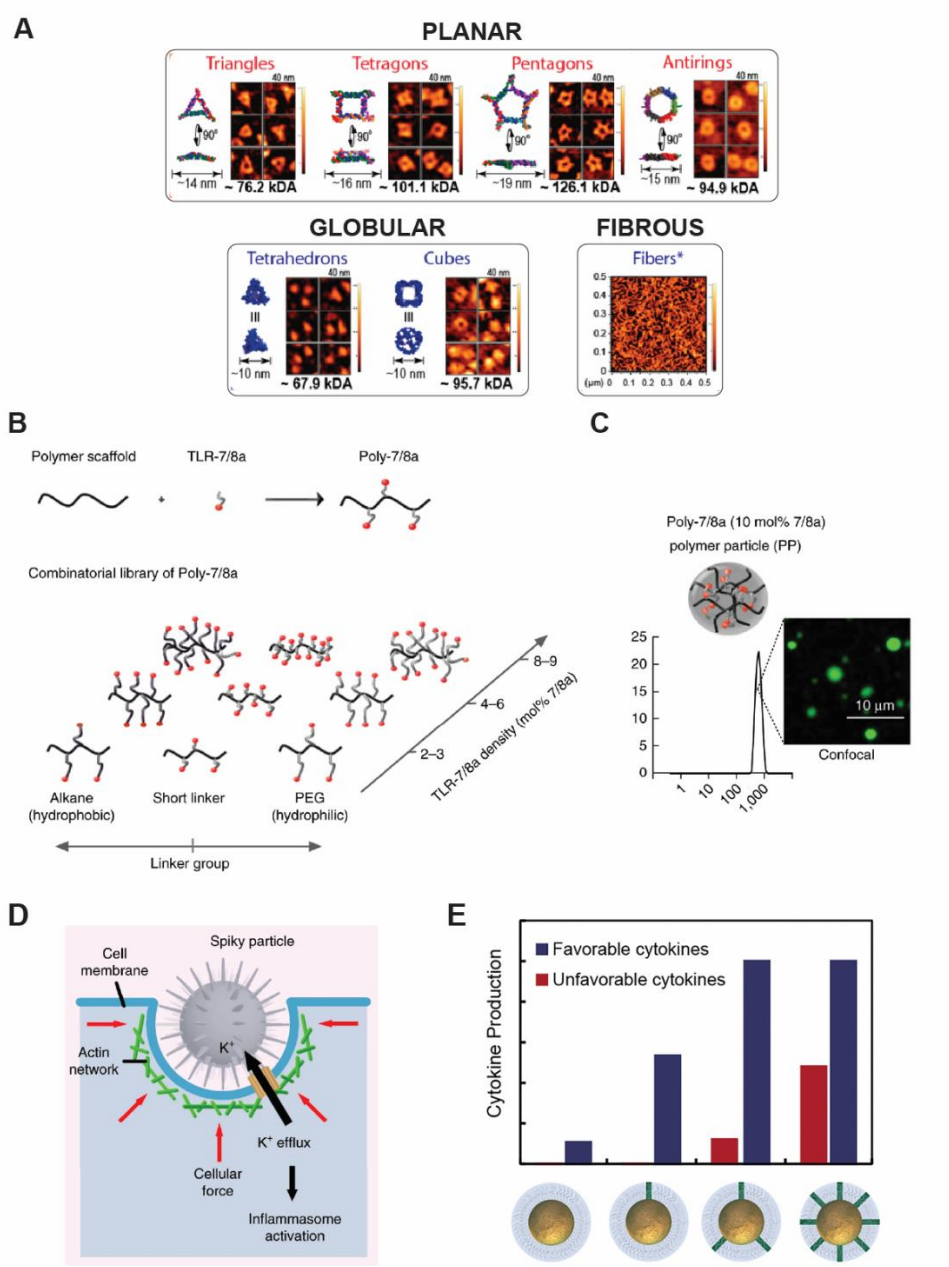

Figure 2.5 Shape and surface characteristics can be tailored to improve delivery of immunostimulatory signals to the immune system

A) A library of self-assembled nucleic acid structures offers tunable activation of innate immune responses. Reproduced with permission. [78] Copyright 2017, American Chemical Society. B) TLR7/8 is conjugated to a polymer scaffold at different densities differentially activate immune cells C) Higher densities of TLR7/8 form polymer particles, while lower density remain as random

coils. Reproduced with permission.[85] Copyright 2015, Nature Publishing Group D) Nanospikes on nanoparticles exert mechanical stress on cells, leading to potassium efflux and inflammasome activation to enhance immune activation by "danger signals". Reproduced with permission.[86] Copyright 2018, Springer Nature. E) Increased loading of CpG improves production of cytokines that promote anti-tumor responses. However, at higher concentrations cytokines that promote tumor growth and survival are produced. Reproduced with permission.[151] Copyright 2019, American Chemical Society.

immunized *intranasally*.[79] Thus, material properties can also be harnessed to improve adjuvanticity and improve safety.

Despite the need for more potent adjuvants, the ability to modulate and carefully manipulate the type and magnitude of response remains an important goal. For example, clinical translation of TLR-based adjuvants requires balancing the induction effective responses with safety concerns sometimes related to generation of excessive systemic inflammatory responses.[152,153]

The modularity of biomaterials can address this need by allowing for tunable loading of adjuvants to optimize immune activation in the absence of undesirable side effects. In one study, CpG was conjugated to gold NPs to improve macrophage activation to promote anti-tumor responses.[151] Maximal immunostimulation was achieved when CpG comprised as little as 5% of total oligonucleotides. NPs with higher compositions of CpG achieved similar levels of immunostimulation and production of inflammatory cytokines that promote anti-tumor immunity (i.e. TNF). However, higher levels of CpG was also associated with elevated levels of cytokines that have been linked to tumor growth (**Figure 2.5E**). As such, it is important to be able to precisely control the magnitude of the response as well as the profile of cytokines produced to stimulate desired responses.

While we previously discussed strategies that employ polymers as scaffolds to increase loading capacity of adjuvants, biomaterial carriers can also alter the immunostimulatory potential by limiting the accessibility of adjuvants. CpG complexes formed through electrostatic assembly with an arginine-based poly(ester amide) have been observed to elicit different immune responses in macrophages based on polymer chain stiffness.[83] CpG complexes lowered immune responses compared to soluble CpG alone, with softer chained polymers exhibiting the greatest reduction in the immune response. The reduction in immune responses was hypothesized to be the result of polymer binding to CpG, with softer chain polymers exhibiting more favorable binding interactions. In similar studies, cationic polymers such as poly(beta-amino esters) (PBAE), which are designed to bind nucleic acid, have also been found to tightly bind CpG to form NP complexes.[84] As such, at higher w/w ratio of PBAE:CpG, CpG remains tightly bound to PBAEs, rendering it inaccessible to activate TLR. Interestingly, however, additional studies revealed that higher w/w ratio of PBAE:CpG facilitated improved CpG uptake over soluble CpG. Thus, although higher interaction strength of polymers for adjuvants can decrease the activating potential, the ability to bind CpG to form NPs is important for promoting uptake. These findings present an example of design considerations that must be balanced for engineering effective vaccines and immunotherapies. From these studies, it is clear that the physicochemical properties of materials can play a key role in altering how innate immune cell receive immune signals. In the next section, we discuss how materials properties can be leveraged to manipulate downstream adaptive responses by controlling antigen encounter.

2.7. Biomaterials Control the Context in Which Antigen is Presented to Tune Adaptive Immune Responses

In this section, we highlight how the physicochemical properties of biomaterials can be used to influence adaptive immune response. We first discuss how controlled APC activation and antigen presentation by biomaterial carriers alters the immune microenvironment (e.g., LNs) in which T cells are activated. Next, beginning in **Section 2.7.3**, we explore how antigen presentation by materials are modulated to directly interact with T cells to activate and polarize their responses, followed by examples in which materials initiate B cell responses. Finally, we highlight examples of how biomaterials can be engineered to promote antigen-specific immune tolerance that could be useful in treating autoimmune disease, inflammatory disease, and for transplantation.

2.7.1 Biomaterials can be engineered to alter the microenvironment in which T cell responses are generated

The modulation of innate immune responses by biomaterials defines the conditions (i.e. immune signal presentation, cytokine milieu) under which induction of antigen specific adaptive immune responses occurs. Immune signal trafficking throughout the host and subsequent intracellular processing of these signals by innate cells all contribute to the types of adaptive immune response that result. Demonstrating that inducing a local inflammatory LN environment can enhance T cell responses, Lynn et. al synthesized polymer-TLR7/8a conjugates with different chemical compositions and chain architectures.[87] These conjugates exhibited distinct molecular conformation and size (e.g., random coil, polymer micelle and particles) to evaluate how these parameters impact the potency of the adjuvant for inducing $CD8^+$ T cell response in mouse models.

Cytokine production in LNs and the number of $CD8^+$ T cells induced against antigen increased with increasing polymer-TLR-7/8a hydrodynamic radius, such that particles induced the highest magnitude responses, followed by micelles, then random coils. The ability of the particle to induce greater T cell responses was attributed to increased particle uptake by macrophages and monocytes within LNs, leading to increased activation of APCs and production of inflammatory cytokines, such as IL-12. Thus, molecular conformation and size of polymers laden with TLR-7/8a influences the local LN environment to improve T cell responses. Follow-up studies demonstrated that the physical form of peptide plays a similar role.[122] Synthetic peptides comprised of an antigen epitope conjugated to 30 amino acid long peptide sequence display different hydrodynamic behaviors depending on the hydrophobicity of peptide sequences. Hydrophobic sequences form particulates that result in 20-fold higher T cell responses compared to hydrophilic sequences that remain soluble in aqueous solution. This is due in part to particle peptides being retained longer in LNs, allowing for prolonged antigen presentation.

In addition to driving the activation of T cell responses, biomaterials can also be tuned to skew the specific features of adaptive responses. For example, the choice of carrier can impact the balance between inflammatory T cell subsets. As one illustration, antigen loaded onto calcium phosphate templates and aluminum hydroxide induced both T_{H1} and T_{H2} responses, which stimulate other T cells and B cells, respectively.[154] Chitosan templates, however, only induced T_{H1} responses. In the context of allergies and autoimmune diseases, the ability to inhibit infiltration of activated APCs at sites of disease can skew T cell responses towards tolerance. One unique approach that has been explored employs drug-free biodegradable NPs lacking any targeting ligands, but composed of different polymers to inhibit specific inflammatory cells from entering

sites of disease.[155] NPs with higher MW polymers and higher hydrophilicity associated with inflammatory cells to redirect their trafficking. In another study, the Shea lab investigated the effects of poly (lactide-co-glycolide) (PLG) and poly (lactide) (PLA) NPs in delivering antigen.[156] Compared to PLG NPs, treatment with PLA NPs markedly ameliorated disease in a mouse model of multiple sclerosis (MS), an autoimmune disease in which immune cells mistakenly attack the myelin insulating neurons (**Figure 2.6A**). The addition of a methyl group in lactide makes PLA more hydrophobic than PLG, which was found to facilitate association with APCs and inhibit expression of costimulatory markers. This translated to reduced numbers of $CD4^+$ T cells and B cells in the CNS. These observations illustrate how engineering to curtail inflammatory cues to T cells can limit immune responses and highlight the importance of modulating the microenvironment that T cells are exposed to.

2.7.2 Biomaterials can alter antigen presentation by APCs to activate $CD4^+$ versus CD8 T^+ cells

The spatial organization of cell surface proteins at immune interfaces is a central aspect of immune cell signaling. While **Section 2.6** discussed antigen processing by APCs, we now turn our focus to antigen presentation. As the bridge between innate and adaptive immunity, APC presentation of antigen is critical and can alter subsequent priming of specific adaptive immune responses. For instance, increasing antigen presentation on APCs can increase the interactions of APCs with T cells. Optimizing the size of PLGA particles to improve uptake of antigen loaded particles can lead to increased peptide presentation in MHC and induce inflammatory cytokines.[157] Equally important is the ability to maintain the structural integrity of the presented antigen, because T cells can only recognize specific peptide sequences under precise conformations. This is a particularly important consideration for antigens conjugated to materials, which must be cleaved

before they can be processed into peptides and loaded onto MHC. One strategy is the use of pH sensitive linkers to control release. In collaboration, the Swartz and Hubbell labs developed a pH sensitive self-immolative linker to conjugate antigen to a glyco-adjuvant conjugate.[88] Importantly, the self-immolative linker used reversible chemistry, allowing for the release of conjugated antigen without additional modifications, unlike other commonly used linkers which often chemically tag the antigen upon release. The ability to release unmodified antigen was revealed to augment antigen presentation to T cells, resulting in improved proliferation of both $CD4^+$ and $CD8^+$ T cells compared to a non-self-immolative linker (**Figure 2.6B**). This study highlights a role for controlled release of antigen to improve T cell activation.

Improving antigen presentation to increase the magnitude of T cell responses, however, is only one dimension to consider. To drive specific T cell subsets, antigens must be also be presented in the correct MHC. We previously discussed the ability of cationic particles to facilitate lysosomal escape (**Section 2.4.2**) to localize immune signals within the cytosol. While this is a key step in cross-presentation, excessive exposure to the endolysosomal environment can also lead to degradation of peptides, hindering its proper presentation following escape into the cytosol. This is evident in a comparison between anionic and cationic liposomes. Cationic, but not anionic liposomes have been found to increase cross-presentation of extracellular antigens.[158] This is due in part to elevation of lysosomal pH by cationic liposomes, which reduces the endolysosomal degradation of antigens. In contrast, anionic liposomes do not affect lysosomal pH. However, a critical limitation is that cationic liposomes can have increased cytotoxicity at higher concentrations, while anionic liposomes typically exhibit no cytotoxicity even at much higher

doses. Thus, alternative biomaterial approaches to promote antigen presentation in the correct MHC are being explored.

In one approach, work by Zupancic et. al demonstrates that the nature of protein association to biomaterial carriers (i.e. adsorbed vs. entrapped) affects how these antigens are processed and displayed on DCs.[91] These studies support the need for antigen protection to promote cross-presentation. Immunization with antigen-adsorbed NPs upregulated MHC-II, while antigen-entrapped NPs upregulated MHC-I. This is significant because these results suggest that antigen-loaded NPs may be more efficient for cross-presentation, perhaps due to cargo protection offered by encapsulation. As previously mentioned, the priming of specific adaptive immune responses requires the presentation of antigen within specific classes of MHC. Thus, the ability to tune the presentation of antigen on MHC-I vs. MHC-II remains a key area of interest. This is exemplified in recent studies by Restrepo et. al, which examined how changes in the mode of antigen delivery – encapsulated antigen vs. antigen decorated on surfaces – could control activation of $CD4^+$ and $CD8^+$ T cell responses.[90] The model antigen OVA was delivered using either NPs or polymersomes (PSs), each composed of hydrophobic polymer poly(propylene sulfide) (PPS) and hydrophilic PEG; this design allowed considerable variation in interactions between the carriers and APCs. The NPs were comprised of a hydrophobic core of PPS and a corona of PEG onto which OVA was readily conjugated using disulfide bonds. In contrast, PSs consist of an aqueous core where antigen is loaded, surrounded by a polymer bilayer of PEG-PPS. These differences in material structure promoted unique T cell subsets. In particular, NPs promoted $CD8^+$ responses, while PS preferentially enhanced $CD4^+$ responses. While both carriers activated DCs to similar levels, they each displayed different intracellular processing of antigen. NPs were primarily found

in early endosomes with uptake studies suggesting that the disulfide link is cleaved from the carrier to allow escape of OVA from the endosome to the cytosol. On the other hand, cargo protection by the polymer bilayer of PSs prevented early degradation, allowing for antigen retention within vesicles until these cellular structures acidified into lysosomes. These differences in processing contribute to differential antigen presentation on MHC-I and MHC-II by APCs, resulting in activation of $CD8^+$ or $CD4^+$ T cells, respectively.

Liu et. al suggest that the strongest responses occur by using a combination of the antigen displays described in the examples above (i.e. antigen adsorption and encapsulation).[89] In this study, nanoparticles with antigen both bound to the surface and encapsulated were compared to particles that localized antigen either on the surface or within particles (**Figure 2.6C**). Antigen loading was dose matched across all formulations. NPs that incorporated antigen through both encapsulation and adsorption were significantly more effectively, as this design offered not only adequate initial antigen exposure, but also long-term antigen persistence at the injection site due to cargo protection. More importantly, this design allowed for antigen presentation through both MHC-I and MHC-II. The ability of particles to simultaneous elicit $CD4^+$ and $CD8^+$ responses is critical for generating immunological memory. These results reveal the unique physical and chemical properties that result from carrier design can also generate distinct immune responses, even when the same building blocks are used. Collectively, these findings highlight how biomaterial design can control the context under which antigen is presented by APCs to ultimately help shape the resulting adaptive immune response.

2.7.3 Biomaterial mimics of APCs can present antigen directly to T cells

Biomaterials can also be engineered to directly interact with T cells to trigger differentiation and expansion into specific phenotypes. One opportunity created by such strategies is the ability to directly alter design parameters such as antigen display density, aspects ratio, or shape to impact T cell activation. Several labs have designed artificial APCs (aAPCs) to control immune signal display to APCs.[159] In one example, researchers in the Schneck lab have designed aAPCs composed of superparamagnetic iron oxide NPs coated with peptide-MHC (pMHC) and a costimulatory molecule, anti-CD28.[17] Magnetic NPs were used to control clustering of NPs. Size (i.e., 50nm, 300nm, 600nm) and stimulatory ligand density were then varied to determine whether these properties could improve the efficiency of T cell activation. In these studies, larger aAPCs more efficiently activated T cells (**Figure 2.6D**). Smaller aAPCs, on the other hand, required saturating doses of pMHC or artificial magnetic clustering of NPs to activate T cells at similar levels compared to the larger particles. These results suggest that T cell activation is dependent on the formation of TCR clusters. This was supported by an inverse relationship between aAPC size and the number of aAPCs needed to provide effective T cell signaling, whereby larger aAPCs required fewer aAPCs. Further, transmission electron microscopy studies revealed that while very few 50nm aAPCs attached to T cells, many more 300nm to 600nm aAPCs attached to T cells. This result suggests that ligand density and size affect the ability of aAPCs to interact with T cells. Collectively, these findings indicate that TCR activation requires multi-receptor ligation and formation of TCR nanoclusters.

Studies by the Mooney lab further elucidate the importance of TCR nanoclusters.[16] Under a different platform using mesoporous silica microrods coated with lipid bilayers to form APC

mimetic scaffolds (APC-ms), similar findings were obtained (**Figure 2.6E**). Again, T cell expansion was observed to be dependent on the density of stimulatory cues and number of APC-ms. Strikingly, however, scaffolds with significantly lower density of stimulatory cues could still promote robust expansion of T cells. These findings were attributed to the presentation of stimuli on a fluid lipid membrane, which better emulated the dynamic process of surface cue presentation on APCs contrary to other synthetic aAPC systems which present immune signals on static surfaces. Additionally, formulations that presented higher amounts of T-cell stimuli (i.e. anti-CD3, anti-CD28, IL-2) skewed T cell expansion towards $CD4^+$, while lower amounts of T-cell stimuli promoted a more balanced of CD4-to-CD8 T cells. These results suggest another role for ligand density in polarizing T cell responses. Supporting this idea, antigen density, in combination with surface area and particle size, has also been found to correlate with the subtype of immune responses generated. In one study, spherical NPs (193nm) with antigen conjugated to the surface produced a T_{H1}-biased response, whereas large rod-shaped particles (1530 nm) produce a T_{H2}-biased response.[160] Thus, the density of costimulatory signals and antigen displayed on biomaterials not only plays a critical role in their ability to interact with and trigger T cells, but can even alter the polarization of T cell responses. In the next section, we discuss how controlling antigen presentation on biomaterials can be harnessed to improve B cell maturation that controls antibody production.

2.7.4 Controlled antigen presentation on biomaterials enhances antibody responses

In addition to presenting antigen to T cells, biomaterials can also be engineered to promote B cell activation and antibody production. Many B cell activation processes begin with cross-linking of surface receptors by antigen, which implies that the conformation in which the antigen is displayed

impacts these events, a criterion which biomaterials are well-suited to leverage. Several labs have demonstrated that particulate shape and size play a key role in eliciting higher levels of antibody titers on different substrates, such as gold[161] and hydroxyapatite.[162] Interestingly, conjugation of antigen to the outer surfaces of these particles typically elicits higher immune responses when conjugated to smaller sized particles with lower surface areas and therefore less antigen per particle. Similar trends have been noted when antigen is chemically grafted onto the shell of nanostructured lipid carriers, such that small anionic lipid particles elicit stronger antibody responses compared to larger, cationic lipid particles.[163] These findings are surprising because contrarily, positively charged particles favor uptake, suggesting that higher antibody responses are not solely dependent on internalization of antigen particles, but that other processing mechanisms may be involved. Because the overall antigen dose is maintained constant across particle types in such studies, a possible explanation is that antigen density may also play a role in eliciting strong humoral responses by offering more optimal antigen interaction with B cells. This possibility is corroborated by Marcandalli et. al, who explored the structure-based design of NP vaccines, using self-assembling proteins.[164] An antigen trimer protein was conjugated to NP subunit building blocks to form icosahedral assemblies that could present up to 20 copies of the trimer with tunable control of the antigen display density. Immunogens that could not assemble into NP complexes promoted much weaker antibody responses even with dose-matched antigen amounts. This result suggests the increase in antibody production was related to the structure of the NP guiding antigen display and interactions with the B cell. Additionally, antigen density on the NP exterior correlated with the magnitude of the response, with higher density eliciting higher levels of antibody production. These findings support the hypothesis that efficient BCR cross-linking by the dense array of antigen on the NP surface, at least in part, improves immunogenicity.

However, high antigen density does not always favor improved antibody responses. In another study, NPs displaying lower densities of viral protein antigens were found to more efficiently stimulated antigen-specific B cells than NPs displaying higher antigen densities.[165] NPs displaying a low density of antigen also increased the number of GC B cells in immunized mice, resulting in higher levels of antigen-specific antibodies. Taken together, these observations suggest that sparse antigen density on NPs allows improved GC reactions that, in turn, give rise to durable memory reservoirs and elevated, long-lived serum antibodies. In the case of more immunogenic antigens, it is possible that antigen density may influence antigen access and handling by innate immune cells localized at the site of immunization. In this scenario, a higher protein density could alter draining to LNs or improve uptake by DCs and macrophages, diminishing the number of NPs available to be efficiently captured and presented to B cells within the draining LN. Alternatively, by displaying antigen at a lower density, epitopes may become more accessible due to less steric hinderance, allowing for improved immunogenicity and activation of a larger percentage of the antigen-specific B cell repertoire.

Building on these findings, another approach to improving B cell responses leverages biomaterials to improve the conformational display of antigens on biomaterial carriers. For example, the Irvine lab conjugated phosphoserine linkers to antigen, allowing for the tunable binding of immunogens to aluminum hydroxide (alum), the gold standard for adjuvants that is used in many FDA approved human vaccines (**Figure 2.6F**).[92] Importantly, this system allowed for both the tuning of antigen orientation and density. Interestingly, B cells were also observed to take up alum-antigen conjugates. These findings suggest that when bound to alum via pSer linkages, antigens can behave as a multivalent, particulate vaccine that are internalized by B cells.

While, the immobilization of antigens to alum allowed for control over the conformation of the antigen, the density of antigen binding to alum could be augmented by increasing the number of serine residues in the linker. Importantly, it was demonstrated that the directed orientation of immunogens with the pSer linker can alter the B cell specificity of the immune response, allowing for B cell specificity to be tuned towards specific epitopes. This is particularly relevant for universal protection against highly mutative viruses such as HIV and influenza, in which specific targeting to more conserved regions of the virus are needed. Because these vaccines are effective only against antigenically-matched viruses, new design strategies that can improve specificity towards conserved regions remains an important area of research. In another approach, Skwarczynski et. al, formed self-assembling amphiphilic particles comprised of antigen coupled to poly(amino acids) comprised of 10 repeat units of hydrophobic amino acids.[166] The hydrophobic properties and conformation were easily modified by changing the type and number of amino acids. These particles were found to be self-adjuvanting, with the most hydrophobic amphiphilic particles displaying the highest level antibody titers. However, only particles that maintained the helical conformation of the antigen could generate strong antibodies against multiple strains of group A Streptococcus. These findings highlight the importance of antigen conformation in promoting strong antibodies responses, which can be facilitated through the modularity of biomaterials.

2.7.5 Tunable loading of antigen onto biomaterials can promote tolerance to combat autoimmune diseases

While biomaterial based immunomodulation has largely focused on generating potent responses, much exciting work is exploiting biomaterials to promote tolerance during autoimmune

disease.[5,167,168] As discussed in **Section 2.6.1**, biomaterials can exhibit intrinsic immunogenic feature, which are heavily influenced by the physicochemical properties of materials. Thus, it is important to understand how features of biomaterials such as size and charge, as well as formulation designs such as antigen loading contribute to immune polarization of immune responses towards tolerance. This insight could support rational design criteria for autoimmune therapies and anti-inflammatory materials.

Pearson et. al developed PLGA NPs with modular loading of one or multiple self-antigen types coupled to the NP surface to study the role of size and antigen loading on T_{REG} induction.[169] Higher antigen loading induced more T_{REGs}, but T_{REG} induction was also dependent on size; 400nm NPs induced more T_{REGs} than 80nm NPs at the same total antigen dose. Contrary to this finding, other studies have observed that smaller particles are more effective at inducing tolerogenic responses. For example, phosphatidylserine liposomes have been reported to induce hyporesponsiveness to an otherwise immunogenic antigen.[170] Investigation of the biophysical properties governing this result revealed that smaller liposomes reduced DC activation and increased secretion of anti-inflammatory TGF-β, polarizing DCs towards a more tolerogenic phenotype and reducing antibody production against the antigen. In other studies, peptides were conjugated onto a HA polymer backbone to form different size antigen arrays.[171] Treatment with smaller sized arrays delayed disease onset and lowered disease incidence in a mouse model of MS. However, the impact of smaller size was only observed at earlier stages of disease. At later time points, antigen arrays displayed similar levels of efficacy across sizes, suggesting a role of smaller size in allowing for quicker drainage to LNs for faster polarization of T cells. These differences in

outcomes highlight the need for further studies to elucidate the role of carrier size in inducing tolerance.

As previously described, T_{REGs} can form during interactions with APCs presenting antigen to a T cell in the absence of costimulation. Similar to the principles discussed in **Section 6.3**, biomaterials that directly interact with T cells can be engineered to create more favorable interactions that promote the formation and expansion of T_{REGs}. As one example, the Santamaria lab demonstrated that peptide presentation density can promote long term interactions with the TCR of T cells to promote T_{REG} formation using a different type of aAPC.[93] In these studies, iron oxide NPs were conjugated with pMHC at different densities. pMHC density was found to play a key role in the activation of $CD8^+$ T cell responses, such that 11 pMHCs per NP resulted in strikingly higher levels of IFN-γ secretion compared to NPs with only 8 pMHCs. This suggested that a clear threshold of pMHC density on NPs is required to activate T cells. Confirming this observation, larger particles required a higher number of pMHC per NP to activate T cells, suggesting that density, rather than the absolute number of pMHC molecules, drives these responses. Importantly, pMHC-NP dose and density were also observed to enhance T_{REG} expansion, but in distinct ways. While density influenced the expression levels of a T_{REG} marker (CD49b), resulting in its upregulation on cells, dose had a more minimal effect on expression levels. However, the proliferation of T_{REGs} was found to be dose-dependent. Thus, it was determined that pMHC density regulated the efficiency of T_{REG} formation, and dose controlled the magnitude of expansion. Because TCRs have been found to organize into nanoclusters with ligands to promote TCR cross-linking[172], it was hypothesized that higher density pMHC improved NP interaction with T cells. Further investigation revealed that binding of pMHC-NP with the TCR

on T cells promoted the formation of TCR microclusters that increased in size with increasing pMHC density. However, below a threshold density, clusters were unable form. These findings suggest that pMHC density controls T_{REG} conversion by promoting sustained assembly of TCR microclusters.

In other studies, Hess et. al have demonstrated that the degree of tolerance induced in a mouse model of MS (EAE) correlates with the density of self-antigen presented on quantum dots.[94] In these studies, myelin peptide (MOG), a self-antigen that is attacked in MS was displayed on quantum dots with tunable control over the density (**Figure 2.6G**). Following disease induction, mice were treated with quantum dots displaying antigen at one of three MOG densities, while maintaining a constant dose of MOG; thus, mice receiving lower ligand densities received a higher number of quantum dots (**Figure 2.6H**). Interestingly, MOG displayed at lower densities on a greater number of the particles exhibited the lowest clinical scores, lowest disease incidence, and healthiest body weights. These findings suggest that a higher number of tolerogenic particles displaying lower levels of self-antigen is more effective for inducing tolerance than fewer particles each displaying a higher density of peptide. Additional studies to elucidate potential mechanisms suggest that improved clinical scores are the result of increased T_{REG} expansion and colocalization of quantum dots with macrophages and scavenger receptors involved in promoting tolerance. This observation is particularly significant because it highlights the importance of antigen density in controlling T cell responses, not only through direct interaction with T cells as described in previous paragraphs, but also by controlling antigen display to APCs that then interact with T cells.

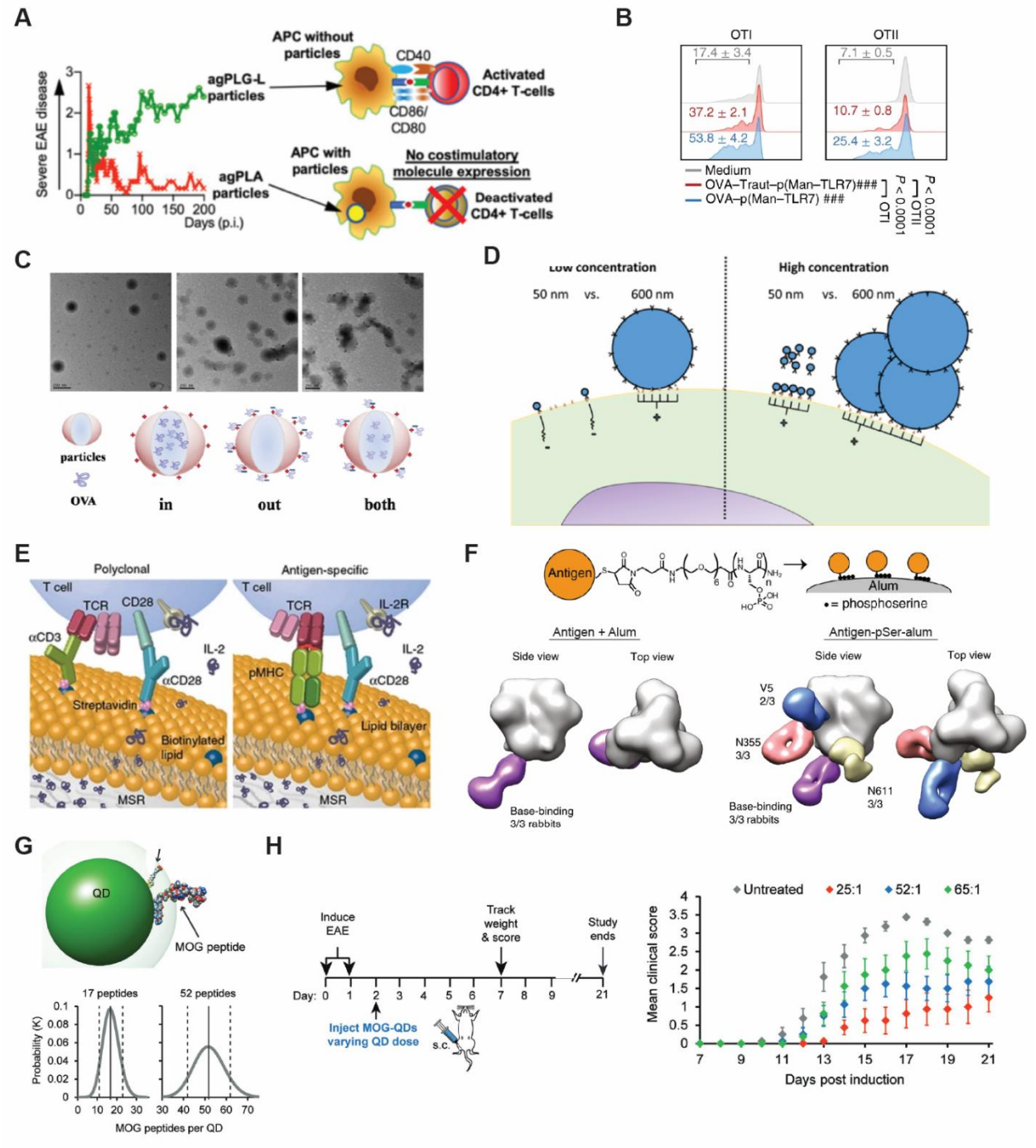

Figure 2.6 Biomaterials modulate the context of antigen delivery to regulate immunity for both immune activation and to promote tolerance

A) NP-cell interactions depend on the type of polymer used. Association of PLA particles with APC inhibit expression of costimulatory molecules to induce tolerance, resulting in lower disease severity. Reproduced with permission.[156] Copyright 2019, Elsevier. B) Reversible chemistry of

OVA-p(Man-TLR7) linker allows for release of unmodified antigen, allowing for improved antigen presentation and downstream proliferation of both $CD4^+$ and $CD8^+$ T cells. Reproduced with permission.[88] Copyright 2019, Nature Publishing. C) TEM and schematic illustrations of different deliery methods of antigen that evoke different intracellular processing mechanisms by APCs. NPs with antigen presented on the surface promote antigen presentation and activation of $CD4^+$ while NPs that encapsulate antigen, promote $CD8^+$ T cell responses. Incorporation of antigen at both locales promotes expansion of both $CD4^+$ and $CD8^+$ T cells. Reproduced with permission.[89] Copyright 2016, Elsevier. D) Antigen presentation density plays an important role in activating T cells. Small aAPCs poorly expand T cells at lower concentrations compared to larger antigen coated particles. When the concentration is raised to improve clustered binding of antigen coated NPs, small aAPCs can expand T cells as well as larger aAPCs. Reproduced with permission.[17] Copyright 2017, American Chemical Society. E) Presentation of stimulatory T cell cues (e.g. anti-CD3, anti-CD28) on lipid bilayers mimcs the dynamic process of surface cue presentation, allowing for robust expansion of T cells even at lower presentation density. Reproduced with permission.[16] Copyright 2018, Nature Publishing. F) Antigen conjugated to alum using a linker composed of repeating phosphoserine units offers conformational control. Single particle electron microscopy analysis of antibodies in treated rabbits revealed that the ability to orient antigen display allowed for targetting of a larger repetoire of antigen epitopes. Reproduced with permission.[92] Copyright 2020, Nature Publishing. G) Antigen density also plays an important role in vaccines and immunotherapies for autoimmune diseases. Quantum dots enable the tuning of antigen display density. H) At constant overall antigen dose, treatment with more particles displaying antigen at a lower density can more effectively reduce clinical scores in a mouse model of multiple sclerosis (EAE). Reproduced according to the terms of the Creative Commons Attribution 4.0 International License.[94] Copyright 2017, Wiley-VCH.

2.8 Biomaterials can be engineered to alter the timescales over which immune signals are available

As alluded to already, the kinetics with which immune signals are encountered play an important role in initiating and directing adaptive immune response. Generation of strong adaptive immune responses often requires multi-step treatments, comprised of an initial “prime” vaccination, and an additional “booster” injection at later time points. Prolonged and targeted adjuvant or antigen uptake by APCs enables sustained DC activation, which contributes to the enhanced immune response seen with particulate vaccine delivery. Additionally, the ability to improve the pharmacokinetics of vaccines and immunotherapies can improve administration schedules, leading to improved safety and compliance.

2.8.1 Material properties can be tuned to prolong retention of immune signals within LNs

Temporally controlled antigen delivery may optimize immune responses for specific diseases of interest when different antigen-APC interaction kinetics lead to distinct downstream signals. In exciting studies, mini osmotic pumps implanted into mice allowed for continuous antigen release over the span of one or two weeks, providing a controlled system to study the importance of antigen persistence in immune response.[173] Continuous antigen exposure increased germinal center and serum antibody responses. These results suggested that regulating antigen kinetics may enable increased vaccine potency, further fueling ongoing interest in controlled release systems for improving vaccines and immunotherapies.

Biomaterials offer a platform to study and tune release kinetics. For instance, unique release rates for PLGA microspheres can be obtained by varying MW and lactide:glycolide ratios.[174] Another strategy for extending antigen release is the use of different linker chemistries to alter release of antigen. Kapadia et. al varied antigen release rate and presentation time by conjugating a model antigen, SIINFEKL, to PEG-hydrogels via a disulfide or thioether linkage (**Figure 2.7A**).[95] Compared to the disulfide linkage, thioether linkage allowed for sustained release of peptide that prolonged antigen presentation over 72 hours. To further examine the mechanism of how NP-peptide formulations deliver antigenic peptide, BMDCs were treated with soluble antigen and antigen NPs, followed by washing with acidic citrate phosphate buffer to remove MHC-I peptide complexes from the surface of BMDCs. Cells were then incubated for an additional 24, 48 and 72 hours, enabling internalized antigens to be processed and re-presented onto the cell surface. Citrate-phosphate treatment completely removed SIINFEKL from p-MHC complexes for cells treated with soluble SIINFEKL but was unable to completely remove cell bound NP-peptide.

At each time point, particle-conjugated SIINFEKL induced significantly higher antigen presentation in BMDCs as compare to soluble SIINFEKL. Slower release from the thioether bond resulted in prolonged antigen release and higher bioavailability, and therefore improved antigen presentation over time. During tumor studies, mice treated with NPs conjugated with either linkage exhibited significantly lower tumor growth compared to mice treated with soluble SIINFEKL and a TLR-based adjuvant, CpG (**Figure 2.7B**). However, due to the improved controlled release of SIINFEKL from thioether-linked NP formulations, tumor growth was delayed up to 14 days, compared to 7 days during treatment with the disulfide linked NP formulation.

Particle size can also impact the duration of peptide/MHC-II presentation.[97] DCs have been observed to display antigens conjugated to larger particles for longer periods of time than when they display antigens on smaller particles. In one study, antigen was conjugated onto polystyrene NPs of varying size by covalent linkages. The overall administered antigen dose, mass of particles, and antigen density was maintained constant across formulations, by altering the amount of antigen per particles and the number of particles administered to mice. For instance, larger particles contained more antigen per particle due to greater surface area, and as such, mice were given fewer particles per mouse, compared to mice that received smaller antigen particles. To assess kinetics of antigen presentation, a traceable antigen, EαGFP was covalently linked to NPs. Smaller NPs showed rapid uptake and presentation as early as 6 hours. Larger antigen NPs, on the other hand, required longer time intervals (within 24 hours) to achieve equivalent levels of uptake by APCs, however, antigen presentation was maintained beyond 72 hours. As such, although larger antigen NPs did not alter the magnitude of antigen presentation, they changed the dynamics of T cell/DC interactions, promoting stable, long-term interactions. The increased presentation duration

ultimately promoted GC formation and antibody production; this sequence exemplifies the importance of sustained antigen presentation in eliciting robust immune responses.

Size and surface chemistry can also play a role in the prolonged retention of biomaterials within LNs. Studies by the Chan lab demonstrated that antigen-conjugated gold NPs 5-15 nm in size are rapidly cleared from LNs, while larger gold NPs 50-100 nm in size are retained for over 5 weeks.[98] This translated to an increase in GC B cell formation, and 5-fold increase in antigen specific antibody production compared to smaller NPs. Interestingly, retention of nanoparticles was found to be facilitated by gold nanoparticle interactions with follicular dendritic cells (FDCs), a specialized set of APCs that can retain antigen within LNs and serve as antigen depots for B cells. Small gold NPs were taken up by FDCs, resulting in their subsequent clearance (**Figure 2.7C**). Larger NPs on the hand were retained on FDC dendrites. Additional studies suggested that serum protein adsorption to NPs during circulation to LNs promoted NP binding to FDCs. Thus, the combination of surface chemistry and increased size, offer another method to promote antigen retention.

2.8.2 Biomaterials can tune the timescales over which multiple immune signals are received

Although biomaterials can be harnessed to mimic specific dosing schedules, temporal control over the delivery of vaccines and immunotherapies can be complicated by the need to deliver multiple signals (i.e. adjuvants and antigen). This is highlighted in studies by Chen et. al. In this work, acetalated dextran (Ace-DEX) MPs with distinct degradation profiles were used to deliver model antigen or adjuvant.[96] Encapsulated adjuvant generated stronger responses then soluble antigen, as indicated by faster-degrading MPs that promoted larger humoral and cellular

responses in mice at earlier time points, while slow-degrading MPs drove stronger responses at later time points. MPs that degraded very quickly were associated with the lowest level of antibody responses. This result was likely due to faster clearance and therefore, less adjuvant exposure. When antigen was encapsulated within Ace-DEX MPs to test for controlled antigen delivery, fast-degrading MPs induced greater antibody and cytokine production throughout the length of the experiment. These findings suggest that faster-degrading Ace-DEX MPs may be beneficial to fighting diseases requiring a rapid antibody response or for individuals who need protection quickly, such post-exposure prophylaxis during accidental exposure to pathogens. Slower degrading MPs may be advantageous for conditions that would benefit from a more sustained immune response. It is also important to note that antibody responses had opposing relationships for the release kinetics of adjuvant versus antigen: delivery of adjuvant with fast-degrading MPs resulted in lower antibody response, but delivery of antigen with fast-degrading MPs induced greater antibody responses. This suggests a possible need for distinct control over adjuvant and antigen delivery.

Further supporting the need for well-designed dosing schedules, Tzeng et. al have demonstrated that effective combination cancer immunotherapy is highly dependent on the order of administration of each individual immunotherapy. [175] In these studies, a tumor specific antibody was combined with immunostimulatory cytokine to activate DCs, IFNα, to treat established tumors in a mouse melanoma model. Interestingly, improved survival rates were achieved only when IFNα was administered at a later time point (48 hours, 96 hours), following treatment with the tumor antibody. This finding suggests a requirement that DC maturation occur after generation of antigenic tumor debris. One hypothesis is that DC maturation results in the loss of the ability to

phagocytose antigen. As such, administration of IFNα prior to treatment with tumor antibody to expose tumor antigens resulted in markedly worse therapeutic outcomes and lower survival rates.

In contrast, studies from the Mirkin lab suggest a need for similar timescales of antigen and adjuvant delivery. [99] Spherical nucleic acids (SNAs) comprised of CpG and peptide antigen that are compositionally similar but vary in antigen incorporation were used to study different mechanisms of co-delivery of antigen and immunostimulatory signals. In this work, superior anti-tumor immune responses were generated when antigen presentation and costimulatory markers were presented in tandem. These constructs were synthesized by absorbing CpG to the surface of liposomes and varying the position and/or conjugation chemistry of antigen peptides by i) encapsulating soluble antigen (SNA-E) ii) absorption of antigen to the liposomal surface (SNA-A) iii) hybridizing peptide to adsorbed CpG (SNA-H) (**Figure 2.7D**). These differences in antigen delivery resulted in different kinetics of peptide presentation, with SNA-A and SNA-H particles inducing peptide presentation at slower rates compared to SNA-E. These differences are likely attributed to the need for processing and dissociation of antigen adsorbed to the surface of SNAs. Importantly, the synchronization of peptide presentation and costimulatory marker expression was found to be important for generating cytotoxic and memory T cell phenotypes. Mice immunized with SNA-H particles exhibited the highest numbers of these antigen-specific $CD8^+$ T cells cell types. Thus, not only can the modularity of biomaterials control release kinetics of immune signals, but they can also be tuned to control the kinetics of immune signal presentation by other cells.

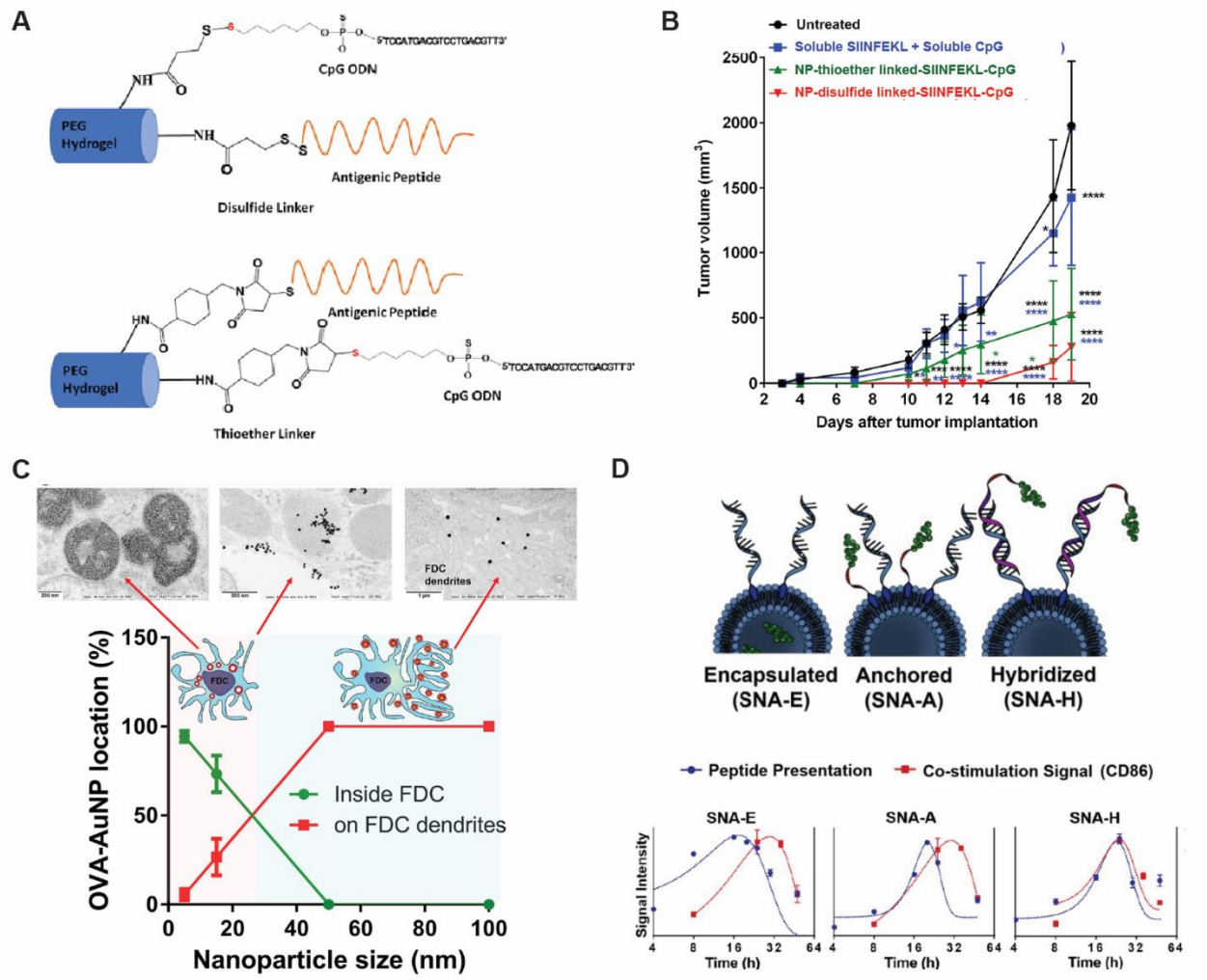

Figure 2.7 Tunable properties of biomaterials allow control over the persistence and pharmacokinetics to improve the quality of adaptive immune responses

A) Slower release of antigen from NPs conjugated to antigen via slower releasing thioether-linkages results in improved antigen presentation over time compared to NPs conjugated to fast releasing disulfide bonds B) Mice vaccinated with NPs conjugated to antigen by thioether linkages exhibit enhanced protection against tumor challenge, resulting in tumor growth inhibition up to 14 days post inoculation compared to 3 days and 7 days for soluble vaccine and NPs conjugated to antigen with disulfide bonds, respectively. Reproduced with permission.[95] Copyright 2017, Elsevier. C) FDCs internalize smaller NPs while larger NPs are retained on the surface, allowing for prolonged antigen availability. Reproduced with permission.[98] Copyright 2019, American Chemical Society. D) Spherical nucleic acids (SNAs) comprised of CpG and peptide antigen that are compositionally similar but vary in the position and/or conjugation chemistry of antigen peptides. Differences in antigen delivery result in different kinetics of peptide presentation and expressions of co-stimulatory markers. Reproduced with permission.[99] Copyright 2019, National Academy of Sciences.

2.9 Concluding Remarks

Despite increased insight into how biomaterials can be engineered to promote immune responses, the interplay between material properties remains a challenge in defining universal design criteria. For instance, changes in shape can alter size. Similarly, surface modifications can introduce changes in both charge and hydrophocity, making it difficult to isolate individual physicochemical parameters. Further, biomaterial carriers span a large collection of platforms each with their own set of optimal design parameters. A detailed understanding of the immune processes that biomaterials can influence and how they can achieve this control will pave the way towards more sophisticated biomaterial designs. Many of the studies discussed here offer new insight into how material properties can be tuned to affect the delivery of immune signals to program the immune system towards immunity or tolerance. Importantly, several biological processes and considerations such as targeting to immune tissue, uptake, controlled delivery of adjuvant and antigens (i.e. conformation, timing) can heavily influence immune responses, offering multiple avenues and targets through which biomaterials can alter innate and adaptive immune function. Studies that isolate specific design parameters (e.g. size, shape) or investigate the relative roles of multiple parameters will allow for greater understanding of these mechanisms and support design of future biomaterial-based vaccines and immunotherapies that serve as precision technologies.

Chapter 3: Polyplex interaction strength as a driver of potency during cancer immunotherapy ‡

3.1 Introduction

Following the review of biomaterial engineering strategies to control immune function provided in **Chapter 2,** this chapter highlights one approach that to improving delivery of immune signals for cancer vaccination. Many experimental cancer vaccines are exploring toll-like receptor agonists (TLRas) such as CpG, a DNA motif that agonizes toll-like receptor 9 (TLR9), to trigger immune responses that are potent and molecule-specific. The ability to tune the immune response is especially important in the immunosuppressive microenvironments of tumors. Because TLR9 is located intracellularly, CpG must be internalized by immune cells for functionality. Polyplexes can be self-assembled through electrostatics using DNA (anionic) condensed by a positively charged carrier. These structures improve cell delivery and have been widely explored for gene therapy. In contrast, here cationic poly (β-amino esters) (PBAEs) are used to assemble polyplexes from CpG as an adjuvant to target and improve immune stimulation in cellular and mouse models. Polyplexes were formed over a range of PBAE:CpG ratios, resulting in a library of complexes with an increasingly positive charge and stronger binding with increasing PBAE:CpG ratios. Although higher PBAE:CpG ratios exhibited improved CpG uptake, lower ratios of PBAE:CpG, which condensed CpG more weakly, activated DCs and tumor-specific T cells more effectively. In a mouse melanoma model, polyplexes with lower binding affinities improved survival more effectively compared with higher binding affinities. These data demonstrate that altering the polyplex interaction strength impacts accessibility of CpG to TLRs in immune cells. Thus, physiochemical properties, particularly the interplay between charge, uptake, and affinity, play a

‡ Adapted from: **Tsai SJ,** Andorko, JI, Zeng X, Gammon JM, and CM Jewell**.** "Polyplex interaction strength as a driver of potency during cancer immunotherapy." *NanoResearch.* **2018**, *11*, 5642-5656.

key role in determining the nature and efficacy of the immune response generated. This insight identifies new design considerations that must be balanced for engineering effective immunotherapies and vaccines.

3.2 Background

Cancer vaccination offers an alternative approach to conventional treatments (i.e. resection, radiation, chemotherapy) by arming immune cells against fragments of tumor termed antigens. These vaccines are comprised of antigens in the form of tumor-associated peptides or proteins, and immunostimulatory molecules called adjuvants. As introduced in **Section 2.3.1**, following immunization, antigen-presenting cells (APCs), such as dendritic cells (DCs) take up and present antigen, express co-stimulatory molecules, and produce distinct cytokines that activate and expand cytotoxic T cells (CTLs) able to attack tumors [1, 2]. However, cancer vaccines fail to elicit strong anti-tumor responses due to poor expansion of T cells specific for weakly immunogenic tumor antigens, and due to the challenge of maintaining anti-tumor responses in the immunosuppressive microenvironment of tumors.

A potential strategy to improve T cell responses to vaccines is use of well-defined molecular adjuvants that activate specific innate immune pathways, signaling that ultimately determines the type and effectiveness of T cell responses that develop. Improved understanding of the innate immune system has allowed for the discovery and design of new immunomodulatory molecules that can target specific pathways to generate robust pro-immune responses and enhance tumor-specific T cell expansion [3–5]. Toll-like receptor (TLR) agonists have emerged as a novel class of adjuvants capable of inducing potent T cell responses [6–8]. As discussed in **Section 2.3.**1, TLRs recognize pathogen-associated molecular patterns that are widely expressed on bacteria and

viruses, but rare in host cells. TLRas serve as adjuvants by mimicking these motifs, which upon binding to TLRs, can trigger specific immune signaling cascades. Several FDA-approved immunotherapies have emerged such as Cervarix (cervical cancer) and Aldara (basal cell carcinoma), which target TLR4 and TLR7/8 respectively, with many others TLR-based trials exploring other indications [182]. Several candidate cancer vaccines have explored CpG – a DNA motif commonly found in bacteria that agonizes toll-like receptor 9 (TLR9) – as a stimulus to trigger more potent immune responses during tumor immunotherapy [183–186]. However, because TLR9 is located intracellularly within endosomes, CpG must be internalized by immune cells to be effective [187].

As discussed in **Chapter 2**, biomaterials offer control over how cargo are internalized and processed, creating a route to enhance TLRa delivery [15-17]. Additionally, loading nucleic acid therapeutics into nanoparticles can provide protection against nucleases and the ability to target cargo to specific cells or intracellular locations. In contrast, the delivery of free DNA molecules is impeded by negative charge, limiting the capacity for endocytosis into cells due to electrostatic repulsion with negatively charged cell membranes. Further, because of the larger size of nucleic acid therapeutics relative to small molecule drugs, nanoparticles offer unique transport properties to control biodistribution of these cargos [18, 19]. Lastly, the physical properties of nanoparticles (i.e., size, shape, and charge) can be tuned to control cargo loading, incorporation of multiple components, and even the immunogenicity of the cargo [20, 21].

An important class of biomaterials in nucleic acid delivery are polyplexes assembled through electrostatic condensation of nucleic acids (anionic) with positively-charged polymers. The resulting nanoparticles improve nucleic acid delivery to cells and have been widely

investigated for gene therapy [22, 23]. Polyplexes increase the delivery level of cargo to cells and offer modularity that can be leveraged in vaccine design. For example, specific nucleic acid adjuvants – or antigens encoded in nucleic acids – can be incorporated into polyplexes without changing the basic electrostatic assembly process. Likewise, many TLRas are based on nucleic acids, offering flexibility to deliver difference classes of adjuvants in polyplexes.

Poly(β-amino esters) (PBAEs) are degradable, cationic polymers that have been intensely explored as vaccine carriers [24, 25] . These polymers readily form polyplexes with nucleic acids and degrade on the order of hours to help release nucleic acids cargo (e.g., DNA encoding antigen) once within the acidic conditions of lysosomes during endocytic uptake processes. Despite these advantages, polyplexes have primarily been explored for antigen delivery, not as a technology to deliver nucleic acid-based adjuvants (e.g., TLRas). Here we investigate this strategy by establishing the immunogenicity of polyplexes formed from PBAEs and CpG (TLR9a). We also link the physical properties – interaction strength between components, for example – to distinct interactions with immune cells, and ultimately, to differences in immunogenicity during cancer vaccination.

Due to the cationic nature of PBAEs, we hypothesized PBAEs could self-assemble into polyplexes with CpG via electrostatic condensation, and further, that these simple, modular nanoparticles could improve immune stimulation by providing cargo protection, improved uptake by dendritic cells (DCs), and controlled adjuvant release in immune cells. We reasoned these effects might be enabled by efficient delivery to endosomes of APCs, where TLR9 receptors are expressed. We confirmed these outcomes in primary cells and animal models. However, using a variety of molecular and immunological tools, we also made an intriguing discovery that the ratio

of PBAE to CpG in polyplexes modulates the interaction strength within the polyplexes. As a result, even when the level of CpG remained constant, these changing interactions altered the accessibility of the TLRa to immune cells, playing a driving role in the strength and efficacy of immune response in cell culture and mouse models of cancer. In particular, the formulations that led to the greatest uptake levels of CpG, were not the most potent, because the TLRa was so tightly bound that APCs were unable to access the adjuvant. Our findings illustrate the powerful role that physicochemical properties play in vaccine and immunotherapy performance, and a need for careful characterization of nanoparticle delivery systems delivering cargo for specific pathways such as TLRas.

3.3 Materials and Methods

3.3.1 Materials

Monomers for polymer synthesis (1,4-butanediol diacrylate and 4,4-trimethylenedipiperidine) were purchased from Alfa Aesar (Ward Hill, MA) and Sigma–Aldrich (St. Louis, MO), respectively. Tetrahydrofuran (THF), diethyl ether, β-mercaptoethanol and sodium acetate (SA) buffer were also purchased from Sigma–Aldrich. RPMI-1640 media was purchased from Lonza (Allendale, NJ). Non-essential amino acids and HEPES solution were purchased from Fisher Scientific (Hampton, NH). CpG DNA (5'-TCC ATG ACG TTC CTG ACG TT-3') was synthesized by IDT. Trp2 peptide (SVYDFFVWL) formulated as a disodium salt was synthesized by Genscript. Fetal bovine serum (FBS) and phosphate buffer solution (PBS) was supplied by Corning (Tewksbury, MA). CD11c microbeads were purchased from Miltenyi Biotech (Cambridge, MA). Spleen Dissociation Medium and CD8 negative selection kits were from STEMCELL Technologies (Vancouver, British Columbia, Canada). DNase I kits with 10X

reaction buffer were from New England Biolabs (Ipswich, MA). Cy5 nucleic acid labelling kits were purchased from Mirus (Madison, WI). Fluorescent antibody conjugates (CD40, CD80, CD86, MHC-II) and enzyme-linked immunosorbent assay (ELISA) were purchased from BD (San Jose, CA) or eBioscience (San Diego, CA). Wheat Germ Agglutinin (WGA), Oregon Green conjugate and Hoescht stain were purchased from Thermo Fisher. 5(6)Carboxy-fluorescein diacetate N-succinimidyl ester (CFSE) was purchased from Sigma–Aldrich.

3.3.2 Cells and animals

All primary cells were isolated from 6-8 week old C57BL/6J mice (Jackson Laboratories). For reporter studies, HEK-Blue™ TLR9 reported cells (Invivogen) were used. For T cell studies, Trp2-clone37 mice (National Cancer Institute, National Institutes of Health), a transgenic strain which has $CD8^+$ T cell receptors specific to Trp2. For tumor studies, 6-week-old female C57BL6J mice from Jackson Laboratories were used. All animals were cared for in compliance with Federal, State, and local guidelines, and using protocols reviewed and approved by the University of Maryland's Institutional Animal Care and USE Committee (IACUC).

3.3.3 PBAE synthesis

PBAE was synthesized via a Michael-type addition reaction as described previously [196]. Briefly, 9mmol of 4,4'trimethylenepiperidine was dissolved in anhydrous THF to form a 500 mg/mL solution. The solution was then added to 9 mmol of 1,4-butanediol diacrylate and the reaction was heated to 50°C and stirred for 16 h. The reaction was cooled to room temperature and the resulting polymer was precipitated in ice cold diethyl ether under vigorously stirring. PBAE was then collected and washed with additional diethyl ether and lyophilized.

3.3.4 CpG polyplex synthesis and degradation

PBAE/CpG particles were assembled via electrostatic condensation by mixing 5 mM PBAE and 31 μM CpG at varying N:P ratio between 1:5 and 5:1, where N:P ratios are determined by comparing the number of amine groups (N) on cationic polymers to the phosphate groups (P) on negatively charged CpG. For each polyplex preparation, 10 μg of CpG was used to form particles with varying quantities of PBAE, while maintaining a fixed overall volume. Thus, the amount of CpG in each polyplex formulation maintained constant irrespective of N:P ratio. For degradation studies, PBAE/CpG complexes were formed in either pH 7 buffer (1X PBS) or pH5 buffer (100mM SA), and incubated at 37°C for specified time intervals up to 48 h.

3.3.5 Characterization of polyplex size and charge

Hydrodynamic diameter and zeta potential of the polyplexes was measured in triplicate using a Malvern Zetasizer Nano ZS90 (Westborough, MA).

3.3.6 DC activation and uptake

CD11+c cells were isolated from spleens by magnetic isolation in accordance with manufacturer protocols (Miltenyi) and plated into 96-well plates at 10^5 cells/well. In RPMI 1640 media supplemented with 10% FBS, 2mM, L-glutamine, 1X non-essential amino acids, 10mM HEPES buffer, 1% penicillin and streptomycin (Gibco), and 55 uM β-mercaptoethanol. For activation studies, DCs were treated with the following: i) buffer ii) 200ng of soluble CpG iii) soluble PBAE iv) 200ng of a random oligonucleotide ("CTRL") complexed with PBAE at 1:1 N:P ratio, or v) 200 ng of CpG complexed with PBAEs at increasing N:P ratio. After 24 h, cells were stained for viability (DAPI) and surface activation markers (CD40, CD80, CD86, and Major

Histocompatibility Complex II (MHC-II)) and analyzed by flow cytometry. For uptake studies, CpG was labelled with Cy5 per manufacturer instructions and Cy5-CpG was used to form complexes. DCs were incubated with polyplexes for 24 h, collected, stained for DAPI, and analyzed by flow cytometry. Flow cytometry data was collected on a Canto II (BD Biosciences) and analyzed by FlowJo (Tree Star). Uptake was also confirmed by confocal microscopy. CD11c+ cells were isolated and 10^6 cells were plated onto glass-bottom dishes with No. 1.5 thickness (MatTek). Again, cells were incubated for 24 h, after which cells were fixed in 4% paraformaldehyde, stained for membrane (wheat germ agglutinin (WGA), Oregon Green conjugate) and resuspended in Hoescht for imaging. Images were taken using a Leica SP5X Laser Scanning Confocal and analyzed by FIJI/ImageJ (National Health Institute).

3.3.7 DC/T Cell Co-culture

Primary $CD11c^+$ cells were isolated as above, plated at 5 x 10^5 cells, and treated with polyplexes. A suboptimal dose of a model antigen (Trp2) in soluble form was added to all wells except indicated controls. After incubation for 24 h, $CD8^+$ T cells were isolated from Trp2-clone 37 mice (National Cancer Institute, NIH), a transgenic strain specific for Trp2. Following negative selection via magnetic isolation in accordance with manufacturer instructions (STEMCELL Technologies), T cells were labelled by incubating with 50 µM CFSE per mL of cells for 5 min at room temperature, followed by washing in media. 1.5 x 10^5 of CFSE labelled Trp2 T cells were then added to treated DC cultures and cultured for an additional 72 h. After incubation, cells were collected and stained for T cell specific surface markers (CD3e, CD8a), and resupended in 4′,6-diamidino-2-phenylindole (DAPI). T cell proliferation was determined by flow cytometry to measure CFSE dilution.

3.3.8 SYBR Green gel migration assay

Polyplexes of varying N:P ratios were loaded onto a 4% agarose gel stained with SYBR green I (Invitrogen) and loading dye and run at 120V for 20 min. The gel was then imaged by a UV illuminator.

3.3.9 Ethidium bromide exclusion assay

Ethidium bromide (EtBr) was added to polyplexes at a 1:5 mass ratio to CpG content and incubated for 1 h. Fluorescence was measured using an excitation wavelength of 540 nm and an emission wavelength of 570 nm. The fluorescence of EtBr alone was subtracted from all samples and an intensity ratio was calculated by comparing the fluorescence of polyplexes with EtBr to the fluorescence of free CpG and EtBr.

3.3.10 Enzymatic degradation assay

Polyplexes of varying N:P ratios were made using Cy5-CpG and PBAE in 100 uL 1X DNA I reaction buffer. The fluorescence was measured using an excitation wavelength of 640 nm and an emission wavelength of 670 nm. 2 units of DNAse I (New England Biolabs) were then added to each complex, mixed, and incubated for 1 h at 37 °C. Following incubation, the fluorescence was immediately measured again and the extent of degradation of Cy5-CpG in polyplexes was determined by comparing fluorescence intensities relative to free Cy5-CpG. Fluorescent measurement was chosen to quantify CpG amount over spectrophotometry because PBAEs exhibit absorbance overlap at 260 nm.

3.3.11 Tumor studies in mice

Mice were shaved and injected *s.c.* at the right hind flank with 5×10^5 B16-OVA cells in 50 μL of PBS, and weighed and monitored daily for tumor growth. Tumor size was calculated as the product of two orthogonal diameters. Mice were treated intratumorally with 50 μL of PBS, PBAE/CTRL or PBAE/CpG when aggregate tumor burden reached 50 mm^2. Each group received an additional three doses every three days following initial treatment. Mice were euthanized according to the IACUC-approved humane endpoints when aggregate tumor burden reached 150 mm^2.

3.3.12 Statistical analysis

One-way ANOVA with a Turkey post-test was used to compare three or more groups for materials characterization and in vitro studies, with post-test corrections for multiple comparisons. Unpaired t-tests were used to compare survival between groups at each study day. For all tests, p values < 0.05 were considered significant. For all figures: *$p < 0.05$, **$p < 0.01$,***$p < 0.001$, ****$p < 0.0001$, ns = not significant.

3.4 Results and discussion

3.4.1 PBAE and CpG self-assemble to form polyplexes

We first tested if polyplex structures could be formed from CpG and PBAEs (**Fig. 1a**). To allow for consistent analysis, the mass of CpG was fixed for all formulations, while the mass of PBAE was varied to form complexes that spanned N:P ratios of 1:5 to 5:1. The N:P ratio is a common parameter to assess the relative charge, defined in our studies as the ratio of positively charged PBAE amines (N) to negatively charged nucleic acid phosphate groups in the CpG

backbone. This design resulted in a library of complexes of similar size, but varying charges, with higher PBAE:CpG forming more positively charged particles (**Fig. 3.1b, 3.1c**). Dynamic light scattering confirmed the formation of complexes with hydrodynamic diameters ranging from 196.0 ± 26.8 to 300.5 ± 105 nm (**Fig. 3.1b**). These sizes were not significantly different across the charge ratios tested. This was an important consideration for our studies since size has been shown to play an important role in vaccine particle uptake, antigen processing, and immune activation [17, 18].

Zeta potential measurements revealed that at lower N:P ratios (i.e. 1:5), polyplexes exhibited negative surface charges, while at higher N:P ratios, the zeta potential increased with the relative amount of PBAE in the polyplexes (**Fig. 3.1c**). Charges ranged from -27.9 ± 1.7 mV (1:5) to 19.4 ± 3.7 mV (5:1), demonstrating the tunability of surface charge. This range of surface charges is particularly interesting since the amount of CpG was fixed. One possibility to explain these values is that the negative surface charges at lower N:P ratios results from exposed CpG on polyplex surfaces, while the positive surface charge at higher N:P ratios results from surfaces comprised primarily of PBAE with CpG condensed within the particles. Another possible arrangement is that the increasing cationic charge compensates the fixed anionic charge as N:P ratio increases, but the entangled PBAE and CpG polymers ensure the particles remain assembled. In both scenarios, higher N:P ratios result from an increased level of PBAEs. We expected this increase to improve adjuvant delivery because of an increased number of electrostatic interactions with CpG, causing tighter condensation of the adjuvant to enable more efficient uptake.

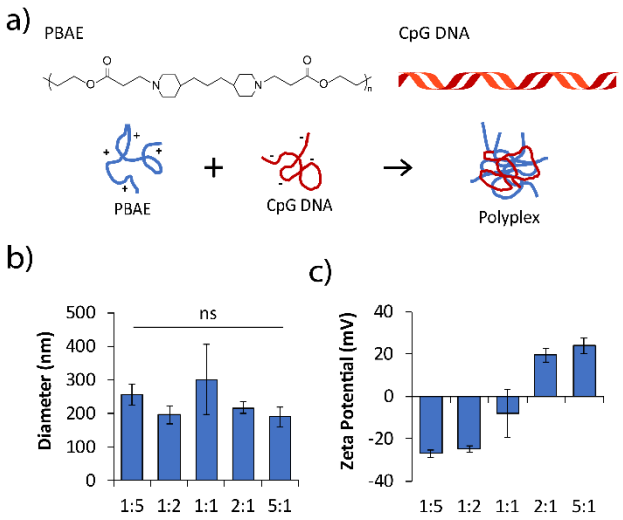

Figure 3.1 PBAE and CpG self-assemble to form polyplexes
(a) Schematic of polyplex assembly with chemical structure of PBAE (b) Hydrodynamic diameter measurements of polyplexes confirming formation of nanoparticular polyplexes. Polyplex diameter does not vary significantly in size across all tested ratios (c) Surface charge is readily tunable by altering the amount of PBAE during polyplex assembly.

3.4.2 PBAE/CpG polyplexes are taken up by DCs in a dose dependent manner

To elicit immune responses, polyplexes must deliver CpG to endosomes within immune cells where CpG can bind TLR9 to initiate immunostimulatory signaling cascades. To begin dissecting this process, we measured the level of polyplexes internalized by primary DCs. DCs were isolated from the spleens of mice, incubated with polyplexes formed from fluorescently-labelled CpG, then analyzed by flow cytometry; corresponding free components were also included as controls. Polyplexes exhibited dose-dependent uptake, with significantly increased

mean fluorescence intensities (MFI) at higher treatment concentrations (**Fig. 3.2a**). Polyplexes were more readily internalized at higher N:P ratios, with the 5:1 ratio supporting the greatest

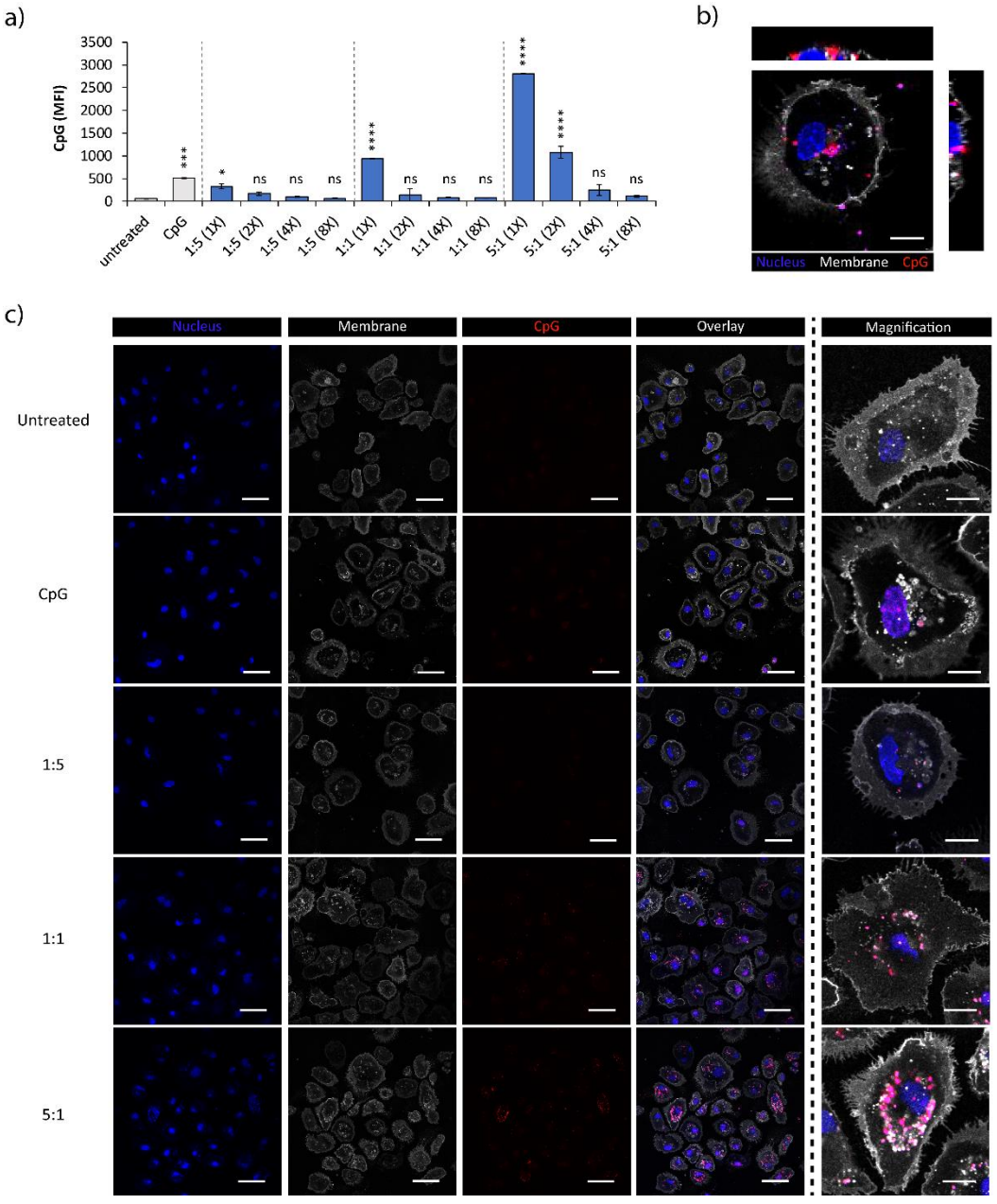

Figure 3.2 Uptake of PBAE/CpG polyplexes for 1:5, 1:1, 5:1 N:P ratio treatments
(a) Uptake of CpG into DCs after 24h incubation as measured by flow cytometry using Cy5-labelled CpG, with untreated and soluble CpG ("CpG") controls. Doses were diluted 1X, 2X, 4X, and 8X to study dose dependency (b) Reconstructed z stack image of DC uptake of 5:1 polyplexes with xz, and yz side view to indicate topographical location, scale bar = 10µm (c) Uptake of CpG

visualized by confocal microscopy with magnified image, scale bar = 10μm, 30μm and for magnified and all others, respectively. *p < 0.05, **p < 0.01, ***p < 0.001, ****p < 0.0001, ns = not significant. Statistical comparisons are vs. untreated.

fluorescence levels. These data are consistent with zeta potential measurements for 5:1 polyplexes, which exhibited a greater positive charge that could improve uptake by increasing interactions with negatively charged cell membranes. DCs were also plated onto glass-bottom dishes, treated with polyplexes, then imaged by confocal microscopy z-stack analysis to determine if polyplexes were internalized by cells, rather than simply associated with the outer membrane. Reconstructed z stack images confirmed polyplexes were contained within cells (**Fig. 3.2b**). Confocal microscopy of cells treated with each formulation also corroborated flow cytometry findings (**Fig. 3.2c**). In particular, greater localization of polyplexes within cells was observed as the N:P ratio increased, with the strongest fluorescent signals for CpG observed in cells treated with the 5:1 ratio, and signal strongly reduced in cells treated with 1:5 ratio polyplexes. High magnification images of cells treated with each formulation revealed polyplexes were distributed throughout the intracellular region, including the nucleus (**Fig. 3.2c**, last column).

3.4.3 PBAE/CpG polyplexes activate DCs & TLR9

To measure how the level of polyplex uptake correlates with DC activation as a function of N:P ratio, DCs were next treated with polyplexes ranging from a 1:5 to 5:1 ratio, or dose-matched free controls. Compared to untreated cells, PBAE/CpG polyplexes significantly increased expression of common surface activation markers, including CD80, CD40, and CD86. Surprisingly, although higher N:P ratios (i.e., 5:1) were associated with the most efficient uptake in **Fig. 3.2**, the activation levels of these polyplexes were significantly lower than 1:5 polyplexes, which were internalized less efficiently (**Fig. 3.3a-c**). Free CpG and 1:5 polyplexes exhibited no

verification that the effects of polyplex ratio were specific to adjuvant in the polyplex (i.e., CpG), we treated reporter cells transduced with human TLR9 and a reporter gene with each N:P ratio. In line with DC activation studies (**Figure 3.3a-c**), these experiments revealed selective activation of TLR9 signaling that was greatest for lower N:P ratios (**Fig. 3.3e**) – which exhibited lower uptake levels in **Fig. 3.2**. Higher N:P ratios – which exhibited greater uptake in **Fig. 3.2** – caused reduced TLR9 signaling (**Fig. 3.3e**). The lowest N:P ratio (1:5) exhibited similar levels of TLR signaling to dose matched free CpG, the highest level of signaling observed. With increasing ratio, TLR activity decreased in a dose-like manner– these findings were attributed to decreasing CpG availability. PBAE/CTRL polyplexes did not trigger TLR9 signaling, further confirming pathway-specific activity driven by CpG. Taken together, these data indicate that while polyplexes with a high N:P ratio are internalized most efficiently, those with a low N:P ratio most potently activate DCs and TLR9 signaling. These effects are not a result of differences in particle size, toxicity, or PBAE-driven stimulation.

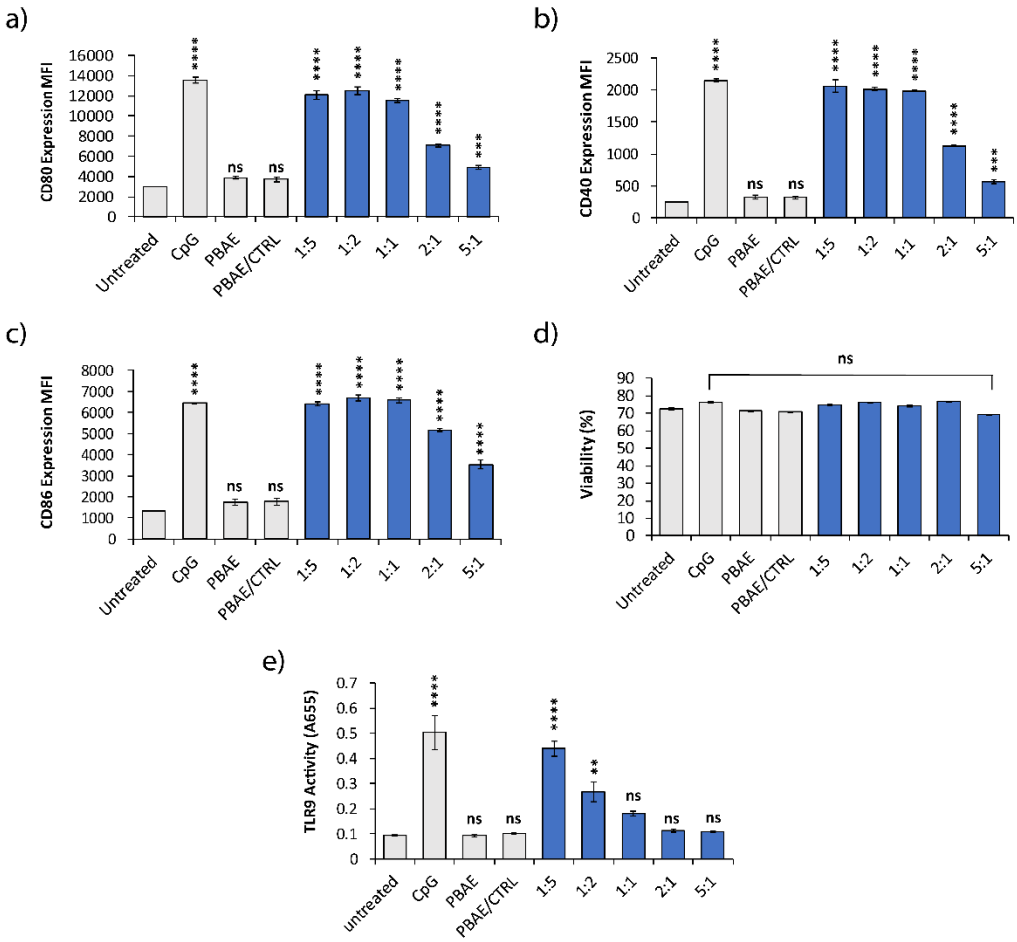

Figure 3.3 Polyplex treatment activates DCs

DC activation was measured by expression levels of immunostimulatory markers (a) CD80 (b) CD40 and (c) CD86 by staining with fluorescent antibody conjugates followed by analysis using flow cytometry (d) Viability of treated DCs was measured by quantifying $DAPI^{(-)}$ cells. (e) DC activation correlates with TLR9 activity, indicated by decreasing activity during treatment with polyplexes exhibiting higher N:P ratio. *$p < 0.05$, **$p < 0.01$, ***$p < 0.001$, ****$p < 0.0001$, ns = not significant. Statistical comparisons are vs. untreated**.**

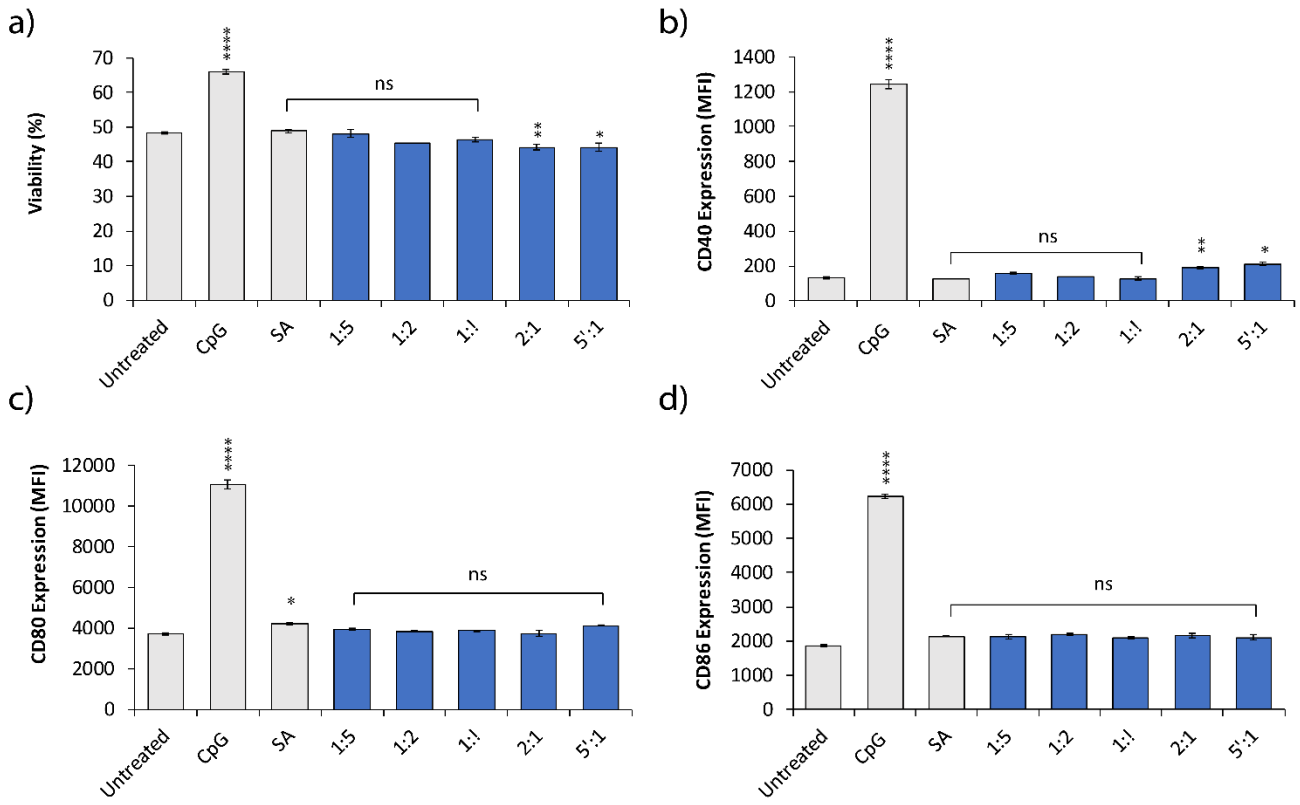

Figure 3.4 PBAE alone does not activate DCs
(a) Viability minimally differs across ratios, while activation is absent or negligible across all ratios as measured in the expression levels of (a) CD40 (b) CD80 or (c) CD86. *****p < 0.05, **p < 0.01, ***p < 0.001, ****p < 0.0001, ns = not significant. Statistical comparisons are vs. untreated.

3.4.4 N:P ratio impacts polyplex interaction strength

We hypothesized decreased adjuvant activity of high N:P ratio polyplexes might result from increased interaction strength between CpG and PBAE compared with low N:P ratios. These interactions could limit the ability of CpG to interact with TLR9 receptors. To measure these differences in binding strength, we analyzed each polyplexes formulation in an ethidium bromide (EtBr) exclusion assay. EtBr is an intercalator that strongly fluoresces when excited while to base pairs of DNA [ref]. CpG was incubated with EtBr, followed by addition of PBAE over a range of ratios (i.e., 1:5-5:1). In these studies, we observed decreased fluorescence as N:P ratio increased,

indicating that increased PBAE content at higher ratios disrupts CpG intercalation by EtBr (**Fig. 3.5a**).

Because PBAE polyplexes are internalized and released under the acidic conditions of endolysosomes [197], we next investigated the interaction strength of polyplexes under acidic pH. Under these acidic buffer conditions, nitrogen groups on PBAEs become protonated, lending to a more positively charged polymer. As a result, in EtBr exclusions studies at pH 5, polyplexes displayed stronger binding interactions compared to pH 7, as indicated by reduced fluorescence (**Fig. 3.5a**).

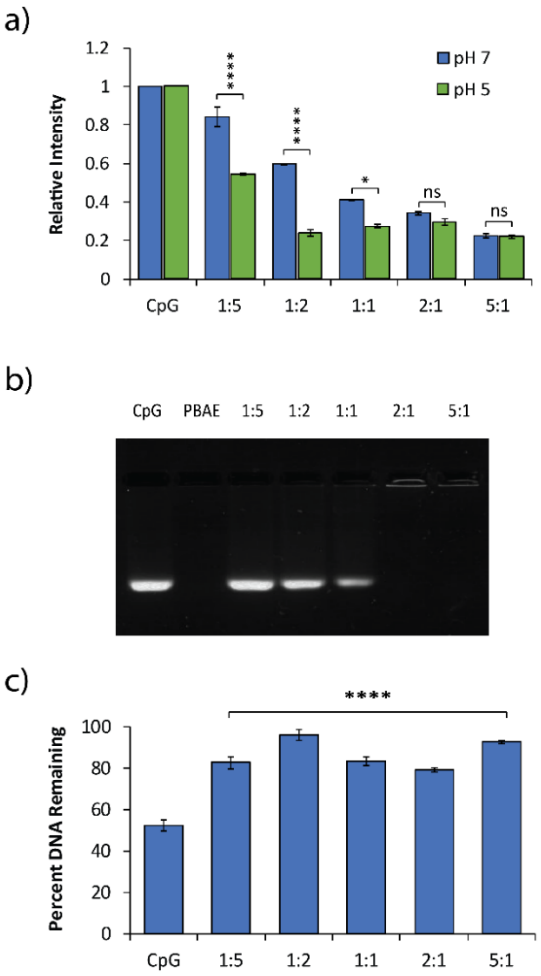

Figure 3.5 Polyplexes N:P ratio impacts interaction strength
(a) Interaction strength was measured by EtBr exclusion assay for polyplexes at pH 7 and pH 5. A reduction in fluorescent intensity relative to soluble CpG control indicates displacement of EtBr by PBAE and stronger binding. (b) Gel migration assay measuring release of CpG using an agarose gel stained with SYBR-Green I. Bands reflect CpG release under applied current. Decreasing fluorescence or absence of bands suggests tight binding of CpG by PBAEs. (c) Complexation with PBAEs provides protection against DNAse degradation. Changes in DNA concentration were determined by comparing fluorescence of PBAE/Cy5-labelled CpG complexes before and after exposure to enzymes *$p < 0.05$, **$p < 0.01$, ***$p < 0.001$, ****$p < 0.0001$, ns = not significant. Statistical comparisons are pH 5 vs pH 7 for exclusion assays, or for enzyme protection assays, before enzyme vs. after enzyme.

To directly assess CpG release from polyplexes as a function of N:P ratio, we carried out a gel migration assay by applying a current to polyplexes loaded in agarose gel. Electrophoresis revealed lower N:P ratio polyplexes were loosely bound, readily releasing CpG under an applied

voltage that migrated at the same rates as free CpG (**Fig. 3.5b**). As N:P ratio increased, this migration band disappeared. Disappearance of fluorescence can also be indicative of tighter binding between CpG and PBAE, resulting in quenching of tightly bound nucleic acids. Thus, at the highest N:P ratios – even though CpG was present at the same concentration in all wells – fluorescent signal was no longer observable. These findings corresponded with the reduced fluorescence measured in the quantitative exclusion assays, but also suggest that at ratios greater than 2:1, complete complexation of the polymer and DNA occurs as indicated by the absence of a free CpG band. At lower ratios, some non-complexed PBAE and CpG may still exist. Nevertheless, zetasizer, uptake, and EtBr exclusion assays reveal significant differences from free CpG indicating that complexation still occurs at lower ratios. In the context of the uptake and activation data, these results suggest that interaction strength plays an important role in determining the immunogenicity of vaccines and immunotherapies delivered in polyplexes or other nanoparticles. In particular, while the 5:1 ratio was internalized to the greatest extent and bound CpG tightest, the activation associate with these particles was lowest. In contrast, 1:5 polyplexes were internalized at lower levels, but exhibited weaker binding of CpG, resulting in much higher levels of activation.

Since we observed differences in interaction strength, we next tested if strong condensation of polyplexes offered protection against enzymatic degradation. Cy5-labelled CpG in free form or complexed with PBAEs was incubated with DNAse for 1 hr. Fluorescent intensity was measured to quantify the amount of DNA present before and after degradation. These studies revealed that polyplexes significantly reduced CpG degradation across all charge ratios relative to free CpG (**Fig. 3.5c**). This is important from a therapeutic standpoint because nucleases in the extracellular environment or within endosomes may degrade nucleic acids, inhibiting TLR activation.

Improving stability may not only increase half-life allowing for better bioavailability, but adjuvant persistence has also been implicated in generation of more potent and longer-lasting immune responses [198].

The data in **Fig. 1-5** indicate that polyplexes formed at the lowest N:P ratio (1:5) exhibit a blend of features between CpG and the polyplexes formed at the highest N:P ratios. For example, the 1:5 ratio results in nanoparticles with sizes similar to that of the 5:1 polyplexes (**Fig. 1b**), also providing significant protection of CpG from degradation (**Fig. 3.5c**). However, these 1:5 polyplexes do not inhibit CpG migration (**Fig. 3.5b**) because of loose binding (**Fig. 3.5a**). The charge of the 1:5 polyplexes is also more negative (**Fig. 1c**), whereas the higher content of positive charge in the 5:1 polyplexes more tightly condenses CpG (**Fig. 3.5a, 3.5b**) and offers more complete protection against DNAse. However, with the 5:1 polyplexes, CpG may be so tightly bound within complexes at these higher N:P ratios that CpG can no longer interact with TLR9 to stimulate DCs (**Fig. 3a-c**). Conversely, at lower N:P ratios, polyplexes are comprised of loosely bound CpG that is internalized by cells at significant levels (**Fig. 2**), readily accessible to interact with TLRs and activate DCs (**Fig. 3**), and still provides significant protection against enzymatic degradation. This tunability and balance of features demonstrates an important benefit over free CpG, highlighting the role of carrier interactions in immune signal delivery.

3.4.5 Expansion of functional tumor-specific T cells by polyplexes depends on N:P ratio

To test if altered DC activation driven by the different interaction strength leads to changes in T cell function, we next conducted DC/T cell co-culture studies. In these experiments splenic $CD11c^+$ DCs were isolated from mice and treated with polyplexes, along with addition of a conserved melanoma peptide (Trp2) to the wells. $CD8^+$ T cells were then isolated from Trp2

transgenic mice and co-cultured with the treated DCs. $CD8^+$ T cells from these mice display T cell receptors specific for Trp2 presented in MHC-I. Upon encountering antigen presentation cells displaying Trp2 in MHC-I with the appropriate co-stimulatory signals, these T cells expand and secrete inflammatory signals. Prior to culture, the T cells were labeled with a fluorescent dye to allow quantification of proliferation as the dye becomes diluted during successive generations of cell division.

Polyplex treatments across all N:P ratios resulted in significant proliferation of T cells when Trp2 was present, but was absent without the presence of antigen in CpG only controls, and greatly reduced when cells were treated with PBAE/CTRL (**Fig. 3.6a, 3.6b**). Importantly, all N:P ratios drove significant T cell proliferation. In agreement with DC activation studies, proliferation was lower in polyplexes with the highest N:P ratio – where DC activation was lowest – although these differences were not statistically significant. However, with respect to changes in T cell function, ELISA measurements on the culture supernatants revealed statistically significant changes in secretion of an important inflammatory cytokine, interferon gamma (IFN-γ) (**Fig. 3.6c**). Importantly, low N:P ratios maximized both T cell expansion and IFN-γ secretion (**Fig. 3.6c**), in agreement with DC activation studies – where activation was greatest following treatment with polyplexes formed at the lowest N:P ratios. Together these data suggests lower N:P ratios result in

loosely bound CpG that, while internalized at lower levels, is more accessible for processing and DC activation, and subsequently, can drive stronger antigen-specific T cell responses.

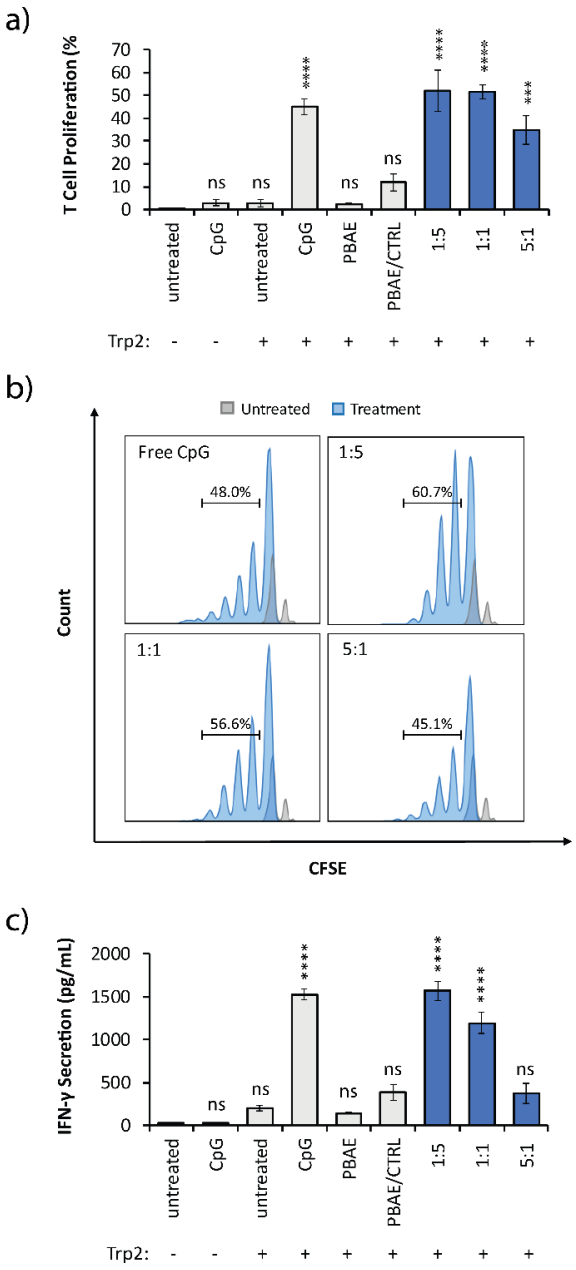

Figure 3.6 Polyplexes activate T cells and increase antigen-specific T cell proliferation
DCs were cultured with Trp2 peptide antigen and treated with soluble CpG or polyplexes. After 24h, T cells labeled with CFSE – a proliferation dye diluted with each generation of cell division – was added to culture (a) Percentage of proliferated T cells. (b) Representative flow cytometry traces illustrating CFSE dilution following treatment in the presence of antigen and compared to untreated cultures. (c) IFN-γ levels secreted in supernatants of DC/T cell co-cultures measured

by ELISA. *p < 0.05, **p < 0.01, ***p < 0.001, ****p < 0.0001, ns = not significant. Statistical comparisons are vs. untreated with Trp2.

3.4.6 Melanoma tumor burden and mouse survival depends on polyplex N:P ratio

Having identified a link between physicochemical properties of polyplexes and innate and adaptive immune responses, we next tested if differences in polyplex characteristics impact tumor progression in a mouse model of melanoma. Mice were inoculated with 5×10^5 B16-OVA cells in the right hind flank. When tumors reached an aggregate tumor size of 0.5 cm^2, mice were treated *intratumorally* with either PBS, PBAE/CTRL, 1:5 PBAE/CpG, or 5:1 PBAE/CpG polyplexes (**Fig. 3.7a**). Mice received three additional treatments every 3 days. In these studies, the dose of CTRL and CpG was constant in all groups containing either of the oligonucleotides.

Mice treated with PBS or PBAE/CTRL polyplexes exhibited mean survivals of 8.5 days, while 1:5 polyplexes and 5:1 polyplexes significantly improved survival, with mean values of 14.0 and 19.4 days, respectively (**Fig. 3.7b, 3.7c**). These improvements were also reflected in the relative rate of increase in tumor burden when assessing individual animals in each group (**Fig. 3.7d**). In particular, while both types of polyplexes slowed tumor growth relative to controls, the low N:P ratio polyplexes were more potent compared to the high N:P ratio, in agreement with the *in vitro* results. Interestingly, one mouse survived through the duration of the study and displayed no changes in tumor size during the final study week.

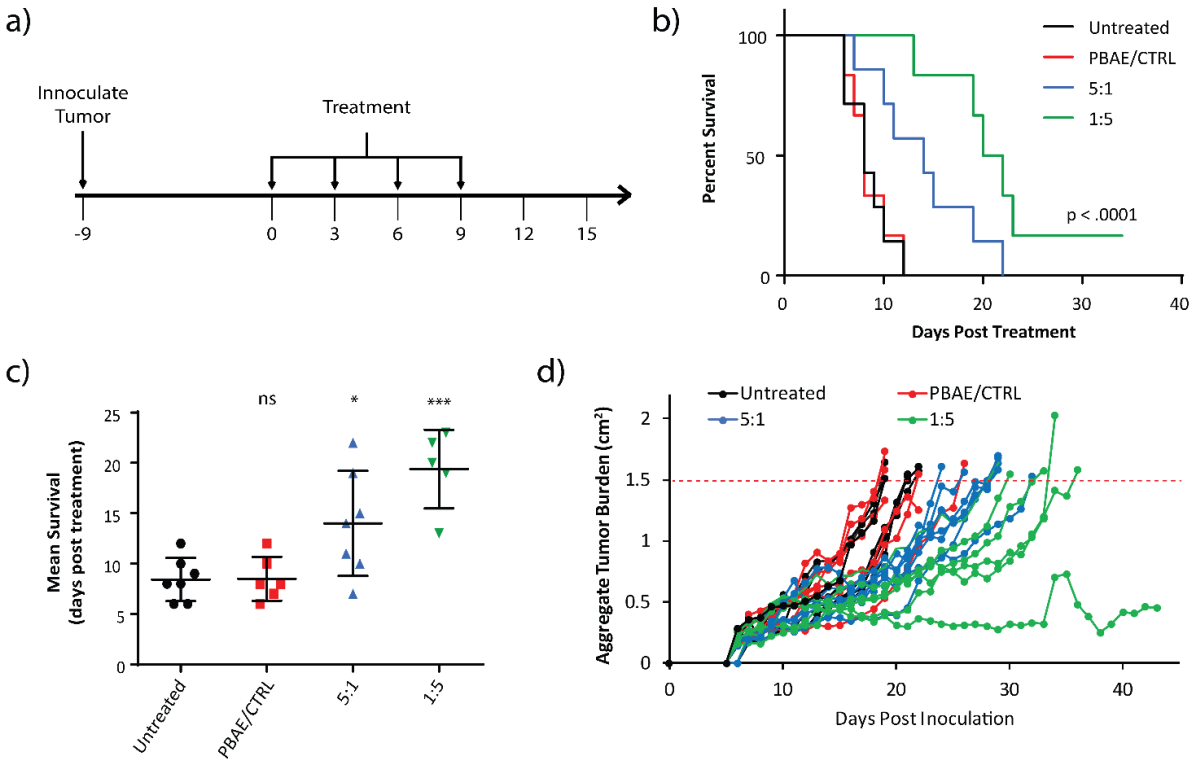

Figure 3.7 *Intratumoral* injection of polyplexes promotes survival and decreased tumor burden in a mouse melanoma model

(a) Schematic of treatment regimen. Mice were inoculated with tumors. When tumor burden reached 0.5 cm^2 (~9 days following inoculation), mice were injected with either: 1) PBS (untreated) 2) PBAE/CTRL polyplexes 3) 5:1 PBAE/CpG polyplexes or 4) 1:5 PBAE/CpG polyplexes. Mice were treated every 3 days for 4 treatments total. (b) survival curves and (c) mean survival for each treatment. Survival was measured as days post treatment. (d) tumor burden curves for each individual mouse in the study. *$p < 0.05$, **$p < 0.01$, ***$p < 0.001$, ****$p < 0.0001$, ns = not significant. Statistical comparisons are vs. untreated.

The abscopal effect occurs when therapeutic interventions at a local tumor site (e.g., resection, introduction of inflammatory cues) allows recruitment of immune cells that subsequently drive general or specific responses that help combat disseminated tumors or relapse [31–33]. For example, direct injection of CpG into tumors can activate DCs within the immunosuppressive tumor microenvironment – which also have ample exposure to tumor antigens, allowing these cells to prime tumor-specific T cells. This generation of tumor-specific

immunity may offer protection from metastasis and prevent relapse. In the context of our studies, this possibility means there is an important opportunity to drive antigen-specific, "vaccine-like" responses through abscopal effects, even though the polyplexes do not contain a tumor antigen. For future studies, we would like to prophylactically treat with different ratio of polyplexes in combination with soluble OVA prior to tumor challenge to investigate if CpG-PBAE interaction strength plays a role in priming antigen specific T cells. Further, our *in vivo* studies reveal that – as with our *in vitro* studies – the physicochemical properties of polyplexes significantly impact the efficacy of anti-tumor immunity, highlighting material characteristics as important design consideration. These effects were evidenced by the difference in anti-tumor efficacy between polyplexes formulation, even though the dose of CpG was fixed.

3.4.7 Physiochemical properties of 1:5 PBAE/CpG evolve with degradation

Since 1:5 polyplexes were the most potent adjuvants during both *in vitro* and *in vivo* studies, we focused on this ratio to test if polyplex stability also impacts processing and function of immune cells. The duration and magnitude of adjuvant exposure have been shown to play important roles in enhancing immune responses, determining cell fate of functional phenotypes (i.e. T_H1 vs. T_H2) and even establishment of memory phenotypes [178]. Because PBAEs readily undergo hydrolysis of the ester bonds (**Fig. 1a**), PBAE polyplexes degrade over time. Degradation of the polymer backbone could lead to increased CpG exposure and release, particularly under acidic conditions that mimic the microenvironment of endolysosomes (pH 5) where TLR9 is activated. These effects could result in more potent immune responses, although at pH 5, there may also be increased interaction strength that counteracts these effects. Additionally, polyplexes

may undergo changes in physiochemical properties, altering interactions with CpG and with immune cells interacting with the polyplexes.

To parse out the relative importance of the possibilities just described, we used 1:5 polyplexes and examined changes in size (**Fig. 3.8a**) as a function of time in both physiological pH (PBS, pH 7) and acidic conditions (sodium acetate buffer, pH 5). Polyplexes were self-assembled and incubated at pH 7 or pH 5 for 0, 1, 4, 24, and 48 hours. At pH 7 size remained constant, while at pH 5, polyplexes increased in size with time, although the changes were not statistically significant because the distributions became more heterogeneous. Zeta potential measurements revealed that over time, 1:5 polyplexes became more positive, with a charge reversal occurring at later time points under acidic conditions (**Fig. 3.8b**). These changes over time may impact association with cells, such that as polyplexes degrade, they are more favorably internalized by the cell because they more likely to interact with the negatively cell membrane. EtBr fluorescent assays demonstrated no significant changes in interaction strength during over time at pH 7 (**Fig. 3.8c**). At pH 5, binding appeared lower compare with pH 7, with some weak trends as a function of time. Because interaction strength is a key driver for immune cell activation with these polyplexes – and we did not observe changes in affinity as a function of time (**Fig. 3.8c**) – the ability of polyplexes to activate DCs was expected to be stable over 48 hrs. However, since polyplexes at pH 7 appeared to bind CpG more weakly than pH 5 at each time point during stability tests (**Fig. 3.8c**), we speculated polyplexes incubated at pH 7 would display higher levels of activation compared with those incubated at pH 5.

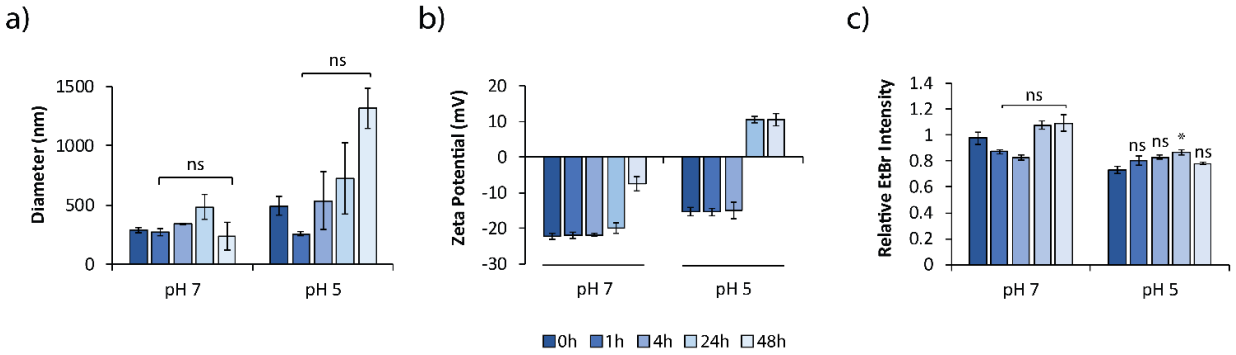

Figure 3.8 Stability of 1:5 polyplexes over time at pH 5 and pH 7
(a) Polyplex diameter does not change significantly but becomes less uniform, while (b) Zeta potential becomes more positive over time. (c) Interaction strength between PBAE and CpG over time at pH 5 and pH 7. *$p < 0.05$, ns = not significant. Statistical are vs. the initial time (i.e., 0h).

3.4.8 PBAE/CpG polyplexes exhibit decreased immunostimulatory potential following incubation in acidic conditions

Based on the rationale just described, we next carried out DC activation studies using 1:5 polyplexes incubated at either pH 5 or pH 7 for up to 48 hrs prior to culturing with primary DCs. As expected based on the data in **Fig. 3.8**, there was generally no dependence on time for either pH 5 or pH 7. For all three markers, polyplexes incubated at pH 7 prior to culture strongly activated DCs at levels that were equal to or greater than those of free CpG. Further, polyplexes incubated at pH 7 before culturing with the DCs activated cells more strongly than polyplexes incubated at pH 5 before culture (**Fig. 3.9a-c**). This was particularly evident for CD40 (**Fig. 3.9a**), where polyplexes incubated at pH 5 did not activate DCs relative to negative controls. Similar but more modest effects were observed for CD80 (**Fig. 3.9b**) and CD86 (**Fig. 3.9c**).

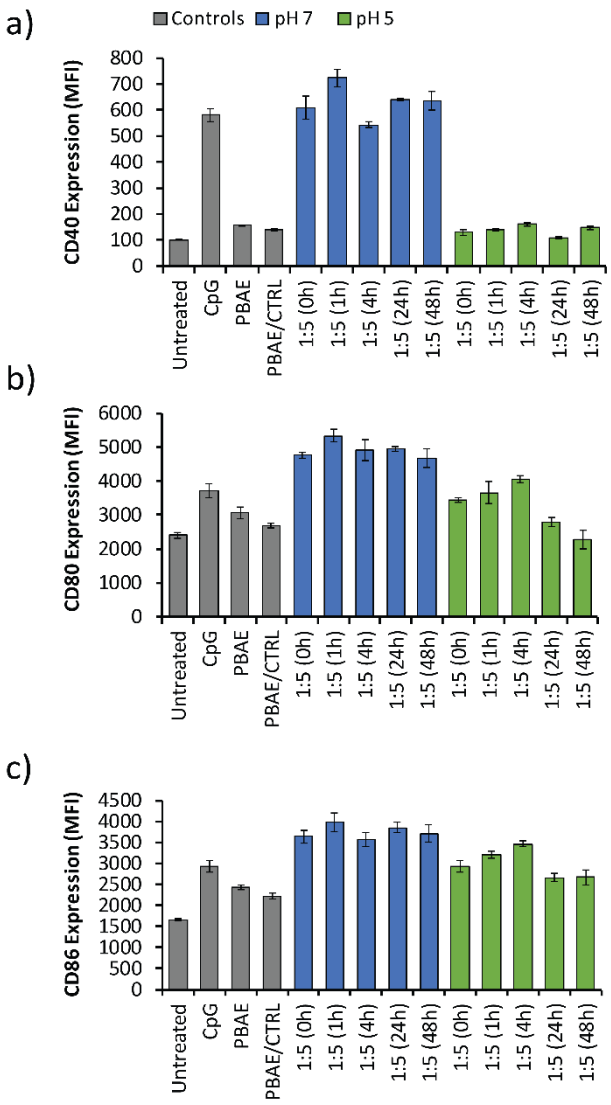

Figure 3.9 Impact of polyplexes stability testing on DC activation
Polyplexes were incubated for the indicated times at either pH 5 or pH 7, then cultured with DCs to assess activation by measuring (a) CD40 (b) CD80 or (c) CD86 expression.

The results in **Fig. 3.9** reveal a strong effect of pH on the activation potential of polyplexes. This is unsurprising since pH alters the protonation state of PBAEs, with lower pH conditions increasing the positive charge of the polymers. In the context of our DC studies, the resulting increase in binding at pH 5 versus pH 7 appears to limit DC activation. Interestingly, for polyplexes incubated at pH 5 before cell culture, there was a weak dependence on time for CD80 and CD86 that peaked at intermediate time points. These times are also approximately where polyplexes

incubated at pH 5 showed small decreases in interaction strength (**Fig. 3.8c**). This pair of observations could provide an initial clue to link changes in CpG binding as PBAEs degrade to the resulting changes in TLR9 accessibility that controls DC activation. However, more in depth studies are required to explore this possibility.

3.5 Conclusions

TLRs are an exciting target to improve the selectivity and potency of vaccines and immunotherapy. Because many of these pathways are spatially restricted within cells, biomaterials offer a means to deliver immunostimulatory signals and protect cargo, but also create the potential to tune physiochemical properties (i.e. size, charge) for improved uptake and potency. Our results demonstrate a simple self-assembly system for delivering TLR agonists to potently activate DCs, which subsequently activate T cells for strong antigen-specific responses. *In vivo* these effects translate to improved survival and reduced tumor burdens. Importantly, our studies reveal a balance of distinct nanoparticle characteristics that are important in nanoparticle design and efficacy. Cargo encapsulation, protection, and improved uptake – while desireable – are not sufficient for immunogenicty; immune signals must also be accessible for processing by APCs, which can be inhibited if interaction strength is too great. This knowledge contributes to the design of new adjuvant carriers for vaccines and immunotherapies. Many of the design considerations presented here are also studied in **Chapter 3** to co-deliver self-assembled structures comprised of both adjuvant and antigen.

Chapter 4: Altering antigen charge to control self-assembly of immune signals during cancer vaccination [§]

4.1 Introduction

As highlighted in **Chapter 2**, biomaterial delivery systems offer unique potential to improve cancer vaccines by offering targeted delivery and modularity to address disease heterogeneity. Here, we develop a simple platform using a conserved human melanoma peptide antigen (Trp2) modified with cationic arginine residues that condenses an anionic toll-like receptor agonist (TLRa), CpG, into polyplex-like nanoparticles. Building upon the advantages of polyplexes demonstrated in **Chapter 3,** we reasoned that these structures could offer several useful features for immunotherapy – such as tunable loading, co-delivery of immune cues, and cargo protection – while eliminating the need for synthetic polymers or other complicating delivery systems. We demonstrate that Trp2/CpG polyplexes can readily form over a range of Trp2:CpG ratios and improve antigen uptake by primary antigen presenting cells. We show antigen loading can be tuned by interchanging Trp2 peptides with defined charges and numbers of arginine residues. Notably, these polyplexes with greater antigen loading enhance the functionality of Trp-2 specific T cells and in a mouse melanoma model, decrease tumor burden and improve survival. This work highlights opportunities to control the biophysical properties of nanostructured materials built from immune signals to enhance immunotherapy, without the added complexity or background immune effects often associated with synthetic carriers.

[§]Adapted from: **Tsai SJ,** Amerman A, Jewell CM. "Altering antigen charge to control self-assembly and processing of immune signals during cancer vaccination." *Frontiers in Immunology.* **2021**.

4.2 Background

As mentioned in **Chapter 3**, cancer vaccines present an exciting new strategy to harness the selective ability of the immune system to target tumor cells [202–204]. Tumors evade normal immune function in part because they are self-derived cells, minimizing immunogenicity and the warning signals pathogens typically display [205]. These innate immune signals are needed to activate dendritic cells (DCs) and other antigen presenting cells to support adaptive immune responses that can combat pathogen or tumors. Additionally, the tumor microenvironment is highly suppressive, hindering the ability of immune cells to maintain anti-tumor responses [179,206]. Improved understanding of the innate immune system has allowed for the discovery and design of new immunomodulatory molecules that can target specific pathways to generate robust pro-immune responses and enhance tumor-specific T cell expansion [102,137]. A number of candidate cancer vaccines are exploring CpG – a DNA motif commonly found in bacteria – to promote an immunostimulatory cascade and potentiate an antigen-specific immune responses through TLR9 binding and activation [207–209].

Following immunization, DCs take up and present antigen, express co-stimulatory molecules, and produce distinct cytokines that activate and expand cytotoxic T cells (CTLs) able to attack tumors [104]. Due to this requirement for dual-presentation of antigen and costimulatory markers, codelivery of antigens and adjuvants can significantly improve the effectiveness of antigen-specific immunotherapies. Thus, the mechanisms of delivery and route of administration remain important considerations [210,211]. As one example, adjuvants delivered alone do not generate durable responses, lack specificity, and can lead to off-target effects. Conversely, delivery of antigens in the absence of immunostimulatory signals can promote immune tolerance [94,212].

Owing to the potential benefits of precision co-delivery, new molecular-scale and nano-scale delivery systems are being explored to improve immunotherapies [27,177,213]. Nanoparticles as carriers for cancer vaccines, for example, offer a platform for enhancing immune responses through controlled release and targeting to sites such as lymph nodes − tissues that coordinate adaptive immunity. Co-adsorption or co-encapsulation of antigen and adjuvant particles onto polymer scaffolds or inorganic templates also provide co-delivery and control over the internalization of immune signals to generate more potent responses [26,89]. Despite these advantages, many challenges remain to fully realize the benefits of these system, including antigen loading efficiency, more complex manufacturing and regulatory characterization, and heterogeneous formulations that can impact safety profiles.

Nanoparticles termed polyplexes have been studied for decades as simple carriers to condense or encapsulate biologic cargo using electrostatic interactions [149,214,215]. Most prominently, synthetic cationic polymers have been developed as gene or protein delivery agents to condense anionic nucleic acid cargo into particulate form that are more readily endocytosed [216]. Additionally, by altering polymer structure and function, molecules features can be installed to address barriers to intracellular delivery, such as endosomal escape. While useful, in the vaccine and immunotherapy fields, there are some unique considerations. For example, as highlighted in **Section 2.6.1** many polymeric carriers intrinsically activate [80], suppress [155], or alter immune signaling [140] even in the absence of other antigens or adjuvants. These intrinsic immune characteristics can be useful, but can also hinder rational vaccine design and translation because the carrier itself may change the immune response to the antigen or other vaccine components. Additionally, as mentioned above, high-density co-display of antigen and adjuvant is important to

generate strong, specific immune responses; in this context polyplexes are particularly well-suited since they by definition juxtapose the condensed components comprising the polyplexes.

To address the issues just highlighted and building on the work discussed in **Chapter 3**, we assembled polyplex-like structures comprised entirely of immune signals: tumor antigens and TLR ligand. In particular, we assembled CpG – an anionic TLR9 agonist, and a conserved human melanoma peptide (Trp2) modified with arginine residues to create a net cationic charge. This approach of building polyplexes from tumor immunotherapy components offers several attractive design features. First, in contrast to traditional polyplexes, these nanostructures are assembled entirely from immune signals; this unique approach simplifies the design by eliminating the complicating immunogenic effects often associated with carriers or excipients. Secondly, the lack of carriers ensures a high density of immune signals, as 100% of the formulation is cargo. Third, polyplexes maintain many of the attractive features of biomaterial carriers, including a particulate nature for improved uptake, cargo protection, and co-delivery of immune signals. As mentioned, the particulate nature of polyplexes can promote uptake and delivery to internal compartments within cells; these are features that can both be leveraged in immunotherapy design. For example, efficient internalization is critical for antigen processing and subsequent presentation by DCs. Further, many TLRs are located intracellularly within endosomes – including TLR9; agonists such as CpG must therefore be internalized by immune cells to be effective. Uniquely, in our approach, we demonstrate that anionic CpG and cationic Trp2 peptide electrostatically self-assemble to juxtapose antigen and adjuvant for co-delivery without need of synthetic polymers or other carriers. Using this platform, we show that Trp2/CpG polyplexes form over a range of Trp2:CpG ratios and improve antigen uptake by DCs. Treatment of primary DCs strongly activated these

cells and promoted Trp2-specific T cell proliferation. Interestingly, polyplexes with higher Trp2:CpG ratios elicit increased inflammatory cytokine production. Leveraging the modularity of this platform, we demonstrate a role of antigen dose using Trp2 peptide modified with different numbers of arginine groups (i.e. 3, 6, and 9). Polyplexes with greater antigen loading enhance T cell functionality which correlates with reduced tumor burden and improved survival in a pre-clinical model of melanoma.

4.3 Materials and Methods

4.3.1 Synthesis of Trp2:CpG Polyplexes

Trp2/CpG polyplexes were assembled by electrostatic condensation by mixing aqueous solutions of CpG DNA (5'-TCC ATG ACG TTC CTG ACG TT-3', IDT) and Trp2 peptide (SVYDFFVWL, Genscript) modified with 3($Trp2R_3$), 6 ($Trp2R_6$) or 9 ($Trp2R_9$) arginine groups. CpG and Trp2R were combined at defined mass ratios ranging from 1:5 to 10:1 $Trp2R_x$:CpG (x=3, 6, 9) by fixing the CpG concentration at 10 µg/mL and varying the amount of $Trp2R_x$ under a fixed total volume. Thus, the amount of CpG in each polyplex formulation remained constant irrespective of mass ratio.

4.3.2. Characterization of Trp2/CpG polyplexes

Polyplex formation was assessed by SYBR green exclusion assay. 10 µL SYBR Green I at 100X was added to 90 µL reaction mixture of complexes and incubated for 1h. Fluorescence was measured using an excitation wavelength of 497 nm and an emission wavelength of 520 nm. The resulting fluorescence was compared to the average fluorescence of free soluble CpG to determine the fraction of CpG that remained uncondensed. Formation and stability of polyplexes was

evaluated by gel retardation assays. 10 µL (100 ng CpG) aliquots of polyplexes were loaded onto a 4% agarose gel with gel loading dye and SYBR Green I (Invitrogen). Electrophoresis was performed at 120V for 20 min in 1X Tris-Borate-EDTA (TBE) buffer. The gel was subsequently imaged using a UV illuminator. The hydrodynamic diameter and zeta potential of complexes were measured in triplicate using a Zetasizer Nano Z590.

4.3.3 Enzymatic degradation assay

CpG was labelled with Cy5 per manufacturer instructions (Mirus, Madison, WI). Polyplexes of varying $Trp2R_9$:CpG ratios were made using Cy5-CpG and $Trp2R_9$ in 100 uL 1X DNA I reaction buffer. Fluorescence was measured using an excitation wavelength of 640 nm and an emission wavelength of 670 nm to determine initial CpG levels. Fluorescent measurement was chosen to quantify CpG amount over spectrophotometry because peptides (i.e. $Trp2R_9$) exhibit absorbance overlap at 260 nm. The complexes were then incubated with 2 units of DNAse I (New England Biolabs) for 30 min at 37ºC. Following incubation, the fluorescence was immediately measured again and the extent of degradation of Cy5-CpG in polyplexes was determined by comparing fluorescence intensities relative before and after the addition of DNAse I.

4.3.4 DC uptake and activation

Splenic $CD11c^+$ cells were isolated from 6-8 week old female C57BL/6J mice (Jackson Laboratories) through positive selection by magnetic isolation in accordance with manufacturer protocols (Miltenyi Biotech, Cambridge, MA). Cells were plated at 5×10^4 cells per well in 96-well plates with RPMI 1640 media (Lonza, Allendale, NJ) supplemented with 10% FBS, 2mM, L-glutamine, 1X non-essential amino acids, 10mM HEPES buffer (Fisher Scientific, Hampton,

NH), 1% penicillin and streptomycin (Gibco), and 55 uM β-mercaptoethanol (Sigma-Aldrich). Cells were treated with either vehicle (water), 200ng of CpG complexed at increasing w/w ratio with $Trp2R_9$, or dose-matched soluble CpG and $Trp2R_9$. For uptake studies, CpG was labelled with Cy5 per manufacturer instructions (Mirus, Madison, WI) and Cy5 CpG was used to form complexes with FITC-$Trp2R_9$ (Genscript). DCs were incubated with treatments for 24h at 37°C, then washed and stained for DAPI, and analyzed by flow cytometry (BD Biosciences). Uptake was also confirmed by confocal microscopy. Splenic CD11c+ cells were isolated and 10^6 cells were plated onto glass-bottom dishes with No. 1.5 thickness (MatTek). Cells were incubated for 24 h, after which cells were fixed in 4% paraformaldehyde, stained for membrane (wheat germ agglutinin (WGA), Texas Red conjugate) and resuspended in Hoescht for imaging. Images were taken using a Leica SP5X Laser Scanning Confocal and analyzed by FIJI/ImageJ (National Health Institute). For activation studies, DCs were incubated with treatments for 24h, then washed and stained for DAPI and surface activation markers: CD40, CD80, CD86 (BD, San Jose, CA). Cells were then analyzed by flow cytometry.

4.3.5 DC/T cell co-culture

Splenic primary $CD11c^+$ cells were isolated as described above, plated at 5×10^4 cells, and treated with polyplexes. After incubation for 24 h, $CD8^+$ T cells were isolated from the spleens of Trp2-clone 37 mice (a gift from Dr. Giorgio Trinchieri, National Cancer Institute, NIH), a Trp2-specific transgenic strain, using negative selection via magnetic isolation in accordance with manufacturer instructions (StemCell Technologies, Vancouver, BC). Trp2-specific T cells were then labelled by incubating with 50 μM 5(6)Carboxy-fluorescein diacetate N-succinimidyl ester (CFSE) (Sigma Aldrich) per mL of cells for 5 min at room temperature, followed by washing in

media. 1.5 x 10^5 of CFSE labelled Trp2 T cells were then added to treated DC and cultured for an additional 72 h. Following incubation, cells were collected and stained for T cell specific surface markers (CD3e, CD8a), and resuspended in DAPI. T cell proliferation was determined by flow cytometry to measure CFSE dilution.

4.3.5 Enzyme-linked immunosorbent assay (ELISA)

Supernatants from DC/T cell cultures were collected. Cytokine secretion levels were analyzed via ELISA for mouse interferon gamma (IFN-γ) secretion, following manufacturer instructions (BD,). 96-well plates were coated with an IFN-γ capture antibody and incubated overnight. Supernatant samples were then added and allowed to bind for 2 hr, followed by an IFN-γ detection antibody and streptavidin-horseradish peroxidase conjugate mixture for 1 h. A tetramethylbenzidine and hydrogen peroxide mixture was added to each well; this reaction was stopped by the addition of 1 M phosphoric acid. Absorbance was read at 450 nm and IFN-γ concentrations were calculated from absorbance by comparing to a standard curve.

4.3.6 Murine tumor models

All studies involving mice (as a source of primary cells) were carried out in compliance with federal, state, and local laws and followed institutional guidelines, including the Guide for the Care and Use of Laboratory Animals and the Animal Welfare Act. All experiments were reviewed and approved by the University of Maryland's Institutional Animal Care and Use Committee (IACUC). Mice were shaved and injected subcutaneously (s.c.) with $3x10^5$ B16-F10 cells in 50 µL of PBS, and weighed and monitored daily for tumor growth. Tumor size was determined as the product of two orthogonal diameters. Mice were treated s.c. with 50 µL of PBS

or 25 μg Trp2R$_x$/CpG polyplex treatments when aggregate tumor burden reached 25 mm^2. Each group received additional doses every 3 days for up to 4 total treatments. Mice were euthanized according to the IACUC-approved humane endpoints when aggregate tumor burden reached 150 mm^2.

4.3.7 Statistics

One-way ANOVA was used to compare three or more groups, with Tukey post-test corrections for multiple comparisons. Log-rank tests were used in analyses of survival. All tests were two-sided analyses and were performed using GraphPad Prism. Error bars in all panels represent mean ± standard error of the mean and p values < 0.05 were considered significant.

4.4 Results

4.4.1 Trp2R$_9$ and CpG self-assemble into polyplex nanoparticles

We first tested if polyplexes could be electrostatically assembled from CpG and Trp2 modified with cationic arginine residues (Trp2R$_9$) (**Fig. 4.1A**). In these studies, the mass of CpG was fixed while the mass of Trp2R$_9$ was varied over a range of 1:5-10:1 Trp2R$_9$:CpG (w/w). This weight ratio range corresponds to a cationic:anionic molecular charge ratio of 0.99-4.94 (**Table 4.1**). To determine the ratios at which polyplex formation occurred, we performed a SYBR green exclusion assay. SYBR green II binds secondary and tertiary structural features on single-stranded DNA by intercalating local regions of stacked base pairs. While unbound SYBR green displays low levels of fluorescence, when bound to DNA, the dye undergoes structural changes resulting in strong fluorescence that increases with nucleic acid concentration. In these studies, the fluorescent intensity of SYBR Green II was measured by UV-vis spectroscopy and normalized to

soluble CpG to determine the amount of free CpG remaining. Soluble CpG controls incubated with SYBR Green II led to a high level of fluorescence **(Fig. 4.1B)**. We observed a significant reduction in fluorescence at 1:1 ratio of $Trp2R_9$:CpG and higher ratios, indicating condensation of CpG into polyplexes. To evaluate the stability of polyplexes, we performed gel migration assays. Electrophoresis of polyplexes loaded in agarose gels confirmed that polyplexes do not form below 1:1 $Trp2R_9$:CpG ratios (**Fig. 4.1C)**. This was indicated by the presence of free CpG under applied voltage. Disappearance of fluorescence above 1:1 $Trp2R_9$:CpG ratio indicated quenching of tightly bound nucleic acids and formation of larger complexes that did not migrate. Our studies revealed weak binding of $Trp2R_9$ and CpG at a 1:1 $Trp2R_9$:CpG weight ratio, as indicated by the presence of a CpG band under applied voltage. Disappearance of fluorescence at 2:1 or higher ratios – even though CpG was present at the same concentration in all wells – confirmed that CpG was fully condensed and $Trp2R_9$ and CpG formed stable polyplexes. These findings corresponded with the reduced fluorescence measured in the quantitative exclusion assays.

Table 4.1 Physicochemical Properties of $Trp2R_x$/CpG polyplexes

$Trp2R_x$:CpG (w/w)	$Trp2R_x$:CpG Charge Ratio			Diameter (nm)			Surface Charge (mV)			Composition (% Trp2)			Composition (% CpG)		
	x=3	x=6	x=9	x=3	x=6	x=9	x=3	x=6	x=9	x=3	x=6	x=9	x=3	x=6	x=9
1:1	0.39	0.76	0.99	*	145.8 ± 6.9	134.6 ± 2.1	*	-24.6 ± 0.2	-34.4 ± 0.7	64.6	60.1	55.0	35.4	39.9	45.0
2:1	0.78	1.51	1.98	81.3 ± 8.9	268.5 ± 19.2	120.8 ± 1.80	-26.1 ± 1.3	18.9 ± 0.5	-25.0 ± 0.4	72.5	59.2	59.0	27.5	40.8	41.0
3:1	1.17	2.26	2.96	199.7 ± 17.3	816.4 ± 60.7	128.6 ± 1.4	-11.5 ± .07	22.1 ± 0.2	21.6 ± 0.2	75.5	61.0	64.7	24.5	39.0	35.3
4:1	1.55	3.02	3.95	1766 ± 83	882.4 ± 37.1	159.9 ± 2.0	-0.6 ± 0.1	24.7 ± 0.3	26.6 ± 0.4	75.3	65.1	66.1	24.7	34.9	33.9
5:1	1.94	3.77	4.94	1664 ± 161	686.1 ± 61.8	199.2 ± 2.8	6.0 ± 0.3	25.5 ± 0.6	26.4 ± 0.2	77.8	64.1	63.1	22.2	35.9	36.9

*particle concentration too dilute to measure

Dynamic light scattering confirmed the formation of nanoscale polyplexes with hydrodynamic diameters of 120.77 ± 1.80 nm to 280.8 ± 6.70 nm (**Fig. 4.1D)**. Following complete complexation of polyplexes (2:1 ratio), polyplex size increased with increasing $Trp2R_9$:CpG ratio. Size measurements could not be obtained below 1:2 $Trp2R_9$:CpG ratios, due to the low concentration of particles at this assembly ratio. Surface potential measurements revealed that at lower $Trp2R_9$:CpG ratios (i.e. 1:1), polyplexes exhibit negative surface charges, while at higher N:P ratios, the surface potential increased with the relative amount of $Trp2R_9$ in the polyplexes (**Fig. 4.1E)**. Charges ranged from -34.43 ± 0.69 mV to 25.4 ± .50mV, demonstrating the tunability of surface charge. As expected, reversal of zeta potential from negative to positive was found to occur between 1:1 and 2:1 $Trp2R_9$:CpG, corresponding to the ratio at which the positive and negative charges between $Trp2R_9$ and CpG are approximately balanced (i.e., a passing through a charge ratio of 1).

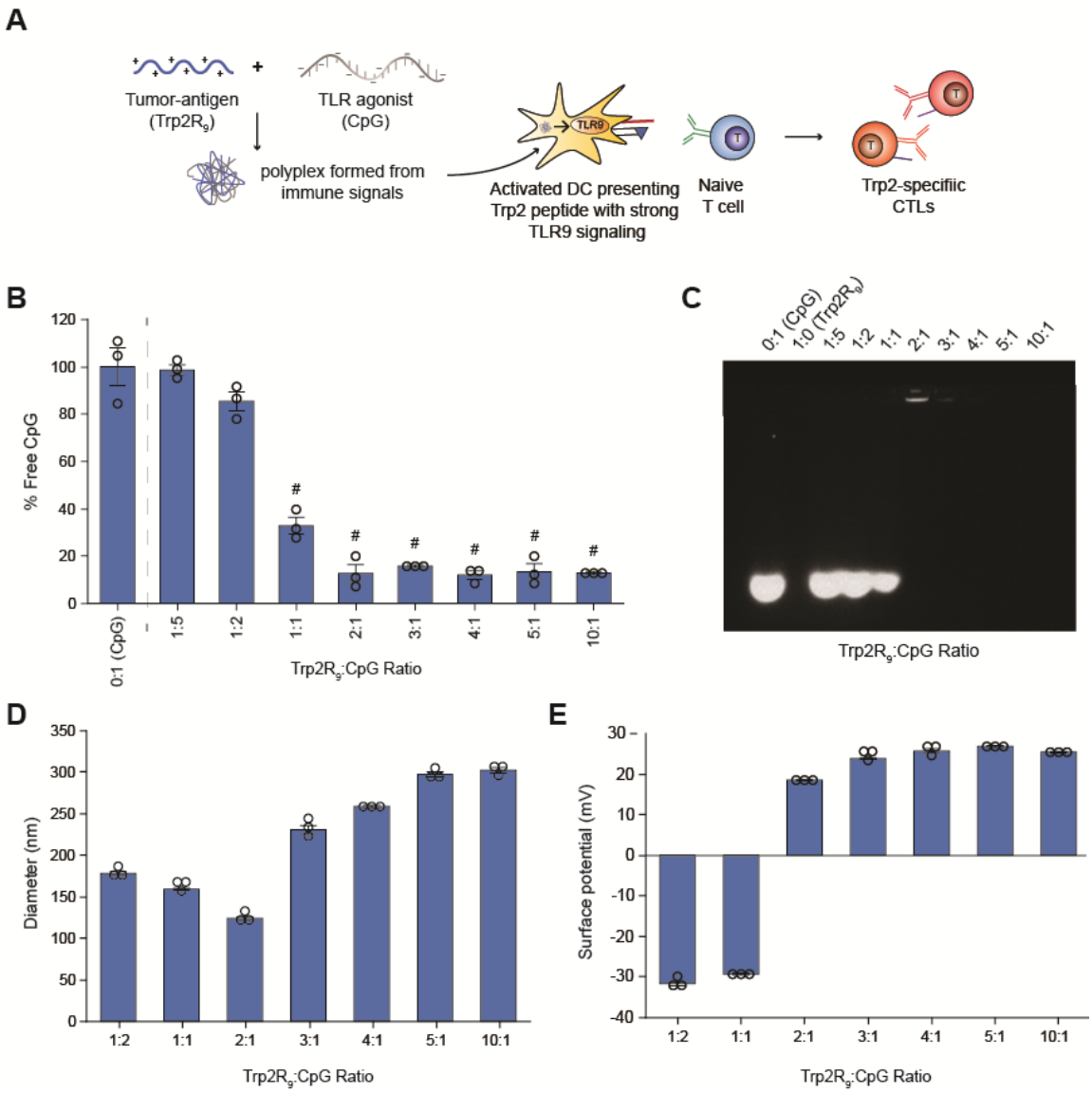

Figure 4.1 Trp2R9 and CpG self-assemble to form polyplexes
(A) Schematic of polyplex assembly to activate cytotoxic T cells (CTLs) **(B)** SYBR Green exclusion assay confirms formation of polyplexes form at 1:1 Trp2R9:CpG ratio **(C)** Gel retardation assay demonstrating the stability of polyplexes above 2:1 Trp2R9:CpG ratio **(D)** Hydrodynamic diameter measurements of polyplexes confirming formation of polyplex nanoparticles. **(E)** Surface charge is readily tunable by altering the amount of Trp2R9 during polyplex assembly. #p < 0.0001. Statistical comparisons are vs. 0:1 (CpG)

4.4.2 CpG is protected from enzyme degradation when complexed with Trp2R$_9$

Nucleic acid TLR ligands delivered *in vivo* are exposed to nucleases in the extracellular environment or within endosomes that may degrade nucleic acids and inhibit TLR activation. Improving stability may not only increase half-life allowing for better bioavailability, but prolong adjuvant persistence which is important in the generation of more potent and longer-lasting immune responses. Thus, we next tested if condensation of Trp2R$_9$/CpG polyplexes could protect CpG from enzymatic degradation. Cy5-labelled CpG in soluble form or complexed with Trp2R$_9$ were incubated with DNAse and the fluorescent intensity was measured to quantify the amount of DNA present before and after degradation. These studies revealed that polyplexes significantly reduced CpG degradation across all charge ratios relative to free CpG, even at lower Trp2R$_9$:CpG ratios that only poorly or weakly condensed CpG (**Fig. 4.2)**. Thus, these wholly immunological polyplexes also maintain the cargo-protecting ability associated with conventional polyplexes that require synthetic polymers to condense cargo.

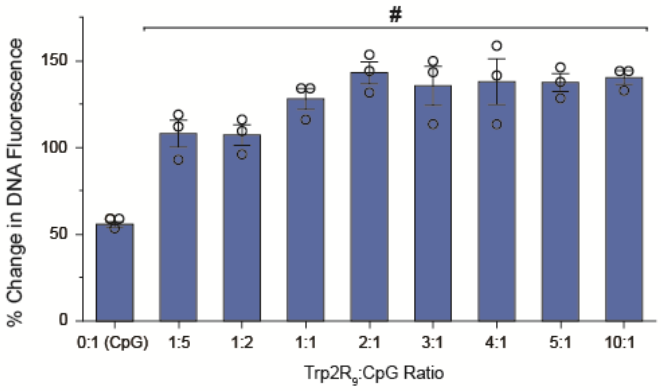

Figure 4.2 Trp2R$_9$/CpG polyplexes protect CpG against enzymatic degradation
#p < 0.0001. Statistical comparisons are vs. 0:1 (CpG)

4.4.3 Polyplexes colocalize delivery of CpG and Trp2 and increase antigen uptake by DCs

Because CpG is an agonist of TLR9, which is expressed intracellularly in endosomes, polyplexes must be internalized by DCs to initiate immunostimulatory signaling cascades. We hypothesized that the particulate nature of polyplexes would improve DC uptake compared to soluble controls. To test this, we next studied the immunological processing of complexes by measuring the level at which polyplexes were internalized by primary DCs. DCs were isolated from mouse spleens and incubated with polyplexes formed from fluorescently-labelled CpG and $Trp2R_9$ for 24 hours. Corresponding dose-matched free CpG and $Trp2R_9$ were also included as controls. Flow cytometry analysis revealed that polyplexes generally provided a significant increase in both CpG (**Fig. 4.3A, 4.3B**) and antigen (**Fig. 4.3C, 4.3D**) relative to soluble forms of CpG and Trp2R9, respectively. This was indicated by increases in the mean fluorescence intensities of each signal. Antigen uptake was dose-dependent with the greatest $Trp2R_9$ uptake associated with the 5:1 $Trp2R_9$:CpG ratio; this ratio also contained the highest loading of $Trp2R_9$.

Initiation of immune responses requires simultaneous presentation of antigen and costimulatory signal. To assess whether polyplexes conferred co-delivery of immune signals within cells, DCs were also plated onto glass-bottom dishes, treated with polyplexes, and imaged by confocal microscopy. Internalized Trp2R9 and CpG signal was localized to similar regions within treated DCs, indicating intra-cellular co-localization of the cargo (**Fig. 4.3E**). This ability to co-delivery signals is important to promote efficient adaptive immune responses, which require encounter of both antigen (e.g.Trp2) and stimulatory (e.g. CpG) signal. Importantly, these studies

also confirmed that polyplexes were taken up by DCs rather than only interacting with the DC surface.

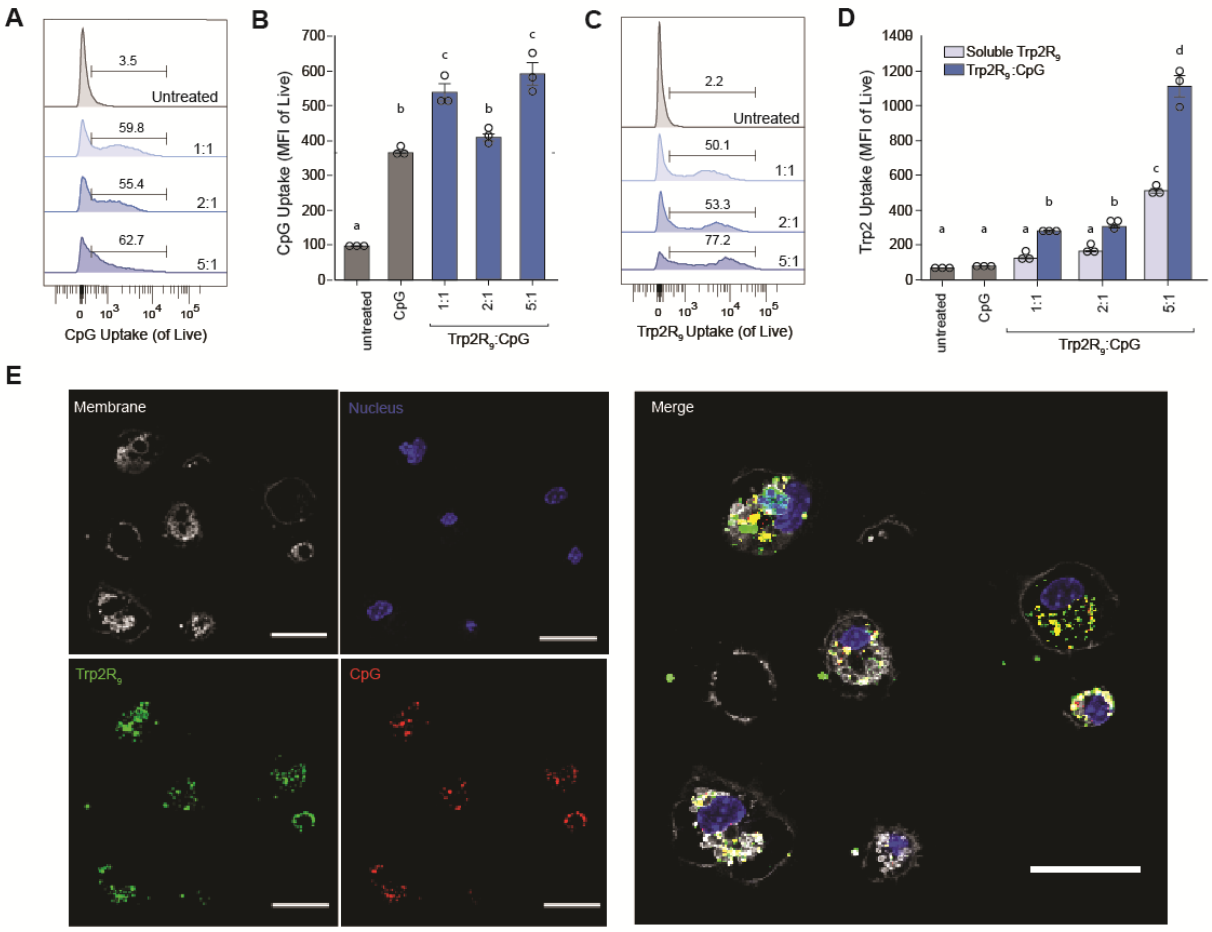

Figure 4.3 Trp2R9/CpG polyplexes improve immune signal uptake by DCs
(A) Representative gates and **(B)** quantification of CpG uptake by DCs following 24h incubation as measured by flow cytometry using Cy5-labelled CpG. **(C)** Representative gates and **(D)** quantification of Trp2R9 uptake was measured using FITC-Trp2R9. Quantitative analysis was performed to compare CpG uptake with soluble CpG controls or dose-matched Trp2R9. **(E)** Confocal images of CpG and Trp2 uptake in DCs (scale bar = 30μm) demonstrate colocalization of immune signals within treated DCs. Different letters indicate statistical significance among means ($p < .05$)

4.4.4 Trp2R9/CpG polyplexes activate DCs

To determine how polyplex uptake impacts DC activation, DCs were next treated with polyplexes ranging from 1:5 to 5:1 ratios. In these studies, polyplexes did not impact viability

relative to other CpG-activated cells **(Fig. 4.4A**). Compared to untreated cells and cells treated with soluble Trp2R$_9$, Trp2R$_9$/CpG polyplexes significantly increased expression of classical surface activation markers CD40, CD86, and CD80 (**Fig. 4.4B-D**). Interestingly, at higher Trp2R$_9$:CpG ratios – which exhibited the most positive potentials (**Fig. 1C**) and likely the strongest binding affinity between components, the polyplexes displayed reduced DC activation compared to soluble CpG; this was despite a constant fixed CpG dose across samples. In control studies, polyplexes formed with a non-immunostimulatory oligonucleotide in place of CpG did not cause any activation, suggesting that any activation activity observed with polyplexes is driven by the CpG component condensed in the polyplexes (**Fig. 4.5**). Together, these results indicate that while the presence of CpG confers polyplex immunogenicity, the affinity and degree of condensation as a result of Trp2R$_9$ binding may influence the availability of CpG to stimulate TLR9.

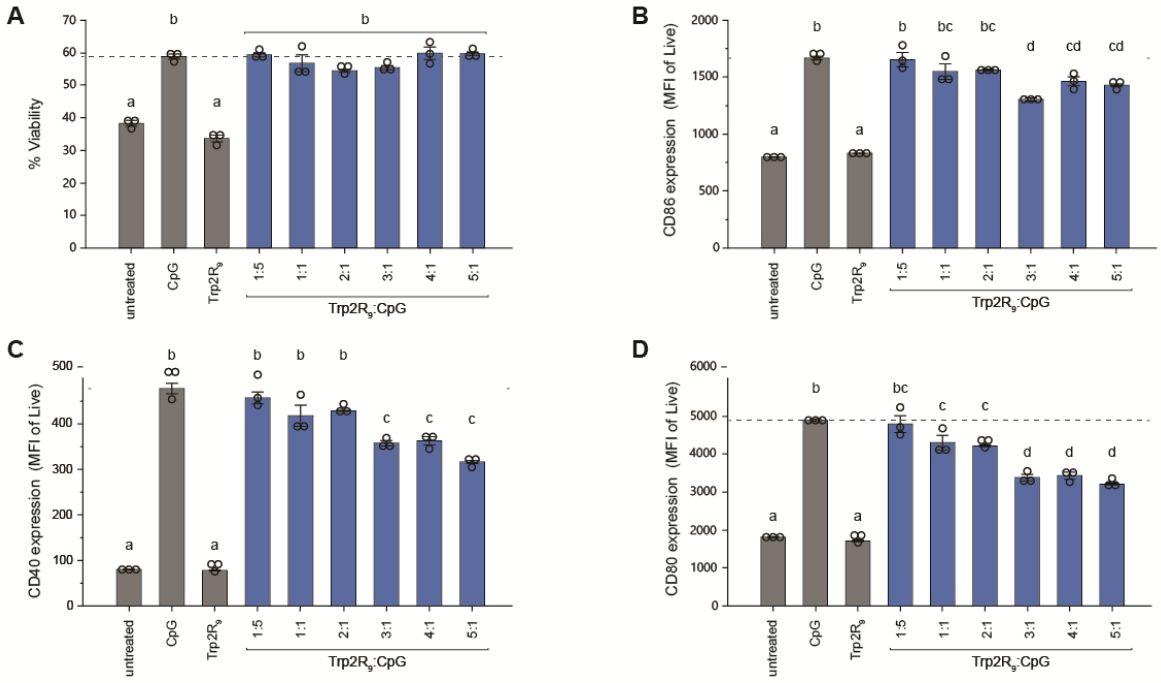

Figure 4.4 Trp2R$_9$/CpG polyplexes are non-toxic and maintain ability to activate DCs

(A) Viability of treated DCs was measured by quantifying DAPI$^-$ cells. DC activation was measured by staining with fluorescent antibody conjugates for immunostimulatory markers **(B)** CD86, **(C)** CD40, and **(D)** CD80 and analyzed for expression levels by flow cytometry. Different letters indicate statistical significance among means ($p < .05$)

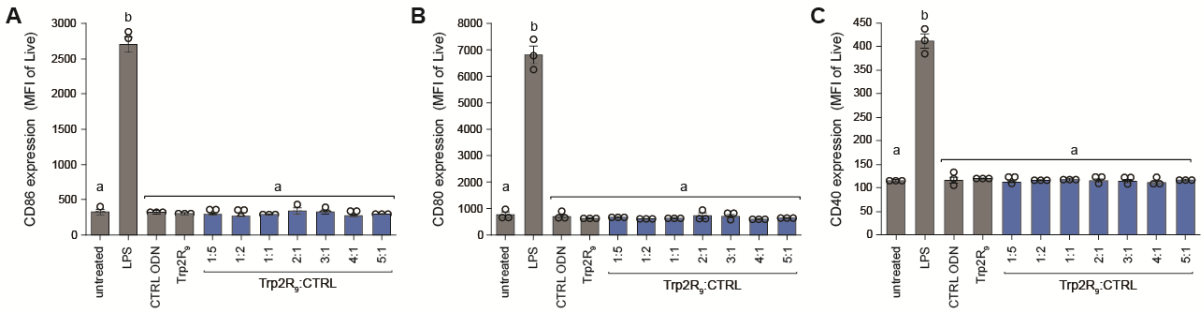

Figure 4.5 Trp2R$_9$/CTRL ODN polyplexes do not activate DCs
Polyplexes were formed by condensing CTRL ODN in place of CpG. Flow cytometry reveal that treated DCs maintained low levels of expression for immunostimulatory markers **(A)** CD86, **(B)** CD40, and **(C)** CD80. Different letters indicate statistical significance among means ($p < .05$)

4.4.5 Polyplexes activate Trp2-specific CD8$^+$ T-cells

The above results indicate that polyplexes differentially alter DC activation, a step that is critical in initiating and potentiating antigen-specific T cell responses. Antigen dose, however, can also play a critical role in shaping the magnitude and nature of adaptive immunity responses to cancer or infection. Thus, we next tested if different Trp2R$_9$:CpG ratios alter T the functional response of Trp2-specific T cells. In these experiments, splenic CD11c$^+$ DCs were isolated from mice and treated with polyplexes and cultured with CD8$^+$ T cells isolated from Trp2 transgenic mice (**Fig. 4.6A)**. CD8$^+$ T cells from these mice display T cell receptors specific for Trp2, and thus expand and secrete cytokines upon encountering antigen presentation with the appropriate co-stimulatory signals. Isolated T cells were labelled with fluorescent proliferation dye that becomes diluted with each generation of proliferation. Following co-culture for 72h, CD8$^+$ T cells were analyzed by flow cytometry to quantify proliferation. Interestingly, altering Trp2R$_9$:CpG ratios

resulted in markedly different proliferation profiles (**Fig. 4.6B)**. Notably, lower ratios of $Trp2R_9$:CpG resulted in a heterogeneous population of T cells comprised of proliferated and unproliferated T cells that had undergone different levels of cell division, as indicated by the presence of several peaks across different intensities. Conversely, higher ratios of $Trp2R_9$:CpG resulted in a more uniform population of T cells undergoing similar levels of cell division, displaying only a few peaks over a narrow range of fluorescent intensity. While T cells treated with soluble CpG did not proliferate, all polyplex formulations resulted in T cells that strongly proliferated at similar levels to soluble CpG + Trp2 treated wells, as quantified by decreasing signal intensity of the proliferation dye (**Fig. 4.6C)**. This confirms the antigen-specific nature of this response. Further, at lower $Trp2R_9$:CpG ratios, combined delivery of CpG with $Trp2R_9$ in polyplexes significantly improved T cell expansion compared to soluble $Trp2R_9$ alone. However, these findings were not observed in polyplexes with higher $Trp2R_9$:CpG ratios, which expanded T cells at similar levels to soluble $Trp2R_9$. Notably, due to fixed CpG levels, lower $Trp2R_9$:CpG ratios contain less $Trp2R_9$, suggesting co-delivery with CpG may be of particular importance at lower antigen doses to drive strong antigen-specific T cell proliferation.

To test if $Trp2R_9$:CpG polyplexes also altered T cell function, we measured interferon-gamma (IFN-γ) levels from culture supernatants by ELISA. IFN-γ is a key inflammatory cytokine and important for augmenting $CD8^+$ T cell cytotoxic function for enhancing anti-tumor and anti-viral effects.[217] In these studies, IFN-γ secretion increased with increasing $Trp2R_9$:CpG ratio; the 5:1 $Trp2R_9$:CpG polyplexes displayed significantly higher levels of IFN-γ levels compared to all other tested ratios and similar levels to dose-matched soluble $Trp2R_9$ control (**Fig. 4.6D)**.

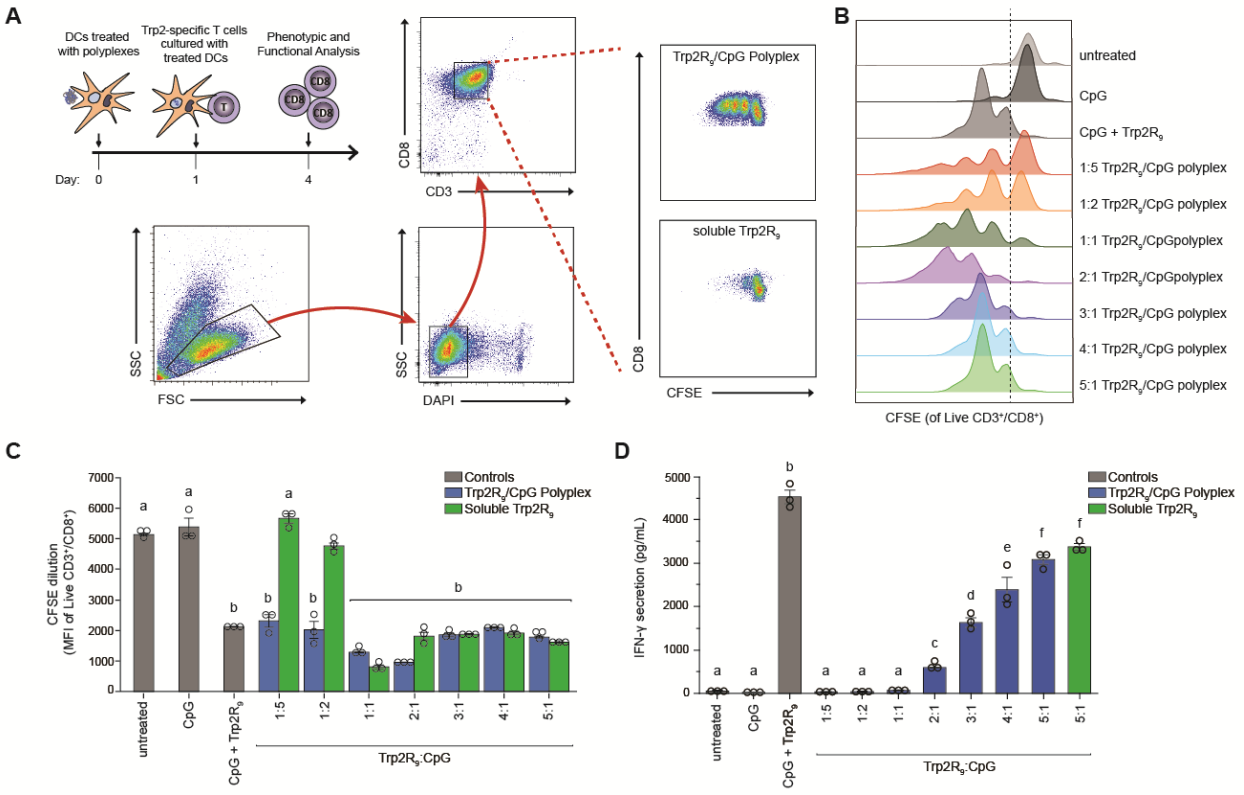

Figure 4.6 Trp2R9/CpG polyplexes promote antigen-specific T cell proliferation
DCs were treated with a library of Trp2R9/CpG polyplex ratios, soluble CpG, or soluble Trp2R9. After 24 h, T cells labeled with CFSE—a proliferation dye diluted with each generation of cell division—was added to culture. **(A)** Schematic of experimental set-up and representative gating schemes for flow cytometry analysis. Comparison is for proliferation of 1:5 Trp2R9:CpG polyplexes and dose matched soluble Trp2 **(B)** Flow cytometry histograms for CFSE dilution illustrating distinct generations of T cell proliferation different proliferation profiles for each tested ratio of Trp2R9:CpG **(C)** MFI of CFSE of $CD3^+/CD8^+$ cells following 72 h of DC/T-cell co-culture revealed that all complexes expanded Trp2-specific T cells with lower Trp2R9:CpG ratios displaying increased levels of proliferation compared to dose-matched soluble Trp2 alone. **(D)** Higher ratios of Trp2R9:CpG display increased levels of IFN-γ levels secreted in supernatants of DC/T cell co-cultures as measured by ELISA. Different letters indicate statistical significance among means ($p < .05$).

4.4.6 Polyplex size, charge, and antigen loading can be tuned

The above results suggest that antigen dose plays an important role in T cell functionality. Thus, to further tune the dose of antigen and the relative number of epitopes – the number of copies

of Trp2 delivered – we next used CpG to condense a series of alternate antigen designs in which Trp2 was modified with fewer arginine residues (i.e. $Trp2R_3$, $Trp2R_6$); this effectively increases the number of epitope copies at a fixed antigen dose. Using a fixed mass of CpG, polyplexes were formed by varying the mass ratio of $Trp2R_x$:CpG from 1:5-10:1. SYBR green exclusion assays revealed that $Trp2R_3$ and $Trp2R_6$ condensed CpG above 1:1 $Trp2R_x$:CpG ratios, as indicated by a significant reduction in fluorescence (**Fig. 4.7A)**. Dynamic light scattering revealed that condensation of CpG with $Trp2R_3$ resulted in smaller particles at 2:1 and 3:1 ratios (< 200nm), while polyplexes above 4:1 $Trp2R_3$:CpG ratio were much larger in size with particles ranging from 1664.33 ± 160.7 nm to 1791.03 ± 102.70 nm (**Fig. 4.7B)**. Sizes for ratios below 2:1 $Trp2R_3$:CpG could not be measured due to the low concentration of particles forming at this range or ratios. Surface charge ranged from -24.57 ± 0.21 mV to 25.53 ± 0.55 mV. As with $Trp2R_9$ complexes, surface charge increased with increasing $Trp2R_3$:CpG, however, charge inversion from negative to positive occurred at a higher $Trp2R_3$:CpG ratio of 2:1 (**Fig.4.7C)**. This shift in zeta potential concurs with the ratio at which the $Trp2R_3$:CpG charge ratio is neutral (**Table 4.1**). Complexes formed using $Trp2R_6$ resulted in polyplexes that varied over a greater range of sizes compared to polyplexes formed using $Trp2R_9$, with hydrodynamic diameters of 145.83 ± 6.87 nm to 882.40 ± 37.08 nm (**Fig. 4.7D)**. Zeta potential measurements revealed that the surface charge for $Trp2R_6$/CpG polyplexes ranged from -24.57 ± 1.21 mV to 28.03 ± 1.93 mV (**Fig. 4.7E)**. Ratios below 1:1 exhibited negative surface charges, while at higher ratios, polyplexes were increasingly positively charged as a function of $Trp2R_6$:CpG ratios and as predicted by changes in charge ratio.

We next measured immune signal loading into complexes to assess how antigen composition was altered by using different levels of arginine modification and altering

$Trp2R_x$:CpG ratios. In these studies, polyplexes formed using Trp2 with fewer arginine modifications (i.e. $Trp2R_3$) resulted in higher absolute yields of antigen within complexes (**Fig. 4.7F)**. 1:1 $Trp2R_x$:CpG ratios resulted in much lower yields of complexed immune signals. Similarly, the relative $Trp2R_x$ and CpG composition of polyplexes could be varied across different levels of arginine modifications and changes in $Trp2R_x$:CpG ratio, with 5:1 $Trp2R_3$:CpG polyplexes displaying the highest levels of antigen loading (**Fig. 4.7G)**. Comparisons of the polyplex diameter, charge, and loading between polyplexes formed by condensing CpG with $Trp2R_3$, $Trp2R_6$, and $Trp2R_9$ are provided in **Table 4.1**.

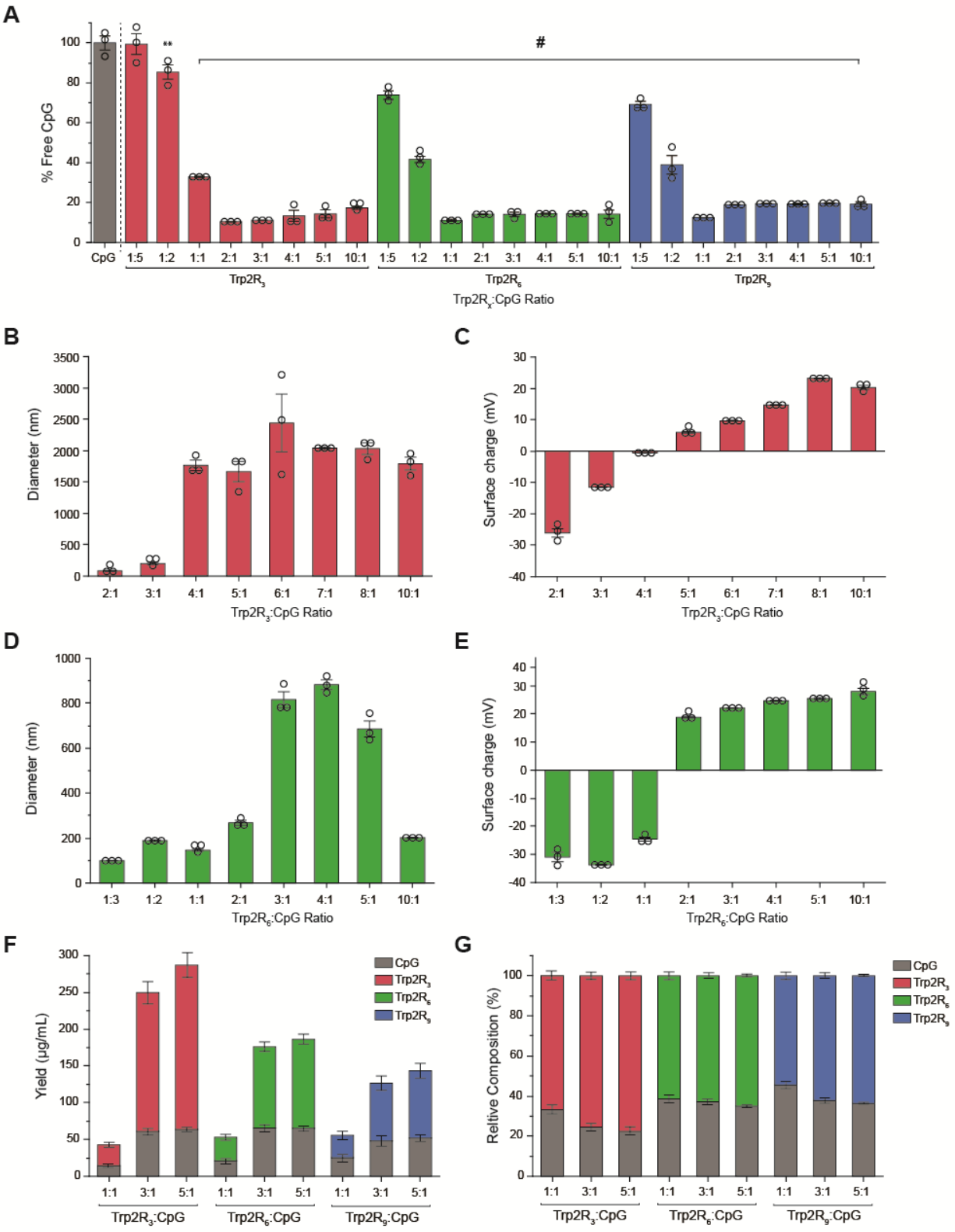
A
% Free CpG
**
#
CpG
1:5 1:2 1:1 2:1 3:1 4:1 5:1 10:1
Trp2R3
Trp2R6
Trp2R9
Trp2Rx:CpG Ratio
B
Diameter (nm)
2:1 3:1 4:1 5:1 6:1 7:1 8:1 10:1
Trp2R3:CpG Ratio
C
Surface charge (mV)
Trp2R3:CpG Ratio
D
Diameter (nm)
1:3 1:2 1:1 2:1 3:1 4:1 5:1 10:1
Trp2R6:CpG Ratio
E
Surface charge (mV)
Trp2R6:CpG Ratio
F
Yield (μg/mL)
CpG
Trp2R3
Trp2R6
Trp2R9
1:1 3:1 5:1
Trp2R3:CpG
Trp2R6:CpG
Trp2R9:CpG
G
Reltive Composition (%)
CpG
Trp2R3
Trp2R6
Trp2R9
1:1 3:1 5:1
Trp2R3:CpG
Trp2R6:CpG
Trp2R9:CpG

Figure 4.7 Trp2/CpG polyplexes can be tuned for size, charge, and loading

Trp2/CpG polyplexes can be assembled with peptide modified with different numbers of arginine groups to form a diverse set of polyplexes with distinct size, charge, and loading characteristics. **(A)** SYBR Green exclusion assay demonstrate formation of polyplexes using Trp2 modified with R_3, R_6, and R_9. The hydrodynamic diameter **(B,D)** and **(C,E)** surface charge varied across $Trp2R_x$:CpG ratio for complexes formed with $Trp2R_3$ and $Trp2R_6$. Immune signal composition of assembled polyplexes was examined by analyzing **(F)** absolute and **(G)** relative loading. All significant comparisons are vs. soluble CpG and indicated, $^{**}p < 0.01$, $\#p < 0.0001$.

4.4.7 Polyplexes with greater amounts of arginine residues drive increased antigen uptake by DCs

The physicochemical properties of immune signal carriers play an important role in altering immune responses. For example, positive surface charges can improve carrier interactions with negatively charged cell membranes, and several studies demonstrate nanoparticles may allow for more efficient uptake compared to larger micron-sized particles. Due to the differences in size, charge and loading of polyplexes, we next compared polyplex uptake by DCs across varying ratios and number of arginine residues. In these studies, DC uptake of CpG was similar to soluble CpG across nearly all polyplexes tested, with the exception of 2:1 $Trp2R_9$, which showed increased CpG uptake (**Fig. 4.8A**). In line with these findings, DC activation studies revealed that all polyplexes activated DCs on similar levels compared to soluble CpG controls (**Fig. 4.9**). Notably, however, $Trp2R_9$ complexes displayed slightly lower levels of activation markers across CD86, CD40, and CD80. These findings may be attributed to tighter condensation of $Trp2R_9$ binding, which may influence the availability of CpG and Trp2 for DC activation and antigen presentation to T cells, respectively. To evaluate Trp2 uptake, soluble $Trp2R_3$, $Trp2R_6$, and $Trp2R_9$ were dose-matched to the highest level of $Trp2R_x$ given for each set of arginine modification (i.e. 5:1 $Trp2R_x$:CpG) (**Fig. 4.8B**). At this dose of antigen, polyplexes increased $Trp2R_x$ uptake compared to their soluble $Trp2R_x$ counterparts. In this study, the most pronounced differences in increased antigen uptake

was observed with increasing $TrpR_x$:CpG ratio. $Trp2R_x$ uptake, however, only modestly increased with increasing number of arginine residues (i.e $Trp2R_3$ vs. $Trp2R_6$ vs. $Trp2R_9$).

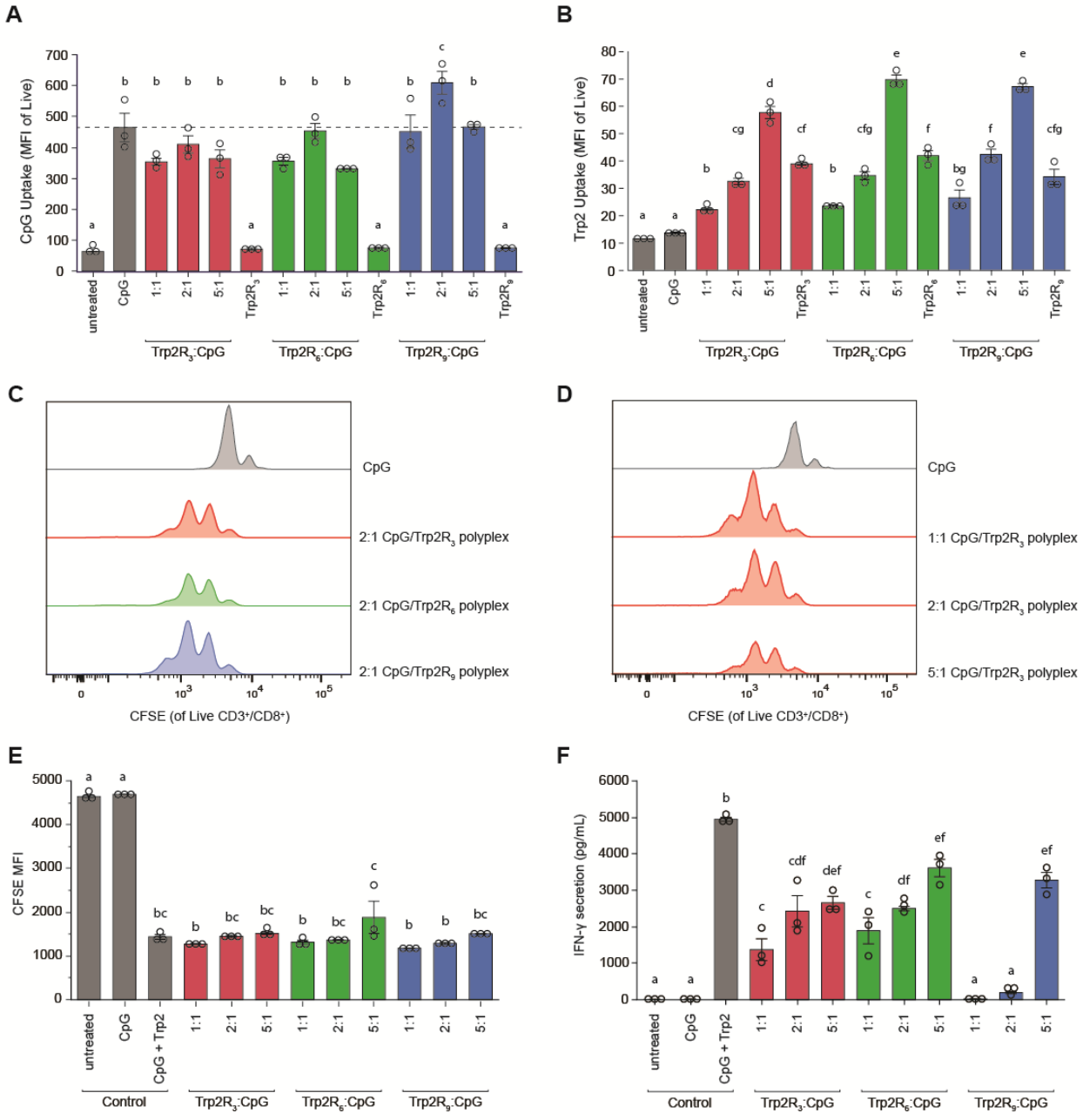

Figure 4.8 Arginine modifications on Trp2/CpG polyplexes influences T cell function
Polyplexes with different arginine modifications on Trp2 retain ability to deliver immune signals and expand T cells, but Trp2 loading in polyplexes influences T cell functionality. Flow cytometry was used to measure **(A)** CpG uptake and **(B)** $Trp2R_x$ uptake following 24h incubation with

$Trp2R_3$, $Trp2R_6$, or $Trp2R_9$ polyplexes. Representative histograms for T cells cultured with treated DCs demonstrate similar levels of T cell proliferation across different **(C)** numbers of arginine modification and **(D)** $Trp2R_x$:CpG ratio, with **(E)** quantification of proliferation by dilution of CFSE MFI. **(F)** ELISAs of supernatants from DC/T cell co-cultures reveal that IFN-γ secretion levels vary with number of arginine modifications and $Trp2R_x$:CpG ratio, with higher IFN-γ correlating with formulations with higher Trp2 loading. Different letters indicate statistical significance among means ($p < .05$).

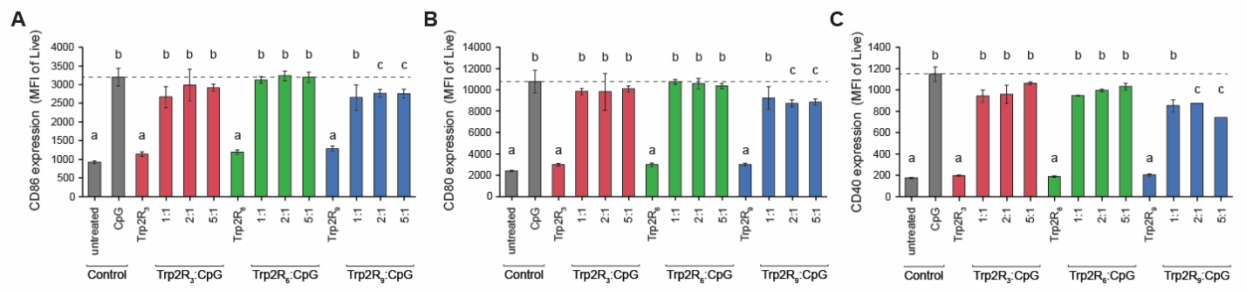

Figure 4.9 Polyplexes formed from Trp2 with different arginine modifications activated DCs on similar levels compared to soluble CpG controls
Different letters indicate statistical significance among means ($p < .05$).

4.4.8 Polyplexes with different arginine modifications retain ability to expand T cells, with higher Trp2 loading displaying improved T cell functionality

Because polyplexes formed with different arginine modifications displayed different antigen compositions, we next tested if different levels of arginine modifications altered T cell proliferation and function. In these studies, $TrpR_x$:CpG polyplexes displayed similar levels of proliferation across both number of arginine modifications and $TrpR_x$:CpG ratio (**Fig. 4.8C-E**). However, although CpG levels were fixed across ratios, we observed marked differences in IFN-γ levels, which increased with increasing $Trp2R_x$:CpG ratio (**Fig. 4.8F**). Polyplexes formed using Trp2 modified with R_3 and R_6, which have improved Trp2 loading over $Trp2R_9$/CpG polyplexes, also promoted more IFN-γ secretion suggesting that Trp2 loading in polyplexes plays a role in promoting T cell functionality.

4.4.9 Trp2-CpG polyplexes slow tumor growth and increase survival time in mice

Having identified a link between antigen dose and activation of adaptive immune responses, we next tested if the relative amount of antigen in polyplexes impacted tumor progression in a mouse model of melanoma. For these studies, we leveraged different levels of arginine modifications to alter the number of epitopes delivered. Mice were inoculated with 3×10^5 B16-F10 cells in the right hind flank (**Fig. 4.10A)**. When tumors reached an aggregate tumor size of 0.25 cm^2 (~ 7 days following inoculation), mice were treated *s.c.* at the tail base on the tumor draining side with either PBS (sham) or polyplexes formed from $Trp2R_3$, $Trp2R_6$, or $Trp2R_9$ at 3:1 $Trp2R_x$:CpG ratio. Mice received three additional treatments at 3 day intervals. In these studies, the dose of CpG was constant in all groups containing oligonucleotide. Mice treated with sham exhibited mean survivals of 15 days, while polyplexes formed from $Trp2R_3$ significantly improved survival to 25.8 days (**Fig. 4.10B-C**). Polyplexes formed from $Trp2R_6$ and $Trp2R_9$ also showed a modest improvement in survival of 21.8 days and 18 days, however, these were not significant. The improvements in survival were also reflected in the relative rate of increase in tumor burden when assessing individual animals in each group (**Fig. 4.10D**). In agreement with *in vitro* results, this study demonstrates that the ability of polyplexes to tune antigen dose and loading can be leveraged to promote significant improved outcomes during cancer vaccination.

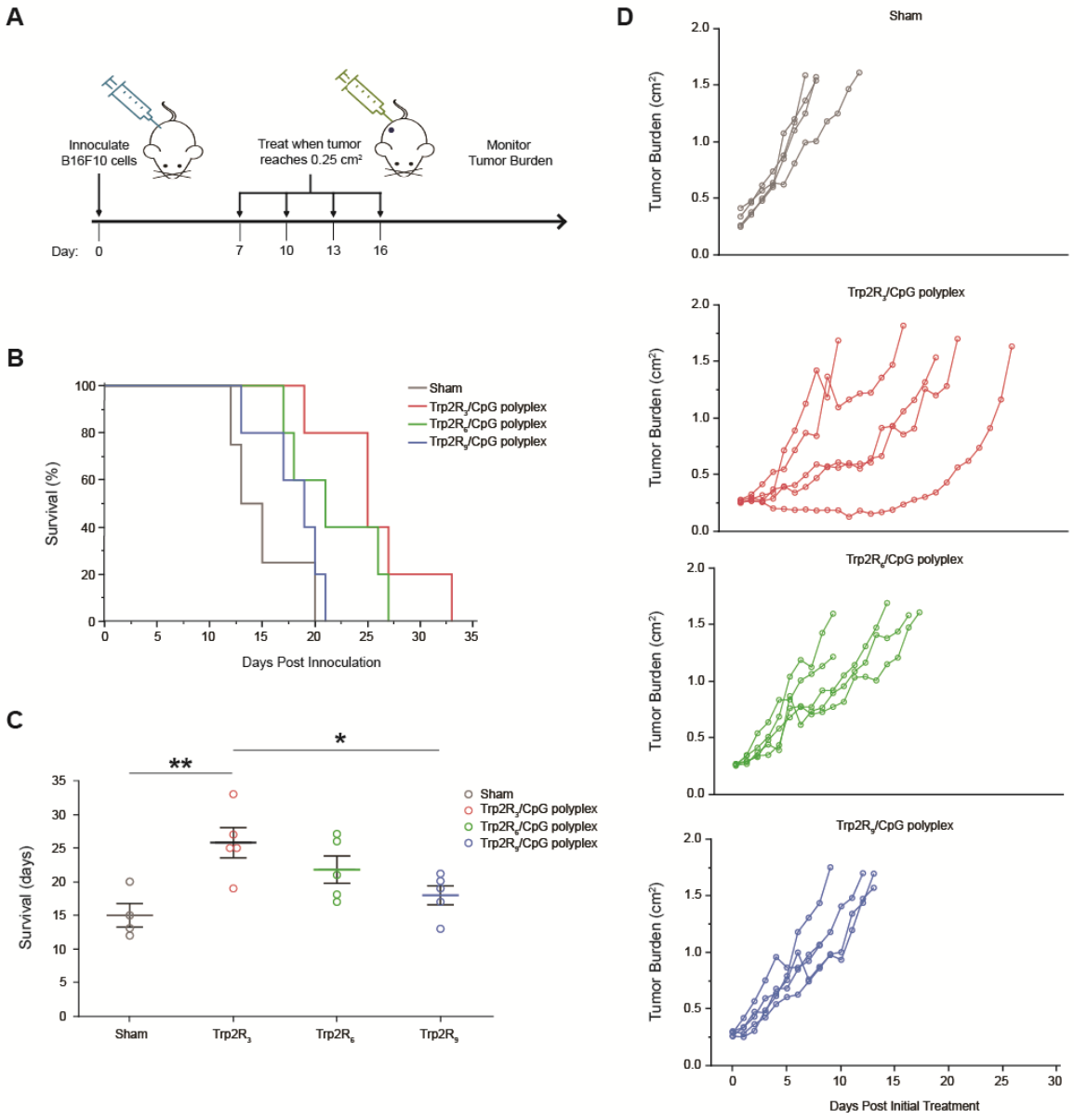

Figure 4.10 Trp2/CpG polyplexes slow tumor growth and increase survival time in mouse melanoma model

(A) Schematic of treatment regimen. Mice were inoculated with tumors and treated with either: 1) PBS (Sham) and polyplexes comprised of CpG condense with Trp2 modified with 2) R_3 3) R_6 4) R_9. Mice were treated every 3 days for 4 treatments total. **(B)** Survival curves and **(C)** mean survival for each treatment. All significant comparisons are indicated *$p < 0.05$, **$p < 0.01$. Survival was measured as days post innoculation. **(D)** Tumor burden curves for each individual mouse in the study. All significant comparisons are indicated *$p < 0.05$, **$p < 0.01$.

4.5 Discussion

Biomaterials offer many opportunities to improve upon current cancer therapies, many of which lack efficacy and fail to prevent relapse. We approached this challenge by harnessing the unique features of polyplexes to enable co-delivery of self-assembled melanoma antigen (Trp2) and a TLR agonist (CpG) in the absence of other carrier components. This approach can facilitate delivery of immune signals at high density to improve activation of potent immune responses. Designing simple, "carrier-free" vaccines provides an opportunity to develop insight into how each immune component impacts vaccine response to inform rational design of future vaccines. Additionally, we demonstrate that the modularity of this platform allows for incorporation of different antigen analogues to alter relative epitope concentration and physicochemical properties such as binding affinity, charge, and size. Importantly, we show that the underlying assembly processes are not impact by changes in the number of arginine modification, which is necessary to alter the amount of antigen in polyplexes. By assembling polyplexes with Trp2 and CpG, Trp2 was more efficiently internalized by DCs, colocalizing with CpG within cells. By tuning epitope concentration, we show that higher levels of antigen loading in polyplexes can promote improved antigen-specific T cell functionality *in vitro*, which translate to improved antitumor responses *in vivo*.

Polyplexes offer the opportunity to eliminate the presence of extraneous carrier materials in cancer vaccines while maintaining the features of traditional polymer platforms to leverage some of the physicochemical properties of biomaterial-based strategies. As one example, we found that polyplexes promoted improve antigen uptake compared to soluble antigen, which may be attributed to the particulate nature of complexes facilitating endocytosis. Additionally, modifying

Trp2 with arginine residues results in a polyR tail, a motif commonly found in cell-penetrating peptides, which may drive transcytosis. Tunable surface charge can also influence uptake as cationic particles can improve material interactions with the negatively charged cell membranes. Surprisingly, in our studies, condensation of negatively charged CpG to form positively charged particles did not improve uptake compared to soluble CpG. One possibility is that surface charge may alter the mechanism of cellular uptake and subsequent intracellular trafficking, which can hinder uptake. Binding affinity may also affect the dissociation and subsequently the delivery and processing of immune signals within cells [83,84].

Leveraging polyplex principles that require internalization in endosomes followed by escape into the cytosol for transcription and translation, our data demonstrates that polyplexes enable two distinct yet critical delivery routes. First, the ability of complexes to activate DCs suggests that polyplexes allow for the delivery and binding of CpG to receptors in endosomes to activate TLR pathways. Secondly, antigen delivered within cells can undergo endosomal escape into the cytosol for loading onto MHC-I, a critical step for activating $CD8^+$ T cells. Elucidating the precise trafficking mechanisms that facilitate polyplex processing through these pathways can offer valuable insight towards improving co-delivery of immune components.

We also observed some interesting differences in how CpG behaved in complexes versus soluble form. During DC activation studies with $Trp2R_9$ polyplexes, although $Trp2R_9$:CpG promoted high expression of activation markers, polyplex treated DCs were less activated compared to free CpG alone, and activation was further attenuated with increasing $Trp2R_9$:CpG (**Fig. 4.4B-D**). One potential explanation is the strong binding between $Trp2R_9$ and CpG at higher ratios of $Trp2R_9$:CpG which could require a longer time for binding and processing or limit the

availability of CpG to TLR9 receptors. Although the SYBR Green exclusion assay suggested similar binding levels (**Fig. 1B**), more sensitive measurements of binding affinity such as surface plasmon resonance might provide additional insight into some of the different effects. Despite the less efficient activation of DCs by some $Trp2R_x$:CpG ratios, all polyplex formulations still promoted strong levels of activation and further, provide other benefits such as improved antigen uptake and protection from enzyme. Importantly in our studies, treatment of cells with free $Trp2R_x$ or $Trp2R_x$-ODN polyplexes generally did not activate cells, suggesting that CpG is the key driver of these observed effects.

Interestingly, polyplexes across all arginine modifications displayed similar levels of uptake, DC activation, and T cell expansion, despite changes in physicochemical properties for each library of Trp2 analogues. We instead observed that polyplexes formed from CpG and Trp2 modified with R_3 generally stronger T cell responses compared to complexes modified with R_6 or R_9. One possibility is that $Trp2R_3$ more closely resembles native Trp2 because it contains the fewest modifications and closest protein length, making it more easily processed by DCs and more readily identifiable by $CD8^+$ T cells specific to Trp2. Alternatively, at a given $Trp2R_x$:CpG ratio, $Trp2R_3$ complexes contained higher levels of Trp2, which may improve tumor-specific T cell activation. Many antigens expressed on tumors are also expressed on normal tissues; thus T cells specific to many tumor antigens are subject to thymic selection which deletes high avidity T-cells recognizing self-antigen [218]. This leaves a repertoire of low avidity T cells that require high doses of antigen to become stimulated [219]. This is corroborated by our findings that increasing the antigen concentration by altering Trp2:CpG by was found to correlate with improved T cell functionality.

4.6 Concluding remarks

Our approach reveals several important questions for future studies. First, we prepared polyplexes using different analogues of the same tumor epitope. While T cells recognize specific epitopes, tumor antigens are larger proteins which present multiple peptide fragments, each with varying degrees of immunogenicity [220]. Thus, additional studies are needed to investigate if the modularity of polyplexes can be extended to other tumor epitopes. Additionally, the polyplexes prepared in these studies contain a single antigen epitope. Recent studies, however, suggest that immunotherapies that target multiple epitopes allows for improved anti-tumor responses [221,222]. As one example, EMD640744, a multi-epitope vaccine for patients with advanced solid tumors, is currently undergoing phase I clinical trials [223]. Targeting multiple epitopes allows for a wider spectrum of antigens that expanded T cells can recognize within heterogenous tumor cell populations. Further, potent anti-tumor responses arise from simultaneous induction of both humoral and cellular responses, requiring different epitopes to activate B cells and multiple subsets of T-cells [224–226]. Thus, there is also motivation to test if multiple epitopes can be incorporated into polyplexes. Lastly, the finding that $Trp2R_3$ elicited the strongest functional T cell responses and subsequently improved tumor-burden raises some interesting implications surrounding the role of antigen in promoting anti-tumor immunity. Our results demonstrate that polyplex structures comprised of immune signals offer a tunable platform to co-deliver CpG and Trp2 peptide, while eliminating carrier components. As highlighted in our studies utilizing different Trp2 peptide modifications, the simple approach and modularity of this platform offers a unique opportunity to study the role of antigen dosing, structure, and co-delivery in stimulating effector T cell responses – this insight can contribute to new therapies to improve tumor-specific immune responses.

Chapter 5: Modular control of lymph node niches to control T cell fate in immune tolerance

5.1 Introduction

As highlighted in the above chapters, biomaterials offer controlled release, targetting, and co-delivery of multiple classes of cargo well suited for improving immune responses in cancer, due to their ability to direct immune responses in a tunable and precise manner. These same properties can be exploited in other diseases to combat immune dysregulation. Biomaterials are now also increasingly being used to study and treat autoimmune diseases – conditions in which immune cells incorrectly attack healthy host tissues – where the balance between inflammation that drives disease and tolerance that regulates inflammation depends on the concentrations and location of immune signals and their integration into LNs.[12,22,227–230] This body of work leverages a biomaterial platform to encapsulated immune signals that are directly deposited into LNs. While the Jewell lab has shown this system to be highly effective for eliciting strong tolerogenic responses, this dissertation work demonstrates that in addition to its potential as a therapeutic platform, iLN treatment also offers a powerful tool to study the role of immune signal integration in LNs. In this chapter, iLN treatment is used to study how 4 specific design parameters for immunotherapies– i) relative tissue location of delivery ii) total dose iii) signal densities and iv) relative signal concentrations– give rise to these exciting outcomes. This approach will improve understanding of how immune signals impact local function to shape strong and durable tolerogenic responses and enable improved therapeutic design for autoimmune diseases such as MS. More broadly, these findings could contribute to a greater understanding of how biomaterial features can be rationally designed to improve immunotherapies.

5.2 Background

Multiple sclerosis (MS) is an autoimmune disease in which immune cells in the central nervous system (CNS) attack myelin peptide on neurons, resulting in inflammation and loss of CNS function.[231–233] Conventional therapies for MS are non-specific and non-curative, which can leave patients immunocompromised and require life-long treatments. These strategies provide important benefits by blocking receptors or inflammatory immune function; however, they fail to differentiate between myelin-reactive cells and healthy lymphocytes. Alternative pre-clinical approaches aim to develop more selective tolerance, such as generating regulatory T cells (Tregs). In preclinical studies, several groups have shown that Tregs can suppress inflammatory cells in an antigen-specific manner,[7,234,235] offering a promising strategy to polarize myelin specific T cells toward tolerogenic phenotypes, without compromising the rest of the immune system.

Because therapeutic induction of antigen-specific immune tolerance is an emerging clinical area in autoimmune therapy that has yet to realize success, new advances would benefit from greater insight into the mechanisms that drive efficacy and selectivity. As mentioned in **Chapter 2**, lymph nodes (LNs) are sites where T cells differentiate and expand against antigens (e.g. myelin) in response to immune cues. Thus, one critical area towards enabling the therapeutic potential of candidate therapies is delivery to LNs and insight into the integration of signals that occurs within these tissues. However, achieving direct control over the concentrations and combinations of signals integrated in LNs to exploit these possibilities has been difficult. One reason for this is the lack of precise control over delivery of immune signals to the LN. Typically, immune signals are administered via conventional delivery routes such as subcutaneously (s.c.) or intramuscularly (i.m.), which must then travel from the periphery to draining LN through the

lymphatics. Alternatively, these signals may be carried to LNs by APCs. Poor targeting efficiency after injection prevents direct control over the combinations and dosage of signals that reach LNs. Even target approaches which increase the amount of signal reaching LNs result in most of the injected material accumulating at the injection site of going to off-target tissues and vessels. Once in LNs, soluble signals are rapidly cleared by lymphatics further limited exposure.[30,236] Moreover, significant loss and degradation of antigen and adjuvant often results in poor efficacy and other undesirable off-target effects due to systemic exposure to drugs. The lack of spatial control remains a major obstacle in understanding how local immune signals affect the LN microenvironment and function in tolerance.

The Jewell lab has developed a modular system to directly deposit antigens and modulatory immune cues, such as rapamycin (Rapa) – a small immunomodulatory molecule that promotes the expansion of Tregs[237] - in LNs. In this approach, tracer dye is administered at the tail base of mice drains to neighboring LNs, allowing for topical visualization of inguinal LNs for direct injection. In this system, MPs are synthesized using double emulsion to prepare MPs that are too large to drain from the LN. Instead, the MPs slowly degrade to locally release peptide antigens and molecular modulators in the LN microenvironment. Previous studies revealed that a single direct intra-LN injection (*iLN*) of tolerogenic microparticles (MPs) containing myelin peptide (MOG) and Rapa can combat immune-mediated neurodegeneration in mouse models of MS (EAE), demonstrating the exciting therapeutic potential of this platform.[238] Further, these therapeutic effects do not occur when MOG/Rapa depots are administered to *muscle* (*i.m.*) instead of LNs or when *soluble antigen* is mixed with Rapa MPs and injected to LNs. Importantly, these findings suggests that local integration of MOG and Rapa within LN play different or perhaps synergistic

roles in determining efficacy and durability. This result motivates a need to elucidate how the geographic distribution of signal in LN affects the recruitment, expansion, and differentiation of antigen specific T cells, and the ultimate impact on regulatory function and the ability of this therapy to induce and maintain systemic tolerance.

Leveraging the unique features of the platform, this body of work highlights iLN injection as a tool to study immune responses in tolerance. Using this platform, we elucidate defining immunological features and mechanisms for inducing robust tolerogenic responses. This is achieved by addressing four tunable design parameters – i) distribution of cargo components with respect to distinct LNs, ii) total cargo dose, iii) cargo density in MPs depots, and iv) the relative concentration of each cargo in the MPs. This body of work demonstrates that iLN injection of MP depots can directly control the concentration and combinations of signals integrated into LNs. Precise spatial control allows for generation of multiple distinct immune responses in different LNs within the same mouse. Leveraging this capability, new mechanistic insights into the role MOG and Rapa integration within LNs in inducing systemic tolerance are gained. The combination of MOG and Rapa promotes the generation and retention of MOG-specific Tregs within treated LNs while supporting higher frequencies of Treg in non-treated LN. In EAE, lower clinical scores are observed in mice that received MOG and Rapa delivered in MPs to the same LN. This is facilitated in part by the ability of MOG/Rapa MPs to lower the frequency of MOG-specific inflammatory T cells. The potency of induced tolerance is dependent on the dose, but the not the density of the delivered immune signals. Finally, the relative signal concentrations of MOG and Rapa plays a role in generating tolerogenic responses. The knowledge obtained through this

work provide critical insight towards therapeutic formulation and design of more potent, long-lasting immunotherapies in MS.

5.3 Materials and Methods

5.3.1 Materials and Reagents

Myelin oligodendrocyte glycoprotein, MOG_{35-55} (MEVGWYRSPFSRVVHLYRNGK), Cy5 fluorescently labelled MOG peptide, and ovalbumin peptide $OVA_{323–339}$ (ISQAVHAAHAEINEAGR) were purchased from GensScript at >98% purity. Rapamycin was purchased from LC Laboratories. Poly(lactide-co-galactide) (PLGA) was purchased from Durect, and poly(vinyl alcohol) (PVA) was purchased from Alfa Aesar.

5.3.2 Animals

6–12-week-old, female age matched mice were used for all experiments. Wildtype (WT) C57BL/6J (Thy1.2), Thy1.1 (B6.PL-*Thy1*^{a}/CyJ), and OT-II (Thy1.2) mice (Tg[TcraTcrb]425Cbn) were purchased from The Jackson Laboratory (Bar Harbor, ME). MOG-specific 2D2 (Thy1.2) TCR transgenic mice (Tg[Tcra2D2,Tcrb2D2]^{1Kuc} were bred in University of Maryland facilities. 2D2.Thy1.1 reporter mouse strains were generated by crossing 2D2 mice with Thy1.1 mice. All 2D2 and 2D2.Thy1.1 mice were genotyped to confirm the appropriate phenotype. All animal studies were fully compliant with local, state, and federal guidelines per the Association for Assessment and Accreditation of Laboratory Animal Care (AAALAC) expectations for animal care and use/ethics. All studies were approved and carried out under the supervision of the University of Maryland Institutional Animal Care and Use Committee (IACUC).

5.3.3 MP Synthesis

Microparticles (MPs) were synthesized by double emulsion and solvent evaporation as previously described.[123] Briefly, an inner aqueous phase of 500 μL was prepared with either water, 1 mg OVA323-339, 1 mg MOG35-55 in 500 μL water. For CpG loaded MPs, the inner aqueous phase was prepared with 0.5-1mg CpG in 1X TAE buffer. A primary emulsion was generated by sonicating 80 mg PLGA dissolved in 5 mL dichloromethane with 500 μL of an inner aqueous phase for 30s at 12W. For Rapa loaded MPs, a 2 mg of aliquot of Rapa was added to the dichloromethane phase prior to synthesis. This initial emulsion was then homogenized with 40 mL water containing 2% w/v polyvinyl alcohol (Alfa Aesar) at 16,000-18,000×g for 3 min, and stirred overnight to allow for solvent evaporation.

MPs were filtered through a 40 μm strainer and collected via centrifugation at 5000×g for 5 min at 4°C. Supernatants were removed, and MPs were washed three times with 1 mL water. MPs were resuspended in 1X PBS for iLN injection. Particle size was determined using an LA-950 laser diffraction analyzer (Horiba). To determine Rapa loading, a known mass of dried MPs was dissolved in dimethyl-sulfoxide, and the absorbance at 278nm was determined using UV/VIS spectrophotometry. Peptide loading was measured using a Micro Bicinchoninic Acid (mBCA) Protein Assay kit (ThermoFisher Scientific Pierce) according to manufacturer's instructions. Standard curves of known concentrations of Rapa and peptide were used to calculate loading, which is reported as the mass of cargo per mass of dried MP formulation. For preparation of fluorescently labeled MPs, 5 μL of DiI or 0.2mg of DiR was dissolved with PLGA prior to the primary emulsion during MP synthesis, and Cy5-labeled MOG was used in place of unlabeled MOG during synthesis.

5.3.4 Intra-Lymph Node MP Injections

Tolerogenic MP treatments were delivered directly to LN using a non-surgical, iLN injection technique as previously described by the Jewell Lab.[123–125] Briefly, prior to injection, mice were shaved above the injection site and remaining fur was removed using a mild depilatory cream. One day prior to iLN injection, a tracer dye (Evans blue, Alfa Aesar) was injected subcutaneously at each side of the tail base. Each mouse received two injections – one into each inguinal LN – containing 0.1-1 mg of each indicated MP formulation in 10 μL of PBS using a 29g syringe.

For iLN treatments prior to disease onset, mice were induced with disease and randomized into treatment groups following induction. For iLN treatments following disease onset, mice were assigned to normalized groups to ensure consistent clinical scores between groups on the day of injection.

5.3.5 In vivo imaging

Imaging of indicated surgically excised LNs was performed using an IVIS Spectrum in vivo imaging system (Perkin-Elmer). DiR (Thermo) Animals were injected *iLN* with fluorescently labelled MPs as described with one LN receive DiR fluorescent MPs, and one LN receive Cy5-MOG DiI MPs. 2 days following *iLN* injection, mice were imaged under anesthesia. Mice were then euthanized and LNs were excised and imaged. Exposure times and lamp settings were determined from single-fluorophore controls. Image analysis was performed using Living Image Software and quantitative analysis was done using doing region of interest (ROI) analysis of total radiant efficiency.

5.3.6 Cell preparation and isolation from tissues

At the indicated time points, immune tissues were collected from mice. Treated inguinal LNs, CNS draining cervical LNs, or spinal cords were collected and manually dissociated through a 40 μm cell strainer. Cells were collected by centrifugation (5 min, 500xg, 4°C). LN cells were washed with PBS without lysis. Cells were collected from spinal cord using a gradient to remove debris (Debris Removal Kit, Miltenyi). Cells were then analyzed by flow cytometry.

5.3.7 Flow cytometry studies

Cells from lymphoid organs, CNS, or ex vivo cultures were resuspended in FACs buffer (PBS with 1% FBS), BD, Clone 2.4G2) for 10min on ice. For analysis of cytokine-producing T cells, recovered lymphocytes were restimulation with $MOG_{35–55}$ peptide for 4h with brefeldin A (BD Bioscience) prior to staining. Cells were then stained with surface marker antibodies for 20 minutes on ice. Cells were then washed two times with FACS buffer and were either analyzed immediately or stained for intracellular markers. For intracellular stains cells were fixed and permeabilized by incubating with fix/perm buffer from the Foxp3/Transcription factor staining buffer set (eBioscience) for 40 min at 4 degrees C. Cells were stained with antibodies against intracellular markers for 30 min at 4 degrees C, followed by two washes with perm/wash buffer. Flow cytometry data was acquired using a Canto II (BD) or FACSCelesta (BD). DAPI or LIVE/DEAD Fixable Viability Dye (Thermofisher). Data was analyzed with FlowJo software (FlowJo LLC).

The following antibodies used for flow cytometry: CD4 (RM4-5), CD11c (N418), CD44 (IM7), CD62L (MEL-14), CD90.1 (OX-7), CD90.2 (53-2.1), B220 (RA3-6B2), CD25 (PC61).

Foxp3 (MF23), Tbet (O4-46), ROR-γ (Q31-378), anti-s6 pS235/S236 (N7-584), IFNγ (XMG1.2), IL-17 (TC11-18H10). Antibodies were purchased from BD Biosciences.

5.3.8. Adoptive Transfer Studies

Naive T cells from spleens and lymph nodes of donor OT-II (Thy1.2), 2D2 (Thy1.2), or 2D2.Thy1.1 mice were isolated using CD4 negative magnetic selection (Stemcell) per the manufacturer's instructions, and then were adoptively transferred to host WT C57BL/6J mice or Thy1.1 mice by intravenous (*i.v.*) injection. Prior to adoptive transfer into naïve or EAE mice, isolated T cells were labeled with CSFE or eFluor450 (Invitrogen) to measure proliferation and in studies where the donor and host T cells could not be differentiated by congenic Thy1.2/Thy1.2 markers. At indicated times following T cell transfer, host mice were sacrificed and LNs were processed and analyzed by flow cytometry. Transferred T cells were identified using a combination of both Thy1.1/Thy1.2 marker stains and CFSE/eFluor450.

5.3.9. Active EAE Induction and Passive EAE Induction

Emulsion was prepared using a 50:50 ratio (v/v) of 2mg/mL $MOG_{35–55}$ peptide in sterile PBS and Complete Freund's Adjuvant (CFA). CFA was made by grinding heat-inactivated *Mycobacterium tuberculosis* H37Ra (BD Difco) with a mortar and pestle and mixing with Incomplete Freund's Adjuvant (BD Difco) at 4mg/mL. This suspension was emulsified using a probe sonicator (Qsonica, CL-18 and 1/8 in. probe, 4422) while in a chilled ice bath and loaded into needles. A total of 200 µl of emulsion was injected into WT mice given as either two 100µl dorsal subcutaneous injections along the midline or as four 50µl dorsal subcutaneous injections spaced on each side of the midline. Two and 24 hours later, mice were injected i.p. with 60 ng of

pertussis toxin (List Biological Laboratories, 179A). Alternatively, EAE was induced using a kit from Hooke laboratories according to the manufacturer's instructions. Validation studies were performed to verify that both methods yielded comparable disease. Clinical signs of disease were monitored according to the following scheme: 0, no symptoms; 0.5, partial tail paralysis; 1, paralyzed (limp) tail; 1.5, decrease in hind limb stability; 2, hind limb weakness and altered gait; 2.5, partial hind limb paralysis; 3, hind limb paralysis; 3.5, hind limb paralysis and trunk weakness; 4, hind limb paralysis and partial front limb paralysis; 4.5, hind and front limb paralysis; and 5, moribund. Humane end points were set for a score of 4 for 2 days or anytime a score was >4.5. Water and food were localized at the cage floor level to accommodate the levels of paralysis during the disease course. To induce passive EAE, active EAE was induced as described above into 10-week-old WT mice. In studies that tracked disease inducing cells, Thy1.1 mice were used. 10-14 days following induction, cells from spleens and LNs from EAE mice were processed into single-cell suspensions, resuspended in Ack lysis buffer (Invitrogen) to remove red blood cells and then washed with PBS. Collected cells were re-stimulated *in vitro* with 10 ng/mL of IL-23 (R&D Systems) and 20 μg/mL of $MOG_{35–55}$ peptide. Activated cells were collected 3 days later and resuspended in PBS. Each mouse was injected i.p. with 10-15 x 10^6 cells in 200μL. Due to faster disease kinetics in the passive model, mice were monitored for clinical symptoms beginning on day 5, using the same scoring criteria outlined above.

5.3.11 Statistical Analysis

Statistical calculations were performed using JMP Pro (v14, SAS Institute). All tests and sample sizes are indicated in the figure legends. Error bars in all panels represent the mean ± standard deviation and p values ≤ 0.05 were considered significant with levels of significance were defined

as *p<0.05, **p<0.01, ***p<0.001, #p<0.0001. For comparisons of more than two groups, one-way ANOVA with Tukey's post test was performed to compare across all groups, or a Dunnett's test was performed to compare each group to a control. For comparisons of two groups, two tailed Welch's t test was performed. For EAE, these tests were used for comparisons at individual time points or comparison of clinical disease burden. Kaplan−Meier survival analysis was performed using a Wilcoxon test to compare global effects as indicated by the exact p-values in the relevant figures.

5.4 Results

5.4.1 iLN delivery offers a platform for spatial control over immune signal delivery to distinct LNs

We previously demonstrated that depots loaded with MOG and Rapa drive strong tolerance with a single treatment. However, how T cells are recruited and polarized as a function of signals in LNs using this approach is unknown. To investigate this, MPs were synthesized and loaded with combinations of MOG and OVA peptides and Rapa or CpG, an adjuvant leveraged for studies in **Chapters 3** and **4**. Loading of these immune signals within MPs can be readily tuned within a size range of 2-5 μm (**Table 5.1**). At this size, MPs are too large to passively drain from the LN, ensuring that most of the cargo in retained in LNs where it can interact with APCs and T cells. Because injected MP depots containing immune signals directly injected into LNs and are size restricted to prevent draining through efferent lymphatics, we hypothesized that iLN injection could be expanded to deliver multiple therapeutic formulations, each of which would be restricted to the treated LN.

Table 5.1 PLGA MP Characterization for Multiple Immune Signals

MP Formulation	Diameter (μm)	Antigen Loading (μg/mg MP)		Immunomodulatory Signal Loading (μg/mg MP)	
		MOG	OVA	CpG	Rapa
Empty	2.82 ± 1.19	n/a	n/a	n/a	n/a
MOG	2.51 ± 0.93	11.00 ± 0.80	n/a	n/a	n/a
Rapa	2.16 ± 0.76	n/a	n/a	n/a	19.7 ± .94
MOG/Rapa (1X)	2.72 ± 1.10	9.59 ± 0.92	n/a	n/a	21.6 ± 1.21
MOG/CpG	4.59 ± 0.54	9.11 ± .59	n/a	15.64 ± 0.10	n/a
OVA/Rapa	3.63 ± 0.49	n/a	9.78 ± 0.88	n/a	16.95 ± 1.46
OVA/CpG	4.64 ± 0.68	n/a	3.39 ± .39	9.70 ± 0.11	n/a
MOG/Rapa (.2x)	2.51 ± 0.98	2.74 ± 0.24	n/a	n/a	4.59 ± 0.26
MOG/Rapa (2X)	2.51 ± 1.01	20.35 ± .76	n/a	n/a	22.08 ± 2.84
80/20 MOG/Rapa	2.92 ± 0.96	6.45 ± 0.28	n/a	n/a	21.82 ± 1.40
50/50 MOG/Rapa	2.76 ± 0.99	12.83 ± .03	n/a	n/a	14.39 ± 1.39
20/80 MOG/Rapa	2.89 ± 1.09	21.22 ± 0.81	n/a	n/a	7.04 ± 1.26

*n/a indicates no loading of specific antigen or immunomodulatory signal into particle

We first confirmed that MPs are retained and restricted to treated LNs. To demonstrate that iLN depots can deliver treatment regimens that are locally restricted to the treated LN, two different MP formulations encapsulating different fluorescent dyes were injected into contralateral LNs. In this study, one LN received MPs fluorescently labelled with DiI encapsulating Cy5-labelled MOG peptide (Cy5-MOG DiI MP), while the contralateral LN received MPs fluorescently labelled with DiR (DiR MPs) (**Fig. 5.1A**). 48 hours after MP treatment, live mice were imaged by IVIS for each fluorescent signal (**Fig. 5.1B)**. To verify that the signals observed in live mice were localized to LNs, the treated LNs were isolated and imaged by IVIS (**Fig. 5.1C**). Cy5-MOG and

DiI signal was observed only in LNs that received Cy5-MOG DiI MP (**Fig. 5.1D**), while only DiR signal was detectable in the LN that received DiR MPs (**Fig. 5.1E**).

Analagous results were observed following processing of LN into single cell suspensions and analysis of immune signal counts using flow cytometry (**Fig. 5.1G-H)**. Importantly, delivered signals were associated with APCs such as dendritic cells ($CD11c^+$) (**Fig. 5.1I-J)** and B cells (data not shown). Further, the immune signals engaged by APCs within treated LNs was restricted to the signals that were delivered to the LN, such that in the Cy5-MOG DiI MP treated LN, immune cells were primarily associated with Cy5-MOG and DiI signals, while immune cells in the DiR MP treated LN were primarily associated with DiR signal. This data demonstrates that iLN treatment allows for restriction of large immune signal reservoirs to treated LNs that immune cells can locally engaged with.

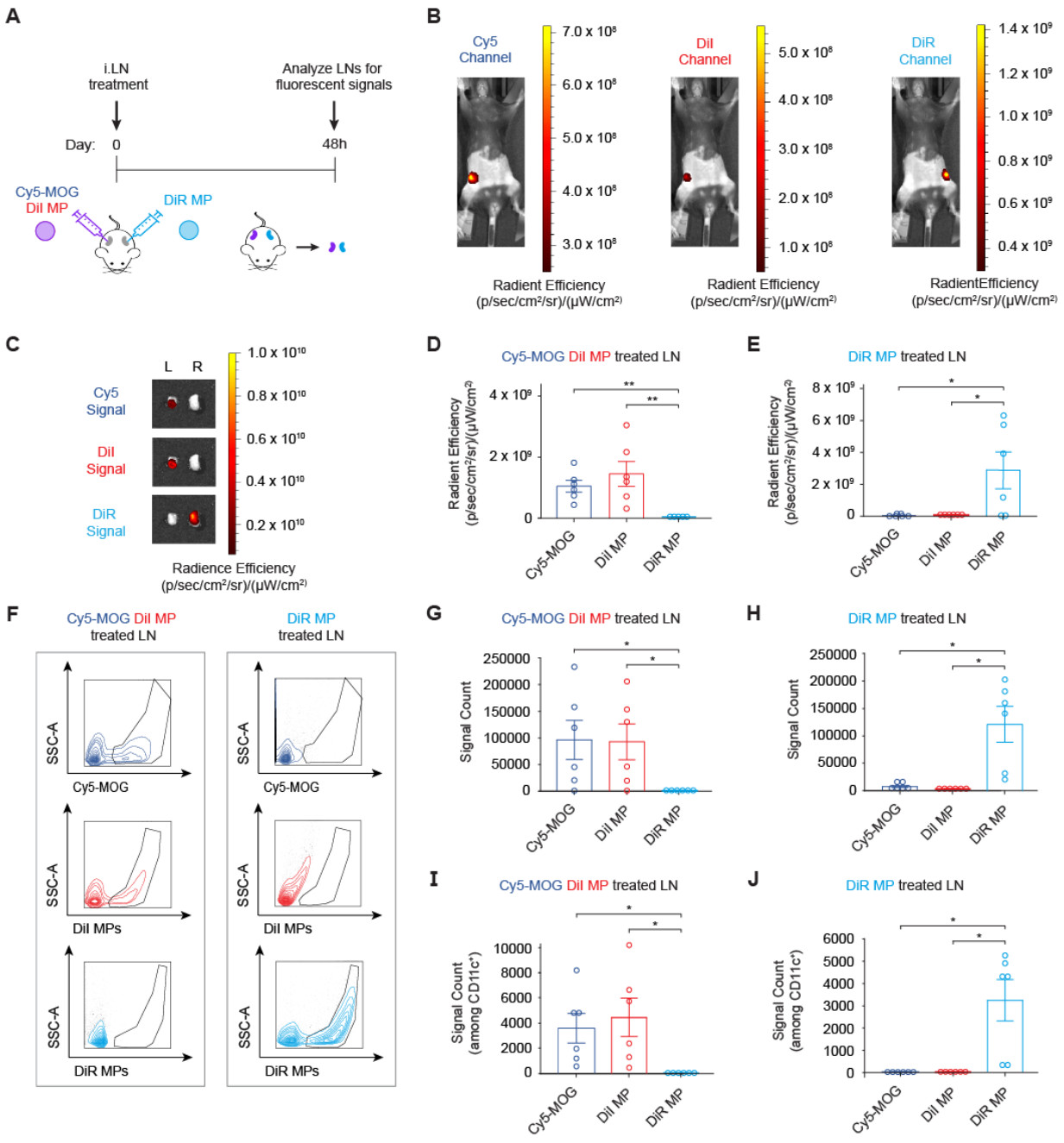

Figure 5.1 iLN injection provides spatial localization of immune signals to specific LNs.
(**A**) Schematic representation of experiment. N = 6 mice used in this experiment. Each data point is individually represented. (**B**) IVIS images of iLN treated mice (**C**) IVIS images of excised treated LNs. (**D**) quantitation of signals in Cy5-MOG DiI MP treated LN and (**E**) DiR treated LNs. One way ANOVA with Tukey's post hoc test was used to compare each treatment group. Individual LNs were used as single data points. Mean ± standard error of the mean (SEM) is shown. (**F**) Representative flow cytometry gating showing Cy5-MOG, DiI MP, and DiR MP signal in treated LNs. Quantification of signal count in (**G**) Cy5-MOG DiI MP treated LN and (**H**) DiR

treated LNs. N = 6 LNs for all groups in all experiments. The mean ± SEM is shown. One way ANOVA with Tukey's post hoc test was used to compare each indicated LNs. Quantification of CD11c engagement with delivered signals in (**I**) Cy5-MOG DiI MP treated LN and (**J**) DiR treated LNs. N = 6 LNs for all groups in all experiments. The mean ± SEM is shown. One way ANOVA with Tukey's post hoc test was used to compare each indicated LNs at each timepoint. *$p < 0.05$, **$p < 0.01$

5.4.2 Local LN delivery provides recruitment and polarization of antigen-specific T cells with geographic control

Because immune cell engagement with delivered immune signals was found to be locally dependent, we next tested if iLN treatment could locally direct multiple immune responses simultaneously within the same host. In these studies, Thy1.1 mice were injected with MPs containing either MOG or OVA antigen in combination with an immunoregulatory cue – Rapa, or a pro-immune cue – CpG (**Fig. 5.2A**). As mentioned in previous chapters, CpG is a DNA motif commonly found in bacteria, that can trigger inflammatory responses and drive T cell proliferation. These mice were then infused with a 1:1 mixture of antigen-specific T cells from recognizing epitopes within MOG (2D2) or OVA (OT-II). Thus, T cells from 2D2 mice recognize only MOG peptide, while T cells from OT-II mice only recognize OVA peptide. Each cohort was injected iLN, with the right inguinal LN receiving antigen and Rapa and the left inguinal LN receiving the same antigen and CpG. One day following treatment, $CD4^+$ T cells specific for MOG and OVA were isolated from 2D2 and OT-II transgenic mice, respectively. The recipient Thy1.1 mice used for these studies are a congenic strain that carry the T cell Thy1.1 allele in place of the wildtype Thy1.2 allele carried by donor 2D2 and OT-II cells. As a result, donor T cells transferred into these mice can easily be distinguished from recipient T cells through their signature Thy1.1 marker. Prior to transfer, each antigen-specific cell population was labelled with distinct fluorescent dyes – either CFSE (2D2) or eFluor450 (OT-II), to enable tracking of each individual cell type and proliferation. CFSE and eFluor proliferation dyes covalently bind intracellularly, lending the

ability to monitor distinct generations of proliferating cells by dye dilution. Three days after transfer, LNs were analyzed for proliferation of antigen-specific subsets and T cell phenotype.

Excitingly, these studies revealed proliferation of transferred T cells was localized to the specific LNs treated with the MPs containing cognate antigen, even when the cells were infused systemically (**Fig. 5.2B-E**). Within treated LNs, 2D2 cells proliferated in mice that received MOG antigen, but remained undivided in mice that received OVA antigen (**Fig. 5.2B**). Conversely, OT-II cells proliferated in mice that received OVA, but remained undivided in mice that received MOG peptide. Within each mouse, the extent of proliferation was dependent on the immunomodulatory molecule delivered (**Fig. 5.2C)**. LNs that received CpG proliferated to a much greater extent than their Rapa-treated counterparts in both MOG (**Fig. 5.2D)** and OVA (**Fig. 5.2E)** treated mice. These findings were in line with established immune functions for both CpG, which drives immune activation and proliferation and Rapa, which inhibits T cell proliferation. These results suggest that iLN injection allows spatial localization of T cell priming and expansion, eliminating the need for systemic cargo delivery. To test if iLN injection likewise allows for locally restricted polarization toward inflammatory or regulatory phenotypes, the transferred T cells within each treated LN were analyzed for Tregs ($CD25^+$ $FoxP3^+$) and Tbet expression. Tbet is a transcription factor that is activated during immunostimulation with CpG and plays a role in proimmune inflammatory Th1 differentiation[239]. Among 2D2 T cells in MOG treated

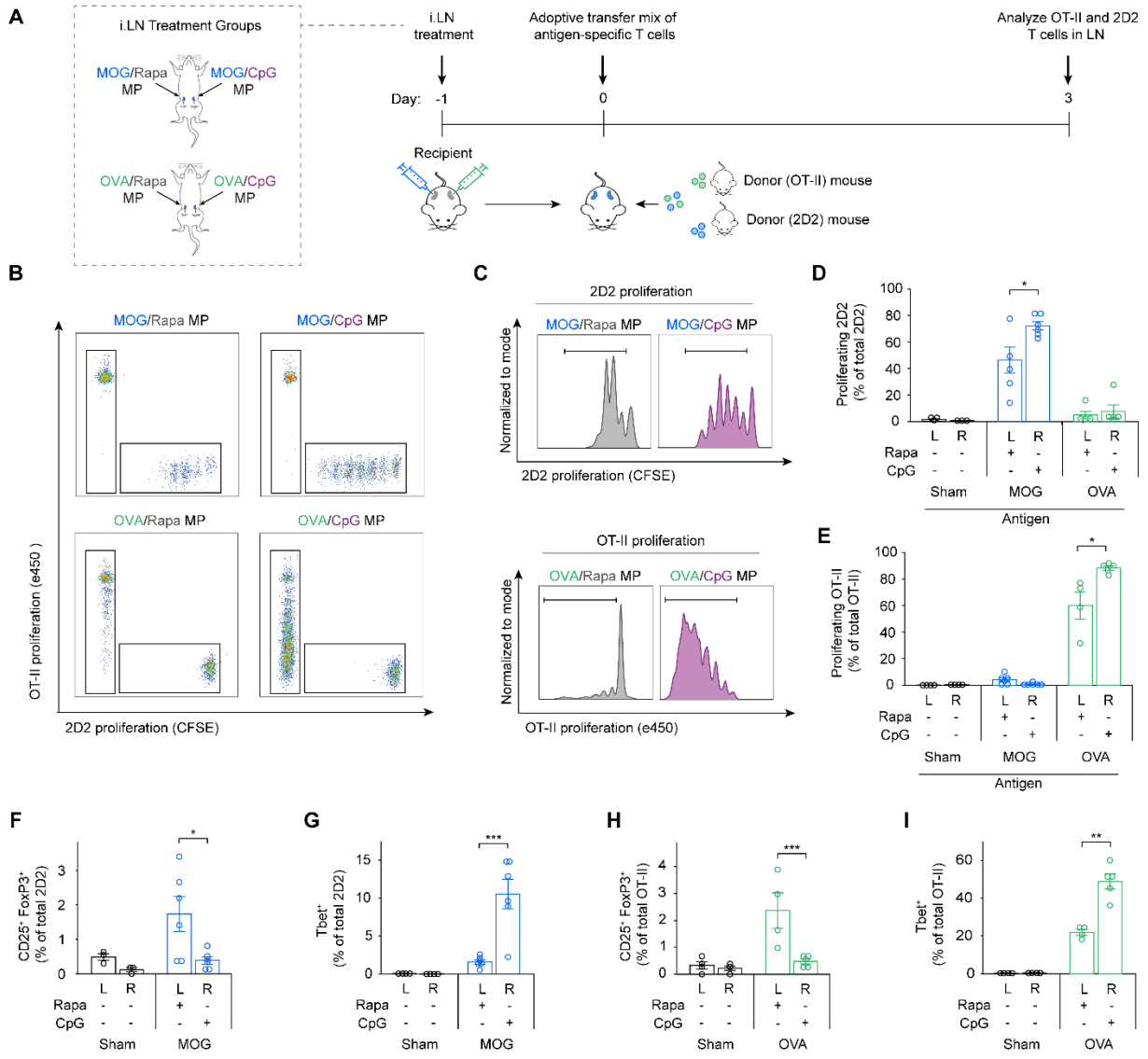

Figure 5.2 Spatial control over immune signal delivery offers precise local tuning of immune response in antigen dependent manner.

(**A**) Schematic representation of experiment. N = 3 mice for sham treatment group and N = 5 for all other treatment groups. Each data point is individually represented. (**B**) Representative flow cytometry plots for proliferation of mixed antigen-specific T cells comprised of MOG and OVA specific T cells. (**C**) Representative proliferation traces for individual MOG and OVA specific T cells. Quantification of proliferation for (**E**) MOG specific T cells and (**F**) OVA specific T cells. N = 3 mice for sham treatment group and N = 5 for all other treatment groups. Individual LNs were used as single data points (L: Left LN; R: Right LN). The mean ± SEM is shown. Two tailed Welch's t-test was used to compare contralateral LNs within treatment groups. Quantification of (**G**) Tregs ($CD25^+$ $FoxP3^+$) and (**H**) Tbet expression among transferred MOG-specific cells. Quantification of (**I**) FoxP3 expression and (**J**) Tbet expression among transferred OVA-specific cells. N = 3 mice for sham treatment group and N = 5 for all other treatment groups. The mean ±

SEM is shown. Individual LNs were used as single data points (L: Left LN; R: Right LN). Two tailed Welch's t-test was used to compare contralateral LNs within each treatment group. *p < 0.05, **p < 0.01, ***p < 0.001.

mice, higher frequencies of Tregs were observed in LNs that received Rapa (**Fig. 5.2F)**, while higher frequencies of Tbet expressing cells were observed in CpG treated LNs (**Fig. 5.2G)**. Similar findings were observed in OVA treated mice (**Fig. 5.2H, 5.2I**).

Having demonstrated the ability of iLN treatment to locally skew immune responses towards proinflammatory or tolerizing functions, we next investigated if antigen-specific proliferation could also be spatially control by providing multiple antigens to specific nodes in the same animal. Using a similar design to above, mice were treated iLN with MOG/Rapa MPs delivered to the left inguinal LN, but with the right inguinal LN receiving the OVA/Rapa MPs (**Fig. 5.3A**). One day after treatment, an equal mixture of 2D2 T cells

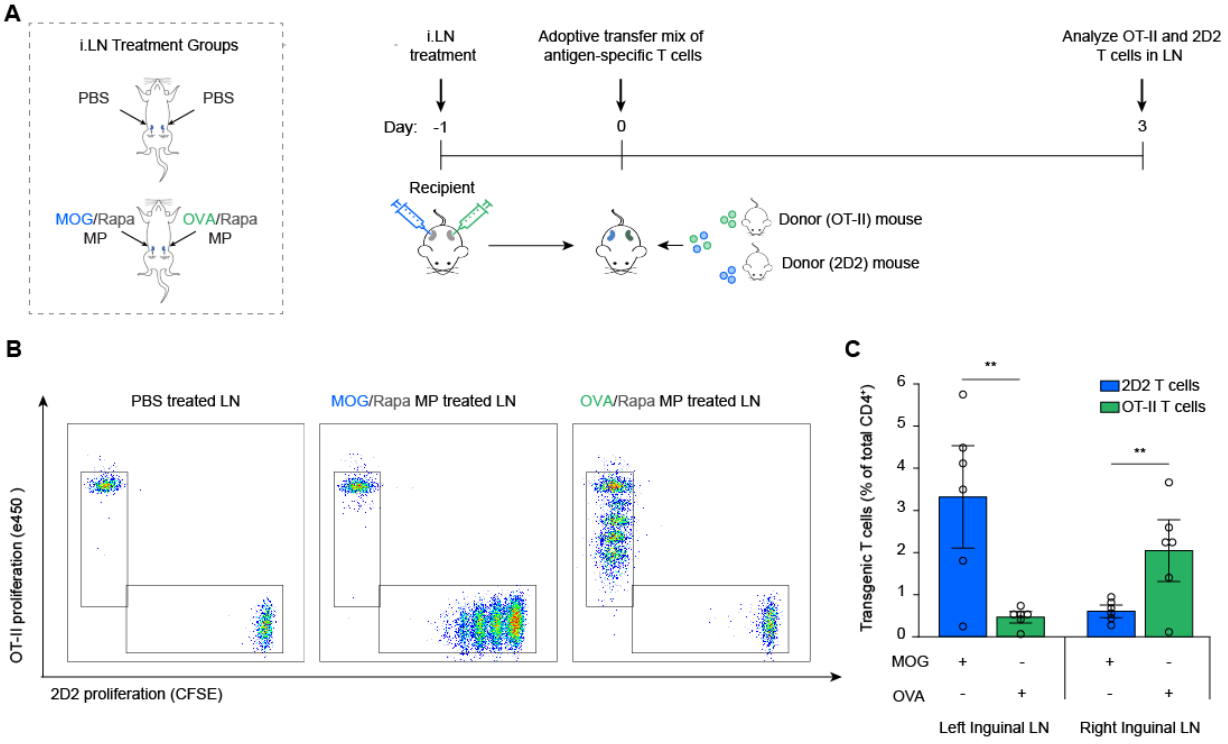

Figure 5.3 Antigen-specific responses are highly localized to the LNs that receive antigen. (**A**) Schematic representation of experiment. Each data point is individually represented. (**B**) Representative flow cytometry plots for proliferation of mixed antigen-specific T cells comprised of MOG and OVA specific T cells. (**C**) of MOG (2D2) and OVA-specific (OT-II) T cells within treated LNs. N = 5 mice plus N = 1 sham treated mouse as a control. The mean ± SEM is shown. Individual LNs were used as single data points (L: Left LN; R: Right LN). Two tailed Welch's t-test was used to compare contralateral LNs within each treatment group. **$p < 0.01$

and OT-II T cells were systemically infused by *i.v.* injection, following labelling with distinct proliferation dyes. In this study, 2D2 T cells only proliferated in LNs that received MOG/Rapa MPs, while OT-II T cells only proliferated in LNs that received OVA/Rapa MPs (**Fig. 5.3B-C**); this was notable since mice received both antigens, spatially localized to specific LNs. These results demonstrate that antigen localization drives proliferation of T cells only in LNs containing cognate antigen and highlight the highly localized manner in which antigen-specific T cell responses are generated. Together, this finding illustrates the role of antigen and immunomodulatory signal in driving T cell responses: while the correct antigen is required to promote proliferation, the extent of proliferation and subsequent T cell fate is dependent on the immunomodulatory signal present within LNs. From a therapeutic perspective, this suggests a powerful opportunity to expand and polarize large populations of antigen specific T cells in vivo without requiring systemic exposure to potent immunoregulatory cues.

5.4.3 Local delivery of a combination of MOG and Rapa reduces antigen specific T cell proliferation while promoting antigen-specific Tregs both locally and systemically

We next focused on the specific signal pairing of MOG and Rapa to explore how the geographic distribution of MOG and Rapa in LNs alters antigen-specific T cell responses to promote tolerance both locally and systemically. Given that antigen-specific T cell proliferation

was highly localized to the LN containing the cognate antigen, we hypothesized that MOG/Rapa MPs promote the localized retention of MOG-specific T cells to the treated LNs. To test this, mice were treated iLN with either i) one LN receiving MOG/Rapa MPs and one LN receiving MOG or ii) a single LN receiving MOG (**Fig. 5.4A**). 2D2.Thy1.1 T cells were then adoptively transferred into iLN treated mice to ensure a large population of antigen-specific T cells for analysis. The Thy1.1 congenic marker is not expressed on donor mice, allowing for facile tracking of the transferred T cells. One day after adoptive transfer, LNs were processed and analyzed transferred T cells. At this early timepoint, transferred T cells have not proliferated, allowing for measurement of the trafficking of the transferred T cells. In these studies, MOG/Rapa MP treated LNs contained significantly higher counts of transferred Thy1.1 T cells, even when compared to the contralateral MOG treated LN (**Fig. 5.4B**). These findings demonstrate that Rapa integration into LNs promotes recruitment or retention of antigen-specific cells, and motivated studies to test if Rapa also induced localized inhibition of mammalian target of rapamycin (mTOR).

mTOR inhibitors have been demonstrated to promote antigen-specific Tregs – localized retention and mTOR inhibition may promote localized induction of Tregs. Using the same approach, mice were treated iLN, then 2D2.Thy1.1 T cells were adoptive transferred. One day after transfer, transferred cells in treated LNs were analyzed for phosphorylated ribosomal s6 protein (ps6) expression, which arises from increased mTOR signaling. Rapa inhibition of mTOR results in lower ps6 expression. Mice which received only MOG displayed high levels of ps6 expression (**Fig. 5.4C**). Interestingly, in mice that received a combination of MOG/Rapa and MOG

in separate LNs, ps6 expression was suppressed in both the MOG/Rapa treated LN and the MOG treated LNs.

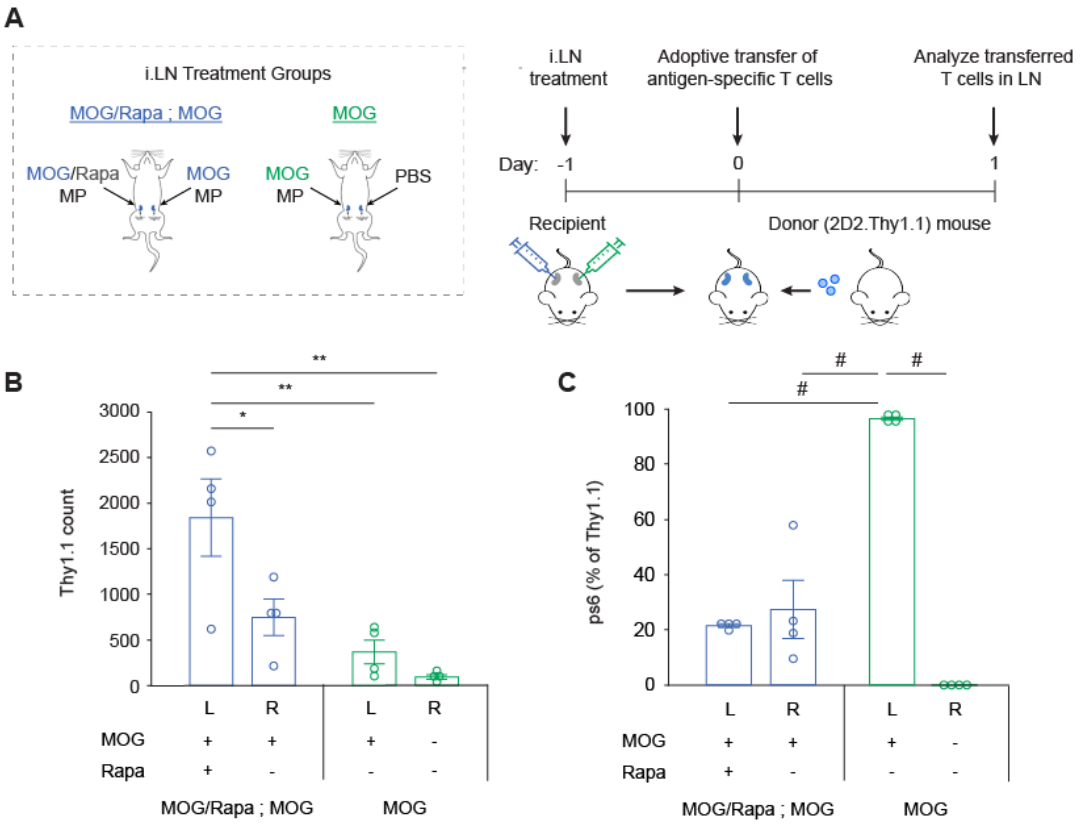

Figure 5.4 Rapa promotes localized antigen-specific T cell retention but inhibits mTOR systemically

(A) Schematic representation of MP treatment and experimental readout for 2D2.Thy1.1 T cell adoptive transfer experiment in naïve mice. **(B)** Quantification of adoptively transferred Thy1.1^{+} MOG specific cells**.** N = 4 mice for each group. Individual LNs were used as single data points (L: Left LN; R: Right LN). The mean ± SEM is shown. One way ANOVA with Tukey's post hoc test was used to compare each treatment within individual lymph nodes. **(C)** Quantification of ps6 expression among transferred Thy1.1^{+} MOG specific cells N = 4 mice for each group. Individual LNs were used as single data points (L: Left LN; R: Right LN). The mean ± SEM is shown. One way ANOVA with Tukey's post hoc test was used to compare each treatment within individual lymph nodes. *p < 0.05, **p < 0.01, #p < 0.0001

We next investigated how the combination of mTOR inhibition and localized retention of antigen-specific cells promote antigen-specific T cell polarization towards Tregs. To test this, naïve mice were injected with fixed doses of MOG and Rapa in MPs either i) together in a single

inguinal LN MP ("combined") or ii) in separate MP formulations ("split") into two LN, with one LN receiving MPs containing only MOG and one LN receiving Rapa MPs (**Fig. 5.5A**). 2D2.Thy1.1 T cells were then adoptively transferred in iLN treated mice. Six days following transfer, treated inguinal LNs and non-treated cervical LNs were isolated to determine MOG-specific T cell retention, proliferation, and Treg number and frequency. This time point allows for sufficient time for the priming of transferred T cells and their subsequent differentiation and expansion. Cell number and proliferation of MOG-specific T cells was significantly higher in all LNs that received MOG MPs or MOG/Rapa MPs, with similar numbers observed in LNs that received either of these formulations (**Fig. 5.5B-C**). However, MOG/Rapa MP treated LNs displayed lower numbers of proliferated cells (**Fig. 5.5C**). This finding supports our findings from the trafficking studies above that MOG/Rapa MPs promotes retention of T cells to LNs. Notably, at this time point, only Combined delivery with MOG/Rapa MPs elicited higher counts of antigen-specific Tregs (**Fig. 5.5D**). Further analysis revealed that LNs that received a combination MOG/Rapa MPs, Tregs were a large proportion of total antigen-specific cells (**Fig. 5.5E-F)**. In mice that received Split treatments of MOG MPs and Rapa MPs, Rapa MPs treated LN also displayed higher Treg frequencies comparable to MOG/Rapa MP treated LNs, however this was not significant compared to the contralateral MOG MP treated LN ($p = .0523$, One-way ANOVA with Tukey post hoc test). These studies demonstrate that MOG is required to expand antigen-

specific T cells in treated and untreated LNs, and inclusion of Rapa is necessary to polarize antigen-specific T cells to Treg.

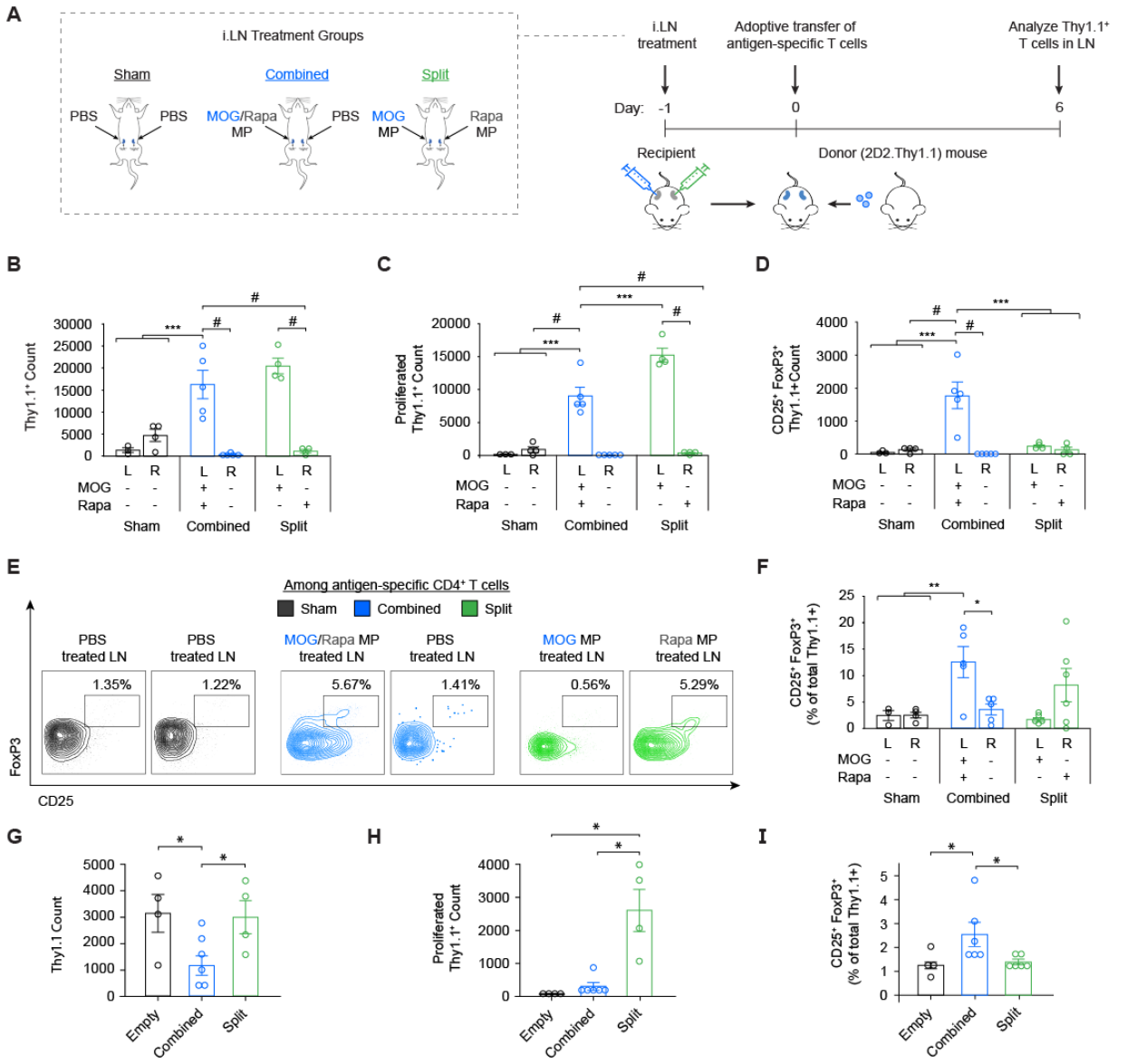

Figure 5.5 Local delivery of a combination of MOG and Rapa reduces antigen specific T cell proliferation while promoting antigen-specific Tregs

(**A**) Schematic representation of MP treatment and experimental readout for 2D2.Thy1.1 T cell adoptive transfer experiment in naïve mice. N = 4 mice for sham treatment group and N = 5 for all other treatment groups. Each data point is individually represented. (**B**) Quantification of Thy1.1$^+$ MOG specific cells (**C**) proliferated cells and (**D**) Thy1.1$^+$ Tregs (CD25$^+$ FoxP3$^+$) in treated LNs. N = 4 mice for sham and split treatment groups and N = 5 for combined. Individual LNs were used as single data points (L: Left LN; R: Right LN). The mean ± SEM is shown. One way ANOVA with Tukey's post hoc test was used to compare each treatment within individual lymph nodes.

(**E**) Representative flow cytometry traces for Treg frequency among MOG specific T cells in treated LNs. (**F**) Quantification of Treg ($CD25^+$ $FoxP3^+$) frequency in treated LNs. N=4 mice for sham and split treatment groups and N=5 for combined. Individual LNs were used as single data points (L: Left LN; R: Right LN). The mean ± SEM is shown. One way ANOVA with Tukey's post hoc test was used to compare each treatment within individual lymph nodes. (**G**) Quantification of $Thy1.1^+$ MOG specific cells and (**H**) proliferated cells in non-treated cervical LNs. N = 4 mice for sham and split treatment groups and N = 5 for combined. Each single data point represents pooled LN from an individual mouse. The mean ± SEM is shown. One way ANOVA with Tukey's post hoc test was used to compare each indicated group. (**I**) Quantification of Treg ($CD25^+$ $FoxP3^+$) frequency in non-treated cervical LNs. N = 4 mice for sham and split treatment groups and N = 5 for combined. Each single data point represents pooled LN from an individual mouse. The mean ± SEM is shown. Two tailed Welch's t-test was used to compare each treatment group. *$p < 0.05$, **$p < 0.01$, ***$p < 0.001$, #$p < 0.0001$.

Interestingly, in non-treated cervical LNs, mice that received combined treatments exhibited lower counts of Thy1.1 T cells, despite increased counts and expansion of Thy1.1 MOG-specific T cells within MOG/Rapa MP treated LNs (**Fig. 5.5G**). This was observed both in comparison to mice that received split treatments, which had comparable numbers of Thy1.1 T cells within MOG MP-treated LNs, and in comparison to sham treated mice, which had low retention and expansion of transferred cells. Only Split MP-treated mice displayed high counts of proliferated MOG-specific cells (**Fig. 5.5H)**. Together, these findings suggest a potential role of Combined MOG/Rapa MP treatment in limiting trafficking and retention of MOG-specific cells to non-treated tissue. Importantly, however, in the non-treated cervical LNs, Combined treatment of MOG/Rapa MPs also displayed higher Treg frequency among MOG-specific cells compared to Empty and Split treatments (**Fig. 5.5I**). This finding suggests that spatial co-localization of MOG and Rapa within the same LN plays an important role in the induction of systemic tolerance.

5.4.4 The combination of MOG/Rapa MPs within the same LN offers the greatest therapeutic efficacy in EAE

To test the hypothesis that the spatial distribution of MOG and Rapa affects induction of systemic tolerance, we next explored the ability of Empty, Combined, and Split iLN treatments to protect against EAE induction (**Fig. 5.6A-B**). Mice were induced with EAE and ten days later were administered fixed doses of MOG and Rapa into both inguinal LNs either as i) MOG/Rapa MPs ("combined" or ii) MOG MPs delivered to one LN and the other LN receiving Rapa MPs ("split"). An Empty MP treated control was included to compare treatment efficacy. Mice were weighed and disease severity (clinical score) was assessed daily starting 7 days after induction. Increasing disease severity is indicated by an increase in clinical score; a score of 0 indicates no paralysis, 1 indicates tail paralysis, 2 indicates partial hind limb paralysis, 3 indicates total hind limb paralysis, and 4 indicates partial front limb paralysis. While mice that received Combined treatments of MOG and Rapa displayed marked reductions in clinical score (**Fig. 5.6C**) and improved morbidity, displaying no reduction in weight loss (**Fig. 5.6D**), Split treatments were significantly less effective in ameliorating disease. Analysis of treated LNs within EAE mice 4 days following iLN treatment revealed higher frequencies of Tregs among total CD4+ only within LNs that received MOG/Rapa MPs (**Fig. 5.6E**).

Within non-treated disease relevant cervical LNs, similar levels of Tregs were observed between Combined and Split treatments (**Fig. 5.6F**). However, lower counts of inflammatory interferon-γ producing T cells (IFN-γ+) were observed in mice that received Combined MP treatments (**Fig. 5.6G**). These findings indicate that co-localization of MOG and Rapa within the same LN plays a role in developing systemic tolerance, by promoting increased Treg induction in

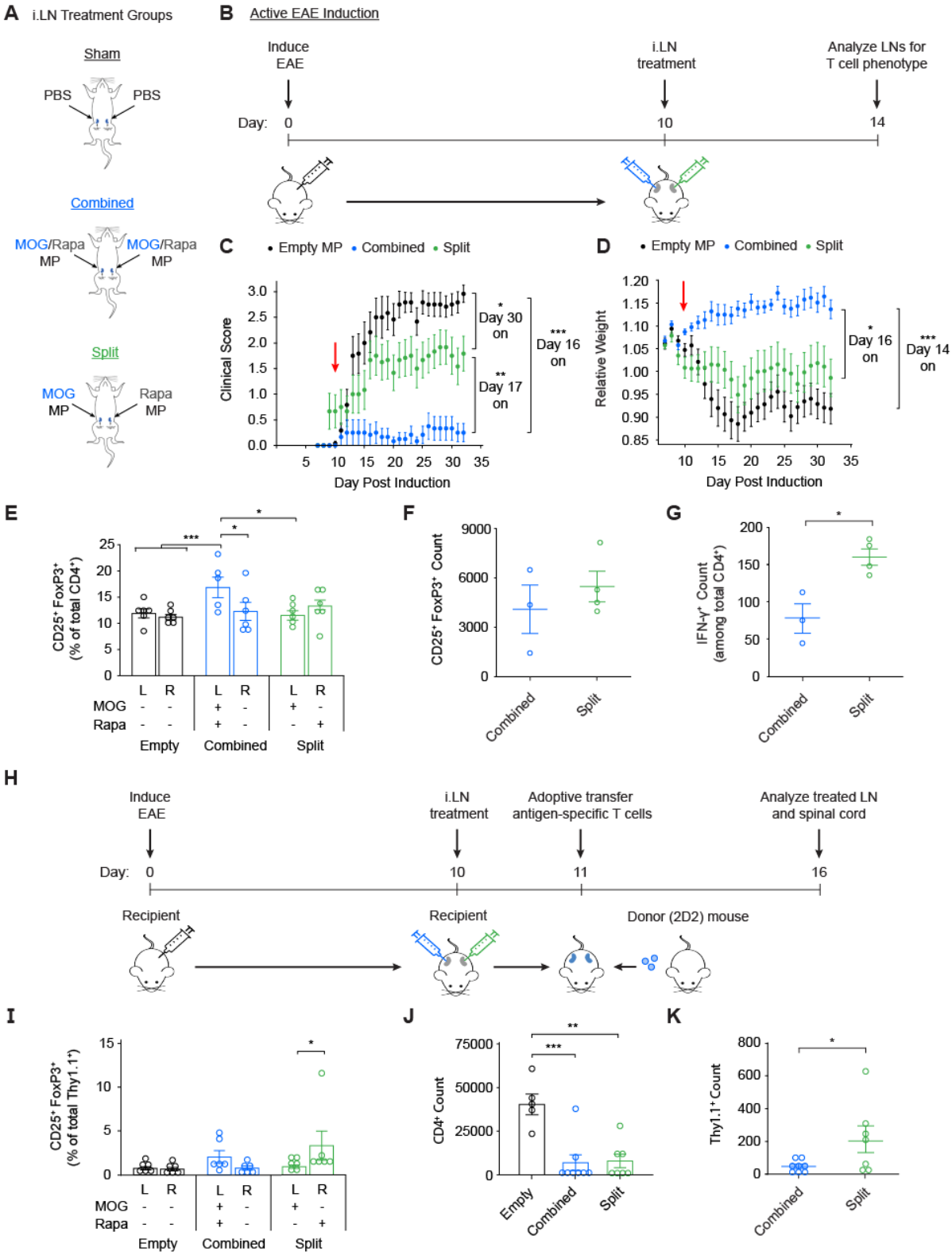
A
i.LN Treatment Groups
Sham
PBS
PBS
Combined
MOG/Rapa MP
MOG/Rapa MP
Split
MOG MP
Rapa MP
B
Active EAE Induction
Induce EAE
i.LN treatment
Analyze LNs for T cell phenotype
Day: 0
10
14
C
Empty MP
Combined
Split
Clinical Score
Day Post Induction
* Day 30 on
** Day 17 on
*** Day 16 on
D
Empty MP
Combined
Split
Relative Weight
Day Post Induction
* Day 16 on
*** Day 14 on
E
CD25+ FoxP3+ (% of total CD4+)
L R L R L R
MOG - - + - + -
Rapa - - + - - +
Empty
Combined
Split
F
CD25+ FoxP3+ Count
Combined
Split
G
IFN-γ+ Count (among total CD4+)
Combined
Split
H
Induce EAE
i.LN treatment
Adoptive transfer antigen-specific T cells
Analyze treated LN and spinal cord
Day: 0
10
11
16
Recipient
Recipient
Donor (2D2) mouse
I
CD25+ FoxP3+ (% of total Thy1.1+)
L R L R L R
MOG - - + - + -
Rapa - - + - - +
Empty
Combined
Split
J
CD4+ Count
Empty
Combined
Split
K
Thy1.1+ Count
Combined
Split

Figure 5.6 Local delivery of a combination of MOG and Rapa reduces antigen specific T cell proliferation while promoting antigen-specific Tregs
(**A)**Schematic representation of MP treatment and experimental readout for 2D2.Thy1.1 T cell adoptive transfer experiment in naïve mice. N = 4 mice for sham treatment group and N = 5 for all other treatment groups. Each data point is individually represented. (**B**) Quantification of Thy1.1$^+$ MOG specific cells (**C**) proliferated cells and (**D**) Thy1.1$^+$ Tregs (CD25$^+$ FoxP3$^+$) in treated LNs. N = 4 mice for sham and split treatment groups and N = 5 for combined. Individual LNs were used as single data points. The mean ± SEM is shown. One way ANOVA with Tukey's post hoc test was used to compare each treatment within individual lymph nodes. (**E**) Representative flow cytometry traces for Treg frequency among MOG specific T cells in treated LNs. (**F**) Quantification of Treg (CD25$^+$ FoxP3$^+$) frequency in treated LNs. N=4 mice for sham and split treatment groups and N=5 for combined. Individual LNs were used as single data points. The mean ± SEM is shown. One way ANOVA with Tukey's post hoc test was used to compare each treatment within individual lymph nodes. (**G**) Quantification of Thy1.1$^+$ MOG specific cells and (**H**) proliferated cells in non-treated cervical LNs. N = 4 mice for sham and split treatment groups and N = 5 for combined. Each single data point represents pooled LN from an individual mouse. The mean ± SEM is shown. One way ANOVA with Tukey's post hoc test was used to compare each indicated group. (**I**) Quantification of Treg (CD25$^+$ FoxP3$^+$) frequency in non-treated cervical LNs. N = 4 mice for sham and split treatment groups and N = 5 for combined. Each single data point represents pooled LN from an individual mouse. The mean ± SEM is shown. Two tailed Welch's t-test was used to compare each treatment group. *$p < 0.05$, **$p < 0.01$, ***$p < 0.001$, #$p < 0.0001$.

treated LNs and reducing inflammatory T cells that can promote disease. We next investigated MOG-specific cells were impacted by these responses to determine if the observed increases in Treg and reduction in inflammatory T cells responses were the result of antigen-specific responses. In this experiment, 2D2.Thy1.1 T cells were adoptively transferred into iLN treated EAE mice to ensure a large population of MOG-specific cells for analysis (**Fig. 5.6H**). After five days, LNs and spinal cords were analyzed for transferred T cells. Higher frequencies of antigen specific cells were observed in LNs that received Rapa only MPs (**Fig. 5.6I**). Combined treatment using MOG/Rapa MPs also trended toward increase Treg frequency, though this did not rise to the level of statistical significance. Within the spinal cords of mice, Combined and Split treatments displayed decreased CD4 infiltration (**Fig. 5.6J**). Further analysis, however revealed higher counts of MOG-specific T cells infiltration in Split treated mice compared to mice that received the

Combined treatment of MOG/Rapa MPs (**Fig. 5.6K**). Together, these results suggest an additional mechanism through which colocalized MOG and Rapa delivery can promote robust systemic tolerogenic responses by limiting MOG-specific T cells in disease-relevant tissue, such as the CNS.

5.4.5 The combination of MOG and Rapa protects against inflammatory T cell challenge and supports Tregs

Having established that the combination of MOG/Rapa MPs offers stronger protection against EAE compared to the Split regimen, we next tested if MOG/Rapa MPs could influence MOG-specific effector cells during EAE to downregulate inflammatory phenotypes. While the study presented above was performed in an active EAE model, for these studies, we utilized a passive model of EAE. In the active EAE model, a depot of MOG and Complete Freund's Adjuvant (CFA) is injected into mice, providing a source of continued disease induction. While the active model is useful for studying the combined activation of innate and adaptive immunity, passive EAE offers an avenue to independently study effector T cells during disease in the absence of adjuvant. To generate disease inflicting inflammatory T cells for the passive model, active EAE is first induced in donor mice. Following disease onset (~day 13), lymphocytes are isolated from emulsion draining LNs and restimulated *ex vivo* with MOG peptide and IL-23, a cytokine that polarizes T cells towards inflammatory Th17 phenotypes. This allows for expansion and enrichment of inflammatory disease-inducing T cells. After three days, cultured lymphocytes - many of which are highly inflammatory MOG-specific T cells that can induce EAE- are transferred into recipient mice. A large proportion of transferred T cells in this model are activated effector cells ($CD44^-/CD62L^+$) that co-express inflammatory transcription factors, ROR-γ and Tbet (**Fig.**

5.7). While ROR-γ has been demonstrated by others to be necessary for passive EAE induction, co-expression with Tbet has been shown to promote more severe disease.[240,241] A schematic illustrating the passive model is provided in **Fig. 5.8A**.

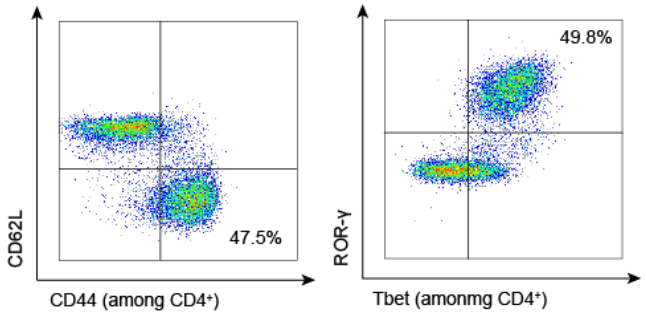

Figure 5.7 Phenotype of Transferred T cells in Passive EAE

In the first experiment, mice were induced with passive EAE and treated with either MOG/Rapa MP or Empty MP on day 10 following establishment of disease (**Fig. 5.8B**). Treatment with MOG/Rapa MPs resulted in reversal of disease as indicated by lower clinical scores (**Fig. 5.8C**) and improvements in relative weight (**Fig. 5.8D**). Analysis of spinal cords from these mice revealed similar numbers of infiltrating $CD4^+$ T cells among MOG/Rapa MP and Empty MP treated groups (**Fig. 5.8E**). Strikingly, higher frequencies of Tregs were observed in the spinal cord of MOG/Rapa treated mice (**Fig. 5.8F**). These results suggest two avenues through which MOG/Rapa MPs promote tolerance: i) by redirecting inflammatory T cell responses while ii) promoting Tregs in disease relevant tissues.

To test the impact of MOG/Rapa MPs on inflammatory T cells, mice were treated iLN with MOG/Rapa MP or Empty MPs, one day prior to passive EAE induction (**Fig. 5.8G**). For this study, donor cells for passive EAE studies were obtained from Thy1.1 mice, allowing for extended tracking of transferred cells. Following stabilization of clinical symptoms in mice that developed

disease, LNs were removed and analyzed for T cell phenotypes. All mice that received MOG/Rapa MPs were protected from disease. No differences in overall Tregs were observed between

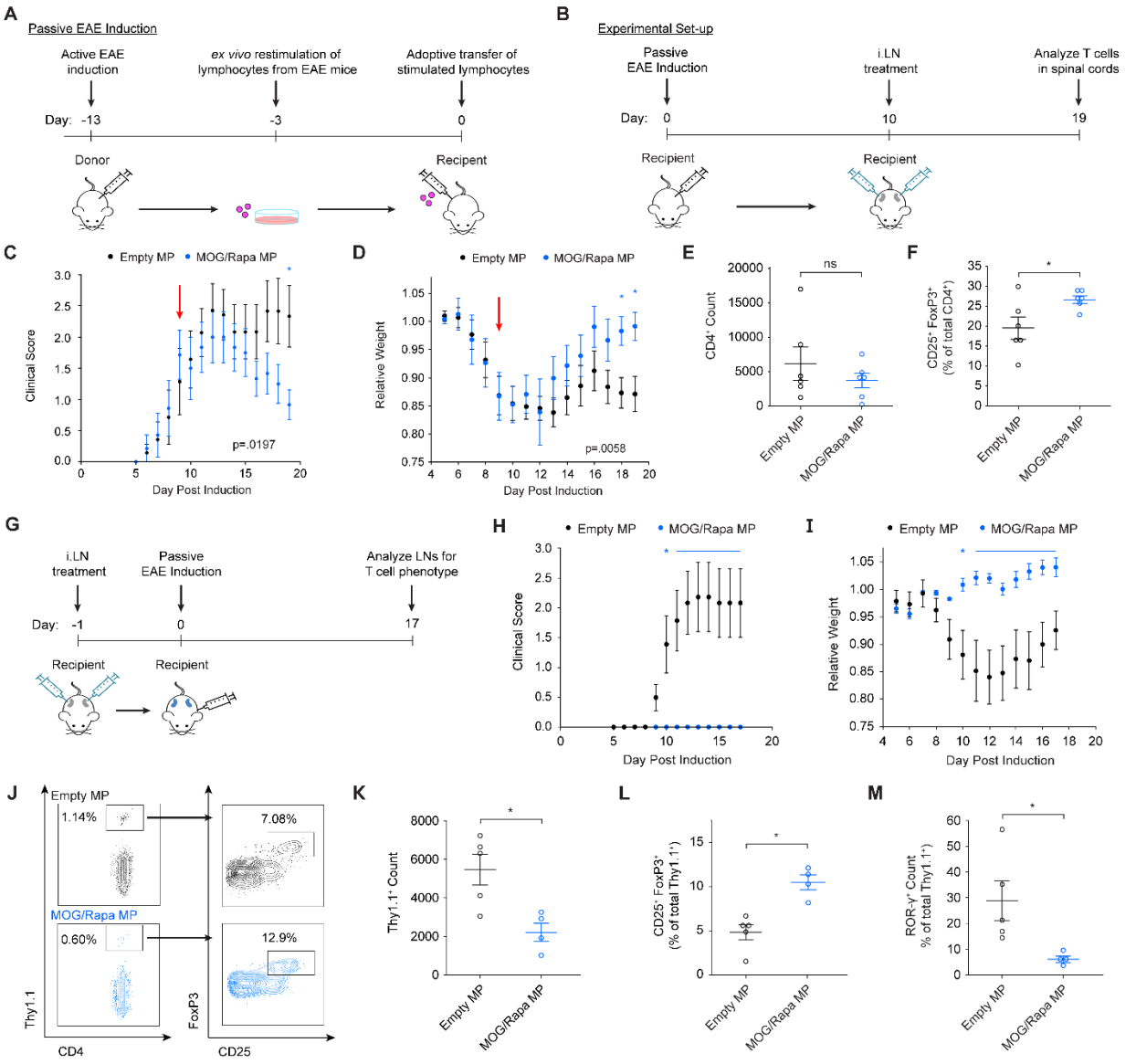

Figure 5.8 The combination of MOG and Rapa protects against inflammatory T cell challenge and supports Tregs

Schematic representation of **(A)** passive EAE induction and (**B**) experiment timeline. (**C**) Average clinical score and (**D**) average relative weight curves for Empty MP treated vs. MOG/Rapa MP treated mice in (B). Treatment timepoint is indicated with a red arrow. N = 6 for each treatment group. The mean ± SEM is shown. Mann-Whitney test was used to compare each treatment at each timepoint. Statistical significance is indicated by (*) for individual significant time points. *p

< 0.05. Quantification of (**E**) $CD4^+$ T cells and (**F**) Treg ($CD25^+$ $FoxP3^+$) frequency in spinal cords from mice in (B). N = 6 for each treatment group. Individual spinal cords from each mouse were used as single data points. The mean ± SEM is shown. Two tailed Welch's t-test was used to compare each treatment group. *p < 0.05 (**G**) Schematic representation of experiment timeline. (**H**) Average clinical score and (**I**) average relative weight curves for Empty MP treated vs. MOG/Rapa MP treated mice in (G). N = 5 for Empty MP treated group and N = 4 for MOG/Rapa treatment groups. The mean ± SEM is shown. Mann-Whitney test was used to compare each treatment group at each timepoint. Statistical significance is indicated by (*) for individual and (bar) for continuously significant time points. *p < 0.05. (**J**) Representative flow cytometry traces for Treg frequency among transferred T cells and respective quantification of (K) transferred T cells to induce passive EAE (Thy1.1), (**L**) Treg ($CD25^+$ $FoxP3^+$) frequency and (**M**) ROR-γ frequency in disease relevant cervical LNs. N = 5 for Empty MP treated group and N = 4 for MOG/Rapa treatment groups. Single data points represent pooled LNs from an individual mouse. The mean ± SEM is shown. Two tailed Welch's t-test was used to compare each treatment group. *p < 0.05

MOG/Rapa and Empty treated mice in treated or disease draining LNs. However, stark differences were observed among the transferred disease inducing T cells (**Fig. 5.8J**). In treated LNs, we observed an increase in Treg frequency and among transferred cells. Within disease relevant cervical LNs, lower counts of transferred cells were observed in MOG/Rapa MP treated mice (**Fig. 5.8K**), and a higher frequency of the transferred cells were Tregs (**Fig. 5.8L**). Critically, MOG/Rapa MP treatments also lowered frequencies of ROR-γ among transferred cells (**Fig. 5.8M**). These results demonstrate that iLN delivery of MOG/Rapa MPs not only reduces the number of transferred inflammatory effector T cells but can also skew the transferred repertoire towards Tregs and away from Th17.

5.4.6 iLN platform can offer dosing guidelines to inform therapeutic formulation

The studies presented thus far demonstrate how iLN injection can be leveraged to alter the geographic distribution of MOG and Rapa in LNs to gain new insight into the role of signal localization in inducing robust tolerance. We next sought to demonstrate that iLN injections could

be leveraged in preclinical applications to study the effect of dose, density, and relative immune signal composition to inform therapeutic design.

For dosing studies, in addition to an Empty MP control, a single formulation of MP co-loaded with MOG and Rapa was used for all treatments. Treatments were administered on ten days following EAE induction using 10-fold serial dilutions. For these studies, dose titrations are represented by the relative formulation used (i.e. 1X, 0.1X, 0.01X) The effectiveness of MOG/Rapa MPs in promoting tolerance was observed to be dose-dependent, with 0.1X treatments displaying intermediate reduction in clinical score, and .01X MOG/Rapa MPs displaying no statistically-significant protection during initial disease onset (**Fig. 5.9A**). These reductions in clinical score were associated with reduced disease incidence (**Fig. 5.9B**). Additional analyses reveals that dose and maximum clinical score are poorly correlated (**Fig. 5.9C**), suggesting that the dose of administered MOG/Rapa MPs affects the number of responders to treatment rather than ameliorating clinical symptoms. Together, these results suggest that a threshold dose of MOG/Rapa MPs is needed to drive immune tolerance.

In parallel studies, to evaluate the role of delivered immune signal density, mice were treated with MPs encapsulating MOG and Rapa at different densities. As with *in vitro* studies, one set of MPs contained MOG and Rapa in MPs at a density 10x that of a second set. However, for high dose particles, mice received 1/10 the number of particles, such that overall administered dose of MOG and Rapa remained constant between cohorts. Due to MOG/Rapa loading constraints and MP dosing limits, for these studies, mice received an overall MOG/Rapa dosing consistent with administration of 0.2X of MOG/Rapa MPs in dosing studies. Mice were induced with EAE and treated on day 10 with either: i) Empty MPs, ii) 1mg of .2X MOG/Rapa MPs, or iii) 0.1mg of 2X

MOG/Rapa MPs. Treatment with MOG/Rapa MPs resulted in modest reductions in clinical score (**Fig. 5.9D**) and slower disease progression (**Fig. 5.9E**), however no differences were noted

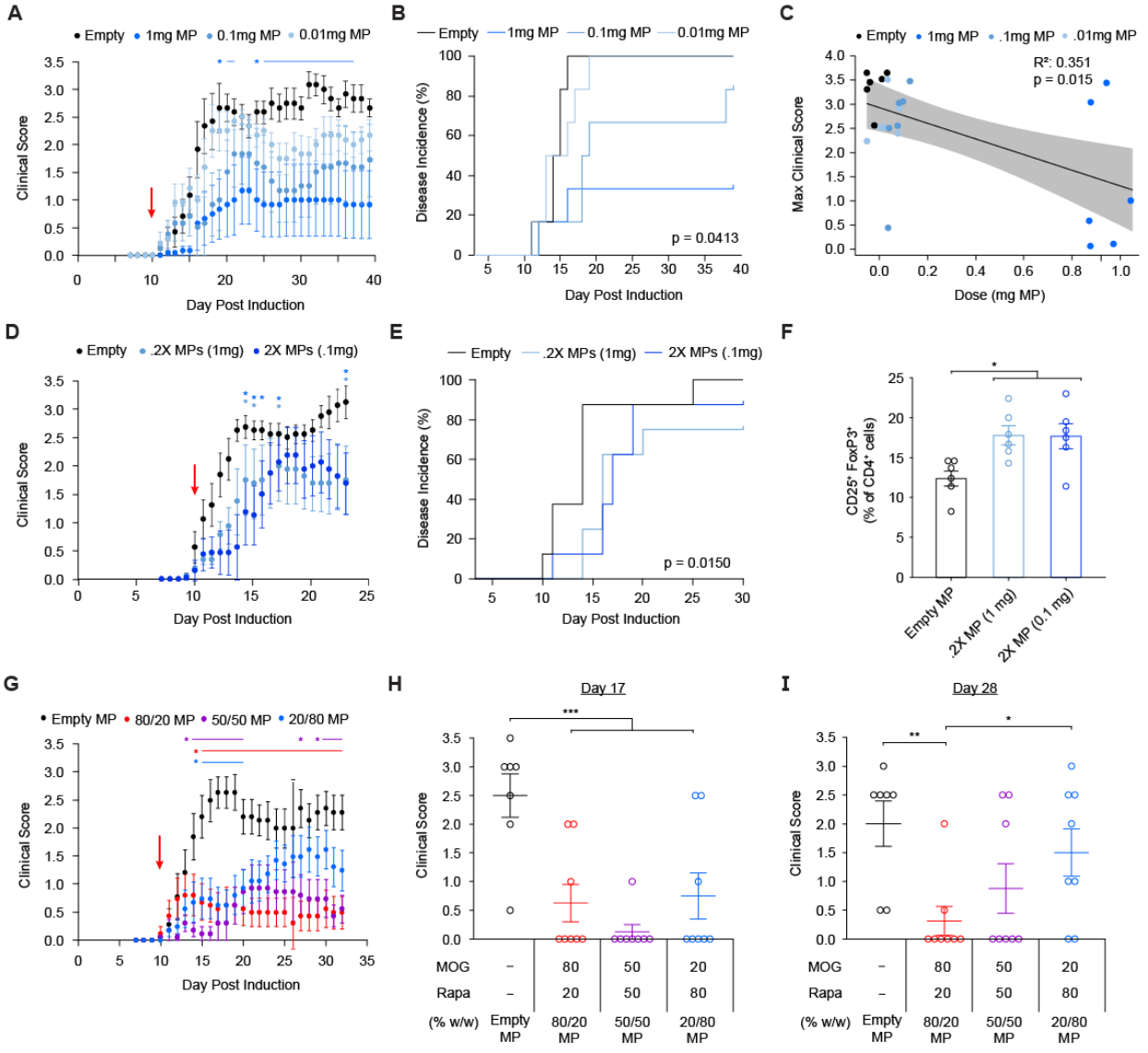

Figure 5.9 Dose and composition play important roles in promoting the strength and durability of induced tolerance

(**A**) Average clinical scores and (**B**) disease incidence for serially diluted doses of MOG/Rapa MPs. Treatment timepoint is indicated with a red arrow. N = 6 for each treatment group. The mean ± SEM is shown. Dunnet test was used to compare each treatment to Empty MP control at each timepoint. Statistical significance is indicated by (*) for individual and (bar) for continuously significant time points. *p < 0.05. Disease onset was analyzed by time-to-event analysis using a Wilcoxon test for global comparison. (**C**) Comparison of maximum clinical score as a function of dose. Moderate R^2 value for line of fit and low p-value (ANOVA) reflects bimodal distribution of

efficacy within treatment groups into responders and non-responders. (**D**) Average clinical scores and (**E**) disease incidence for low density: .2X MPs (1mg) and high density: 2X MPs (.1mg) loaded MOG/Rapa MPs. The overall administered dose of MOG and Rapa is normalized between low density and high density groups. Treatment timepoint is indicated with a red arrow. N = 6 for each treatment group. The mean ± SEM is shown. Mann-Whitney test was used to compare each treatment at each timepoint. Statistical significance is indicated by (*) for individual significant time points. *p < 0.05. (**F**) Quantification of Treg ($CD25^+$ $FoxP3^+$) frequency in treated LNs for mice in (D,E). N = 6 for each treatment group. Single data points represent pooled LNs from an individual mouse. The mean ± SEM is shown. One way ANOVA with Tukey's post hoc test was used to compare each indicated group. *p < 0.05. (**G)** Average clinical scores for different compositions of MOG:Rapa (w/w) ratios. The total administered dose of MOG and Rapa was normalized across all treatment groups at 25μg of MOG plus Rapa per MP. Treatment timepoint is indicated with a red arrow. N = 8 for each treatment group. The mean ± SEM is shown. Dunnet test was used to compare each treatment to Empty MP control at each timepoint. Statistical significance is indicated by (*) for individual and (bar) for continuously significant time points. *p < 0.05. Individual clinical scores for (G) at (**H**) Day 17 (peak disease) (**I**) Day 28 (late stage disease). N = 8 for each treatment group. Individual clinical scores were used as single data points. The mean ± SEM is shown. One way ANOVA with Tukey's post hoc test was used to compare each indicated group. *p < 0.05, **p < 0.01, ***p < 0.001.

between different densities of MOG/Rapa loading treatment. Correlating with this, density did not affect Treg induction, with both MOG/Rapa MPs displaying similar increases in Treg frequency **Fig. 5.9F**. These findings suggest that for the direct delivery of immune signals to LNs the microscale concentration of immune signals within LNs (i.e. density) does not play a significant role. Rather tolerance induction is largely dependent on the concentration of immune signals that reach LNs.

Finally, the role of immune signal composition on tolerance induction was investigated to evaluate the relative contribution of each component in generating tolerance. For these studies, a set of MPs was formulated to encapsulate a similar total mass of both MOG and Rapa, but at varying w/w ratio of MOG:Rapa yielding 4 different groups: i) Empty MPs, ii) 80/20 MOG/Rapa MPs, iii) 50/50 MOG/Rapa MPs, and iv) 20/80 MOG/Rapa MPs (**Table 5.1**). As before, mice were treated iLN 10 days following EAE induction, and monitored daily for changes in clinical

scores (**Fig. 5.9G)**. In these studies, all formulations of MOG/Rapa MPs offered early protection against EAE (**Fig. 5.9H)**. However, formulations containing more MOG displayed more robust protection against disease progression- only treatment with 80/20 and 50/50 MOG/Rapa ratios resulted in lower clinical scores at later time points (**Fig. 5.9I)**. These findings suggest that the relative amounts of MOG and Rapa impacts the quality of generated tolerance.

5.5 Discussion

MS therapies could benefit from greater control over delivery of immune signals and from improved understanding of the conditions needed to generate strong tolerogenic responses. The studies presented in this chapter were motivated by a need for improved understanding over how tolerogenic responses in LNs develop. Using fixed total doses of MOG and Rapa with iLN injection, we achieved localization that cannot be achieved with peripheral injections, allowing for studies to isolate the role of individual and combined immune signals on local and systemic tolerance. This body of work investigated how the geographic distribution and localization of MOG and Rapa within LNs induce local and systemic tolerance during iLN treatment. The studies reveal that MOG and Rapa work synergistically to promote tolerance in three ways. First, MOG-drives expansion of myelin-specific T cells. Second, Rapa promotes the retention and polarization of these antigen-specific cells toward Tregs within treated LNs. The ability of MOG/Rapa to maintain of Tregs within treated tissue may support increased frequencies of MOG-specific Tregs in peripheral tissues including disease relevant LNs and spinal cords. Third, the combination of MOG and Rapa reduces disease inducing inflammatory T cell subsets, both locally and systemically.

Our findings highlight the importance of combined of MOG and Rapa within treated LNs. In naive mice, we found that MOG treated LNs had higher numbers of total transferred MOG-specific T cells (**Fig. 5.5B**) and proliferating T cells (**Fig. 5.5B**). However, higher counts of Tregs were observed only when MOG and Rapa were geographically localized within the same LN (**Fig. 5.5C**). These findings have important implications particularly in the context of disease, during which systemic inflammation may polarize expanding T cells towards undesirable inflammatory subsets in the absence of Rapa. We observed that Split treatments of MOG and Rapa were significantly less effective in stopping EAE (**Fig. 5.6C**), and exhibited higher counts of IFN-γ producing cells (**Fig. 5.6G**). IFN- γ is a distinguishing feature of inflammatory Th1 T cells and has been demonstrated to promote EAE pathogenesis, particularly in earlier stages of disease.[242] Notably, we observed higher levels of trafficked MOG-specific T cells within the spinal cords of mice that received Split MP treatments, while spinal cords from mice that received combined doses of MOG/Rapa MPs had significantly lower counts of MOG-specific T cells (**Fig. 5.6K**).

Importantly, our results suggest that in addition to promoting Tregs, combined MOG/Rapa MP treatment can also redirect pathogenic T cells in peripheral tissues. Additional studies are needed to elucidate how MOG/Rapa MPs affect antigen-specific pathogenic T cells. In the presented work, the passive EAE model is used to study the isolate the effects of MOG/Rapa MPs on effector T cells during disease. Therapeutic treatments in this model demonstrate that MOG/Rapa MPs can revert T cell mediated pathogenesis (**Fig. 5.8C,D**). Increased frequencies of Tregs in spinal cords of MOG/Rapa MP treated mice compared to Empty control group (**Fig. 5.8F**) suggest that generation of potent Tregs can suppress inflammatory T cell activity and function. Treg depletion studies following iLN treatment could reveal if Tregs play a role in the observed

disease reversal. Additionally, Treg suppression assays can offer insight into whether MOG/Rapa MP treatments improve Treg function, and is ongoing work described in **Chapter 6**. iLN Treatment with prior to passive EAE induction reveals even more striking results: MOG/Rapa MP treated mice were completely protect against disease. In MOG/Rapa MP treated mice, lower counts of the transferred disease inducing cells were observed (**Fig. 5.8F**), suggesting a second potential mechanism through which MOG/Rapa MP treatment can control disease: by eliminating pathogenic T cells from the T cell repertoire. Interestingly, MOG/Rapa MP injections also induced a notable recomposition of the T cell subtypes present among cells transferred to induce EAE, promoting higher frequencies of Tregs but lower frequencies of ROR-γ^+ T cells. These results suggest a third way through which MOG/Rapa MPs may affect pathogenic T cells, by promoting their transdifferentiation towards Tregs that can modulate disease.

5.6 Concluding remarks

Precise delivery of immune signals to the LN promises to promote desired immune responses. Findings from these studies will allow us to generate rational design criteria for generating effective and selective therapies for autoimmunity. Since many developing antigen-specific therapies require drainage to LNs or spleen, this information with fill a critical gap in knowledge regardless of injection route.

Excitingly, the knowledge gained from these studies have several clinical implications for iLN injection of tolerogenic MPs as a therapy. For instance, we demonstrate that generation of immune responses by iLN can be highly compartmentalized and confined to the LNs in which immune signals are delivered. Using this platform, we are able to deliver both immunostimulatory

CpG and immunomodulatory Rapa to elicit two distinct responses: one pro-immune reflected in large expansion of T cells and polarization of T cells to express Tbet, and one of tolerance with restrained proliferation and polarization towards Tregs. The ability to generate multiple opposing immune responses establishes a potential avenue to introduce immunotherapies for MS while leaving the remainder of the immune system intact to mount immune responses as part of normal immunity. Additionally, advances towards clinical translation requires a sound understanding the mechanisms that drive efficacy and selectivity. This work offers insight into several potential mechanisms through which MOG/Rapa MPs induce tolerance. Lastly, leveraging the modularity of the iLN platform we identify key design criteria for the spatial distribution, dose, and relative concentration of immune signals, information that can be leveraged to design more potent therapeutic formulations that are more likely to succeed in clinical trials.

Chapter 6: Outlook and Future Work

6.1 Outlook

The work in this dissertation focused on leveraging biomaterials to tune immune responses by controlling immune signal delivery. Using multiple biomaterial systems, I demonstrate how the tunability of biomaterials can elucidate rational design considerations in promoting robust immune function against cancer and autoimmune disease. The knowledge generated adds to the working knowledge of important biomaterial considerations needed to generate potent immune responses in cancer, and demonstrates how a new biomaterial platform can be used as a tool to advance understanding of a potential myelin-specific treatment for MS.

In my first body of work, I engineered self-assembled cancer vaccine nanoparticles with tunable charge and cargo loading for the delivery of pro-immune signals in the right combination and doses without compromising function. The studies performed here revealed a balance of nanoparticle characteristics that are important in nanoparticle design and efficacy. In one set of studies, I demonstrated that cargo encapsulation, protection, and improved uptake were not sufficient for immunogenicity and that immune signals must also be accessible for processing by APCs, which can be inhibited if interaction strength is too great. In a second set of studies, I demonstrated that stronger antigen dosing elicited more functional anti-tumor responses. These findings offer several contributions to the field of cancer vaccines. First, this body of work illustrates a novel approach to immune signal delivery using polyplexes. While previous work using polyplexes has focused on delivery of mRNA to encode antigen peptide to geneate immune responses, here I demonstrate that polyplex structures can directly deliver both antigen and

adjuvant. Secondly, codelivery of Trp2 and CpG traditionally necessitates a biomaterial carrier (i.e. polymer, inorganic template), which as discussed in **Section 2**, can lead to undesired activation of other immune pathways. This work demonstrates codelivery of both Trp2 and CpG in the absence of a carrier.

In my second body of work, I used a biomaterial-based platform to control immune signal delivery and gain new insight into how the localized combination of MOG and Rapa promote immune tolerance. Our lab previously demonstrated that iLN depots reverse and protect against disease in multiple models of MS, and that efficacy is dependent on MOG/Rapa delivery. This dissertation demonstrates the robustness of iLN depots in generating tolerance by demonstrating that iLN reverse and protect against disease in an additional model of MS: passive EAE. Additionally, I highlight three additional criteria for the efficacy of iLN depots: i) MOG and Rapa must be delivered to the same LN ii) there is a clear dosing threshold that must be achieved to generate tolerance iii) higher ratios of MOG:Rapa offer improved protection against disease. Finally, I investigate how iLN depots impact disease inducing T cells – a previously unexplored area – and demonstrate that MOG/Rapa treatment results in the elimination and transdifferentiation of T cells that promote disease. However, because T cell transdifferentiation is a nascent field, future studies should aim to corroborate this mechanism.

While this work defined many critical features for the induction of tolerance – for example, retention and expansion of antigen-specific cell towards Tregs by a combination of MOG and Rapa in LNs – these findings motivate further areas to explore using intra-LN delivery as a tool to understand immune responses. There are several ongoing and future studies in the Jewell lab that I am leading that will progress the presented work to improve our understanding of how robust

tolerance is generated. These studies focus on understanding the durability of induced tolerance, particularly in the context of induced Tregs. Ongoing studies are exploring if MOG/Rapa MPs promote more functional Tregs with improved capabilities to counter inflammatory antigen-specific T cells. Additional studies explore the durability of induced Tregs by testing for memory markers. Lastly, several ongoing studies aim to improve rigor of the present findings by exploring generation of immune tolerance by localized MOG/Rapa MPs in male mice.

6.2 Ongoing and future studies: Explore role of immune signals on regulatory T cell functionality

The studies completed in **Chapter 5** demonstrated that MOG/Rapa MPs i) induce expansion and polarization of MOG-specific T cells towards Tregs and ii) reduction in inflammatory MOG-specific T cells during disease. To test if the reduction in inflammatory MOG-specific T cells in mediated by Tregs, ongoing studies are exploring suppressive capacity of MOG/Rapa induced Tregs to suppress MOG-specific T cells. In this *in vitro* assay, Tregs are cocultured with activated naïve T cells (Tconv). Activation of naïve T cells in cultures mediated by a combination of anti-CD3 and anti-CD28.[243] Naïve T cells are obtained by cell sorting for $CD44^{-}/CD62L^{+}$, while Tregs are obtained by cell sorting from FoxP3.GFP reporter mice (**Fig. 6.1A**). Pilot data demonstrates that Tregs obtained from LNs of MOG/Rapa treated mice can suppress activated T conv cells (**Fig. 6.1B**). In this assay, Treg suppression is measured by plating Treg at serially diluted ratios of Treg:Tconv plating densities and comparing proliferation index for each Treg:Tconv ratio to Tconv alone. Ongoing studies are exploring if Tregs from MOG/Rapa treated mice display greater suppressive capacity compared to Tregs from Empty MP or MOG MP treated mice. Future studies will also explore if induced Tregs can suppress Tconv in an antigen-dependent manner.

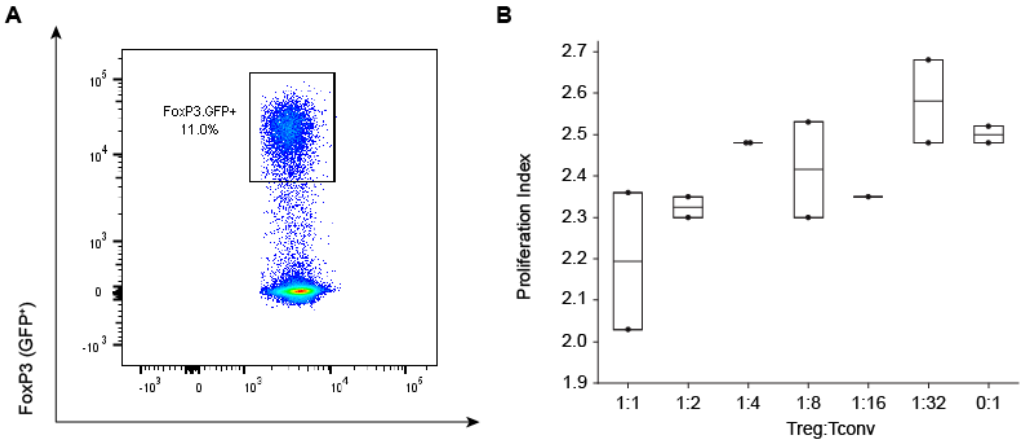

Figure 6.1 Treg suppression of MOG-specific T cells
(**A**) Representative gating for sorting GFP cells from FoxP3.GFP reporter mice (**B**) Quantification of Tconv proliferation by proliferation index at different Treg:Tconv ratio. N=2 wells per dilution with 50k cell plating density

6.3 Ongoing and future studies: Defining and tuning the durability of immune responses

The studies completed in **Chapter 5**, as well as work in the Jewell lab indicates that MOG/Rapa MPs can induce and maintain long-lasting tolerance. This motivates additional studies to investigate if development and maintenance of tolerance is driven by geographical localization of immune signals within LNs. Towards this goal, I have been working with Jewell lab staff immunologist, Dr. Senta Kapnick. In pilot studies, iLN treatment with MOG/Rapa MPs 28 days prior to EAE induction protects mice from developing paralysis, highlighting that tolerance induced by MOG/Rapa treatment provides durable protection against disease onset (**Fig. 6.2A**). These findings suggest a potential for lasting tolerance and regulatory memory. One hypothesis is that MOG/Rapa MPs locally promote retention and maintenance of Tregs. Using a similar set-up to the study described in **Chapter 5.4.3**, early pilots demonstrate that Tregs delivered into naïve

mice are retained within LNs at Day 14 (**Fig. 6.2B**) and Day 28 (**Fig. 6.2C**), but only within MOG/Rapa treated LNs.

Figure 6.2 iLN injection of MOG/Rapa MPS promotes durable tolerogenic responses
(A) Average clinical scores for mice treated 28 days prior to injection. N=8 mice per group. The

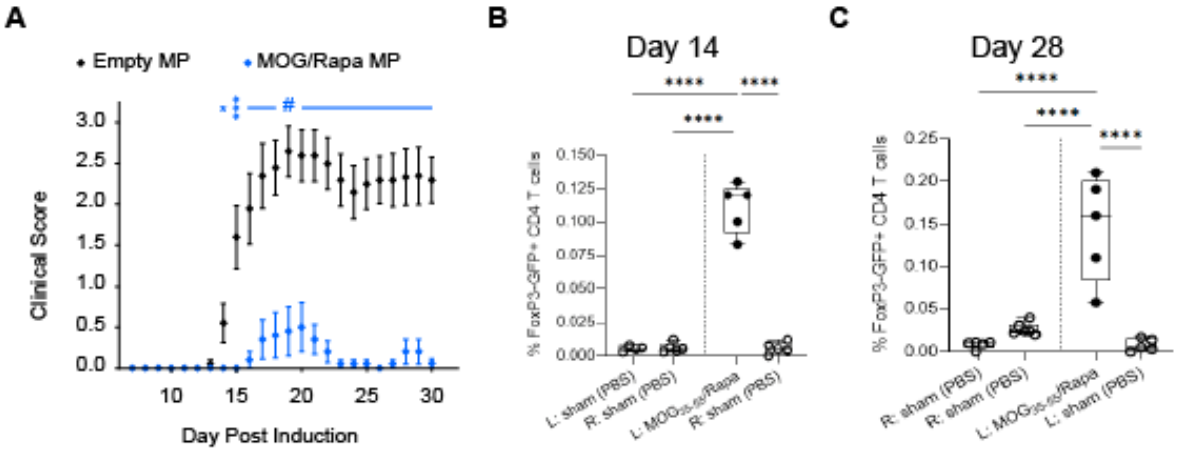

mean ± SEM is shown. Dunnet test was used to compare each treatment to Empty MP control at each timepoint. Statistical significance is indicated by (*) for individual and (bar) for continuously significant time points. *p < 0.05; ***p < 0.001; #p < 0.0001. Transferred MOG-specific Treg frequency among total $CD4^+$ cells at (**B**) 14 days and (**C**) 28 days post transfer. N=8 mice per group. The mean ± SEM is shown. One-way ANOVA with Tukey post-hoc test was used to compare each treatment group. ****p < 0.0001.

Based on *in vitro* release studies of MPs, at this timepoint, it is expected that delivered cargo is no longer present, suggesting a possibility of regulatory memory. This posit is supported by recent studies that have demonstrated mTOR pathway inhibition during expansion of naïve T cells polarizes central memory phenotype among Treg, which display increased persistence *in vivo*. Ongoing studies are testing the hypothesis that Treg responses polarized during mTOR inhibition may also be durable. To test whether inclusion of MOG/Rapa MPs enhances memory-like phenotype among self-reactive Treg, we are exploring expression of several key memory markers, such as CD44, CD62L, CCR7, and CD127. Canonical central memory T cells are

frequently classified as $CD44^+/CD62L^+/CCR7^+$.[244] CD44 is a marker expressed by activated T cells; CD62L and CCR7 drive homing to LNs, where long lived memory T cells persist. $CD127^+/KLRG1^-$ T cells are considered precursors for long-term memory T cells.[245] CD127 is the receptor for IL-7, an important survival signal for memory T cells within LNs, while KLRG1 is commonly expressed on short-lived effector T cells.

6.4 Ongoing and future studies: Improve robustness and rigor with studies in male mice

iLN treatment in male mice are underway to improve rigor of the present studies and demonstrate the robustness of iLN injection as a therapy. The study presented in **Chapter 5.4.3** was repeated in male mice. To review, this study explored retention of antigen-specific cells to promote antigen-specific T cell polarization towards Tregs. To test this, naïve mice were administered fixed doses of MOG and Rapa either i) together in a single inguinal LN ("combined") or ii) in separate MP formulations into two LN, with one LN receiving MPs containing only MOG and one LN receive Rapa MPs. 2D2.Thy1.1 T cells were then adoptively transferred in iLN treated mice. Six days following transfer, treated inguinal LNs and non-treated cervical LNs were isolated to determine MOG-specific T cell retention, proliferation, and Treg frequency. We obtained similar results to those observed in female mice, with LNs that received MOG displaying higher levels of MOGs-specific cells, but only the LN that received Combined MOG/Rapa MPs had higher frequencies of Tregs. Ongoing studies are exploring if iLN treatment of MOG/Rapa MPs into male mice protects against disease

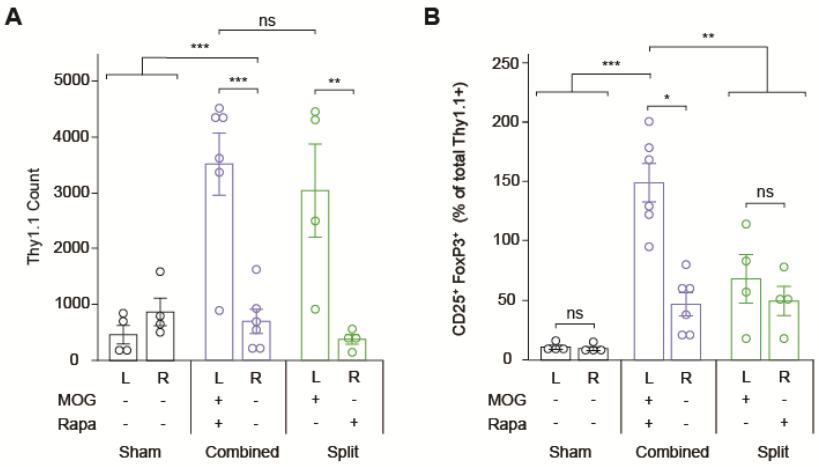

Figure 6.3 Local delivery of a combination of MOG and Rapa promotes antigen-specific Tregs in male mice

(**A**) Quantification of Thy1.1^{+} MOG specific cells and (**B**) Thy1.1^{+} Treg (CD25^{+} FoxP3^{+}) in treated LNs. N = 4 mice for sham and N = 6 for combined and split. Individual LNs were used as single data points (L: Left LN; R: Right LN). The mean ± SEM is shown. One way ANOVA with Tukey's post hoc test was used to compare each treatment within individual lymph nodes.

Chapter 7: Contributions

7.1 Research Publication Contributions

The work I completed to date during my PhD has resulted in 4 published manuscripts – two first author original research articles, one first author review, and one second author review. I also have two first author original research articles in progress, with one recently submitted, and one in preparation.

One first author paper, presented in **Chapter 3**, focuses on understanding how self-assembled delivery vehicles can be used to control immune signal integration to improve immunotherapies. The paper investigates rapidly-degradable poly(β-amino esters (PBAEs) for improved delivery of CpG, a negatively-charged immune activator. Using electrostatic assembly, I show that while positively charged assemblies improved CpG uptake, these formulations were poor immune cell activators. My studies reveal that PBAEs are strongly bound to CpG in more positively charged complexes, limiting access to immune processing machinery; this suggests a critical role for interaction strength between cargo and carrier in the generation of strong immune responses. This work provided a basis for delivery of self-assembled complexes using CpG.

In a follow-up to the above work, another first author paper explored complexes comprised of CpG assembled with a conserved human melanoma peptide antigen, Trp2 (cationic). Uniquely, this work demonstrated co-delivery of immune signals in the absence of a polymer carrier. In these studies, improved Trp2 loading efficiency by altering Trp2 charge using cationic arginine residues led to improved survival in a mouse melanoma model. This work was accomplished in conjunction with former high school mentee, Allie Amerman.

The review of biomaterials for modulating immune responses presented in **Chapter 2** was published as a first author review paper. This paper highlighted modular features of biomaterials that could be leveraged to stimulate or regulate immunity for improved vaccine and immunotherapy design.

Two additional first author papers are currently in progress. The work for these papers are outlined in **Chapter 6.** Both papers motivate clinical research using the iLN platform. One paper focuses on using the iLN platform as a tool to further pre-clinical studies by providing new insight into immune signal dosing, spatial and combinatorial requirements to generate robust tolerance and inform therapeutic formulations. The second paper will be published as a first co-author manuscript in collaboration with fellow Jewell lab members Emily Gosselin and Senta Kapnick to demonstrate the clinical translational potential of the iLN as a novel MS therapy. My work adds mechanistic insight demonstrating that iLN treatment of tolerogenic microparticles drives local programming and persistence of regulatory T cell in LNs in an antigen-dependent manner.

For my contributing author publications, my contributions include conducting experimental procedures, assistance in animal studies, study design, statistical analysis, and input in writing the paper.

7.2 Research Conference Presentations

I have presented research at four national and international conferences focused on biomaterials and immunology including: one annual meeting of the American Association of Immunology, one annual meeting of the Biomedical Engineering Society, one national meeting of the American Chemical Society, and a Keystone Symposia on T cell Memory. For these

conferences, I have been awarded a number of travel awards, including a BMES Student Travel Award, as well as the Jacob K. Goldhaber Travel Award from the UMD Graduate School.

7.3 Research Funding Support and Awards

My research has been enabled by a number of fellowships and awards. I received two years of funding from the National Cancer Institute Training Award (3-4 awarded at UMD per year) in the second year and one year of funding from the National Institute of Health T32 Host Pathogen Interactions Award (3-4 awarded at UMD per year) in my fourth year. I am also a recipient of the 2021 Clark Doctoral Fellows Mid-Career Award (awarded to 2% of graduate students from Clark School per year).

7.4 Service and Mentoring

Throughout my PhD, I have been involved in service and mentoring both on campus in the community. Through the NSF-funded Program to Enhance Participation in Research, I have mentored three underserved students from Wheaton High School over the course of a year. I helped my mentees identify a research topic, find and read scientific literature, and prepare a research poster to present at a symposium at UMD.

In lab, I mentored a high school student for two years. I designed her project, tangentially related to mine, to help her gain key research skills – experimental techniques, scientific reading, and communication. In her first year, she received 8 awards at the Regional Science Fair including 1st place in the Biology category, Qiagen 1st place award, Commissioned Officers Association of the United States Public Health Service 1st place award, and the MIT Certificate of Excellence. In her second year, she qualified for the highly competitive Intel International

Science Fair, and competed in the Translational Medicine Division earning 2nd in the category. In addition, my mentee earned co-authorship on the work that was presented in **Chapter 4.**

Appendix: List of Publications

Published First Author:

1. **Tsai SJ,** Amerman A, Jewell CM. "Altering antigen charge to control self-assembly and processing of immune signals during cancer vaccination." *Frontiers in Immunology.* **2021**.

2. **Tsai SJ**, Black SB, Jewell CM. "Leveraging the modularity of biomaterial carriers to tune immune responses."*Advanced Functional Materials.* **2020**.

3. **Tsai SJ,** Andorko, JI, Zeng X, Gammon JM, and CM Jewell**.** "Polyplex interaction strength as a driver of potency during cancer immunotherapy." *NanoResearch.* **2018**, *11*, 5642-5656.

Published Contributing Author:

4. Bookstaver, ML, **Tsai SJ**, Bromberg JS, Jewell CM. "Improving vaccine and immunotherapy design using biomaterials." *Trends in Immunology.* **2017**, 2, 135-150.

In Progress:

5. **Tsai SJ**, Rui Y, Carey ST, Kapnick S, Yanis A, Eppler HB, Black SB, Zeng X, Gammon JM, Jewell CM. "Modular control of lymph node niches to control T cell fate in immune tolerance." (in preparation)

6. Gosselin EA*, Kapnick S*, **Tsai SJ***, Carey ST, Froimchuck Y, Shah S, Eppler HB, Yanis A, Black SB, Zeng X, Jewell CM. "Intra-Lymph Node Delivery of Tolerogenic Microparticles Promotes Immune Tolerance, Reverses Paralysis, and Prevents Relapse in a Model of Multiple Sclerosis" (in preparation)
   * indicates equal contributions

7. Andorko JI, **Tsai SJ**, Carey ST, Edwards C, Shah S, Gammon JM, Zeng X, Gosselin EA, Hess KL, Jewell CM. "Spatial delivery of immune cues as a platform to define therapeutic outcomes in cancer vaccination." (submitted)

8. Gammon JM, Carey ST, Saxena V, Eppler HB, **Tsai SJ**, Paluskievicz P, Xiong Y, Li L, Tostanoski LH, Gosselin EA, Zeng X, Bromberg JS, Jewell CM. "Engineering the lymph node environment to promote durable antigen-specific tolerance in type 1 diabetes and allogeneic islet transplantation" (submitted)

References

1. Andorko, J. I., Gammon, J. M., Tostanoski, L. H., Zeng, Q. & Jewell, C. M. Targeted Programming of the Lymph Node Environment Causes Evolution of Local and Systemic Immunity. *Cell. Mol. Bioeng.* **9**, 418–432 (2016).
2. Pape, K. A., Catron, D. M., Itano, A. A. & Jenkins, M. K. The humoral immune response is initiated in lymph nodes by B cells that acquire soluble antigen directly in the follicles. *Immunity* **26**, 491–502 (2007).
3. Hughes, C. E., Benson, R. A., Bedaj, M. & Maffia, P. Antigen-Presenting Cells and Antigen Presentation in Tertiary Lymphoid Organs. *Front. Immunol.* **7**, 481 (2016).
4. Luo, X., Miller, S. D. & Shea, L. D. Immune Tolerance for Autoimmune Disease and Cell Transplantation. *Annu. Rev. Biomed. Eng.* **18**, 181–205 (2016).
5. Gammon, J. M. & Jewell, C. M. Engineering Immune Tolerance with Biomaterials. *Adv. Healthc. Mater.* **8**, 1801419 (2019).
6. Sabatos-Peyton, C. A., Verhagen, J., Wraith, D. C., Waldmann, H. & Greene, M. Antigen-specific immunotherapy of autoimmune and allergic diseases This review comes from a themed issue on Immune tolerance Edited. *Curr. Opin. Immunol.* **22**, 609–615 (2010).
7. von Boehmer, H. & Daniel, C. Therapeutic opportunities for manipulating TReg cells in autoimmunity and cancer. *Nat. Rev. Drug Discov.* **12**, 51–63 (2013).
8. O'Shea, J. J. & Paul, W. E. Mechanisms underlying lineage commitment and plasticity of helper CD4+ T cells. *Science* **327**, 1098–102 (2010).
9. Burrell, B. E. & Bromberg, J. S. Fates of CD4+ T cells in a tolerant environment depend on timing and place of antigen exposure. *Am. J. Transplant* **12**, 576–89 (2012).
10. Snook, J. P., Kim, C. & Williams, M. A. TCR signal strength controls the differentiation of CD4+ effector and memory T cells. *Sci. Immunol.* **3**, (2018).
11. van Panhuys, N. TCR Signal Strength Alters T–DC Activation and Interaction Times and Directs the Outcome of Differentiation. *Front. Immunol.* **7**, 6 (2016).
12. Su, L. F. *et al.* Antigen exposure shapes the ratio between antigen-specific Tregs and conventional T cells in human peripheral blood. doi:10.1073/pnas.1611723113
13. Colegio, O. R. *et al.* Functional polarization of tumour-associated macrophages by tumour-derived lactic acid. *Nature* **513**, 559–563 (2014).
14. Rothoeft, T., Gonschorek, A., Bartz, H., Anhenn, O. & Schauer, U. Antigen dose, type of antigen-presenting cell and time of differentiation contribute to the T helper 1/T helper 2 polarization of naive T cells. *Immunology* **110**, 430–9 (2003).
15. Turner, M. S., Kane, L. P. & Morel, P. A. Dominant role of antigen dose in CD4+Foxp3+ regulatory T cell induction and expansion. *J. Immunol.* **183**, 4895–903 (2009).
16. Cheung, A. S., Zhang, D. K. Y., Koshy, S. T. & Mooney, D. J. Scaffolds that mimic antigen-presenting cells enable ex vivo expansion of primary T cells. *Nat. Biotechnol.* **36**, 160–169 (2018).
17. Hickey, J. W., Vicente, F. P., Howard, G. P., Mao, H.-Q. & Schneck, J. P. Biologically Inspired Design of Nanoparticle Artificial Antigen-Presenting Cells for Immunomodulation. *Nano Lett.* **17**, 7045–7054 (2017).
18. Zhang, P., Andorko, J. I. & Jewell, C. M. Impact of dose, route, and composition on the immunogenicity of immune polyelectrolyte multilayers delivered on gold templates.

Biotechnol. Bioeng. **114**, 423–431 (2017).
19. Li, X., Wang, X. & Ito, A. Tailoring inorganic nanoadjuvants towards next-generation vaccines. *Chem. Soc. Rev.* **47**, 4954–4980 (2018).
20. Ebrahimian, M. *et al.* Co-delivery of Dual Toll-Like Receptor Agonists and Antigen in Poly(Lactic-Co-Glycolic) Acid/Polyethylenimine Cationic Hybrid Nanoparticles Promote Efficient In Vivo Immune Responses. *Front. Immunol.* **8**, 1077 (2017).
21. Ehl, S. *et al.* Antigen persistence and time of T-cell tolerization determine the efficacy of tolerization protocols for prevention of skin graft rejection. *Nat. Med.* **4**, 1015–1019 (1998).
22. Zinkernagel, R. M. *et al. Antigen localisation regulates immune responses in a dose-and time-dependent fashion: a geographical view of immune reactivity*. *ImmunoJogJco/Reviews* **156**, (1997).
23. Zinkernagel, R. M. Localization dose and time of antigens determine immune reactivity. *Semin. Immunol.* **12**, 163–171 (2000).
24. Scully, R., Qin, S., Cobbold, S. & Waldmann, H. Mechanisms in CD4 antibody-mediated transplantation tolerance: kinetics of induction, antigen dependency and role of regulatory T cells. *Eur. J. Immunol.* **24**, 2383–2392 (1994).
25. Weishaupt, A. *et al.* Molecular mechanisms of high-dose antigen therapy in experimental autoimmune encephalomyelitis: rapid induction of Th1-type cytokines and inducible nitric oxide synthase. *J. Immunol.* **165**, 7157–63 (2000).
26. Hess, K. L., Medintz, I. L. & Jewell, C. M. Designing inorganic nanomaterials for vaccines and immunotherapies. *Nano Today* (2019). doi:10.1016/J.NANTOD.2019.04.005
27. Bookstaver, M. L., Tsai, S. J., Bromberg, J. S. & Jewell, C. M. Improving Vaccine and Immunotherapy Design Using Biomaterials. *Trends Immunol.* **39**, 135–150 (2017).
28. Kapnick, S. M. The Nanoparticle-Enabled Success of COVID-19 mRNA Vaccines and the Promise of Microneedle Platforms for Pandemic Vaccine Response. *https://home.liebertpub.com/dna* **41**, 25–29 (2022).
29. Faria, M. *et al.* Minimum information reporting in bio–nano experimental literature. *Nat. Nanotechnol.* **13**, 777–785 (2018).
30. Senti, G. & Kündig, T. M. Intralymphatic immunotherapy. *World Allergy Organ. J.* **8**, 1–5 (2015).
31. Park, H. J. *et al.* Intralymphatic immunotherapy with tyrosine-adsorbed allergens: a double-blind, placebo-controlled trial. *Respir. Res.* **22**, 1–13 (2021).
32. Schwaab, T. *et al.* Clinical and immunologic effects of intranodal autologous tumor lysate-dendritic cell vaccine with Aldesleukin (Interleukin 2) and IFN-{alpha}2a therapy in metastatic renal cell carcinoma patients. *Clin. Cancer Res.* **15**, 4986–4992 (2009).
33. Morisaki, T. *et al.* Intranodal Administration of Neoantigen Peptide-loaded Dendritic Cell Vaccine Elicits Epitope-specific T Cell Responses and Clinical Effects in a Patient with Chemorefractory Ovarian Cancer with Malignant Ascites. *Immunol. Invest.* **50**, 1–18 (2021).
34. Barrat, F. J., Elkon, K. B. & Fitzgerald, K. A. Importance of Nucleic Acid Recognition in Inflammation and Autoimmunity. *Annu. Rev. Med.* (2015). doi:10.1146/annurev-med-052814-023338
35. Reis, E. S., Mastellos, D. C., Ricklin, D., Mantovani, A. & Lambris, J. D. Complement in

cancer: untangling an intricate relationship. *Nat. Rev. Immunol.* **18**, 5–18 (2018).
36. Hancock, R. E. W., Haney, E. F. & Gill, E. E. The immunology of host defence peptides: beyond antimicrobial activity. *Nat. Rev. Immunol.* **16**, 321–334 (2016).
37. Sharma, P. & Allison, J. P. Leading Edge Review Immune Checkpoint Targeting in Cancer Therapy: Toward Combination Strategies with Curative Potential. *Cell* **161**, 205–214 (2015).
38. Diamond, M. S., Ledgerwood, J. E. & Pierson, T. C. Zika Virus Vaccine Development: Progress in the Face of New Challenges. *Annu. Rev. Med.* **70**, 121–135 (2019).
39. Yang, Y. *et al.* The deadly coronaviruses: The 2003 SARS pandemic and the 2020 novel coronavirus epidemic in China. *Journal of Autoimmunity* **109**, 102434 (2020).
40. Koopmans, M. *et al.* Familiar barriers still unresolved—a perspective on the Zika virus outbreak research response. *The Lancet Infectious Diseases* **19**, e59–e62 (2019).
41. Focosi, D., Tuccori, M. & Maggi, F. Progressive multifocal leukoencephalopathy and anti-CD20 monoclonal antibodies: What do we know after 20 years of rituximab. *Rev. Med. Virol.* **29**, (2019).
42. Leach, D. G., Young, S. & Hartgerink, J. D. Advances in immunotherapy delivery from implantable and injectable biomaterials. *Acta Biomaterialia* **88**, 15–31 (2019).
43. Sestito, L. F. & Thomas, S. N. Biomaterials for Modulating Lymphatic Function in Immunoengineering. *ACS Pharmacol. Transl. Sci.* **2**, 293–310 (2019).
44. Zhao, Y., Guo, Y. & Tang, L. Engineering cancer vaccines using stimuli-responsive biomaterials. *Nano Research* **11**, 5355–5371 (2018).
45. Vishwakarma, A. *et al. Engineering Immunomodulatory Biomaterials To Tune the Inflammatory Response. Trends in Biotechnology* **34**, 470–482 (2016).
46. A Study of V503 (A Multivalent Human Papillomavirus [HPV] L1 Virus-Like Particle [VLP] Vaccine) in Preadolescents and Adolescents (V503-002) - Full Text View - ClinicalTrials.gov. Available at: https://clinicaltrials.gov/ct2/show/NCT00943722. (Accessed: 19th April 2020)
47. Phase 3 Pivotal Trial of NanoFlu^{TM} in Older Adults - Full Text View - ClinicalTrials.gov. Available at: https://clinicaltrials.gov/ct2/show/NCT04120194?term=NanoFlu&draw=2&rank=2. (Accessed: 19th April 2020)
48. Amsterdam UMC Clinical Trial With a Native-like HIV-1 Envelope Vaccine - Full Text View - ClinicalTrials.gov. Available at: https://clinicaltrials.gov/ct2/show/NCT03961438?term=liposome+AND+vaccine&draw=2&rank=2. (Accessed: 19th April 2020)
49. Dendritic Cell Activating Scaffold in Melanoma - Full Text View - ClinicalTrials.gov. Available at: https://clinicaltrials.gov/ct2/show/NCT01753089. (Accessed: 19th April 2020)
50. Study of the Safety, Pharmacodynamics, Efficacy, and PK of TIMP-GLIA in Subjects With Celiac Disease - Full Text View - ClinicalTrials.gov. Available at: https://clinicaltrials.gov/ct2/show/NCT03738475. (Accessed: 19th April 2020)
51. Enhanced Epidermal Antigen Specific Immunotherapy Trial -1 - Full Text View - ClinicalTrials.gov. Available at: https://clinicaltrials.gov/ct2/show/NCT02837094. (Accessed: 19th April 2020)
52. Moon, J. J., Huang, B. & Irvine, D. J. Engineering nano- and microparticles to tune

immunity. *Adv. Mater.* **24**, 3724–46 (2012).
53. Gause, K. T. *et al.* Immunological Principles Guiding the Rational Design of Particles for Vaccine Delivery. *ACS Nano* **11**, 54–68 (2017).
54. Jasinski, D., Haque, F., Binzel, D. W. & Guo, P. Advancement of the Emerging Field of RNA Nanotechnology. *ACS Nano* **11**, 1142–1164 (2017).
55. Toy, R. & Roy, K. Engineering nanoparticles to overcome barriers to immunotherapy. *Bioeng. Transl. Med.* **1**, 47–62 (2016).
56. Bracho-Sanchez, E., Xia, C. Q., Clare-Salzler, M. J. & Keselowsky, B. G. Micro and Nano Material Carriers for Immunomodulation. *American Journal of Transplantation* **16**, 3362–3370 (2016).
57. Pati, R., Shevtsov, M. & Sonawane, A. Nanoparticle vaccines against infectious diseases. *Frontiers in Immunology* **9**, 2224 (2018).
58. Nicolas, J. *et al. Best Practices for New Polymers and Nanoparticulate Systems*. *Chemistry of Materials* **30**, 6587–6588 (American Chemical Society, 2018).
59. Howard, G. P. *et al.* Critical size limit of biodegradable nanoparticles for enhanced lymph node trafficking and paracortex penetration. *Nano Res.* **12**, 837–844 (2019).
60. Talamini, L. *et al.* Influence of Size and Shape on the Anatomical Distribution of Endotoxin-Free Gold Nanoparticles. *ACS Nano* **11**, 5519–5529 (2017).
61. Zhang, R. *et al.* Peptide Amphiphile Micelle Vaccine Size and Charge Influence the Host Antibody Response. *ACS Biomater. Sci. Eng.* **4**, 2463–2572 (2018).
62. Kelly, S. H. *et al.* Enabling sublingual peptide immunization with molecular self-assemblies. *Biomaterials* **241**, 119903 (2020).
63. De Koker, S. *et al.* Engineering Polymer Hydrogel Nanoparticles for Lymph Node-Targeted Delivery. *Angew. Chemie Int. Ed.* **55**, 1334–1339 (2016).
64. Moynihan, K. D. *et al.* Enhancement of Peptide Vaccine Immunogenicity by Increasing Lymphatic Drainage and Boosting Serum Stability. *Cancer Immunol. Res.* **6**, 1025–1038 (2018).
65. Zhu, D. *et al.* Co-delivery of antigen and dual agonists by programmed mannose-targeted cationic lipid-hybrid polymersomes for enhanced vaccination. *Biomaterials* **206**, 25–40 (2019).
66. Bahmani, B. *et al.* Targeted delivery of immune therapeutics to lymph nodes prolongs cardiac allograft survival. *J. Clin. Invest.* **128**, 4770–4786 (2018).
67. Son, S. *et al.* Sugar-Nanocapsules Imprinted with Microbial Molecular Patterns for mRNA Vaccination. *Nano Lett.* **20**, 1499–1509 (2020).
68. Xia, Y. *et al.* Exploiting the pliability and lateral mobility of Pickering emulsion for enhanced vaccination. *Nat. Mater.* **17**, 187–194 (2018).
69. Palomba, R. *et al.* Modulating Phagocytic Cell Sequestration by Tailoring Nanoconstruct Softness. *ACS Nano* **12**, 1433–1444 (2018).
70. Miura, R., Sawada, S. I., Mukai, S. A., Sasaki, Y. & Akiyoshi, K. Antigen Delivery to Antigen-Presenting Cells for Adaptive Immune Response by Self-Assembled Anionic Polysaccharide Nanogel Vaccines. *Biomacromolecules* **21**, 621–629 (2020).
71. Fromen, C. A. *et al.* Nanoparticle surface charge impacts distribution, uptake and lymph node trafficking by pulmonary antigen-presenting cells. *Nanomedicine Nanotechnology, Biol. Med.* **12**, 677–687 (2016).
72. Phanse, Y. *et al.* Functionalization promotes pathogen-mimicking characteristics of

polyanhydride nanoparticle adjuvants. *J. Biomed. Mater. Res. Part A* **105**, 2762–2771 (2017).
73. Yang, Y. *et al.* Multi-shelled Dendritic Mesoporous Organosilica Hollow Spheres: Roles of Composition and Architecture in Cancer Immunotherapy. *Angew. Chemie Int. Ed.* **56**, 8446–8450 (2017).
74. Manna, S. *et al.* Immunomodulation of the NLRP3 Inflammasome through Structure-Based Activator Design and Functional Regulation via Lysosomal Rupture. *ACS Cent. Sci.* **4**, 982–995 (2018).
75. Wang, Y.-Q. *et al.* Improving adjuvanticity of quaternized chitosan–based microgels for H5N1 split vaccine by tailoring the particle properties to achieve antigen dose sparing effect. *Int. J. Pharm.* **515**, 84–93 (2016).
76. Xing, Y. *et al.* Synthesis of Poly(acyclic orthoester)s: Acid-Sensitive Biomaterials for Enhancing Immune Responses of Protein Vaccine. *Angew. Chemie Int. Ed.* anie.202001169 (2020). doi:10.1002/anie.202001169
77. Guo, S. *et al.* Size, Shape, and Sequence-Dependent Immunogenicity of RNA Nanoparticles. *Mol. Ther. - Nucleic Acids* **9**, 399–408 (2017).
78. Hong, E. *et al.* Structure and Composition Define Immunorecognition of Nucleic Acid Nanoparticles. *Nano Lett.* **18**, 4309–4321 (2018).
79. Tazaki, T. *et al.* Shape-dependent adjuvanticity of nanoparticle-conjugated RNA adjuvants for intranasal inactivated influenza vaccines †. *RSC Adv.* **8**, 16527–16536 (2018).
80. Andorko, J. I., Hess, K. L., Pineault, K. G. & Jewell, C. M. Intrinsic immunogenicity of rapidly-degradable polymers evolves during degradation. *Acta Biomater.* **32**, 24–34 (2016).
81. Andorko, J. I., Pineault, K. G. & Jewell, C. M. Impact of molecular weight on the intrinsic immunogenic activity of poly(beta amino esters). *J. Biomed. Mater. Res. - Part A* **105**, 1219–1229 (2017).
82. Allen, R. P., Bolandparvaz, A., Ma, J. A., Manickam, V. A. & Lewis, J. S. Latent, Immunosuppressive Nature of Poly(lactic- *co* -glycolic acid) Microparticles. *ACS Biomater. Sci. Eng.* **4**, 900–918 (2018).
83. You, X. *et al.* Arginine-based poly(ester amide) nanoparticle platform: From structure–property relationship to nucleic acid delivery. *Acta Biomater.* **74**, 180–191 (2018).
84. Tsai, S. J., Andorko, J. I., Zeng, X., Gammon, J. M. & Jewell, C. M. Polyplex interaction strength as a driver of potency during cancer immunotherapy. *Nano Res.* **11**, 5642–5656 (2018).
85. Lynn, G. M. *et al.* In vivo characterization of the physicochemical properties of polymer-linked TLR agonists that enhance vaccine immunogenicity. *Nat. Biotechnol.* **33**, 1201–1210 (2015).
86. Wang, J. *et al.* Physical activation of innate immunity by spiky particles. *Nat. Nanotechnol.* **13**, 1078–1086 (2018).
87. Lynn, G. M. *et al.* Impact of Polymer-TLR-7/8 Agonist (Adjuvant) Morphology on the Potency and Mechanism of CD8 T Cell Induction. *Biomacromolecules* **20**, 854–870 (2019).
88. Wilson, D. S. *et al.* Antigens reversibly conjugated to a polymeric glyco-adjuvant induce protective humoral and cellular immunity. *Nat. Mater.* **18**, 175–185 (2019).

89. Liu, L. *et al.* Immune responses to vaccines delivered by encapsulation into and/or adsorption onto cationic lipid-PLGA hybrid nanoparticles. (2016). doi:10.1016/j.jconrel.2016.01.050
90. Rincon-Restrepo, M. *et al.* Vaccine nanocarriers: Coupling intracellular pathways and cellular biodistribution to control CD4 vs CD8 T cell responses. *Biomaterials* **132**, 48–58 (2017).
91. Zupančič, E. *et al.* Rational design of nanoparticles towards targeting antigen-presenting cells and improved T cell priming. *J. Control. Release* **258**, 182–195 (2017).
92. Moyer, T. J. *et al.* Engineered immunogen binding to alum adjuvant enhances humoral immunity. *Nat. Med.* **26**, 430–440 (2020).
93. Singha, S. *et al.* Peptide-MHC-based nanomedicines for autoimmunity function as T-cell receptor microclustering devices. *Nat. Nanotechnol.* **12**, 701–710 (2017).
94. Hess, K. L. *et al.* Engineering Immunological Tolerance Using Quantum Dots to Tune the Density of Self-Antigen Display. *Adv. Funct. Mater.* **27**, 1700290 (2017).
95. Kapadia, C. H. *et al.* Extending antigen release from particulate vaccines results in enhanced antitumor immune response. *J. Control. Release* **269**, 393–404 (2018).
96. Chen, N. *et al.* Tunable degradation of acetalated dextran microparticles enables controlled vaccine adjuvant and antigen delivery to modulate adaptive immune responses. *J. Control. Release* **273**, 147–159 (2018).
97. Benson, R. A. *et al.* Antigen presentation kinetics control T cell/dendritic cell interactions and follicular helper T cell generation in vivo. *Elife* (2015). doi:10.7554/eLife.06994.001
98. Zhang, Y. N. *et al.* Nanoparticle Size Influences Antigen Retention and Presentation in Lymph Node Follicles for Humoral Immunity. *Nano Lett.* **19**, 7226–7235 (2019).
99. Wang, S. *et al.* Rational vaccinology with spherical nucleic acids. *Proc. Natl. Acad. Sci. U. S. A.* **116**, 10473–10481 (2019).
100. Kreer, C., Rauen, J., Zehner, M. & Burgdorf, S. Cross-presentation: how to get there – or how to get the ER. *Front. Immunol.* **2**, 87 (2012).
101. Joffre, O. P., Segura, E., Savina, A. & Amigorena, S. Cross-presentation by dendritic cells. *Nat. Rev. Immunol.* **12**, 557–569 (2012).
102. Latz, E. *et al.* TLR9 signals after translocating from the ER to CpG DNA in the lysosome. *Nat. Immunol.* **5**, 190–198 (2004).
103. Oakes, R. S., Froimchuk, E. & Jewell, C. M. Engineering Biomaterials to Direct Innate Immunity. *Adv. Ther.* **2**, 1800157 (2019).
104. Le Gall, C. M., Weiden, J., Eggermont, L. J. & Figdor, C. G. Dendritic cells in cancer immunotherapy. *Nat. Mater.* **17**, 474–475 (2018).
105. Garg, A. D., Coulie, P. G., Van den Eynde, B. J. & Agostinis, P. Integrating Next-Generation Dendritic Cell Vaccines into the Current Cancer Immunotherapy Landscape. *Trends Immunol.* **38**, 577–593 (2017).
106. Tostanoski, L. H., Gosselin, E. A. & Jewell, C. M. Engineering Tolerance Using Biomaterials to Target and Control Antigen Presenting Cells. *Discov. Med.* **21**, 403–410 (2016).
107. Mesin, L., Ersching, J. & Victora, G. D. Germinal Center B Cell Dynamics. *Immunity* **45**, 471–482 (2016).
108. Stavnezer, J., Guikema, J. E. J. & Schrader, C. E. Mechanism and Regulation of Class Switch Recombination. *Annu. Rev. Immunol.* **26**, 261–292 (2008).

109. McCullough, K. C. & Summerfield, A. Basic Concepts of Immune Response and Defense Development. *ILAR J.* **46**, 230–240 (2005).
110. Sahdev, P., Ochyl, L. J. & Moon, J. J. Biomaterials for nanoparticle vaccine delivery systems. *Pharm. Res.* **31**, 2563–2582 (2014).
111. Dai, Q. *et al.* Cell-Conditioned Protein Coronas on Engineered Particles Influence Immune Responses. (2017). doi:10.1021/acs.biomac.6b01545
112. Ke, X. *et al.* Physical and chemical profiles of nanoparticles for lymphatic targeting. *Advanced Drug Delivery Reviews* **151**–**152**, 72–93 (2019).
113. Schudel, A., Francis, D. M. & Thomas, S. N. Material design for lymph node drug delivery. *Nature Reviews Materials* **4**, 415–428 (2019).
114. Reddy, S. T., Rehor, A., Schmoekel, H. G., Hubbell, J. A. & Swartz, M. A. In vivo targeting of dendritic cells in lymph nodes with poly(propylene sulfide) nanoparticles. *J. Control. Release* **112**, 26–34 (2006).
115. Yu, X. *et al.* Melittin-lipid nanoparticles target to lymph nodes and elicit a systemic anti-tumor immune response. *Nat. Commun.* **11**, (2020).
116. Shukla, S. *et al.* Plant viral nanoparticles-based HER2 vaccine: Immune response influenced by differential transport, localization and cellular interactions of particulate carriers. *Biomaterials* **121**, 15–27 (2017).
117. Liu, H. *et al.* Structure-based programming of lymph-node targeting in molecular vaccines. *Nature* **507**, 519–522 (2014).
118. Fenton, O. S., Olafson, K. N., Pillai, P. S., Mitchell, M. J. & Langer, R. Advances in Biomaterials for Drug Delivery. *Adv. Mater.* **30**, 1705328 (2018).
119. Hasani-Sadrabadi, M. M. *et al.* Mechanobiological Mimicry of Helper T Lymphocytes to Evaluate Cell-Biomaterials Crosstalk. *Adv. Mater.* **30**, 1706780 (2018).
120. Zhu, G. *et al.* Albumin/vaccine nanocomplexes that assemble in vivo for combination cancer immunotherapy. *Nat. Commun.* **8**, 1–15 (2017).
121. Darrah, P. A. *et al.* Prevention of tuberculosis in macaques after intravenous BCG immunization. *Nature* **577**, 95–102 (2020).
122. Lynn, G. M. *et al.* Peptide–TLR-7/8a conjugate vaccines chemically programmed for nanoparticle self-assembly enhance CD8 T-cell immunity to tumor antigens. *Nat. Biotechnol.* **38**, 320–332 (2020).
123. Andorko, J. I., Tostanoski, L. H., Solano, E., Mukhamedova, M. & Jewell, C. M. Intra-lymph Node Injection of Biodegradable Polymer Particles. *J. Vis. Exp.* e50984 (2014). doi:10.3791/50984
124. Jewell, C. M., Bustamante López, S. C. & Irvine, D. J. In situ engineering of the lymph node microenvironment via intranodal injection of adjuvant-releasing polymer particles. *Proc. Natl. Acad. Sci.* **108**, 15745–15750 (2011).
125. Tostanoski, L. H. *et al.* Reprogramming the Local Lymph Node Microenvironment Promotes Tolerance that Is Systemic and Antigen Specific. *Cell Rep.* **16**, 2940–2952 (2016).
126. Garapaty, A. & Champion, J. A. Tunable particles alter macrophage uptake based on combinatorial effects of physical properties. *Bioeng. Transl. Med.* **2**, 92–101 (2017).
127. Hui, Y. *et al.* Understanding the Effects of Nanocapsular Mechanical Property on Passive and Active Tumor Targeting. *ACS Nano* **12**, 2846–2857 (2018).
128. del Pino, P. *et al.* Basic Physicochemical Properties of Polyethylene Glycol Coated Gold

Nanoparticles that Determine Their Interaction with Cells. *Angew. Chemie Int. Ed.* **55**, 5483–5487 (2016).
129. Wen, Y., Waltman, A., Han, H. & Collier, J. H. Switching the Immunogenicity of Peptide Assemblies Using Surface Properties. *ACS Nano* **10**, 9274–9286 (2016).
130. Wang, W. *et al.* Dual-targeting nanoparticle vaccine elicits a therapeutic antibody response against chronic hepatitis B. *Nat. Nanotechnol.* 1–11 (2020). doi:10.1038/s41565-020-0648-y
131. Tonigold, M. & Mailänder, V. Endocytosis and intracellular processing of nanoparticles in dendritic cells: routes to effective immunonanomedicines. *Nanomedicine* **11**, 2625–2630 (2016).
132. Gros, M. & Amigorena, S. Regulation of antigen export to the cytosol during cross-presentation. *Frontiers in Immunology* **10**, 41 (2019).
133. Sun, B. *et al.* Enhanced Immune Adjuvant Activity of Aluminum Oxyhydroxide Nanorods through Cationic Surface Functionalization. *ACS Appl. Mater. Interfaces* **9**, 21697–21705 (2017).
134. Li, A. W. *et al.* A facile approach to enhance antigen response for personalized cancer vaccination. *Nat. Mater.* **17**, 528–534 (2018).
135. Seydoux, E. *et al.* Size-dependent accumulation of particles in lysosomes modulates dendritic cell function through impaired antigen degradation. *Int. J. Nanomedicine* **9**, 3885–902 (2014).
136. Coffman, R. L., Sher, A. & Seder, R. A. Vaccine Adjuvants: Putting Innate Immunity to Work. *Immunity* **33**, 492–503 (2010).
137. Maisonneuve, C., Bertholet, S., Philpott, D. J. & De Gregorio, E. Unleashing the potential of NOD- and Toll-like agonists as vaccine adjuvants. *Proc. Natl. Acad. Sci.* **111**, 12294–12299 (2014).
138. Jones, K. S. Biomaterials as vaccine adjuvants. *Biotechnol. Prog.* **24**, 807–814 (2008).
139. Peleteiro, M. *et al.* Polymeric Nanocapsules for Vaccine Delivery: Influence of the Polymeric Shell on the Interaction With the Immune System. *Front. Immunol.* **9**, 791 (2018).
140. Zhu, M. *et al.* Cell-Penetrating Nanoparticles Activate the Inflammasome to Enhance Antibody Production by Targeting Microtubule-Associated Protein 1-Light Chain 3 for Degradation. *ACS Nano* (2020). doi:10.1021/acsnano.0c00962
141. Chen, X. *et al.* Shape-Dependent Activation of Cytokine Secretion by Polymer Capsules in Human Monocyte-Derived Macrophages. *Biomacromolecules* **17**, 1205–1212 (2016).
142. Jasinski, D. L., Li, H. & Guo, P. The Effect of Size and Shape of RNA Nanoparticles on Biodistribution. *Mol. Ther.* **26**, 784–792 (2018).
143. Chandler, M., Afonin, K. A., Chandler, M. & Afonin, K. A. Smart-Responsive Nucleic Acid Nanoparticles (NANPs) with the Potential to Modulate Immune Behavior. *Nanomaterials* **9**, 611 (2019).
144. Parlea, L. *et al.* Cellular Delivery of RNA Nanoparticles. *ACS Comb. Sci.* **18**, 527–547 (2016).
145. Nasi, A. *et al.* Dendritic cell reprogramming by endogenously produced lactic acid. *J. Immunol.* **191**, 3090–9 (2013).
146. Loftus, C., Saeed, M., Davis, D. M. & Dunlop, I. E. Activation of Human Natural Killer Cells by Graphene Oxide-Templated Antibody Nanoclusters. (2018).

doi:10.1021/acs.nanolett.8b01089
147. Gale, E. C. *et al.* A Nanoparticle Platform for Improved Potency, Stability, and Adjuvanticity of Poly(I:C). *Adv. Ther.* **3**, 1900174 (2020).
148. Sofias, A. M., Andreassen, T. & Hak, S. Nanoparticle Ligand-Decoration Procedures Affect in Vivo Interactions with Immune Cells. *Mol. Pharm.* **15**, 5754–5761 (2018).
149. Cui, J. *et al.* Mechanically Tunable, Self-Adjuvanting Nanoengineered Polypeptide Particles. *Adv. Mater.* **25**, 3468–3472 (2013).
150. Kakizawa, Y., Lee, J. S., Bell, B. & Fahmy, T. M. Precise manipulation of biophysical particle parameters enables control of proinflammatory cytokine production in presence of TLR 3 and 4 ligands. *Acta Biomater.* **57**, 136–145 (2017).
151. Pallares, R. M. *et al.* Manipulating Immune Activation of Macrophages by Tuning the Oligonucleotide Composition of Gold Nanoparticles. *Bioconjug. Chem.* **30**, 2032–2037 (2019).
152. Petrovsky, N. Comparative Safety of Vaccine Adjuvants: A Summary of Current Evidence and Future Needs. *Drug Safety* **38**, 1059–1074 (2015).
153. Batista-Duharte, A., Martínez, D. T. & Carlos, I. Z. Efficacy and safety of immunological adjuvants. Where is the cut-off? *Biomedicine and Pharmacotherapy* **105**, 616–624 (2018).
154. Abkar, M., Alamian, S. & Sattarahmady, N. A comparison between adjuvant and delivering functions of calcium phosphate, aluminum hydroxide and chitosan nanoparticles, using a model protein of Brucella melitensis Omp31. *Immunol. Lett.* **207**, 28–35 (2019).
155. Saito, E. *et al.* Designing drug-free biodegradable nanoparticles to modulate inflammatory monocytes and neutrophils for ameliorating inflammation. *J. Control. Release* **300**, 185–196 (2019).
156. Saito, E. *et al.* Design of biodegradable nanoparticles to modulate phenotypes of antigen-presenting cells for antigen-specific treatment of autoimmune disease. *Biomaterials* **222**, 119432 (2019).
157. Jia, J. *et al.* Adjuvanticity Regulation by Biodegradable Polymeric Nano/microparticle Size. *Mol. Pharm.* **14**, 14–22 (2017).
158. Gao, J., Ochyl, J., Yang, E. & Moon, J. J. Cationic liposomes promote antigen cross-presentation in dendritic cells by alkalizing the lysosomal pH and limiting the degradation of antigens. *Int. J. Nanomedicine* **12**, 1251–1264 (2017).
159. Gosselin, E. A., Eppler, H. B., Bromberg, J. S. & Jewell, C. M. Designing natural and synthetic immune tissues. *Nature Materials* **17**, 484–498 (2018).
160. Kumar, S., Anselmo, A. C., Banerjee, A., Zakrewsky, M. & Mitragotri, S. Shape and size-dependent immune response to antigen-carrying nanoparticles. *J. Control. Release* **220**, 141–148 (2015).
161. Dykman, L. A. *et al.* Gold nanoparticles as an adjuvant: Influence of size, shape, and technique of combination with CpG on antibody production. *Int. Immunopharmacol.* **54**, 163–168 (2018).
162. Hayashi, M. *et al.* Optimization of physiological properties of hydroxyapatite as a vaccine adjuvant. *Vaccine* **34**, 306–312 (2016).
163. Courant, T. *et al.* Tailoring nanostructured lipid carriers for the delivery of protein antigens: Physicochemical properties versus immunogenicity studies. *Biomaterials* **136**, 29–42 (2017).

164. Marcandalli, J. *et al.* Induction of Potent Neutralizing Antibody Responses by a Designed Protein Nanoparticle Vaccine for Respiratory Syncytial Virus. *Cell* **176**, 1420-1431.e17 (2019).
165. Brewer, M. G. *et al.* Nanoparticles decorated with viral antigens are more immunogenic at low surface density. *Vaccine* **35**, 774–781 (2017).
166. Skwarczynski, M. *et al.* Poly(amino acids) as a potent self-adjuvanting delivery system for peptide-based nanovaccines. *Sci. Adv.* **6**, (2020).
167. Northrup, L., Christopher, M. A., Sullivan, B. P. & Berkland, C. Combining antigen and immunomodulators: Emerging trends in antigen-specific immunotherapy for autoimmunity. *Adv. Drug Deliv. Rev.* **98**, 86–98 (2016).
168. Pearson, R. M., Casey, L. M., Hughes, K. R., Miller, S. D. & Shea, L. D. In vivo reprogramming of immune cells: Technologies for induction of antigen-specific tolerance. *Adv. Drug Deliv. Rev.* **114**, 240–255 (2017).
169. Pearson, R. M. *et al.* Controlled Delivery of Single or Multiple Antigens in Tolerogenic Nanoparticles Using Peptide-Polymer Bioconjugates. *Mol. Ther.* **25**, (2017).
170. Ramakrishnan, R., Balu-Iyer, S. V, Balu-Iyer, S. V, Sathyamangalam, F. & Balasubramanian, V. Effect of Biophysical Properties of Phosphatidylserine Particle on Immune Tolerance Induction Toward Factor VIII in a Hemophilia A Mouse Model. *J. Pharm. Sci.* **105**, 3039–3045 (2016).
171. Sestak, J. O., Fakhari, A., Badawi, A. H., Siahaan, T. J. & Berkland, C. Structure, size, and solubility of antigen arrays determines efficacy in experimental autoimmune encephalomyelitis. *AAPS J.* **16**, 1185–93 (2014).
172. Martin-Blanco, N. *et al.* A window of opportunity for cooperativity in the T Cell Receptor. *Nat. Commun.* **9**, 2618 (2018).
173. Tam, H. H. *et al.* Sustained antigen availability during germinal center initiation enhances antibody responses to vaccination. *Proc. Natl. Acad. Sci.* (2016). doi:10.1073/pnas.1606050113
174. Guarecuco, R. *et al.* Immunogenicity of pulsatile-release PLGA microspheres for single-injection vaccination. *Vaccine* **36**, 3161–3168 (2018).
175. Tzeng, A. *et al.* Temporally Programmed CD8α+ DC Activation Enhances Combination Cancer Immunotherapy. *Cell Rep.* **17**, 2503–2511 (2016).
176. Reed, S. G., Orr, M. T. & Fox, C. B. Key roles of adjuvants in modern vaccines. *Nat. Med.* **19**, 1597–1608 (2013).
177. Gammon, J. M. *et al.* Improving the clinical impact of biomaterials in cancer immunotherapy. *Oncotarget* **7**, 15421–15443 (2016).
178. Moyer, T. J., Zmolek, A. C. & Irvine, D. J. Beyond antigens and adjuvants: formulating future vaccines. *J. Clin. Invest.* **126**, 799–808 (2016).
179. Gu, L. & Mooney, D. J. Biomaterials and emerging anticancer therapeutic: engineering the tumor microenvironment. *Nat. Rev. Cancer* **16**, 56–66 (2016).
180. Drake, C. G., Lipson, E. J. & Brahmer, J. R. Breathing new life into immunotherapy: review of melanoma, lung and kidney cancer. *Nat. Rev. Clin. Oncol.* **11**, 24–37 (2014).
181. O'Neill, L. A. J., Golenbock, D. & Bowie, A. G. The history of Toll-like receptors — redefining innate immunity. *Nat. Rev. Immunol.* **13**, 453–460 (2013).
182. Karolinska, C. *et al.* Therapeutic vaccines for cancer: an overview of clinical trials. *Nat. Publ. Gr.* **11**, 509–524 (2014).

183. Kuai, R., Ochyl, L. J., Bahjat, K. S., Schwendeman, A. & Moon, J. J. Designer vaccine nanodiscs for personalized cancer immunotherapy. *Nat. Mater.* **16**, (2016).
184. Leleux, J. A., Pradhan, P. & Roy, K. Biophysical Attributes of CpG Presentation Control TLR9 Signaling to Differentially Polarize Systemic Immune Responses. *Cell Rep.* **18**, 700–710 (2017).
185. Chen, H. C., Zhan, X., Tran, K. K. & Shen, H. Selectively targeting the toll-like receptor 9 (TLR9) - IRF 7 signaling pathway by polymer blend particles. *Biomaterials* **34**, 6464–6472 (2013).
186. Krieg, A. M. Development of TLR9 agonists for cancer therapy. *J. Clin. Invest.* **117**, 1184–1194 (2007).
187. Blasius, A. L. & Beutler, B. Intracellular Toll-like Receptors. *Immunity* **32**, 305–315 (2010).
188. Andorko, J. I. & Jewell, C. M. Designing biomaterials with immunomodulatory properties for tissue engineering and regenerative medicine. *Bioeng. Transl. Med.* **2**, 139–155 (2017).
189. Kaphingst, K. A., Persky, S. & Lachance, C. Biomaterials for Nanoparticle Vaccine Delivery Systems. **14**, 384–399 (2010).
190. Jia, X., Wan, L. & Du, J. In situ polymerization on biomacromolecules for nanomedicines. *Nano Res.* 1–21 (2018). doi:10.1007/s12274-018-2080-2
191. Tay, C. Y., Yu, Y., Setyawati, M. I., Xie, J. & Leong, D. T. Presentation matters: Identity of gold nanocluster capping agent governs intracellular uptake and cell metabolism. *Nano Res.* **7**, 805–815 (2014).
192. Chen, G. *et al.* Development of fluorinated polyplex nanoemulsions for improved small interfering RNA delivery and cancer therapy. *Nano Res.* 1–16 (2017). doi:10.1007/s12274-017-1946-z
193. Démoulins, T. *et al.* Self-replicating RNA vaccine functionality modulated by fine-tuning of polyplex delivery vehicle structure. *J. Control. Release* **266**, 256–271 (2017).
194. Wilson, D. R. *et al.* Biodegradable STING agonist nanoparticles for enhanced cancer immunotherapy. *Nanomedicine* **14**, 237–246 (2018).
195. Shmueli, R. B., Anderson, D. G. & Green, J. J. Electrostatic surface modifications to improve gene delivery. *Expert Opin. Drug Deliv.* **7**, 535–550 (2010).
196. Lynn, D. M. & Langer, R. Degradable poly(beta-amino esters): Synthesis, characterization, and self-assembly with plasmid DNA. *J. Am. Chem. Soc.* **122**, 10761–10768 (2000).
197. Pack, D. W., Hoffman, A. S., Pun, S. & Stayton, P. S. Design and development of polymers for gene delivery. *Nat. Rev. Drug Discov.* **4**, 581–593 (2005).
198. Kasturi, S. P. *et al.* Programming the magnitude and persistence of antibody responses with innate immunity. *Nature* **470**, 543–547 (2011).
199. Ngwa, W. *et al.* Using immunotherapy to boost the abscopal effect. *Nat. Rev. Cancer* **18**, 313–322 (2018).
200. Thomas, S. N., Vokali, E., Lund, A. W., Hubbell, J. A. & Swartz, M. A. Targeting the tumor-draining lymph node with adjuvanted nanoparticles reshapes the anti-tumor immune response. *Biomaterials* **35**, 814–824 (2014).
201. Chen, Q. *et al.* Photothermal therapy with immune-adjuvant nanoparticles together with checkpoint blockade for effective cancer immunotherapy. *Nat. Commun.* **7**, 13193 (2016).

202. Mougel, A., Terme, M. & Tanchot, C. Therapeutic cancer vaccine and combinations with antiangiogenic therapies and immune checkpoint blockade. *Frontiers in Immunology* **10**, 467 (2019).
203. Santos, P. M. & Butterfield, L. H. Based Cancer Vaccines − Dendritic Cell Dendritic Cell–Based Cancer Vaccines. *J Immunol J. Immunol. by guest* **200**, 443–449 (2018).
204. Vermaelen, K. Vaccine strategies to improve anticancer cellular immune responses. *Frontiers in Immunology* **10**, (2019).
205. Muenst, S. *et al.* The immune system and cancer evasion strategies: therapeutic concepts. *J. Intern. Med.* **279**, 541–562 (2016).
206. Tormoen, G. W., Crittenden, M. R. & Gough, M. J. Role of the immunosuppressive microenvironment in immunotherapy. *Advances in Radiation Oncology* **3**, 520–526 (2018).
207. Cai, Z. *et al.* Photodynamic Therapy Combined with Antihypoxic Signaling and CpG Adjuvant as an In Situ Tumor Vaccine Based on Metal–Organic Framework Nanoparticles to Boost Cancer Immunotherapy. *Adv. Healthc. Mater.* **9**, 1900996 (2020).
208. Cano-Mejia, J., Bookstaver, M. L., Sweeney, E. E., Jewell, C. M. & Fernandes, R. Prussian blue nanoparticle-based antigenicity and adjuvanticity trigger robust antitumor immune responses against neuroblastoma. *Biomater. Sci.* **7**, 1875–1887 (2019).
209. Cha, B. G., Jeong, J. H. & Kim, J. Extra-Large Pore Mesoporous Silica Nanoparticles Enabling Co-Delivery of High Amounts of Protein Antigen and Toll-like Receptor 9 Agonist for Enhanced Cancer Vaccine Efficacy. *ACS Cent. Sci.* **4**, 484–492 (2018).
210. Bookstaver, M. L., Hess, K. L. & Jewell, C. M. Self-Assembly of Immune Signals Improves Codelivery to Antigen Presenting Cells and Accelerates Signal Internalization, Processing Kinetics, and Immune Activation. *Small* **14**, 1802202 (2018).
211. Zhu, M. *et al.* Co-delivery of tumor antigen and dual toll-like receptor ligands into dendritic cell by silicon microparticle enables efficient immunotherapy against melanoma. *J. Control. Release* **272**, 72–82 (2018).
212. Zinzow-Kramer, W. M., Weiss, A. & Au-Yeung, B. B. Adaptation by naïve CD4+ T cells to self-antigen–dependent TCR signaling induces functional heterogeneity and tolerance. *Proc. Natl. Acad. Sci. U. S. A.* **116**, 15160–15169 (2019).
213. Irvine, D. J., Hanson, M. C., Rakhra, K. & Tokatlian, T. Synthetic Nanoparticles for Vaccines and Immunotherapy. *Chem. Rev.* **115**, 11109–11146 (2015).
214. Lu, Y. *et al.* Engineering a "PEG-g-PEI/DNA nanoparticle-in- PLGA microsphere" hybrid controlled release system to enhance immunogenicity of DNA vaccine. *Mater. Sci. Eng. C* **106**, 110294 (2020).
215. Wongrakpanich, A. *et al.* The absence of CpG in plasmid DNA-chitosan polyplexes enhances transfection efficiencies and reduces inflammatory responses in murine lungs. *Mol. Pharm.* **11**, 1022–1031 (2014).
216. Zhang, M. *et al.* ROS Activatable siRNA-Engineered Polyplex for NIR-Triggered Synergistic Cancer Treatment. *ACS Appl. Mater. Interfaces* **12**, (2020).
217. Ivashkiv, L. B. IFNγ: signalling, epigenetics and roles in immunity, metabolism, disease and cancer immunotherapy. *Nature Reviews Immunology* **18**, 545–558 (2018).
218. Kieback, E. *et al.* Thymus-Derived Regulatory T Cells Are Positively Selected on Natural Self-Antigen through Cognate Interactions of High Functional Avidity. *Immunity* **44**, 1114–1126 (2016).

219. Carretero-Iglesia, L. *et al.* High Peptide Dose Vaccination Promotes the Early Selection of Tumor Antigen-Specific CD8 T-Cells of Enhanced Functional Competence. *Front. Immunol.* **10**, 3016 (2020).
220. Zhang, Y. *et al.* The Immunogenicity and Anti-tumor Efficacy of a Rationally Designed Neoantigen Vaccine for B16F10 Mouse Melanoma. *Front. Immunol.* **10**, 2472 (2019).
221. Alipour Talesh, G. *et al.* Poly (I: C)-DOTAP cationic nanoliposome containing multi-epitope HER2-derived peptide promotes vaccine-elicited anti-tumor immunity in a murine model. *Immunol. Lett.* **176**, 57–64 (2016).
222. Zhang, L. Multi-epitope vaccines: A promising strategy against tumors and viral infections. *Cell. Mol. Immunol.* **15**, 182–184 (2018).
223. Lennerz, V. *et al.* Immunologic response to the survivin-derived multi-epitope vaccine EMD640744 in patients with advanced solid tumors. *Cancer Immunol. Immunother.* **63**, 381–394 (2014).
224. Tsou, P., Katayama, H., Ostrin, E. J. & Hanash, S. M. The Emerging Role of B Cells in Tumor Immunity. *Cancer Res* **76**, (2016).
225. Duong, H. T. T. *et al.* Degradation-regulated architecture of injectable smart hydrogels enhances humoral immune response and potentiates antitumor activity in human lung carcinoma. *Biomaterials* **230**, 119599 (2020).
226. Zhong, X. *et al.* An aluminum adjuvant-integrated nano-MOF as antigen delivery system to induce strong humoral and cellular immune responses. *J. Control. Release* **300**, 81–92 (2019).
227. Maldonado, R. A. *et al.* Polymeric synthetic nanoparticles for the induction of antigen-specific immunological tolerance. doi:10.1073/pnas.1408686111
228. Mueller, S. N., Tian, S. & DeSimone, J. M. Rapid and Persistent Delivery of Antigen by Lymph Node Targeting PRINT Nanoparticle Vaccine Carrier To Promote Humoral Immunity. *Mol. Pharm.* **12**, 1356–65 (2015).
229. Johansen, P. *et al.* Antigen kinetics determines immune reactivity. *Proc. Natl. Acad. Sci. U. S. A.* **105**, 5189–94 (2008).
230. Gratz, I. K. *et al.* Cutting edge: Self-antigen controls the balance between effector and regulatory T cells in peripheral tissues. *J. Immunol.* **192**, 1351–5 (2014).
231. Ontaneda, D., Hyland, M. & Cohen, J. A. Multiple Sclerosis: New Insights in Pathogenesis and Novel Therapeutics. *Annu. Rev. Med.* **63**, 389–404 (2012).
232. Sospedra, M. & Martin, R. IMMUNOLOGY OF MULTIPLE SCLEROSIS. *Annu. Rev. Immunol.* **23**, 683–747 (2005).
233. Racke, M. K. Immunopathogenesis of multiple sclerosis. *Ann. Indian Acad. Neurol.* **12**, 215–20 (2009).
234. Abdel-Gadir, A., Massoud, A. H. & Chatila, T. A. Antigen-specific Treg cells in immunological tolerance: implications for allergic diseases. *F1000Research* **7**, 38 (2018).
235. Yeste, A., Nadeau, M., Burns, E. J., Weiner, H. L. & Quintana, F. J. Nanoparticle-mediated codelivery of myelin antigen and a tolerogenic small molecule suppresses experimental autoimmune encephalomyelitis. doi:10.1073/pnas.1120611109
236. Rice, J., Ottensmeier, C. H. & Stevenson, F. K. DNA vaccines: precision tools for activating effective immunity against cancer. *Nat. Rev. Cancer* **8**, 108–120 (2008).
237. Powell, J. D., Pollizzi, K. N., Heikamp, E. B. & Horton, M. R. Regulation of Immune Responses by mTOR. *Annu. Rev. Immunol.* **30**, 39 (2012).

238. Tostanoski, L. H. *et al.* Reprogramming the Local Lymph Node Microenvironment Promotes Tolerance that Is Systemic and Antigen Specific. *Cell Rep.* **16**, 2940–2952 (2016).
239. Lipford, B. *et al.* Lethal Murine Leishmaniasis in Trigger Protective and Curative Th1 Responses Cutting Edge: CpG Oligodeoxynucleotides. *J Immunol Ref.* **3627**, 3627–3630 (1998).
240. Butcher, M. J. & Zhu, J. (Jeff). Plasticity and functionality of Th17 subsets in EAE. *J. Immunol.* **200**, (2018).
241. Grifka-Walk, H. M., Lalor, S. J. & Segal, B. M. Highly polarized Th17 cells induce EAE via a T-bet-independent mechanism. *Eur. J. Immunol.* **43**, 2824–2831 (2013).
242. Arellano, G., Ottum, P. A., Reyes, L. I., Burgos, P. I. & Naves, R. Stage-specific role of interferon-gamma in experimental autoimmune encephalomyelitis and multiple sclerosis. *Front. Immunol.* **6**, 492 (2015).
243. Collison, L. W. & Vignali, D. A. A. In Vitro Treg Suppression Assays. *Methods Mol. Biol.* **707**, 21–37 (2011).
244. Rosenblum, M. D., Way, S. S. & Abbas, A. K. Regulatory T cell memory. *Nat. Rev. Immunol.* **16**, 90 (2016).
245. Renkema, K. R. *et al.* KLRG1 + Memory CD8 T Cells Combine Properties of Short-Lived Effectors and Long-Lived Memory . *J. Immunol.* **205**, 1059–1069 (2020).